Metallacarboranes derived from 1,1′-bis(*o*-carborane)

Dipendu Mandal

Submitted for the degree of Doctor of Philosophy at Heriot-Watt University, on completion of research in the School of Engineering and Physical Sciences

September 2016

Abstract

Chapter one gives an overview of single cage heteroborane chemistry, particularly the areas of 12- and 13-vertex metallacarboranes and their isomerisations. Also included is the chemistry of bis(carboranes), with recent developments on chelating derivatives of 1,1′-bis(*o*-carborane), as well as reduction/metallation of bis(*o*-carborane).

Chapter two describes metallation of the [7-(1′-1′,2′-*closo*-$C_2B_{10}H_{11}$)-7,8-*nido*-$C_2B_9H_{10}]^{2-}$ dianion with various $\{NiPP\}^{2+}$, $\{PdNN\}^{2+}$ or $\{NiP_2\}^{2+}$ fragments (PP = chelating diphosphine; NN = chelating diamine; P = monodentate phosphine or phosphite) and which leads either to unisomerised 3,1,2-MC_2B_9 species or to isomerised 4,1,2-MC_2B_9 or 2,1,8-MC_2B_9 species, all with a pendant C_2B_{10} substituent. The products were fully characterised spectroscopically and crystallographically as appropriate. Overall the results suggest that an important factor in a 3,1,2 to 4,1,2 isomerisation is the relief gained from steric crowding, whereas a 3,1,2 to 2,1,8 isomerisation appears to be favoured by strongly electron-donating ligands on the metal.

Chapter three describes capitation of the [7-(7′-7′,8′-*nido*-$C_2B_9H_{10}$)-7,8-*nido*-$C_2B_9H_{10}]^{4-}$ tetraanion with $\{NiPP\}^{2+}$ and $\{BX\}^{2+}$ fragments (PP = chelating diphosphine; X = Br, I, Ph). This results in examples of MC_2B_9-MC_2B_9 architectures (3′,1′,2′-3,1,2; 4′,1′,2′-3,1,2) or bis(carborane) derivatives. Thermal isomerisation of the bis(nickelacarboranes) is studied. Unexpected interconversion is observed between bis(nickelacarborane) diastereoisomers (*rac* and *meso* isomers of 3′,1′,2′-NiC_2B_9-3,1,2-NiC_2B_9) ligated by dmpe and the mechanism of this interconvesion is considered. A stereospecific product was observed in the nickelacarborane ligated by dppe and this is rationalised by DHB. Formation of 4′,1′,2′-NiC_2B_9-4,1,2-NiC_2B_9 and 2′,1′,8′-NiC_2B_9-4,1,2-NiC_2B_9 isomers on thermolysis of 3′,1′,2′-3,1,2 or 4′,1′,2′-3,1,2 MC_2B_9-MC_2B_9 precursors is elucidated in terms of DHB. Finally a new naming convention is introduced for these 12-vertex/12-vertex bis(nickelacarboranes) to distinguish the chirality between cages.

Chapter four elaborates the thermolysis of a *rac*/*meso* mixture of the species [1-(1′-4′-Cp-4′,1′,6′-*closo*-$CoC_2B_{10}H_{11}$)-4-Cp-4,1,6-*closo*-$CoC_2B_{10}H_{11}$] to yield a *rac*/*meso* mixture of [1-(1′-4′-Cp-4′,1′,12′-*closo*-$CoC_2B_{10}H_{11}$)-4-Cp-4,1,12-*closo*-$CoC_2B_{10}H_{11}$]. Cage carbon-atom identification is accomplished by both the VCD and BHD methods. Polyhedral

expansion of the *rac* and *meso* isomers of 4′,1′,12′-CoC_2B_{10}-4,1,12-CoC_2B_{10} was also attempted targeting 14-vertex metallacarborane/14-vertex metallacarborane derivatives.

Chapter five contains the experimental procedures leading to, and characterisation details for, all new compounds reported herein. Crystallographic data is listed in the Appendix together with structure solution and refinement details.

DEDICATION

To my Parents

Mr. Nakul Chandra Mandal

&

Mrs. Kabita Mandal

and

To my elder brother

Mr. Sukhendu Sekhar Mandal

Acknowledgements

First of all my sincerest thanks go to my supervisor, Prof. Alan J. Welch. I'm grateful for him giving me an opportunity to work in the Heteroborane Group, for all his guidance, support and advice throughout the research. I would like to also acknowledge the generous financial support of the James-Watt Scholarship throughout last three years.

I also wish to give great thanks to Dr Wing Y. Man for the initial introduction in the lab and support during the project. A special thanks go to Dr Alasdair P. M. Robertson who has been an invaluable source of information and knowledge. On top of this they have been great friends, and helpful with assistance in all kind of problems.

In my duration in the group all members were very friendly and made my research experience in the group more enjoyable and less frustrating. Special thanks go to Samuel Powley and Laura E. Riley who were incredibly supportive. Thanks also go to Antony P. Y. Chan, John J. Jones, Amanda Benton and all MChem and BSc project students during my stay in the group.

I would like to gratefully acknowledge Dr Koenraad M. P. Collart and Dr Brian Hutton for CHN analysis, Dr Dave Ellis for NMR spectroscopy, Dr Georgina M. Rosair for all her efforts in *X*-ray crystallography and Dr David McKay for DFT calculations. Acknowledgement must go to Dr Brian Hutton for lending me some reagents. A special acknowledgement goes to Dr Alasdair P. M. Robertson and Laura E. Riley for proof reading.

I was fortunate to have good friends in Edinburgh during the research. A special thanks go to Prof. Ajoy Kar and his family for caring and support. Special thanks go to my very good friend Sebabrata Mukherjee for his support and chatting in general.

Finally I would like to thank my family for all their support, especially my mother and elder brother for all their support. A great thanks goes to my best friend and fiancée Ashima Hazari for all her unwavering support and encouragement.

Table of Contents

Chapter 3

Nickelacarboranes: double dec/met of 1,1′-bis(*o*-carborane)

Chapter 4

Supraicosahedral bis(cobaltacarboranes)

Chapter 5

Experimental Section

Abbreviations

40-60	Boiling between 40 and 60 ^{o}C (petroleum ether)
2c-2e	Two centre two electron
3c-2e	Three centre two electron
δ	Chemical shift in ppm
PhCN	Benzonitrile (C_6H_5CN)
μ	Bridging
Å	Ångström, 1 x 10^{-10} m
Ueq	Equivalent isotropic thermal displacement parameter
app	apparent
benz	benzene
BTMA	benzyltrimethylammonium
BHD	Boron-Hydrogen Distance
BNCT	Boron Neutron Capture Therapy
br	broad
CHN	Elemental analysis
Cp	Cyclopentadienyl (C_5H_5)
p-cym	η-$C_{10}H_{14}$, 1-^{i}Pr,4-MeC_6H_4
d	doublet
DFT	Density Functional Theory
dec	decapitation
dmpe	1,2-bis(dimethylphosphino)ethane
dppe	1,2-bis(diphenylphosphino)ethane
DSD	Diamond-Square-Diamond
EIMS	Electron Ionisation Mass Spectrometry
Et	Ethyl group (-CH_2CH_3)
Et_2O/ether	Diethyl ether $(CH_3CH_2)_2O$
FMO	Frontier Molecular Orbital
g	gram(s)
h/hrs	hour(s)
K	Kelvin
kcal mol^{-1}	kilocalories per mole
LN	Lithium Napthalenide

mes	mesitylene
m	multiplet
M	Molar concentration (molarity)
M^+	Molecular Parent ion
mg	milligram(s)
mL	millilitre(s)
MHz	megahertz
met	metallation
mmol	millimole(s)
MO	Molecular Orbital
MW	Molecular Weight
m/*z*	Mass-to-charge ratio
n-BuLi	*n*-butyl lithium, $[C_4H_9]Li$
NMR	Nuclear Magnetic Resonance
OEt	Ethoxy group ($-OCH_2CH_3$)
Ph	Phenyl group ($-C_6H_5$)
ppm	parts per million
PS	Proton-Sponge
PSEPT	Polyhedral Skeletal Electron Pair Theory
q	quartet
red	reduction
R_f	Retention factor
Room temperature	16 - 20 °C
Δ	slipped parameter
s	singlet
t	triplet
TFR	Triangular Face Rotation
THF	Tetrahydrofuran
tmeda	tetramethylenediamine
TLC	Thin Layer Chromatography
VCD	Vertex-Centroid Distance

Abbreviations for Compounds

1 [1-(1′-1′,2′-*closo*-$C_2B_{10}H_{11}$)-3-dppe-3,1,2-*closo*-$NiC_2B_9H_{10}$]

2 [2-(1′-1′,2′-*closo*-$C_2B_{10}H_{11}$)-4-dppe-4,1,2-*closo*-$NiC_2B_9H_{10}$]

3 [8-(1′-1′,2′-*closo*-$C_2B_{10}H_{11}$)-2-dmpe-2,1,8-*closo*-$NiC_2B_9H_{10}$]

4 [1-(1′-1′,2′-*closo*-$C_2B_{10}H_{11}$)-3,3-$(PMe_3)_2$-3,1,2-*closo*-$NiC_2B_9H_{10}$]

5 [7-(1′-1′,2′-*closo*-$C_2B_{10}H_{11}$)-10-(PMe_3)-7,8-*nido*-$C_2B_9H_{10}$]

6 [1-(1′-1′,2′-*closo*-$C_2B_{10}H_{11}$)-3-Cl-3-PMe_3-8-PMe_3-3,1,2-*closo*-$NiC_2B_9H_9$]

7 [1-(1′-1′,2′-*closo*-$C_2B_{10}H_{11}$)-3,3-$(PMe_2Ph)_2$-3,1,2-*closo*-$NiC_2B_9H_{10}$]

8 [7-(1′-1′,2′-*closo*-$C_2B_{10}H_{11}$)-10-(PMe_2Ph)-7,8-*nido*-$C_2B_9H_{10}$]

9 [2-(1′-1′,2′-*closo*-$C_2B_{10}H_{11}$)-4,4-$(PMePh_2)_2$-4,1,2-*closo*-$NiC_2B_9H_{10}$]*

10 1-(1′-1′,2′-*closo*-$C_2B_{10}H_{11}$)-3-Cl-3-PMe_3-8-PMe_3-3,1,2-*closo*-$PdC_2B_9H_9$]*

11 1-(1′-1′,2′-*closo*-$C_2B_{10}H_{11}$)-3-tmeda-3,1,2-*closo*-$PdC_2B_9H_{10}$]

12 [8-(1′-1′,2′-*closo*-$C_2B_{10}H_{11}$)-2-tmeda-2,1,8-*closo*-$PdC_2B_9H_{10}$]

13 [1-(1′-1′,2′-*closo*-$C_2B_{10}H_{11}$)-3,3-$\{P(OMe)_3\}_2$-3,1,2-*closo*-$NiC_2B_9H_{10}$]

14 [1-(1′-1′,2′-*closo*-$C_2B_{10}H_{11}$)-2,2-$\{P(OMe)_3\}_2$-2,1,8-*closo*-$NiC_2B_9H_{10}$]

15 *cis*-$[NiBr_2\{P(OMe)_3\}_2]$*

16 [1-(1′-1′,2′-*closo*-$C_2B_{10}H_{11}$)-3,3-$\{P(OEt)_3\}_2$-3,1,2-*closo*-$NiC_2B_9H_{10}$]*

---

17 $[Tl]_2$[1-(1′-3′,1′,2′-$TlC_2B_9H_{10}$)-3,1,2-$TlC_2B_9H_{10}$]*

18 *rac*-[1-(1′-3′-(dmpe)-3′,1′,2′-*closo*$^{\circlearrowleft}$-$NiC_2B_9H_{10}$)-3-(dmpe)-3,1,2-*closo*$^{\circlearrowleft}$-$NiC_2B_9H_{10}$]

19 *meso*-[1-(1′-3′-(dmpe)-3′,1′,2′-*closo*$^{\circlearrowleft}$-$NiC_2B_9H_{10}$)-3-(dmpe)-3,1,2-*closo*$^{\circlearrowleft}$-$NiC_2B_9H_{10}$]

20 [7-(7′-7′,8′-*nido*-$C_2B_9H_{12}$)-7,8-*nido*-$C_2B_9H_{12}$]

21 *rac*-[1-(1′-3′-Ph-1′,2′-*closo*$^{\circlearrowleft}$-$C_2B_{10}H_{10}$)-3-Ph-1,2-*closo*$^{\circlearrowleft}$-$C_2B_{10}H_{10}$]

22 *meso*-[1-(1′-3′-Ph-1′,2′-*closo*$^{\circlearrowleft}$-$C_2B_{10}H_{10}$)-3-Ph-1,2-*closo*$^{\circlearrowleft}$-$C_2B_{10}H_{10}$]

23 $[HNMe_3]_2$[7-(7′-3′-Ph-7′,8′-*nido*-$C_2B_9H_{10}$)-3-Ph-7,8-*nido*-$C_2B_9H_{10}$] ($[HNMe_3]_2$[**23**])*

$[BTMA]_2$[7-(7′-3′-Ph-7′,8′-*nido*-$C_2B_9H_{10}$)-3-Ph-7,8-*nido*-$C_2B_9H_{10}$] ($[BTMA]_2$[**23**])

24	*rac*-[1-(1′-3′-(dppe)-3′,1′,2′-*closo*^{5}-$NiC_2B_9H_{10}$)-3-(dppe)-3,1,2-*closo*^{5}-$NiC_2B_9H_{10}$]
25	[1-(2′-4′-(dppe)-4′,1′,2′-*closo*^{5}-$NiC_2B_9H_{10}$)-3-(dppe)-3,1,2-*closo*^{5}-$NiC_2B_9H_{10}$]
26	[2-(8′-2′-(dppe)-2′,1′,8′-*closo*^{5}-$NiC_2B_9H_{10}$)-4-(dppe)-4,1,2-*closo*^{5}-$NiC_2B_9H_{10}$]
27	[2-(2′-4′-(dppe)-4′,1′,2′-*closo*^{5}-$NiC_2B_9H_{10}$)-4-(dppe)-4,1,2-*closo*^{5}-$NiC_2B_9H_{10}$]
28	*rac*-[1-(1′-4′-Cp-4′,1′,12′-*closo*-$CoC_2B_{10}H_{11}$)-4-Cp-4,1,12-*closo*-$CoC_2B_{10}H_{11}$)]
29	*meso*-[1-(1′-4′-Cp-4′,1′,12′-*closo*-$CoC_2B_{10}H_{11}$)-4-Cp-4,1,12-*closo*-$CoC_2B_{10}H_{11}$)]

*No crystallographic details.

Chapter 1

Introduction

1.1 Boron

Boron chemistry particularly cluster chemistry has expanded through several decades starting from the boron hydrides to carboranes and finally to metallaboranes and metallacarboranes. Carboranes, metallaboranes and metallacarboranes are classified as heteroboranes since heteroatoms have been incorporated into the boron cage.

In 1808 elemental boron was first isolated by Davy, Gay-Lussac and Thenard from the reduction of boric acid with potassium.[1] Although boron is not found freely in nature, it can be extracted in pure form from naturally occurring ores such as borax ($Na_2B_4O_7{\cdot}7H_2O$) or kernite ($Na_2B_4O_7{\cdot}4H_2O$). The natural abundances of the two isotopes of boron are 19.78% (^{10}B) and 80.22% (^{11}B).

Boron-rich clusters, heteroboranes in particular, exhibit high thermal, chemical and photochemical stability. Therefore these molecules can be easily functionalised and are capable of undergoing various transformations. These properties make these compounds versatile and useful in real life applications. There are many applications [2] (Figure 1.1.1) of these boron-rich species including catalysis with exo-metallated carboranes,[3] monocarbon carboranes in catalysis,[4] stabilisation of highly reactive cations,[5] inclusion in metal-organic frameworks,[6] radionuclide extraction [7] and as a part of molecular machines.[8] Boron containing derivatives show stability and are not harmful within the cell. Therefore these compounds can be used in various biomedical applications. A unique application of boron currently ongoing and developing is Boron-Neutron Capture Therapy.[9] The treatment is used to kill cancerous cells. This involves neutron beam irradiation of cancer cells that have been tagged by an appropriate ^{10}B rich species. BNCT exploits the great tendency of ^{10}B to capture a slow neutron due to its large neutron capture cross section. By capturing a neutron ^{10}B forms an $\{^{11}B\}$ species which subsequently undergoes nuclear fission by releasing ^{4}He (α particle) and ^{7}Li nuclei. This process also

gives 2.4 MeV of kinetic energy and weak gamma radiation (Equation 1). Since the energetic α particle travels only about one cell diameter in tissue, it is capable of killing cancerous tissue within that area by incorporating innocent ^{10}B nuclei on or within only the target cells.

$$^{10}_{5}B + ^{1}_{0}n \rightarrow \{^{11}_{5}B\} \rightarrow ^{4}_{2}He + ^{7}_{3}Li + \gamma + 2.4\ MeV \ldots\ldots \text{Equation 1}$$

A requirement of this treatment is the presence of a high percentage of ^{10}B to destroy each tumour cell. Therefore to enhance BNCT application, it is necessary to design high boron content compounds. However the development of highly boron rich compounds remains as a challenging task.

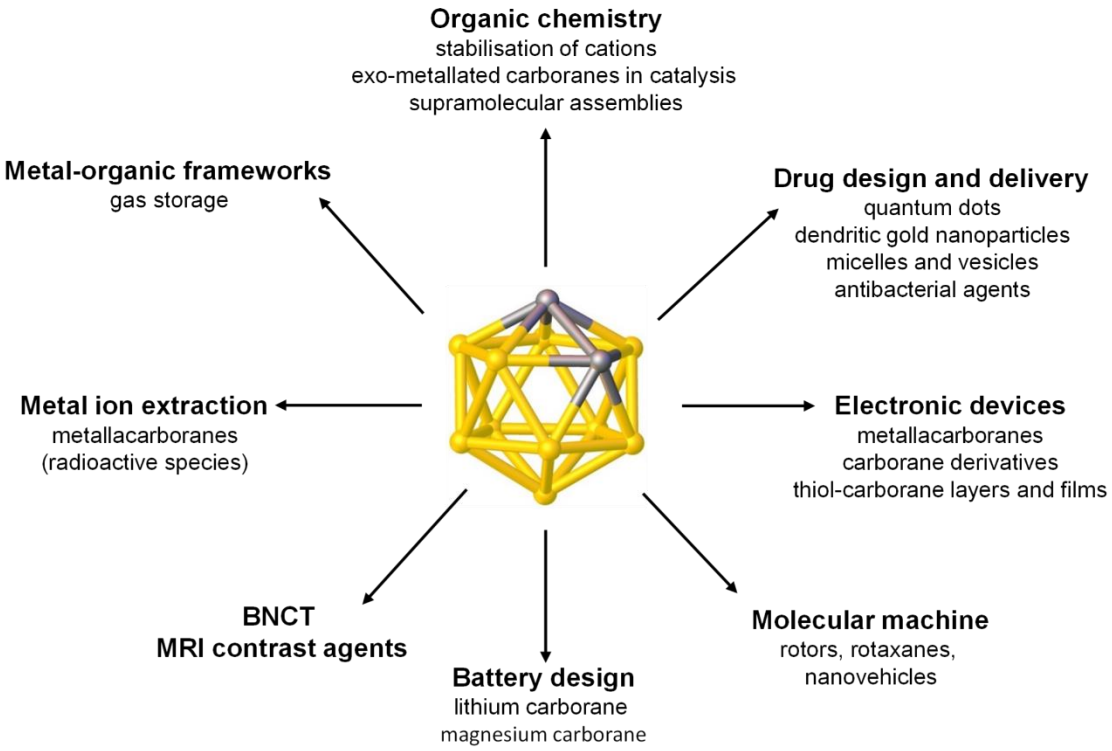

Figure 1.1.1 Applications of heteroboranes summarised pictorially.

1.2 Boranes

The simplest boron compounds are boron hydrides or boranes containing only boron and hydrogen. The very first boranes were reported by Alfred Stock in the 1930's.[10] They synthesised a series of boron hydrides which were identified by spectroscopic means only. Stock and his co-workers were able to isolate B_2H_6, B_4H_{10}, B_5H_{11}, $B_{10}H_{14}$ and other similar boranes. This ground breaking report illustrates that boron does form a series of hydrides. Subsequently boranes were classified into two distinct homologous series: B_nH_{n+4} and B_nH_{n+6}.

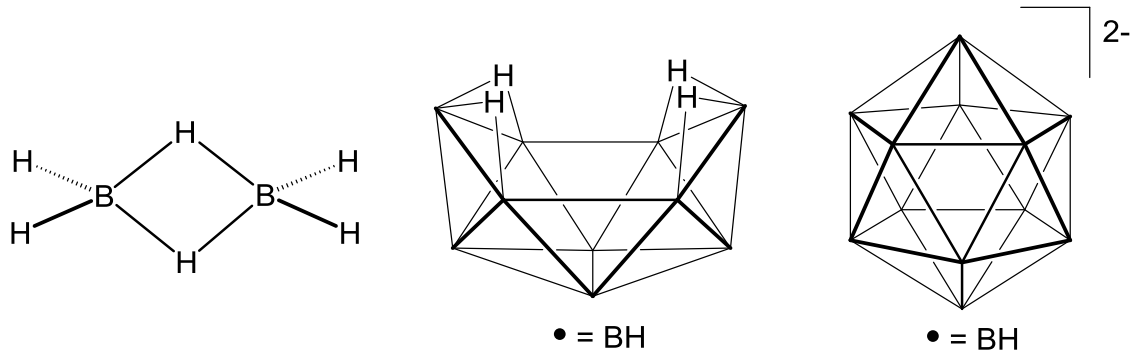

Figure 1.2.1 Structure of B_2H_6 (left), $B_{10}H_{14}$ (centre) and icosahedral $[B_{12}H_{12}]^{2-}$ (right).

Complete characterisations were not possible due to the unavailability of modern spectroscopic tools which limited understanding of bonding and connectivities of boranes. In the 1950's, the development of the single crystal *X*- ray diffraction technique assisted the understanding of the bonding in diborane, B_2H_6, by confirming the molecular structure (Figure 1.2.1, left). [11,12] Subsequently the molecular structure of decaborane, $B_{10}H_{14}$, (Figure 1.2.1, centre) was also determined crystallographically.[11,12] In the mid 1950's Longuet-Higgins and Roberts predicted theoretically the geometry of the 12-vertex borate, $[B_{12}H_{12}]^{2-}$, as an icosahedral, 20-sided polyhedron (Figure 1.2.1, right).[13b,c] Shortly afterwards, Hawthorne and Pitochelli confirmed the closed polyhedral structure of the dianionic species by isolation of the potassium salt.[14] It was found that the $[B_{12}H_{12}]^{2-}$ species is a robust material, inert toward most reagents and thermally stable even at 800 °C.

Polyhedral clusters with more than twelve vertices are called supraicosahedral. Lipscomb computed theoretically the geometries of the series of boron hydrides $[B_nH_n]^{2-}$ for n = 13-24.[15a] Following this Schleyer also calculated the energies of successive {BH} unit addition to a smaller borate with a higher level of theory.[16] A trend of increasing stability was observed from $[B_5H_5]^{2-}$ to $[B_{12}H_{12}]^{2-}$ upon successive addition of a {BH} unit. The process is also exothermic up to $[B_{12}H_{12}]^{2-}$. However the addition of a {BH} unit to icosahedral $[B_{12}H_{12}]^{2-}$ making $[B_{13}H_{13}]^{2-}$ is computed to be a highly unfavourable endothermic process. This endothermic nature continues up to $[B_{15}H_{15}]^{2-}$ upon cumulative addition of {BH} units to $[B_{12}H_{12}]^{2-}$. Therefore these borates are not viable synthetically as these are thermodynamically unstable with respect to $[B_{12}H_{12}]^{2-}$. However additional vertices added after $[B_{15}H_{15}]^{2-}$ are exothermic and these species should be accessible. Addition of four or five {BH} units to $[B_{12}H_{12}]^{2-}$ to obtain $[B_{16}H_{16}]^{2-}$ or $[B_{17}H_{17}]^{2-}$ is thermodynamically possible. The diagram (Figure 1.2.2) shows the cumulative {BH} addition energy tends to go down with respect to the addition of vertices which indicates the high stability of larger borates not yet discovered.

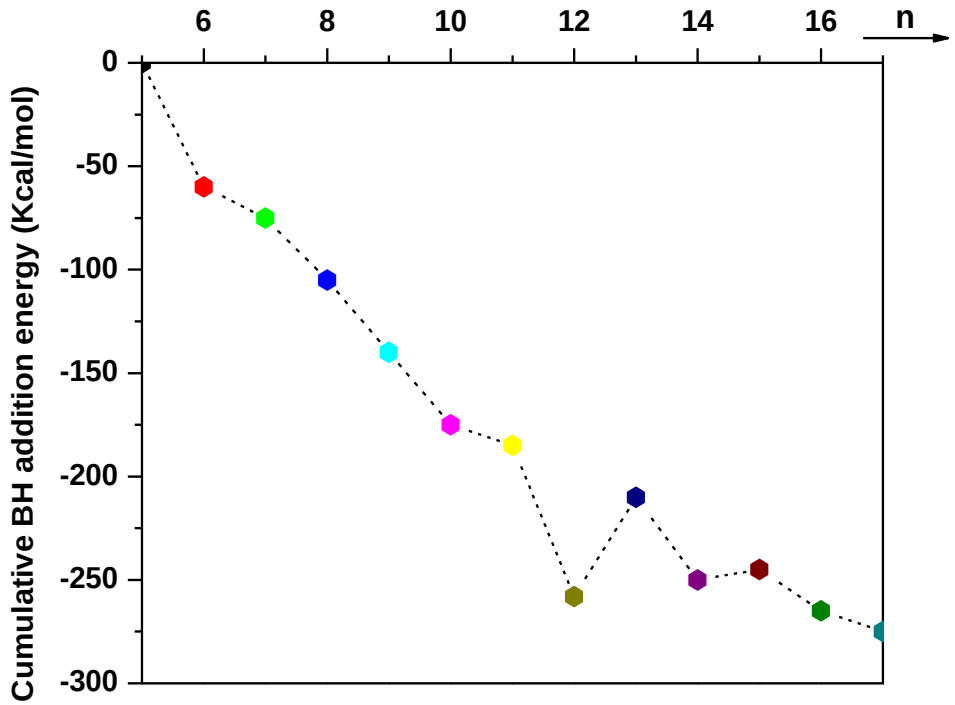

Figure 1.2.2 Plot of cumulative {BH} addition energy (kcal mol^{-1}) vs n for $[B_nH_n]^{2-}$.

1.2.1 Bonding in Boranes

Several theories have been postulated for the understanding of bonding in boranes and many attempts have been made to study these molecules computationally through modern quantitative molecular orbital techniques. The simplest borane BH_3 does not exist as a carbon-like hydride CH_4 but forms the dimer B_2H_6 due its strong Lewis acidity. In 1943 Longuet-Higgins and Bell proposed that the formation of diborane from BH_3 occurs through 3c-2e bonding.[13a] Further, the 3c-2e bonding concept was used by Lipscomb when he developed a method of combining 3c-2e and 2c-2e bonds for the understanding of the structures of boranes. The method is known as Lipscomb's *styx* rules.[15b] These rules used a combination of three nuclei B-H-B and B-B-B bonds along with two nuclei B-B and B-H bonds. However whilst the rule is applicable for smaller boranes, it is more complicated for larger boranes and fails to determine exact structures.

In 1971, Wade proposed a relationship between shape and the available number of skeletal electrons popularly known as Wade's rules [17] or Wade-Mingos rules.[18] This is less complicated than *styx* rules and easier to apply. Wade's rules or polyhedral skeletal electron pair theory (PSEPT) is based on MO theory and also applies to heteroboranes and metal cluster compounds. The method involves counting the number of skeletal electrons in the cluster to determine its 3D geometry. The cluster is broken down into fragments at each individual vertex and the number of electrons employed in cluster bonding by each gives the total number.

For a main group vertex, the electronic input to the skeletal framework (s) is given by Equation 2. For a transition metal vertex, due to different orbitals used, either Equation 3 for 18e species or Equation 4 for 16e species is followed.

$$s = v + x - 2 \ldots\ldots \text{Equation 2}$$
$$s = v + x - 12 \ldots\ldots \text{Equation 3}$$
$$s = v + x - 10 \ldots\ldots \text{Equation 4}$$

Where v = number of valence electrons of the vertex atom; x = number of electrons provided by exopolyhedral groups or atoms.

All the s values are summed to afford the total number of electrons involve in skeletal bonding and this number is then divided by two to obtain the total number of PSEPs. The number of PSEPs is directly related to the number of vertices present in the polyhedron, and the shape of the polyhedron. The geometry of the polyhedron can be determined by the following simple rules:

If there are (n+1) PSEPs the structure is closo	closed polyhedron
If there are (n+2) PSEPs the structure is nido	one vertex removed
If there are (n+3) PSEPs the structure is arachno	two adjacent vertices removed

1.3 Carboranes

Icosahedral carboranes represent the most widely utilised member among all carboranes and are commercially available. Swapping of a {BH} fragment of $[B_{12}H_{12}]^{2-}$ by an isolobal $\{CH\}^{+}$ fragment results in the mono-carborane $[CHB_{11}H_{11}]^{-}$. Further replacement of a {BH} vertex of the anion $[CHB_{11}H_{11}]^{-}$ with $\{CH\}^{+}$ gives neutral dicarborane $[C_2B_{10}H_{12}]$ retaining the same icosahedral geometry of its precursor (Figure 1.3.1). We will discuss here the chemistry of dicarborane.

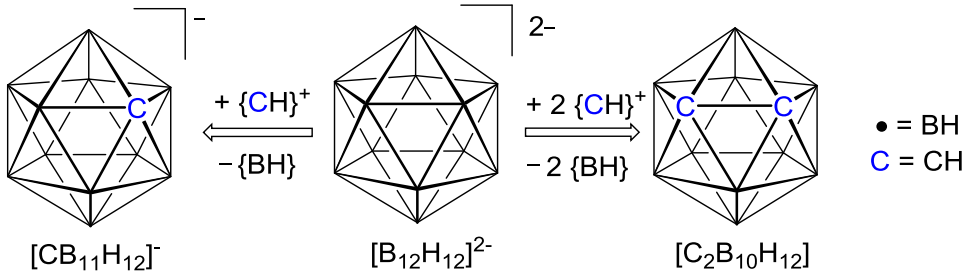

Figure 1.3.1 Conversion of borane to mono- and dicarborane.

The first dicarborane was [1,2-*closo*-$C_2B_{10}H_{12}$] or trivially *ortho*-carborane, prepared by Heying and co-workers in 1963 [19] and characterised by Bohn *et al*. in 1971.[20] The method adopted by Heying and co-workers involved the reaction of decaborane-Lewis base adducts with ethyne, and has been utilised in the synthesis of a variety of C substituted carboranes (Figure 1.3.2).[21] The reaction of *nido*-$B_{10}H_{14}$ with an electron donor ligand (L) results in an arachno $L_2B_{10}H_{12}$ complex by the displacement of two bridging hydrogen atoms and the more open arachno geometry of the complex enables an easier alkyne insertion.

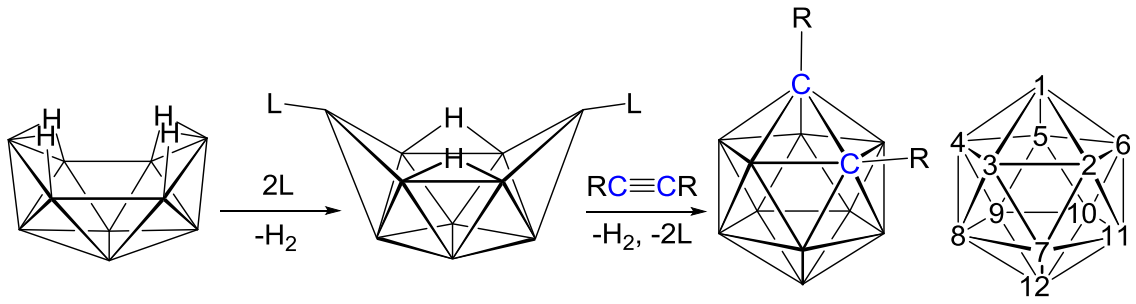

Figure 1.3.2 Carborane synthesis and 12-vertex numbering scheme (heteroatoms are given lowest possible numbers and the numbering starts at the top as shown).

1.4 Decapitation/metallation of *o*-carborane: metallacarboranes

As carbon is more electronegative than boron, the B3 and B6 atoms are more electrophilic than other B vertices and can be removed by nucleophiles. A strong base can remove one of these boron atoms producing an 11-vertex nido deboronated or decapitated carborane. This nido species can be isolated as either a neutral derivative [*nido*-$C_2B_9H_{13}$] or the mono-anion [*nido*-$C_2B_9H_{12}]^-$ [22-26] which has been structurally characterised as different salts.[27-31] Out of these $[(Me_2SO)_2H]^+$, $[(Me_2N)_3PNH_2]^+$ and $[PSH]^+$ salts [27-29] contain well defined [*nido*-7,8-$C_2B_9H_{12}]^-$ clusters (**A** or **B** in Figure 1.4.1) where all hydrogens could be identified. From the theoretical calculations of Welch *et al.* [27] the HOMO of $[C_2B_9H_{11}]^{2-}$ (**B**-H^+**)** is localised on B(10) (41%), B(9) (13%) and B(11) (13%) vertices. The constituents from these atoms are *sp* hybrids pointing outwards from the open face (**C** in Figure 1.4.1). The anticipated site of protonation of [*nido*-7,8-$C_2B_9H_{11}]^{2-}$ is therefore above B(10) giving an endo-H. However a neutron diffraction study by Hughes *et al.* [29] reveals that there is an asymmetric B–H–B bridging hydrogen in the $[PSH]^+$ salt of [*nido*-7,8-$C_2B_9H_{12}]^-$.

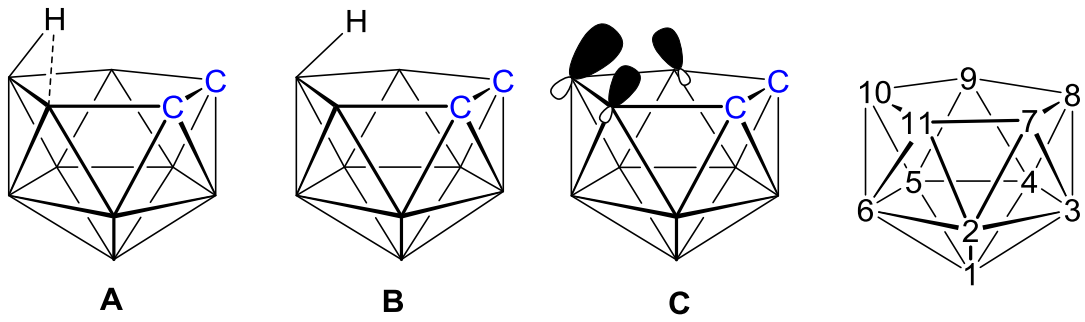

Figure 1.4.1 Geometries of [*nido*-7,8-$C_2B_9H_{12}]^-$ species (**A**, **B**), the HOMO of $[C_2B_9H_{11}]^{2-}$ (**C**) and numbering scheme.

The endo/bridging proton of the mono-anion [*nido*-$C_2B_9H_{12}]^-$ can be easily removed using a strong base resulting in a dicarbollide dianion, [*nido*-7,8-$C_2B_9H_{11}]^{2-}$, which is an important precursors to many *closo* icosahedral metallacarboranes in which the twelfth vertex is occupied by a metal atom. Recapitation of [*nido*-7,8-$C_2B_9H_{11}]^{2-}$ with a {ML} (L = ligand) fragment results in metallcarborane species and with a {BX} (X = halogen/alkyl/aryl) fragment affords carborane derivatives.

In 1965 the first metallcarboranes were synthesised by Hawthorne *et al.*, [32a] and showed the potential for carborane anions to behave as ligands in a similar way to the cyclopentadienide anion. The open pentagonal face of [*nido*-7,8-$C_2B_9H_{11}]^{2-}$ contains five FMOs bearing six electrons similar to that of the $[Cp]^-$ anion. In fact, they are isolobal in nature *i.e.* the FMOs of these two fragments contain same number of electrons and are of similar energy and symmetry. By reacting two equivalents of [*nido*-7,8-$C_2B_9H_{11}]^{2-}$ with $FeCl_2$, a process analogous to the preparation of a metallocene complex, ferrocene, the first metallcarborane sandwich complex [3,3-Fe-(1,2-*closo*-$C_2B_9H_{11})_2]^{2-}$ was generated. The use of the dicarbollide dianion as a ligand actually adds to the overall stability of these compounds compared to that of analogous metallocenes. The FMOs of dicarbollide are more favourably oriented to bind to a metal as they point inwards, due to the inclination of the exo hydrogen atoms, instead of them all being parallel to each other, giving greater overlap with metal orbitals (Figure 1.4.2). Further metallation of [*nido*-7,8-$C_2B_9H_{11}]^{2-}$ with a $\{CpFe\}^{2+}$ fragment affords a mixed sandwich species (Figure 1.4.3).[32b] The wide variety of fragments isolobal to {BH} has resulted in thousands of icosahedral metallcarboranes.[33]

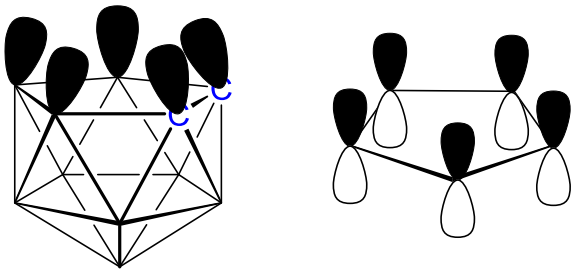

Figure 1.4.2 FMOs orientation of dicarbollide dianion and cyclopentadienide anion.

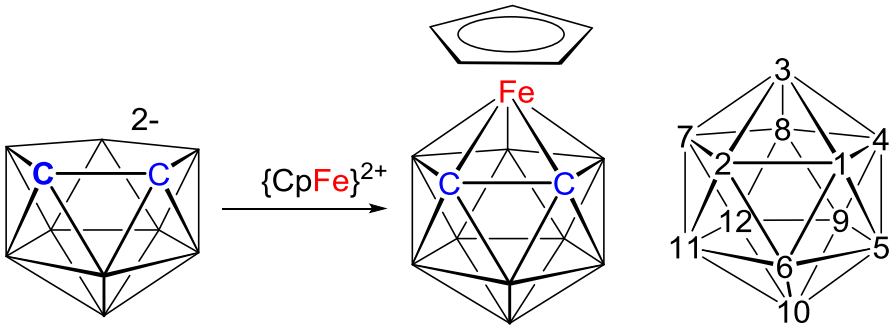

Figure 1.4.3 Formation of [3-Cp-3,1,2-*closo*-$FeC_2B_9H_{11}$] and numbering scheme (left) (the numbering is similar to a 1,2-*closo*-$C_2B_{10}H_{12}$ and carbon is usually given precedence over metals).

1.5 Isomerisation in icosahedral heteroboranes

[1,2-*closo*-$C_2B_{10}H_{12}$] (*ortho*-carborane) is among the most thermally stable known covalently bonded molecules. However, upon heating above 425 °C it produces the 1,7-isomer [1,7-*closo*-$C_2B_{10}H_{12}$] (*meta*-carborane) which is even more robust and thermodynamically stable. At even higher temperature, 600 °C, it rearranges to [1,12-*closo*-$C_2B_{10}H_{12}$], *para*-carborane (Figure 1.5.1).[34,35] Although, at this high temperature, there is some decomposition, carborane survives even at 700 °C. The rationale behind this isomerisation is the electrostatic repulsion between the partially charged carbon nuclei. In *para*-carborane the separation of carbon atoms is greatest, hence it is the most thermodynamically stable isomer. The reverse isomerisation is also observed *via* 2e reductions and oxidations. A 2e reduction of the 1,12-isomer followed by oxidation results in the 1,7 isomer being formed.[36a] Likewise, the same redox process transforms the 1,7-isomer back to the 1,2-isomer (Figure 1.5.1).[36b]

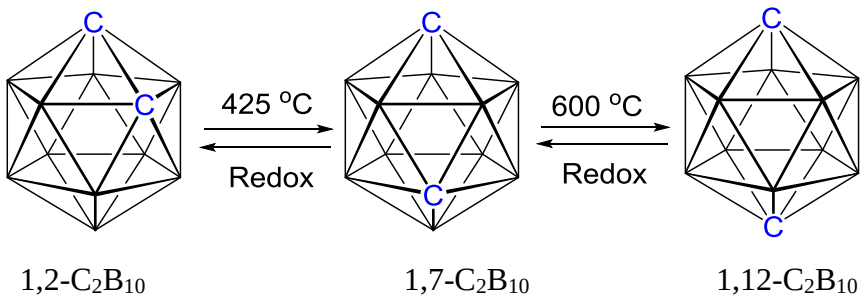

Figure 1.5.1 Thermal and electrochemical rearrangement in carboranes.

The elucidation of the mechanistic details of the isomerisation process *i.e*. *o*-carborane and its thermal isomerisation to *m*- and *p*-carborane has been targeted by many theoretical chemists and experimentalists. Although several theories have been proposed, the actual mechanism is not yet proved. The most accepted mechanisms for these isomerisation steps are DSD [37] or TFR [38] rearrangements. DSD comprises the breaking of a common edge between two triangular faces to create a single square face followed by the creation of two different triangular faces with a common edge perpendicular to the original broken one (Figure 1.5.2, left). DSD mechanisms requires minimum bond-stretching and are of low activation energy.

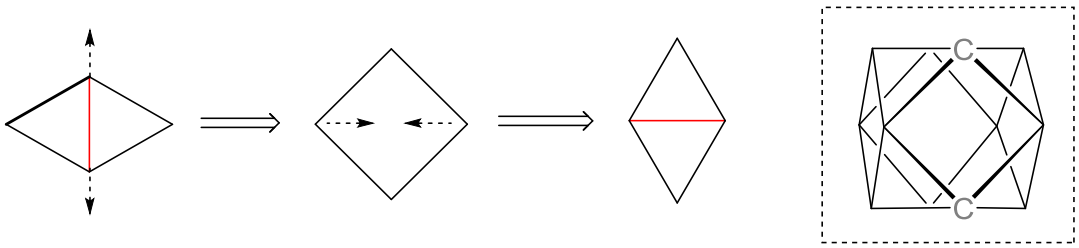

Figure 1.5.2 DSD mechanism (left) and cuboctahedral intermediate (right).

The DSD mechanism was first used by Lipscomb for the rationalisation of the isomerisation. He proposed a cuboctahedral intermediate which occurs during the DSD process (Figure 1.5.2, right). The DSD mechanism was therefore proposed to account for the 1,2- to 1,7-$C_2B_{10}H_{12}$ isomerisation. However, the activation energy of the cuboctahedral intermediate was suggested by Wales to be too high and thus not accessible for the isomerisation process.[39] Welch and co-workers [40] isolated a derivative of a non-icosahedral intermediate which supports Wales' suggestions.

Another isomerisation mechanism, TFR, involves the 120° rotation of a single triangular 1-2-3 face (Figure 1.5.3). The 1,2-$C_2B_{10}H_{12}$ to 1,7- isomerisation followed by further rearrangement to the 1,12- species can be explained by sequential TFR processes. Theoretical studies reveal a low energy TFR 1,2- to 1,7-$C_2B_{10}H_{12}$ path.[41] One TFR is equivalent to three DSD steps and so in reality DSD and TFR are effectively the same process.

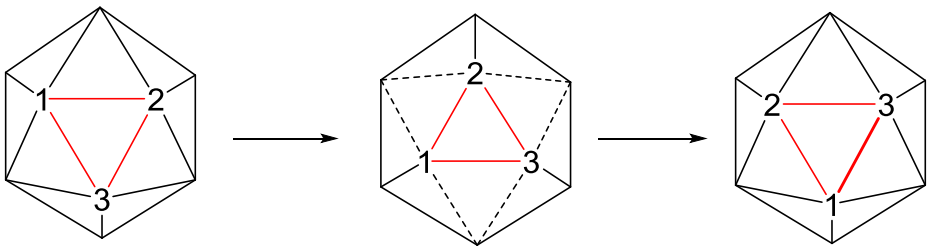

Figure 1.5.3 TFR mechanism.

The isomerisation of icosahedral metallacarborane cages is of special interest in 12-vertex clusters because of their close relationship to the extensively studied $C_2B_{10}H_{12}$ rearrangements. Whereas only three isomers are possible in the latter system, there are nine possible MC_2B_9 icosahedra. The metallation of C-substituted carboranes has been

studied to understand the isomerisation behaviour. Among many factors, steric effects are important in the isomerisation of metallacarboranes. The isomerisation of [3,1,2-$(Me_2PhP)_2Pt(PhC_2B_9H_{10})$] on mild heating affords two carbon-separated isomers (**D**, **E** in Figure 1.5.4).[42] Also remarkable is the fact that the reaction of [*nido*-7,8-$Ph_2C_2B_9H_9]^{2-}$ with $\{Pt(PMe_2Ph)_2\}^{2+}$ at room temperature gives as the only product [2,1,8-$(Me_2PhP)_2Pt(Ph_2C_2B_9H_9)$] indicating that steric crowding can cause rearrangement even without heating.[42]

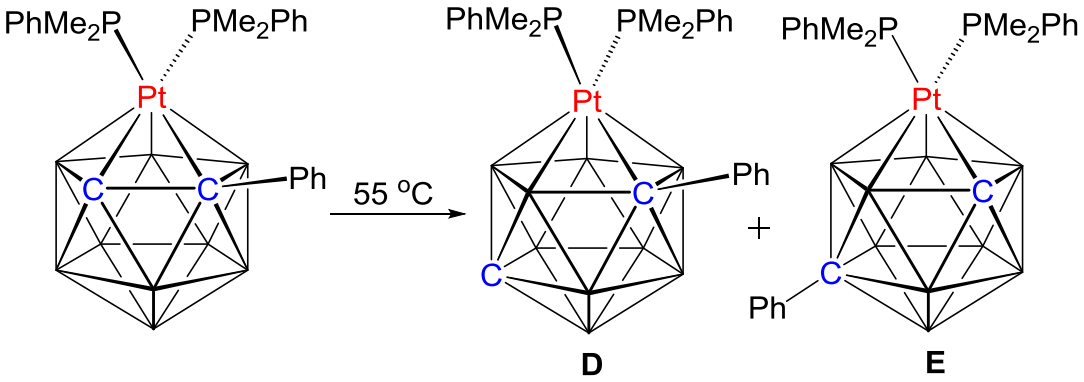

Figure 1.5.4 Isomerisation of [3,1,2-$(Me_2PhP)_2Pt(PhC_2B_9H_{10})$] species.

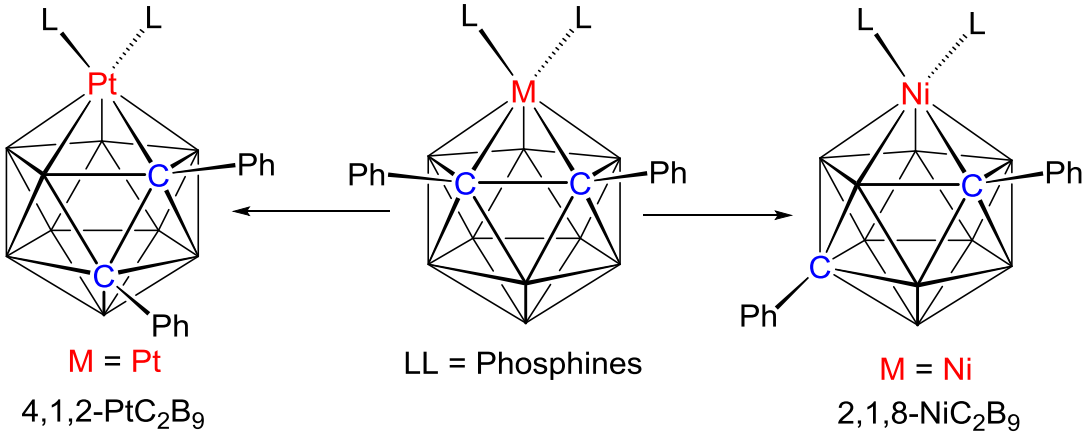

Figure 1.5.5 Platination and nickelation of the [7,8-Ph_2-7,8-*nido*-$C_2B_9H_9]^{2-}$ species.

Several studies on the platination and nickelation of [7,8-*nido*-$Ph_2C_2B_9H_9]^{2-}$ have been carried out.[43] Platination of [7,8-*nido*-$Ph_2C_2B_9H_9]^{2-}$ with a bulky $\{PtLL\}^{2+}$ (LL = phosphines) fragment leads to isomerisation to 2,1,8-MC_2B_9 products (1,2→1,7 C atom isomerisation) at or near room temperature.[43c,43e,43f] In contrast, the addition of bulky $\{NiLL\}^{2+}$ fragments (LL = typically phosphines) yields 4,1,2-NiC_2B_9 products arising

from 1,2→1,2 C atom isomerisation [43d,43e,43a] though occasionally 2,1,8-NiC_2B_9 species are also formed [43d,43e] (Figure 1.5.5). The products of these isomerisation are most easily explained by either one or two triangle face rotation steps starting from the crowded 3,1,2-MC_2B_9 transient. Isomerisation studies of the species containing substituent tagged boron vertices have also been considered.[43b-f]

Some insight into the mechanism of icosahedral cage rearrangement is provided by a study by Welch and co-workers on molybdacarboranes [44] resulting from the reaction of the $[Ph_2C_2B_9H_9]^{2-}$ dianion with the $\{(\eta-C_7H_7)Mo\}^{2+}$ fragment (Figure 1.5.6). The presumed unstable species formed initially (**F**) isomerises at room temperature to five new $(\eta-C_7H_7)Mo(Ph_2C_2B_9H_9)$ isomers. **G** has a pseudocloso cage geometry and is analogous to a RuC_2B_9 cluster.[45] This species transforms on standing in solution to a red non-icosahedral isomer (**H**), which in turn rearranges to the green icosahedron 2,1,8-$(\eta-C_7H_7)Mo(Ph_2C_2B_9H_9)$ (**I**). Interestingly the geometry of **H** is same as that calculated by Wales [39] as an intermediate in the isomerisation of 1,2- to 1,7-$C_2B_{10}H_{12}$. The non-isolable **J** and $(\eta-C_7H_7)Mo(Ph_2C_2B_9H_9)$ (**K**) clearly form *via* a different route in which the latter is formed by rearrangement of less stable **J**, suggested to have a non-icosahedral structure is similar to **H** (Figure 1.5.6**)**.[44]

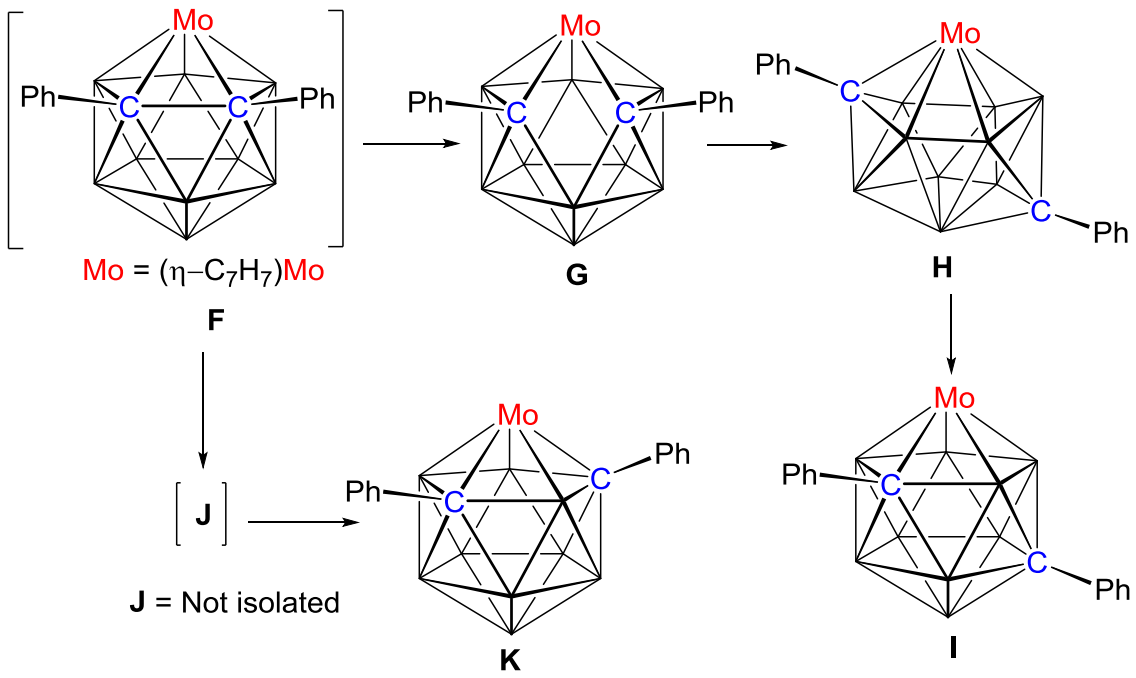

Figure 1.5.6 Alternative pathways for the isomerisation of 3,1,2-$(\eta-C_7H_7)Mo(Ph_2C_2B_9H_9)$.

1.6 Supraicosahedal metallacarboranes

An emerging area in (hetero)borane chemistry is the development of supraicosahedral heteroboranes where there are more than twelve vertices present in the cluster. These compounds are prepared by a method popularly known as polyhedral expansion. The first example of a 13-vertex metallcarborane was reported by Hawthorne by following the polyhedral expansion method (Figure 1.6.1). Two electron reduction of [1,2-*closo*-$C_2B_{10}H_{12}$] gives an open face [7,9-*nido*-$C_2B_{10}H_{12}]^{2-}$ species where the two carbon atoms are separated by a boron atom. Subsequent addition of a $\{CoCp\}^+$ fragment followed by oxidation results in the 13-vertex cobaltacarborane, [4-Cp-4,1,6-*closo*-$CoC_2B_{10}H_{12}$].[46] Additionally on thermolysis many 4,1,6-MC_2B_{10} compounds can be converted to the increasingly more thermodynamically stable analogous 4,1,8- and 4,1,12-isomers.[47]

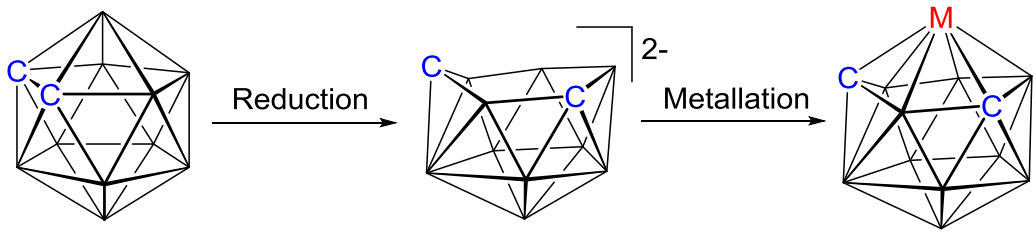

Figure 1.6.1 Reduction/metallation of 1,2-$C_2B_{10}H_{12}$.

The polyhedral expansion can be taken a step further to produce 14-vertex structures with a bicapped hexagonal antiprismatic geometry. The first examples of 14-vertex metallacarboranes were cobaltacarboranes synthesised by Hawthorne [48] in 1974 (Figure 1.6.2**)**. Reduction followed by metallation of the 13-vertex 4,1,12- and 4,1,8-CoC_2B_{10} precursors yielded [1,14-Cp_2-1,14,2,10-*closo*-$Co_2C_2B_{10}H_{12}$] (Figure 1.6.2) and [1,14-Cp_2-1,14,2,9-*closo*-$Co_2C_2B_{10}H_{12}$] (Figure 1.6.3) respectively.[49] Similarly 1,14,2,10-$MRuC_2B_{10}$ homo- and heterobimetallic compounds were prepared by Welch using the polyhedral expansion method.[50] Recently Welch also isolated asymmetric 1,8/13,2,x-$M_2C_2B_{10}$ 14-vertex metallacarboranes by the direct electrophilic insertion reaction.[51] There are limited examples of higher supraicosahedral heteroboranes (15-vertex, 16-vertex).[52]

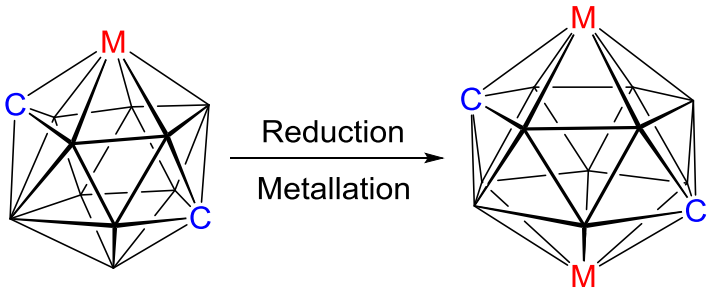

Figure 1.6.2 Reduction/metallation of 4,1,12-MC_2B_{10} isomer.

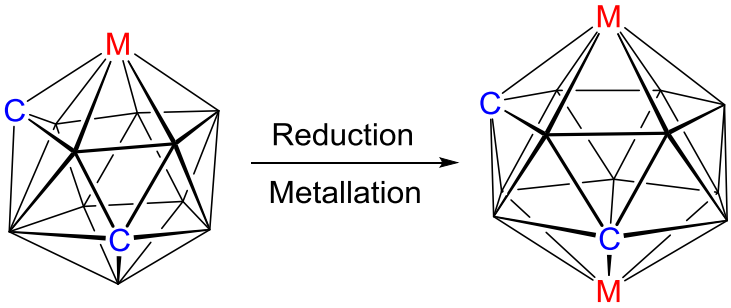

Figure 1.6.3 Reduction/metallation of 4,1,8-MC_2B_{10} isomer.

1.7 Bis(carboranes)

One of the most active areas of heteroborane chemistry is that of metallacarboranes, and as noted above these molecules are generally prepared from *closo*-carboranes either by polyhedral subrogation (dec/met) or by polyhedral expansion (red/met). Single cage carborane chemistry is well developed as summarised in previous sections, however the analogous bis(carborane) chemistry is not well developed. This is possibly due to the previous lack of a high yielding synthetic route to the starting precursor bis(carborane). Theoretically many isomers of bis(carborane) are possible *via* B-B, B-C or C-C linking. Practically there are three major bis(carboranes): (a) [1-(1′-1′,2′-*closo*-$C_2B_{10}H_{11}$)-1,2-*closo*-$C_2B_{10}H_{11}$)], trivially 1,1′-bis(*o*-carborane) (two *o*-carborane units are linked with a C-C bond at the 1,1′ positions); (b) [1-(1′-1′,7′-*closo*-$C_2B_{10}H_{11}$)-1,7-*closo*-$C_2B_{10}H_{11}$)], trivially 1,1′-bis(*m*-carborane) (two *m*-carborane units are linked through a C-C linkage at the 1,1′ positions); (c) [1-(1′-1′,12′-*closo*-$C_2B_{10}H_{11}$)-1,12-*closo*-$C_2B_{10}H_{11}$)], trivially 1,1′-bis(*p*-carborane) (two *p*-carborane cages are joint through a C-C bond at 1,1′ positions) (Figure 1.7.1). Here the chemistry of 1,1′-bis(*o*-carborane) will be discussed.

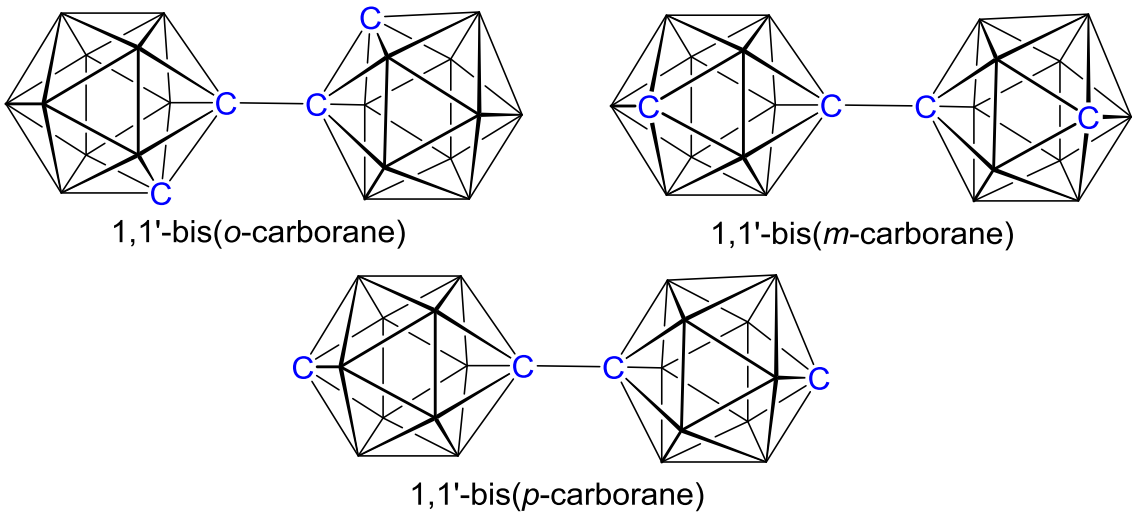

Figure 1.7.1 Major isomers of bis(carborane).

In 1964 Hawthorne *et al*. first reported the synthesis of 1,1′-bis(*o*-carborane) by adopting the same protocol for the synthesis of *ortho*-carborane, in low yield (overall 21%) by reacting bis(acetonitrile)decaborane, $B_{10}H_{12}{\cdot}2CH_3CN$ with diacetylene, HC≡C–C≡CH at reflux temperature.[53] After a few years, the same group developed an improved synthesis of 1,1′-bis(*o*-carborane) by replacing $B_{10}H_{12}{\cdot}2CH_3CN$ with $B_{10}H_{12}{\cdot}2SEt_2$ and lowering

the temperature to -25 °C in order to reduce volatilisation of diacetylene.[54] Later on, using $CuCl_2$, Hawthorne coupled two dilithiated *o*-carborane units to produce a mixture of 1,1′-bis(*o*-carborane), 1,3′-bis(*o*-carborane) and 1,4′-bis(*o*-carborane) in 31% overall yield with respect to dilithiated *o*-carborane as starting material.[55] Hawthorne then repeated the same reaction except that monolithiated *o*-carborane was used as the starting material instead of dilithiated *o*-carborane and the yield was improved to 45%.[55] However, in 2008, Xie and co-workers developed a new method to synthesise 1,1′-bis(*o*-carborane) in high yield (83%) (Figure 1.7.2) by using CuCl instead of $CuCl_2$ in order to avoid C-B and B-B coupled isomeric products.[56] The coupling reaction was carried out in toluene.

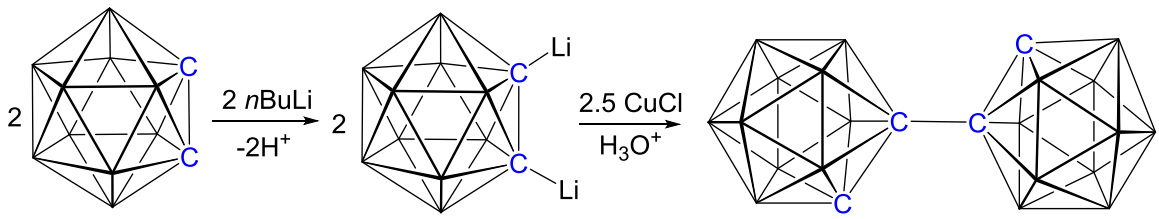

Figure 1.7.2. Synthesis of bis(*o*-carborane) by Cu(I) coupling.

1.7.1 Recent chemistry of 1,1′-bis(*o*-carborane)

The efficient synthesis of 1,1′-bis(*o*-carborane) gives the opportunity to explore new chemistry of this species. Chelated bis(carborane) transition metal complexes in the form $[M(C_2B_{10}H_{10})_2]_2^{n-}$ (where n = 1, 2 and M = Cu, Ni and Co) were first reported by Hawthorne *et al*.[57] Recently bis(carborane) as a κ^2 co-ligand has been further developed by Welch *et al*.[58] The salt elimination reaction of dilithiated 1,1′-bis(*o*-carborane) with $[(PP)NiCl_2]$ (PP = dmpe, dppe) afforded chelated complexes where doubly-deprotonated 1,1′-bis(*o*-carborane) bonds as a κ^2 co-ligand to a Ni^{II} centre (Figure 1.7.1.1). Further similar derivatives were prepared by Spokoyny *et al*. by following the same procedure using the fragments $\{M(dppe)\}^{2+}$ (M = Ni, Pd, Pt) and $\{Pt(dtb\text{-}bpy)\}^{2+}$ (dtb-bpy = 4,4′-di-*t*butyl-2,2′-bipyridine) (Figure 1.7.1.1).[59] Additionally photophysical properties of these derivatives have been studied. The results shown that the dianionic bis(carborane) ligand is photophysically inactive and also prevents intermolecular interactions by creating sufficient steric crowding which stops luminescence quenching. These properties are remarkable and potentially these materials could be used in OLED devices.

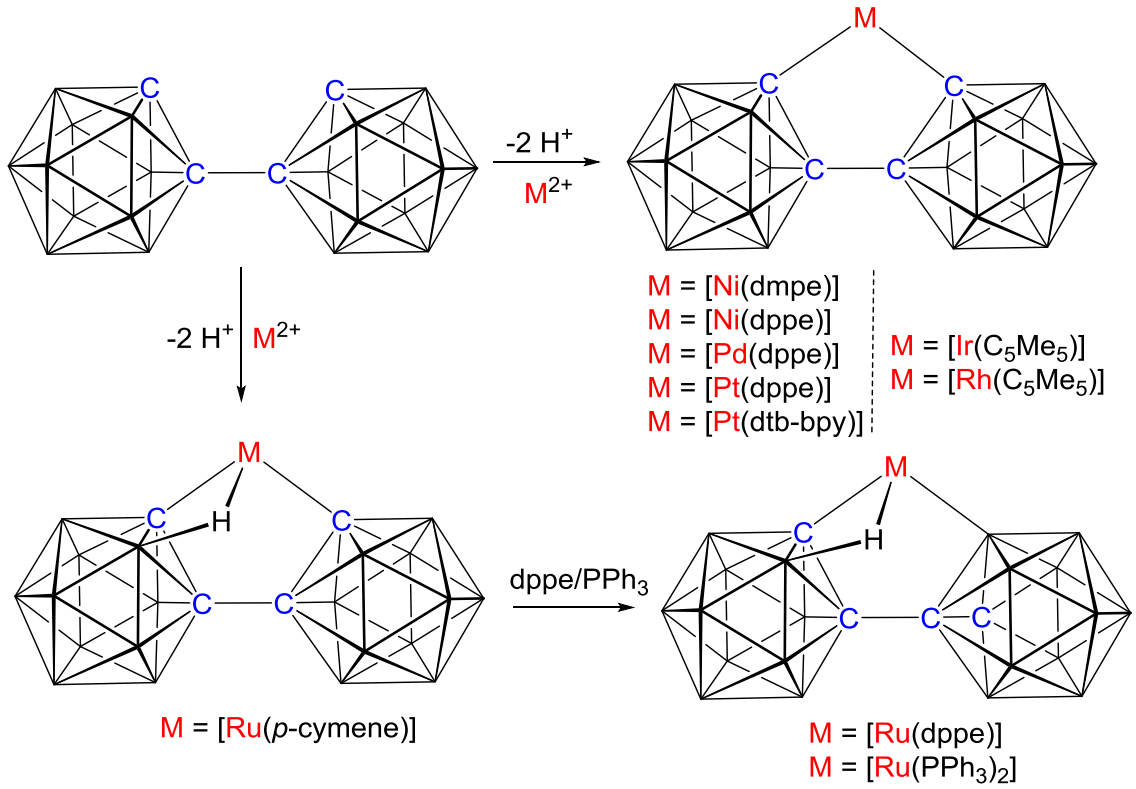

Figure 1.7.1.1 Recent chelation chemistry of 1,1′-bis(*o*-carborane).

Jin and co-workers reported 16e "pseudo-aromatic" bis(carborane) iridium and rhodium complexes with no B-H→M (M = Ir, Rh) agostic interaction (Figure 1.7.1.1).[60] In contrast Welch *et al*. prepared 18e ruthenium derivative where the Ru centre benefits from a B-H→Ru agostic interaction.[61] Here the bis(carborane) unit shows flexible bonding which can be tuned by reaction with an additional ligand *e.g*. the $X_2(C,C')L$ ligating mode in the cymene complex changes to $X_2(C,B')L$ on displacement of the *p*-cymene with dppe or PPh_3 (two equivalents) (Figure 1.7.1.1).

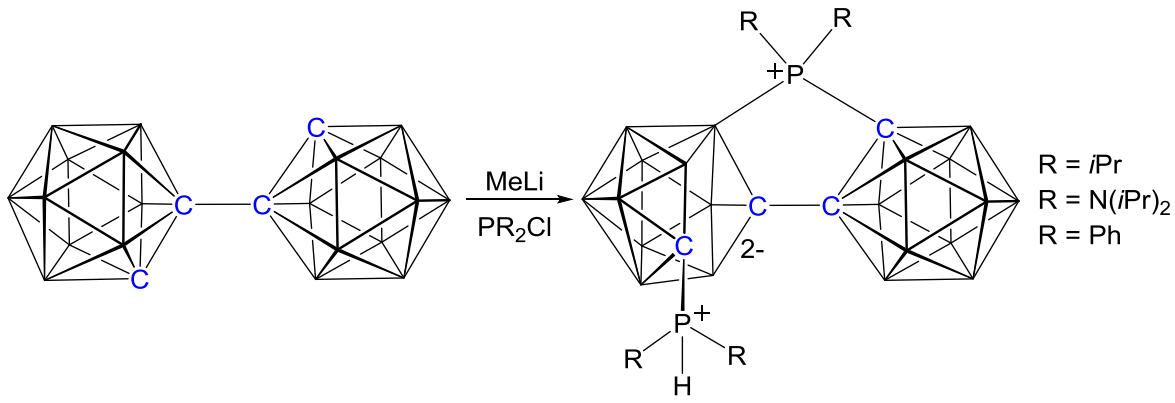

Figure 1.7.1.2 Synthesis of *closo*-C_2B_{10}/*nido*-C_2B_{10} biscarborane derivatives.

Very recently Peryshkov *et al*. reported 12-vertex-*closo*-C_2B_{10}/12-vertex-*nido*-C_2B_{10} biscarborane derivatives through regioselective metal-free B-H activation by a sterically hindered P^{III} centre.[62] The salt elimination reaction of dilithiated bis(carborane) with bulky R_2PCl (R = alkyl/ aryl) afforded a zwitterionic cluster containing one *closo*-C_2B_{10} and one *nido*-C_2B_{10} cage (Figure 1.7.1.2).

1.7.2 Reduction/metallation of 1,1′-bis(*o*-carborane)

The supraicosahedral metallacarborane chemistry of 1,1′-bis(*o*-carborane) has not been much explored. Hawthorne first isolated 2e and 4e reduced species of bis(*o*-carborane).[63] In solution, $[PPh_3Me]^+$ and $[(15\text{-crown-}5)_3Na_2]^{2+}$ salts of the 2e reduced species are identical, whilst in the solid state the anion of the $[PPh_3Me]^+$ salt has two partially-open 4-atom CBCB faces [64] and the anion of the $[(15\text{-crown-}5)_3Na_2]^{2+}$ salt has one 4-atom CBCB face which is partially-open and one 5-atom CBCBB face which is rather more open.[63] However reduction/metallation chemistry of bis(carborane) has not been explored until 2010.

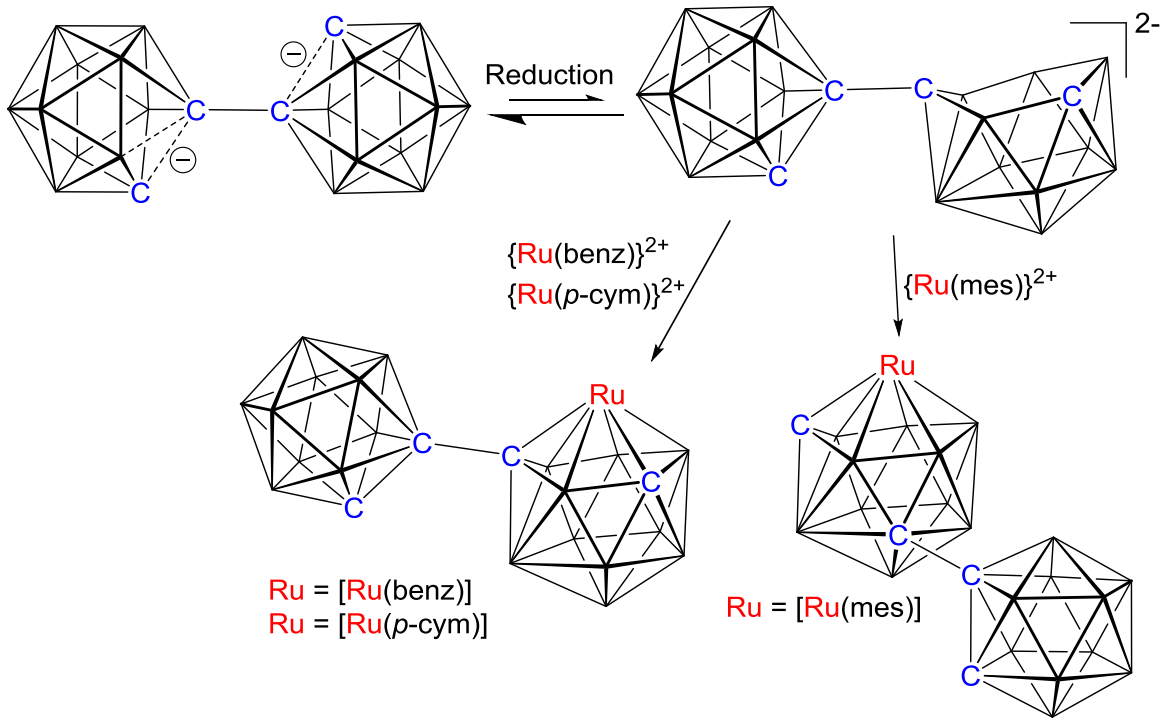

Figure 1.7.2.1 Synthesis of 4,1,6-RuC_2B_{10}-1′,2′-C_2B_{10} and 4,1,8-RuC_2B_{10}-1′,2′-C_2B_{10}.

Stoichiometric 2e reduction and metallation of 1,1′-bis(*o*-carborane) was investigated by Welch *et al*. who synthesised the first examples of 14-vertex metallacarborane/12- vertex carborane species *via* a direct electrophilic insertion reaction.[65] Stoichiometric reduction of bis(carborane) using 2e affords [7-(1′-1′,2′-*closo*-$C_2B_{10}H_{11}$)-7,9-*nido*-$C_2B_{10}H_{11}]^{2-}$ in equilibrium with a dianion which has a formal negative charge on each cage, as shown in Figure 1.7.2.1. Then metallation of the 7,9-nido dianion with a suitable metal fragment such as $\{Ru(arene)\}^{2+}$ results in 13-vertex ruthenacarborane/12-vertex carborane species. Metallation with $\{Ru(\eta\text{-benz})\}^{2+}$ and $\{Ru(\eta\text{-}p\text{-cym})\}^{2+}$ fragments gives [1-(1′-1′,2′-*closo*-$C_2B_{10}H_{11}$)-4-(η-benz)-4,1,6-*closo*-$RuC_2B_{10}H_{11}$] and [1-(1′-1′,2′-*closo*-$C_2B_{10}H_{11}$)-4-(η-*p*-cym)-4,1,6-*closo*-$RuC_2B_{10}H_{11}$] respectively (Figure 1.7.2.1), whereas metallation with $\{Ru(\eta\text{-mes})\}^{2+}$ gives [8-(1′-1′,2′-*closo*-$C_2B_{10}H_{11}$)-4-(η-mes)-4,1,8-*closo*-$RuC_2B_{10}H_{11}$] where the 13-vertex ruthenacarborane is isomerised to a 4,1,8-RuC_2B_{10} architecture and the carborane substituent has moved to the degree 5 atom C8. Further stoichiometric reduction of [8-(1′-1′,2′-*closo*-$C_2B_{10}H_{11}$)-4-(η-mes)-4,1,8-*closo*-$RuC_2B_{10}H_{11}$] using 2e followed by metallation with $\{Ru(arene)\}^{2+}$ fragments results in 14-vertex $Ru_2C_2B_{10}$/12-vertex C_2B_{10} species by direct electrophilic insertion and minor 13-vertex $Ru_2C_2B_9$/12-vertex C_2B_{10} species (Figure 1.7.2.2).[65]

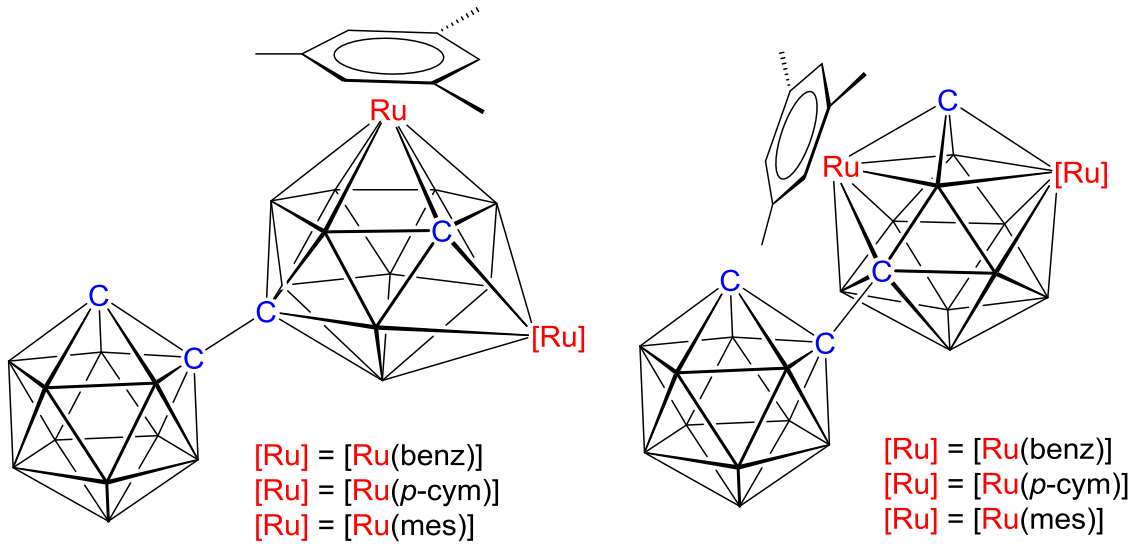

Figure 1.7.2.2 1,13,2,9-RuC_2B_{10}-1′,2′-C_2B_{10} (left) and 1,13,2,10-RuC_2B_{10}-1′,2′-C_2B_{10} isomers (right).

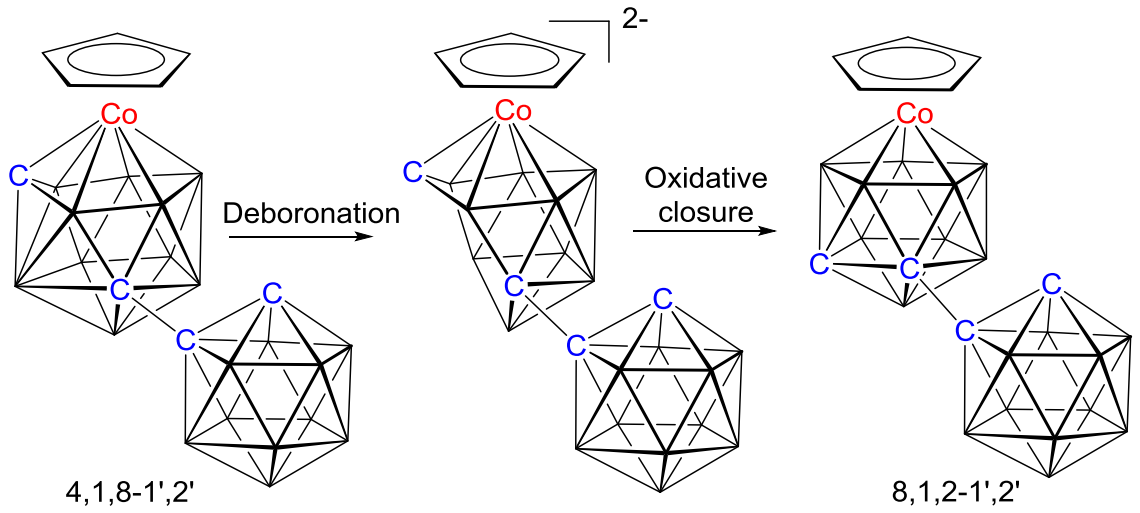

Figure 1.7.2.3 Formation of a 8,1,2-CoC_2B_9-1′,2′-C_2B_9 isomer.

Again using a 2e reduction/metallation strategy, a rare example of a 8,1,2-*closo*-MC_2B_9 isomeric form of an icosahedral metallacarborane was derived from 1,1′-bis(*o*-carborane).[66] A trace amount of a 8,1,2-CoC_2B_9-1′,2′-C_2B_9 species was isolated during the 2e reduction and metallation of bis(*ortho*-carborane). The precursor of the 8,1,2-CoC_2B_9-1′,2′-C_2B_9 species is the corresponding 13-vertex/12-vertex 4,1,8-CoC_2B_9-1′,2′-C_2B_9 compound. In 4,1,8-CoC_2B_9-1′,2′-C_2B_9 species the unique degree-6 boron atom B5 is susceptible to deboronation in the presence of a suitable nucleophile. The deboronation of 4,1,8-1′,2′, removal of {B5H} affords the corresponding *nido*-derivative which *in situ* undergoes oxidative ring closure to yield a 8,1,2-CoC_2B_9-1′,2′-C_2B_9 product (Figure 1.7.2.3).

The excess reduction and metallation chemistry of a bis(carborane) was explored by Welch *et al*. in 2010. The reduction of 1,1′-bis(*o*-carborane) with an excess of Li in degassed THF followed by metallation with [Ru(*p*-cym)Cl_2]$_2$ interestingly affords an unexpected compound.[67] Instead of each cage being capped by one metal, an exotic "flyover" type complex was produced as illustrated in Figure 1.7.2.4. The most interesting feature of this complex is that its formation involves the breaking of an aromatic C-C bond at room temperature. The reduction of 1,1′-bis(*o*-carborane) with excess lithium in presence of a catalytic amount of naphthalene followed by metallation with NaCp/$CoCl_2$ has shown that the double polyhedral expansion of 1,1′-bis(*o*-carborane) is possible in the same way as for mono-carborane. This yielded the first supraicosahedral bis(heteroborane), afforded as a mixture of diastereoisomers.[68] This will be discussed in

detail in chapter 4. Very recently, Xie *et al*. have explored reduction/metallation of a tethered bis(carborane) derivative. Excess reduction of C,C′ linked bis(carborane) followed by metallation with $[Ru(p\text{-cym})Cl_2]_2$ yields polyhedral expansion, triple cage B–H oxidative addition and cage carbon extrusion products (Figure 1.7.2.5).[69]

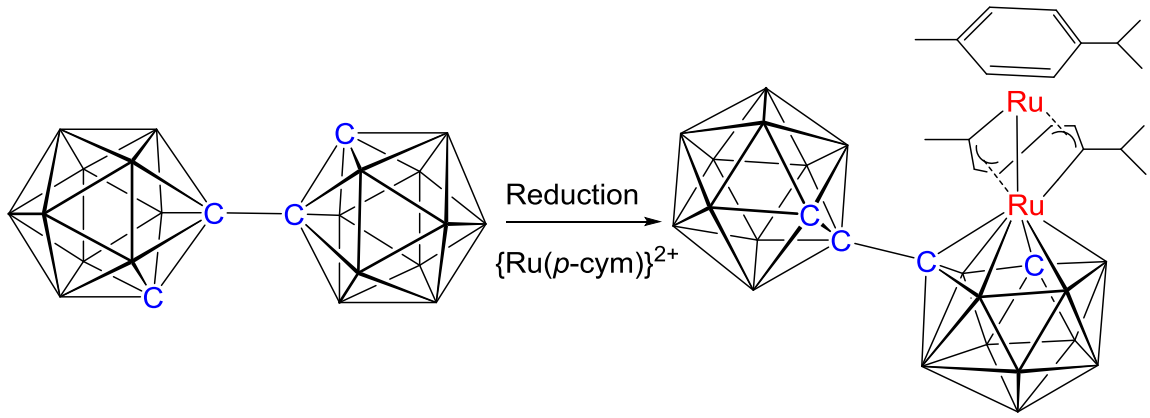

Figure 1.7.2.4 Formation of a fly-over complex.

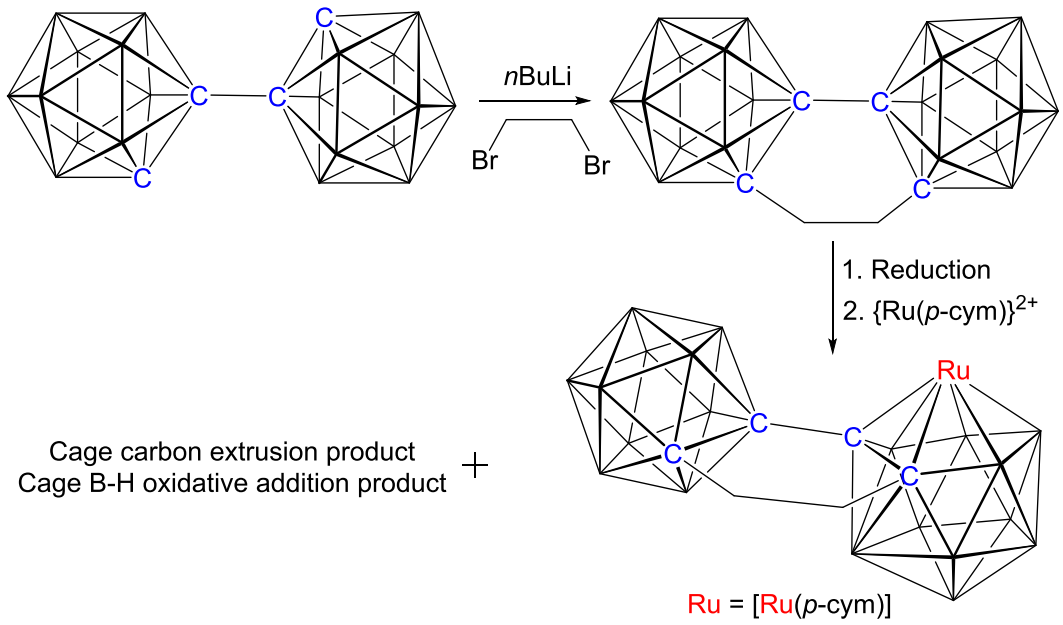

Figure 1.7.2.5 Reduction/metallation of C,C′-tethered bis(carborane).

1.8 VCD and BHD methods for carboranes and metallacarboranes

An important aspect of the chemistry of carboranes and metallacarboranes is determination of C and B atoms unambiguously in the crystallographically determined structure. The distinguishing of C and B vertices in the structures is not trivial since C and B have similar *X*-ray scattering powers as a simple consequence of their period adjacency in the Periodic Table. The two conventional approaches (low U_{eq} value for C and shorter cage connectivities) are not always reliable in distinguishing C and B atoms. Welch *et al*. described the *Vertex-Centroid Distance* (VCD) *Method* [70] and the *Boron-H Distance* (BHD) *Method* [51] to resolve this problem. The atomic radius of C is smaller than that of B due to a larger effective nuclear charge.[71] Therefore the distances between topologically-equivalent vertices and the polyhedral centroid will be shorter when the vertex is occupied by a C atom compared to a B atom. The distinctiveness of the vertex can be determined by measuring and comparing appropriate VCDs within the cage. In the BHD method we examine B-H distances and determine the C atoms as having the shortest B-H distances.

For the identification of the correct positions of the cage C atoms in the crystallographically-determined structures we use these methods if the C atoms do not carry exo-polyhedral substituents other than H. Before using VCDs to confirm C atom positions in carboranes and metallacarboranes, it is essential to know which vertices to use to calculate the polyhedral centroid. For the VCD method applied to icosahedral carboranes (*closo*-C_2B_{10}) all ten vertices are used to define the polyhedral centroid. In the case of icosahedral metallcarboranes (*closo*-MC_2B_{10}) it is different as the atomic radii of all metals are larger than those of C and B. Thus inclusion of the metal vertex displaces the centroid towards it. To test this, the polyhedral centroids were determined for 3,1,2-MC_2B_9 structures in two ways, firstly including all 12 vertices (cent1) and secondly excluding metal and the antipodal atom (cent2), as shown in Figure 1.8.1 (middle).[70] This gives Δ (Δ = cent1– cent2 distance) which is *ca*. 0.05 Å for a first row transition metal. That means Δ is never zero *i.e*. cent1 and cent2 never coincide. Thus for a MC_2B_9 structure, the polyhedral centroid is calculated by excluding the metal vertex and the antipodal atom to the metal.

Experimentally, for 12-vertex cages the vertices were numbered for either C_2B_{10} or MC_2B_9 compounds (Figure 1.8.1, left) and all the vertices except the metal atom for

MC_2B_9 were assumed to be B atoms. Structures were refined to convergence including free refinement of cage H using *OLEX2* [72] producing a model known as the *Prostructure*. Using the Prostructure, the centroid is determined by considering all the 12 vertices for C_2B_{10} compounds but neglecting M3 and the antipodal atom 10 for MC_2B_9 compounds (Figure 1.8.1, right). Then the vertex or vertices having the shortest distance between vertex and centroid is determined as a C atom. This is also confirmed by shortest boron to hydrogen distance.

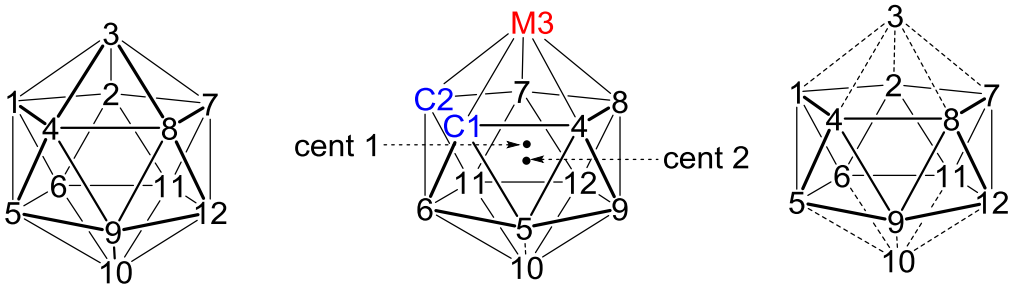

Figure 1.8.1 The numbering scheme (left), the polyhedral centroids for a 3,1,2-MC_2B_9 icosahedron (middle) and vertices used to calculate polyhedral centroid in 12-vertex metallacarborane (right).

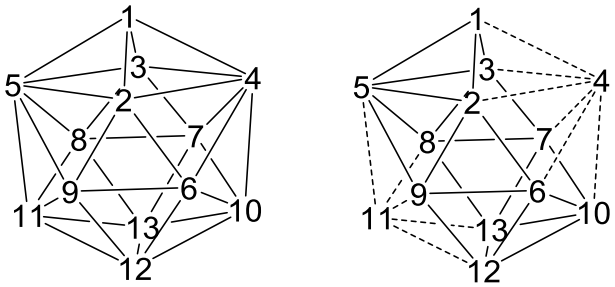

Figure 1.8.2 The numbering scheme of docosahedron (left) and docosahedral vertices used to calculate polyhedral centroid (right).

A variety of isomeric forms exist for 13-vertex $MC_2B_{10}H_{12}$ compounds but always the metal atom is at the degree-6 vertex 4 and one cage C atom is at the unique degree-4 vertex 1 (Figure 1.8.2, left). For docosahedral MC_2B_{10} compounds, the calculation of polyhedral centroid is more complex as it belongs to a low symmetry point group (C_{2v}). However the effective symmetry reduces to C_s symmetry (eliminating C or B) with the metal atom at vertex 4 and one cage C atom at vertex 1, with the mirror plane passing through the vertices 1, 4, 5, 10 and 11. Thus topologically-equivalent vertices exist as

groups (2/3, 6/7/8/9, 10/11 and 12/13) and VCDs for these can aid C atom identification. Here the centroid is calculated by excluding the metal vertex 4 and atom 11, antipodal to the metal (Figure 1.8.2, right).

Both VCD and BHD methods have been used for the determination of the exact crystallographic structure for all compounds, as appropriate, described in this thesis.

1.9 Scope of Thesis

Chapter 1 provides an overview of the relevant literature on single cage borane and heteroborane chemistry which is a basis for the work in this thesis. Bis(carboranes) are then introduced including recent advances. The metallcarborane chemistry of 1,1′-bis(*o*-carborane) and its isomerisation is an area of emerging interest and the main aspects of this thesis.

Chapter 2 discusses steric *versus* electronic factors in metallacarborane isomerisation. Following our previous study on basicity-induced isomerisation, we have examined the factors influencing the isomerisation processes of MC_2B_9-C_2B_{10} heteroboranes. Metallation was studied with various $\{NiPP\}^{2+}$ or $\{NiP_2\}^{2+}$ fragments (PP = chelating diphosphine; P = monodentate phosphine). The study revealed the isomerisation of a 3,1,2-MC_2B_9-1′,2′-C_2B_{10} was the result of either electronic or steric factors. To confirm, further metallation with $\{NiP_2\}^{2+}$ fragments (P = monodentate phosphite) have been studied. Following difficulties encountered in the preparation of phosphite nickelacarboranes, alternative pathways *i.e*. metallation with the $\{Ni(tmeda)\}^{2+}$ fragment and *in situ* addition of $P(OMe)_3$, have been developed. The work yielded the first examples of phosphite based 3,1,2-1′,2′ and 2,1,8-1′,2′ architectures, the latter being a rare example. Direct metallation was also examined using [$NiBr_2P_2$] [P = $P(OMe)_3$, $P(OEt)_3$]. In a related study, two examples of 3,1,2-PdC_2B_9-1′,2′-C_2B_{10} and 2,1,8-PdC_2B_9-1′,2′-C_2B_{10} are also reported.

The requirement for harsh conditions in the double decapitation of 1,1′-bis(*o*-carborane) and the possibilities of the formation of diastereoisomers have been described in Chapter 3. The first examples the architectures 3,1,2-3′,1′,2′; 3,1,2-4′,1′,2′; 4,1,2-2′,1′,8′ and 4,1,2-4′,1′,2′ of bis(nickelcarboranes) have been reported. We have observed unexpected interconversion between diastereoisomers in the case of the small phosphine dmpe and the mechanism of this transformation has been considered. A stereospecific product was observed using the bulky phosphine dppe and this has been rationalised by dihydrogen bonding. This concept has been also applied to the products obtained from the thermolysis of 3,1,2-NiC_2B_9-3′,1′,2′-NiC_2B_9 derivatives. A new naming convention for icosahedral bis(metallcarboranes) is reported.

Following difficulties associated with the separation of the diastereoisomers of 4,1,6-4′,1′,6′ bis(cobaltacarboranes), the isomerisation of these species was examined by using a mixture and this is described in Chapter 4. The study reveals that the isomerisation occurs at high temperature and yielded the first examples of 4,1,12-CoC_2B_{10}-4′,1′,12′-CoC_2B_{10} diastereoisomers. The polyhedral expansion of these species was attempted.

Finally, Chapter 5 details the synthesis, spectroscopic and structural characterisation of all new compounds.

1.10 References

1 J. Daintith, *Dictionary of Chemistry 3rd Ed.*, Oxford University Press, 1996.

2 For review see: R. N. Grimes, *Dalton Trans*., 2015, **44**, 5939.

3 For selected examples see: Z. Yinghuai, K. Carpenter, C. C. Bun, S. Bahnmueller, C. P. Ke, V. S. Srid, L. W. Kee and M. F. Hawthorne, *Angew. Chem. Int. Ed*., 2003, **42**, 3792.

4 For selected example see: (a) N. J. Patmore, C. Hague, J. H. Cotgreave, M. F. Mahon, C. G. Frost and A. S. Weller, *Chem. Eur. J*., 2002, **8**, 2088; (b) O. Allemann, S. Duttwyler, P. Romanato, K. K. Baldridge and J. S. Siegel, *Science*, 2011, **332**, 574.

5 For review see: (a) S. H. Strauss, *Chem. Rev*. 1993, **93**, 927; for selected example see: (b) Y. Shoji, N. Tanaka, K. Mikami, M. Uchiyama and T. Fukushima, *Nature Chem*., 2014, **6**, 498.

6 For selected example see: (a) O. K. Farha, A. M. Spokoyny, K. L. Mulfort, M. F. Hawthorne, C. A. Mirkin and J. T. Hupp, *J. Am. Chem. Soc*., 2007, **129**, 12680; (b) Y.-S. Bae, O. K. Farha, A. M. Spokoyny, C. A. Mirkin, J. T. Hupp and R. Q. Snurr, *Chem. Commun*., 2008, 4135.

7 For selected example see: (a) J. Plešek, *Chem. Rev*., 1992, **92**, 269; (b) J. Rais, P. Selucky and M. J. Kyrs, *J. Inorg. Nucl. Chem*., 1976, **38**, 1376.

8 For selected example see: J. Brus, A. Zhigunov, J. Czernek, L. Kobera, M. Uchman and P. Matějiček, *Macromolecules*, 2014, **47**, 6343 and references cited therein.

9 (a) A. H. Soloway, H. D. Hatanaka and M. A. Davis, *J. Med. Chem*., 1967, **10**, 714; (b) H. D. Hatanaka and Y. Nakagawa, *Int. J. Radiat. Oncol. Biol. Phys*., 1994, **28**, 1061; Reviews: (c) R. F. Barth, J. A. Coderre, M. G. H. Vicente and T. E. Blue, *Clin. Cancer Res*. 2005, **11**, 3987; (d) I. B. Sivaev and V. I. Bregadze, *Eur. J. Inorg. Chem*., 2009, 1433.

10 A. Stock, *Hydrides of Boron and Silicon*, Cornell University Press, Ithaca, New York, 1933.

11 (a) H. W. Smith and W. N. Lipscomb, *J. Chem. Phys*., 1949, **46**, 275; (b) K. Hedberg and V. Schomaker, *J. Am. Chem. Soc*., 1951, **73**, 1482.

12 (a) J. S. Kasper, C. M. Lucht and D. Harker, *Acta Cryst*., 1950, **3**, 436; (b) E. B. Moore Jnr., R. E. Dickson and W. N. Lipscomb, *J. Chem. Phys*., 1957, **27**, 209.

13 (a) H. C. Longuet-Higgins and R. P. Bell, *J. Chem. Soc*., 1943, **46**, 250; (b) H. C. Longuet-Higgins and M. de V. Roberts, *Proc. Roy. Soc. (London)*, 1954, **A224**, 336; (c) *idem*, *Proc. Roy. Soc. (London)*, 1955, **A230**, 110.

14 A. R. Pitochelli and M. F. Hawthorne, *J. Am. Chem. Soc*., 1960, **82**, 3228.

15 (a) L. D. Brown and W. N. Lipscomb, *Inorg. Chem*., 1977, **16**, 2989; (b) W. N. Lipscomb, *Boron Hydrides*, W. A. Benjamin, Inc., New York, 1963.

16 P. von R. Schleyer, K. Najafian and A. M. Mebel, *Inorg. Chem.*, 1998, **37**, 6765.

17 (a) K. Wade, *J. C. S. D*, 1971, 792; (b) K. Wade, *Adv. Inorg. Radiochem*., 1976, **18**, 1.

18 D. M. P. Mingos, *Acc. Chem. Res*., 1984, **17**, 311.

19 T. L. Heying, J. W. Ager Jnr., S. L. Clark, D. J. Mangold, H. L. Goldstein, M. L. Hillman, R. J. Polak and J. W. Szymanski, *Inorg. Chem*., 1963, **2**, 1089.

20 R. K. Bohn and M. D. Bohn, *Inorg. Chem*., 1971, **10**, 350.

21 (a) M. M. Fein, J. Bobinski, N. Meyers, N. Schwartz and M. S. Cohen, *Inorg. Chem*., 1963, **2**, 1111; (b) M. F. Hawthorne, T. D. Andrews, P. M. Garrett, F. P. Olsen, M. Reintjes, F. N. Tebbe, L. F. Warren, P. A. Wegner and D. C. Young, *Inorg. Synth*., 1967, **10**, 91; (c) R. N. Grimes, *Carboranes*, 2nd Edition, Academic Press, Oxford, UK, 2011.

22 R. A. Wiesboeck and M. F. Hawthorne, *J. Am. Chem. Soc*., 1964, **86**, 1642.

23 L. I. Zakharkin and V. N. Kalinin, *J. Gen. Chem. USSR. (Engl. Transl.)*, 1965, **35**, 1693.

24 M. F. Hawthorne, D. C. Young, P. M. Garrett, D. A. Owen, S. G. Schwerin, F. N. Tebbe and P. A. Wegner, *J. Am. Chem. Soc*., 1968, **90**, 862.

25 J. Plešek and S. Heřmánek, *Chem. Ind. (London)*, 1973, 381.

26 D. C. Busby and M. F. Hawthorne, *Inorg. Chem*., 1982, **21**, 4101.

27 J. Buchanan, E. J. M. Hamilton, D. Reed and A. J. Welch, *J. Chem. Soc., Dalton Trans*., 1990, 677.

28 M. G. Davidson, M. A. Fox, T. G. Hibbert, J. A. K. Howard, A. Mackinnon, I. S. Neretin and K. Wade, *Chem. Commun*., 1999, 1649.

29 M. A. Fox, A. E. Goeta, J. A. K. Howard, A. K. Hughes, A. L. Johnson, D. A. Keen, K. Wade and C. C. Wilson, *Inorg. Chem*., 2001, **40**, 173.

30 R. C. B. Copley and D. M. P. Mingos, *J. Chem. Soc., Dalton Trans*., 1996, 491.

31 K. Chiu, Z. Zhang, T. C. W. Mak and Z. Xie, *J. Organomet. Chem*., 2000, **614-615**, 107.

32 (a) M. F. Hawthorne, D. C. Young and P. A. Wegner, *J. Am. Chem. Soc*., 1965, **87**, 1818; (b) M. F. Hawthorne, D. C. Young, T. D. Andrews, D. V. Howe, R. L. Pilling, A. D. Pitts, M. Reintjes, L. F. Warren, Jr., and P. A. Wegner, *J. Am. Chem. Soc*., 1968, **90**, 879.

33 (a) M. F. Hawthorne, *Acc. Chem. Res*., 1968, **1**, 281; (b) R. N. Grimes, *Comprehensive Organometallic Chemistry II*, edited by E. W. Abel, F. G. A. Stone and G. Wilkinson, Volume 1, Chapter 9, Pergamon Press, Oxford, England, 1995, 373.

34 D. Grafstein and J. Dvorak, *Inorg. Chem*., 1963, **2**, 1128.

35 S. Papetti and T. L. Heying, *J. Am. Chem. Soc.*, 1964, **86**, 2295.

36 (a) L. I. Zakharkin, V. N. Kalinin and L. S. Podivisotskaya, *Izv. Akad. Nauk SSSR, Ser. Khim*., 1967, 2310; (b) L. Zakharkin and V. Kalinin, *ibid*., 1969, 194; (c) V. Stanko, Y. V. Gol'tyapin and V. Brattsev, *Zh. Obsch. Khim*., 1969, **39**, 1175.

37 W. N. Lipscomb, *Science*, 1966, **153**, 373.

38 E. L. Muetterties and W. N. Knoth, *Polyhedral Boranes*, Marcel Dekker, New York, 1968, 55 and 70.

39 D. J. Wales, *J. Am. Chem. Soc*., 1993, **115**, 1557.

40 S. Dunn, G. M. Rosair, Rh. Ll. Thomas, A. S. Weller and A. J. Welch, *Angew. Chem. Int. Ed*., 1997, **36**, 645.

41 C. A. Brown and M. L. McKee, *J. Mol. Model*., 2006, **12**, 653.

42 D. R. Baghurst, R. C. B. Copley, H. Fleischer, D. M. P. Mingos, G. O. Kyd, L. J. Yellowlees, A. J. Welch, T. R. Spalding and D. O'Connell, *J. Organomet. Chem*., 1993, **447**, C14.

43 (a) R. M. Garrioch, P. Kuballa, K. S. Low, G. M. Rosair and A. J. Welch, *J. Organomet. Chem*., 1999, **575**, 57; (b) S. Robertson, D. Ellis, T. D. McGrath, G. M. Rosair and A. J. Welch, *Polyhedron*, 2003, **22**, 1293; (c) S. Robertson, D. Ellis, G. M. Rosair and A. J. Welch, *J. Organomet. Chem*., 2003, **680**, 286; (d) S. Robertson, D. Ellis, G. M. Rosair and A. J. Welch, *Appl. Organomet. Chem*., 2003, **17**, 516; (e) S. Robertson, R. M. Garrioch, D. Ellis, T. D. McGrath, B. E. Hodson, G. M. Rosair, A. J. Welch, *Inorg. Chim. Acta*, 2005, **358**, 1485; (f) D. Ellis, R. M. Garrioch, G. M. Rosair and A. J. Welch, *Polyhedron*, 2006, **25**, 915.

44 R. D. McIntosh, D. Ellis, B. T. Giles, S. A. Macgregor, G. M. Rosair and A. J. Welch, *Inorg. Chim. Acta*, 2006, **359**, 3745.

45 A. V. Safronov, F. M. Dolgushin, P. V. Petrovskii and I. T. Chizhevsky, Organometallics, 2005, **24**, 2964.

46 (a) D. F. Dustin, G. B. Dunks and M. F. Hawthorne, *J. Am. Chem. Soc*., 1971, **95**, 1109; (b) G. B. Dunks, M. M. McKown and M. F. Hawthorne, *J. Am. Chem. Soc*., 1971, **93**, 2541.

47 (a) D. F. Dustin, G. B. Dunks and M. F. Hawthorne, *J. Am. Chem. Soc*., 1973, **95**, 1109; (b) D. F. Dustin, W. J. Evans, C. J. Jones, R. J. Wiersema, H. Gong, S. Chan and M. F. Hawthorne, *J. Am. Chem. Soc*., 1974, **96**, 3085; (c) A. Burke, R. McIntosh, D. Ellis, G. M. Rosair and A. J. Welch, *Collect. Czech. Chem. Commun*., 2002, **67**, 991.

48 W. J. Evans and M. F. Hawthorne, *J. Chem. Soc., Chem. Commun*., 1974, 38.

49 A. McAnaw, M. E. Lopez, D. Ellis, G. M. Rosair and A. J. Welch, *Dalton Trans*., 2013, **42**, 671.

50 D. Ellis, M. E. Lopez, R. McIntosh, G. M. Rosair and A. J. Welch, *Chem. Commun*., 2005, 1917.

51 A. McAnaw, M. E. Lopez, D. Ellis, G. M. Rosair and A. J. Welch, *Dalton Trans*., 2014, **43**, 5095.

52 (a) R. D. McIntosh, D. Ellis, G. M. Rosair and A. J. Welch, *Angew. Chem. Int. Ed*., 2006, **45**, 4313; (b) L. Deng, J. Zhang, H. S. Chan and Z. Xie, *Angew. Chem. Int. Ed*., 2006, **45**, 4309; (c) D. K. Roy, S. K. Bose, R. S. Anju, B. Mondal, V. Ramkumar and S. Ghosh, *Angew. Chem. Int. Ed*., 2013, **52**, 3222.

53 J. A. Dupont and M. F. Hawthorne, *J. Am. Chem. Soc*., 1964, **86**, 1643.

54 T. E. Paxson, K. P. Callahan and M. F. Hawthorne, *Inorg. Chem*., 1973, **12**, 708.

55 X. Yang, W. Jiang, C. B. Knobler, M. D. Mortimer and M. F. Hawthorne, *Inorg. Chim. Acta*, 1995, **240**, 371.

56 S. Ren and Z. Xie, *Organometallics*, 2008, **27**, 5167.

57 (a) D. A. Owen and M. F. Hawthorne, *J. Am. Chem. Soc*., 1970, **92**, 3194; (b) D. A. Owen and M. F. Hawthorne, *J. Am. Chem. Soc*. 1971, **93**, 873; (c) D. E. Harwell, J. McMillan, C. B. Knobler and M. F. Hawthorne, *Inorg. Chem*., 1997, **36**, 5951.

58 M. J. Martin, W. Y. Man, G. M. Rosair and A. J. Welch, *J. Organomet. Chem*., 2015, **798**, 36.

59 K. O. Kirlikovali, J. C. Axtell, A. Gonzalez, A. C. Phung, S. I. Khan and A. M. Spokoyny, *Chem. Sci*., 2016, **7**, 5132.

60 Z.-J. Yao, Y.-Y. Zhang and G.-X. Jin, *J. Organomet. Chem*., 2015, **798**, 274.

61 L. E. Riley, A. P. Y. Chan, J. Taylor, W. Y. Man, D. Ellis, G. M. Rosair, A. J. Welch and I. B. Sivaev, *Dalton Trans*., 2016, **45**, 1127.

62 Y. O. Wong, M. D. Smith and D. V. Peryshkov, *Chem. Eur. J*., 2016, **22**, 6764.

63 T. D. Getman, C. B. Knobler and M. F. Hawthorne, *Inorg. Chem*., 1992, **31**, 101.

64 T. D. Getman, C. B. Knobler and M. F. Hawthorne, *J. Am. Chem. Soc*., 1990, **112**, 4594.

65 W. Y. Man, D. Ellis, G. M. Rosair and A. J. Welch, *Angew. Chem. Int. Ed.*, 2016, **55**, 4596.

66 W. Y. Man, S. Zlatogorsky, H. Tricas, D. Ellis, G. M. Rosair and A. J. Welch, *Angew. Chem. Int. Ed*., 2014, **53**, 12222.

67 D. Ellis, D. McKay, S. A. Macgregor, G. M. Rosair and A. J. Welch, *Angew. Chem. Int. Ed.*, 2010, **49**, 4943.

68 D. Ellis, G. M. Rosair and A. J. Welch, *Chem. Commun.*, 2010, **46**, 7394.

69 D. Zhao, J. Zhang, Z. Lin and Z. Xie, *Chem. Commun.*, 2016, **52**, 9992.

70 A. McAnaw, G. Scott, L. Elrick, G. M. Rosair and A. J. Welch, *Dalton Trans*., 2013, **42**, 645.

71 J. C. Slater, *J. Chem. Phys*., 1964, **41**, 3199.

72 O. V. Dolomanov, L. J. Bourhis, R. J. Gildea, J. A. K. Howard and H. Puschmann, *J. Appl. Cryst.*, 2009, **42**, 339.

Chapter 2

Nickelacarboranes: single dec/met of 1,1′-bis(*o*-carborane)

2.1 Introduction

Hawthorne's classic decapitation reaction of *o*-carborane is that 1,2-*closo*-$C_2B_{10}H_{12}$ can be readily decapitated in presence of KOH/EtOH under reflux to an open face [7,8-*nido*-$C_2B_9H_{11}]^{2-}$ species.[1a] The decapitated nido species, [7,8-*nido*-$C_2B_9H_{11}]^{2-}$ can be easily capitated with a metal fragment to avail an icosahedral *closo*-metallacarborane (Figure 2.1.1).[1b]

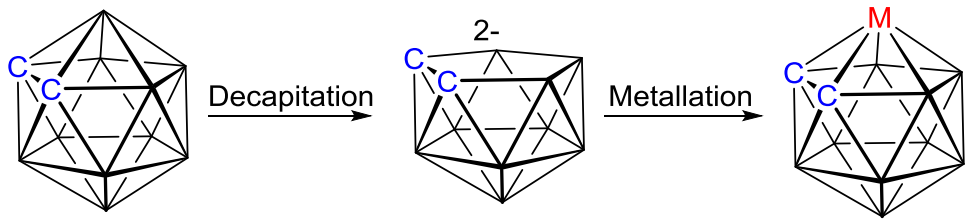

Figure 2.1.1 Synthesis of 3,1,2-MC_2B_9 species.

In 1983, Hawthrone *et al* reported single cage icosahedral bis(phosphine)nickelacaboranes by the reaction of $[NiCl_2(R_3P)_2]$ with [7,8-*nido*-$C_2B_9H_{11}]^{2-}$, [7,9-*nido*-$C_2B_9H_{11}]^{2-}$ and [2,9-*nido*-$C_2B_9H_{11}]^{2-}$ species.[2] Heating of 3,3-$(PPh_3)_2$-3,1,2-*closo*-$NiC_2B_9H_{11}$ at 80 ºC led to the formation of corresponding hydrido complex by interchange of phosphine and hydrido ligands (Figure 2.1.2). However no isomerisations (separation of C atoms) were observed for these nickelacarboranes. Further treatment of hydrido complex with dry HCl gave [3,8-$(PPh_3)_2$-3-Cl-3,1,2-*closo*-$NiC_2B_9H_{11}$]. Heating to reflux [3,3-$(PPh_3)_2$-3,1,2-*closo*-$NiC_2B_9H_{10}$] in presence of CO at 80 ºC gave dimeric nickelacarborane carbonyl species. Additionally, Eremenko and co-workers also synthesised [3,3-$(PPh_3)_2$-3,1,2-*closo*-$NiC_2B_9H_{11}$] by the reactions of salts of bis(*o*-dicarbollyl)nickel(III) or neutral bis(*o*-dicarbollyl)nickel(IV) with triphenylphosphine in ethanol reflux.[3]

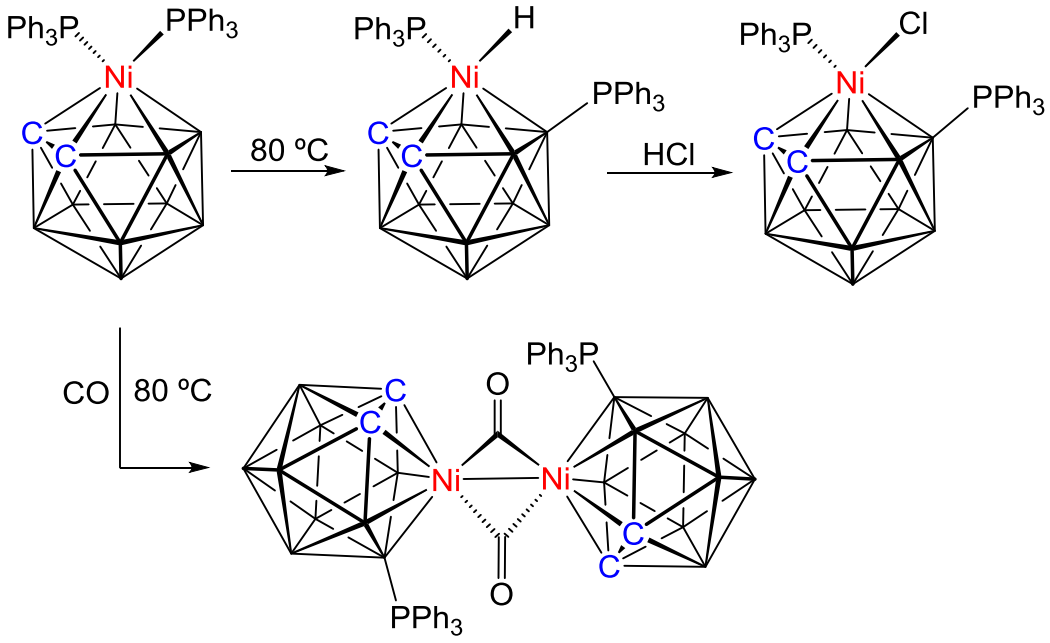

Figure 2.1.2 Derivatisation of 3,3-$(PPh_3)_2$-3,1,2-*closo*-$NiC_2B_9H_{11}$.

When two 1,2-*closo*-$C_2B_{10}H_{12}$ units are connected by a C–C bond at C1 positions, it generates [1-(1′-1′,2′-*closo*-$C_2B_{10}H_{11}$)-1,2-*closo*-$C_2B_{10}H_{11}$], the trivial name for which is 1,1′-bis(*o*-carborane). $Cu^{II}Cl_2$-mediated coupling reactions of mono- or di-lithiated salts of *ortho*-carborane were introduced initially for the synthesis of 1,1′-bis(*o*-carborane).[4] Subsequently, the high yielding synthetic route of 1,1′-bis(*o*-carborane) using $Cu^{I}Cl$-coupling reactions of dilithiated *ortho*-carborane was developed by Xie.[5]

Mono-deboronation (single decapitation) of 1,1′-bis(*o*-carborane) was initially reported by Hawthrone using one equivalent ethoxide ion, $[EtO]^-$ generated from one equivalent KOH in ethanol reflux, but the resultant decapitated nido-derivative was not fully characterised.[6] However, Welch and co-workers recently reported single decapitation of 1,1′-bis(*o*-carborane) using one equiv. KOH by refluxing in ethanol.[7] Isolation of the decapitated intermediate as trimethyl ammonium salt affords $[HNMe_3]$[7-(1′-1′,2′-*closo*-$C_2B_{10}H_{11}$)-7,8-*nido*-$C_2B_9H_{11}$] in moderately high yield (Figure 2.1.3).[7] This was characterised by NMR spectroscopy, elemental analysis and, as the BTMA salt, crystallography. A limitation of this method is that using more than one equivalent KOH leads to the formation of double deboronated nido derivative which will be discussed in detail in Chapter 3.

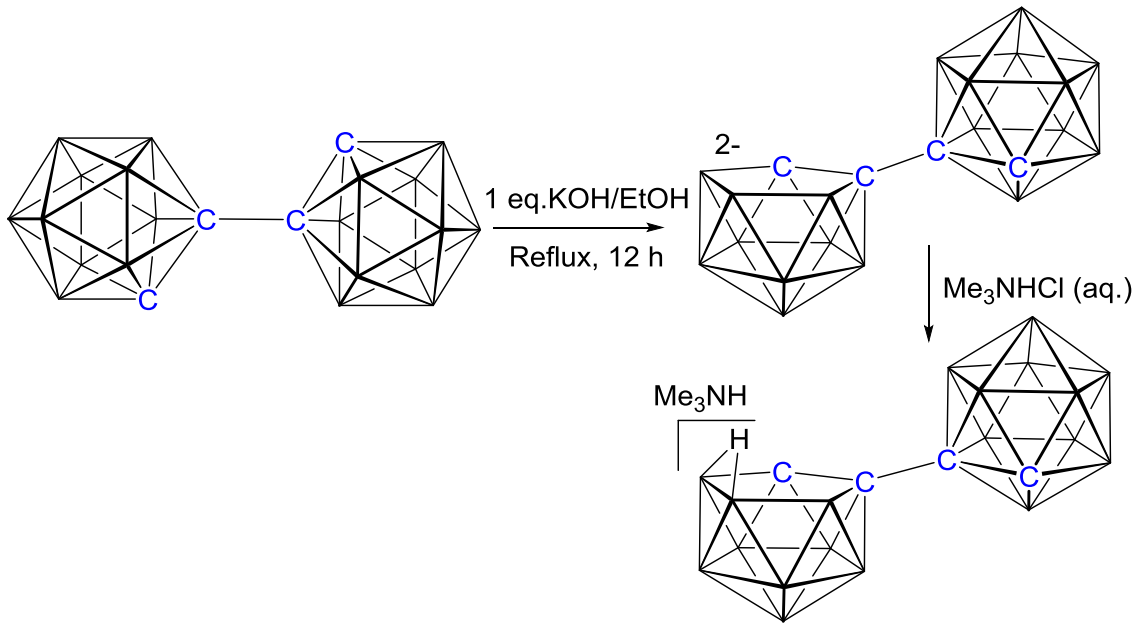

Figure 2.1.3 Single decapitation of 1,1′-bis(*o*-carborane).

Very recently Sivaev *et al* reported selective single decapitation of 1,1′-bis(*o*-carborane) under mild conditions using water/acetonitrile. This easily affords the corresponding nido/closo derivative of bis(carborane) in almost a quantitative yield (Figure 2.1.4).[8] No deboronation of the second carborane cage was found either at room temperature or under reflux conditions. This can be explained by effective suppression of the electron-withdrawal effect of the carborane cage upon its deboronation.

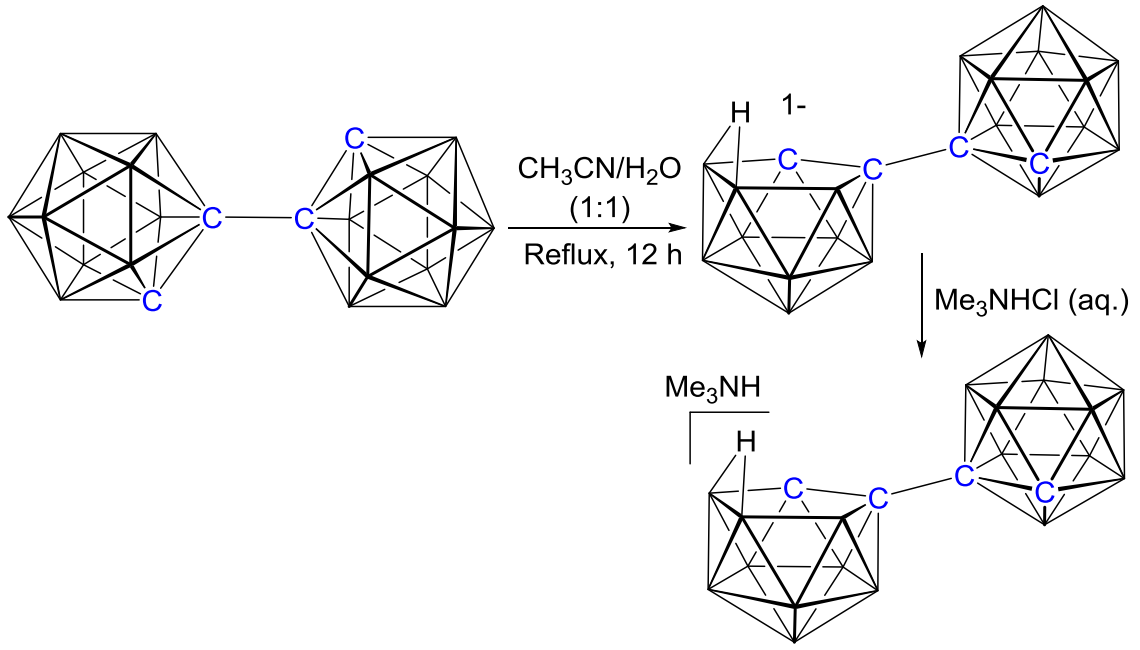

Figure 2.1.4 Single decapitation of 1,1′-bis(*o*-carborane) in mild condition.

The single decapitation and metallation chemistry of 1,1′-bis(*o*-carborane) has not been fully explored. However Welch and co-workers recently [7] reported the results of metallation of [7-(1′-1′,2′-*closo*-$C_2B_{10}H_{11}$)-7,8-*nido*-$C_2B_9H_{11}]^{2-}$ with both $\{CoCp\}^{+}$ (oxidised to $\{CoCp\}^{2+}$) and $\{Ru(p\text{-cymene})\}^{2+}$ fragments. Metallation with the {Ru(*p*-cymene)} fragment yields both the unisomerised [1-(1′-1′,2′-*closo*-$C_2B_{10}H_{11}$)-3-(*p*-cymene)-3,1,2-*closo*-$RuC_2B_9H_{10}$] and the isomerised [8-(1′-1′,2′-*closo*-$C_2B_{10}H_{11}$)-2-(*p*-cymene)-2,1,8-*closo*-$RuC_2B_9H_{10}$] species. Further, 3,1,2-RuC_2B_9-1′,2′-C_2B_{10}, the kinetic product, readily goes to the thermodynamically stable isomer 2,1,8-RuC_2B_9-1′,2′-C_2B_{10} under reflux in THF (Figure 2.1.5). Fully analogous compounds are formed with the $\{CoCp\}^{+/2+}$ fragment but depend on the source of the metal unit. Using [$CoCpI_2$(CO)] the product is [1-(1′-1′,2′-*closo*-$C_2B_{10}H_{11}$)-3-Cp-3,1,2-*closo*-$CoC_2B_9H_{10}$] whereas using $CoCl_2$/NaCp followed by aerial oxidation results in the formation of [8-(1′-1′,2′-*closo*-$C_2B_{10}H_{11}$)-2-Cp-2,1,8-*closo*-$CoC_2B_9H_{10}$]. Although the 3,1,2-CoC_2B_9-1′,2′-C_2B_{10} species does not isomerise to 2,1,8-CoC_2B_9-1′,2′-C_2B_{10} even at 110 °C (toluene reflux), it occurs if it is reduced by addition of one equivalent sodium naphthalenide and then reoxidised at room temperature (Figure 2.1.6). This perhaps suggests that the basicity of the metal fragment might play a role in the ease and nature of the isomerisation of metallacarboranes, a concept that has some literature precedence.[9]

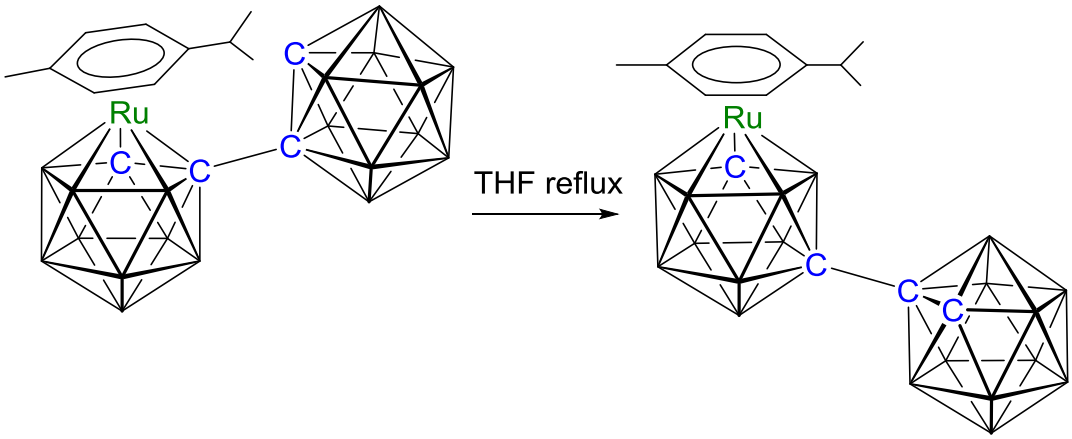

Figure 2.1.5 Isomerisation of 1-C_2B_{10}-3,1,2-RuC_2B_9 to 8-C_2B_{10}-2,1,8-RuC_2B_9 species.

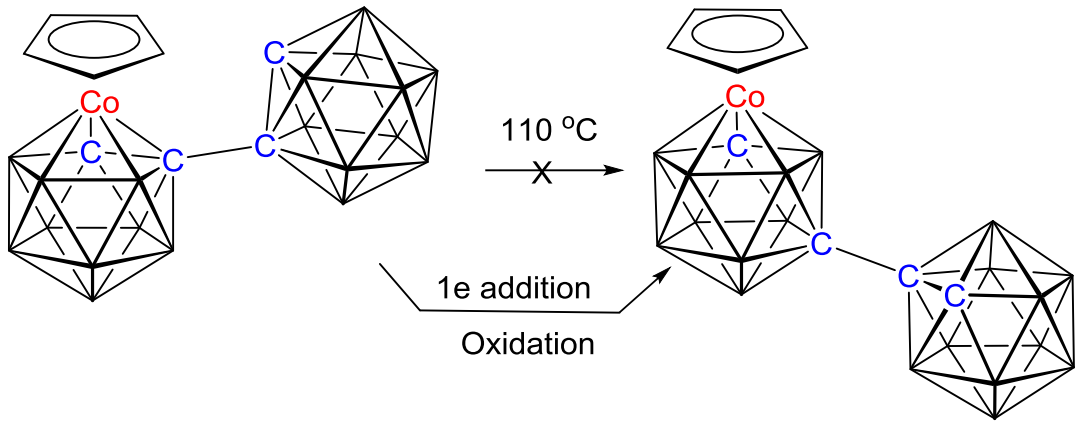

Figure 2.1.6 Isomerisation of 1-C_2B_{10}-3,1,2-CoC_2B_9 to 8-C_2B_{10}-2,1,8-CoC_2B_9 species.

We utilised initially one equivalent KOH/EtOH to prepare [$HNMe_3$][7-(1′-1′,2′-*closo*-$C_2B_{10}H_{11}$)-7,8-*nido*-$C_2B_9H_{11}$] and later on CH_3CN/H_2O (1:1) as a selective decapitating reagent. Capping with metal fragments $\{Ni(dppe)\}^{2+}$, $\{Ni(dmpe)\}^{2+}$, $\{Ni(PMe_3)_2\}^{2+}$, $\{Ni(PMe_2Ph)_2\}^{2+}$, $\{Ni(PPh_2Me)\}^{2+}$, $\{Ni(tmeda)\}^{2+}$, $\{Ni(P(OMe)_3)_2\}^{2+}$, and $\{Ni(P(OEt)_3)_2\}^{2+}$ fragments led to the synthesis of new 12-vertex metallacarborane/12-vertex carborane compounds and their derivatives. We have also attempted capitation of [7-(1′-1′,2′-*closo*-$C_2B_{10}H_{11}$)-7,8-*nido*-$C_2B_9H_{10}]^{2-}$ with the fragments $\{Ni(PPh_3)_2\}^{2+}$, $\{Ni(PiPr_3)_2\}^{2+}$, $\{Ni(P(p\text{-tol})_3)_2\}^{2+}$. For the purpose of investigation of the isomerisation of nickelacarboranes, we have also studied the metallation chemistry of [7-(1′-1′,2′-*closo*-$C_2B_{10}H_{11}$)-7,8-*nido*-$C_2B_9H_{10}]^{2-}$ with metal fragments $\{Pd(NCPh)_2\}^{2+}$, $\{Pd(PMe_3)_2\}^{2+}$, $\{Pd(P(OMe)_3)_2\}^{2+}$, $\{Pd(tmeda)\}^{2+}$, and $\{Pd(en)\}^{2+}$. This Chapter describes the results obtained from these metallation reactions and their isomerisation behaviour.

2.2 Results and discussion

2.2.1 Synthesis of [1-(1′-1′,2′-*closo*-$C_2B_{10}H_{11}$)-3-dppe-3,1,2-*closo*-$NiC_2B_9H_{10}$] (1) and [2-(1′-1′,2′-*closo*-$C_2B_{10}H_{11}$)-4-dppe-4,1,2-*closo*-$NiC_2B_9H_{10}$] (2)

Dianion [7-(1′-1′,2′-*closo*-$C_2B_{10}H_{11}$)-7,8-*nido*-$C_2B_9H_{11}]^{2-}$ is conveniently prepared *in situ*, as its lithium salt, by treatment of [$HNMe_3$][7-(1′-1′,2′-*closo*-$C_2B_{10}H_{11}$)-7,8-*nido*-$C_2B_9H_{11}$] ([$HNMe_3$]**I**) with 2.2 equivalent *n*-BuLi in THF. Addition of [$NiCl_2$(dppe)] to a THF solution of the dianion at –196 °C followed by warming to room temperature and stirring for 12 h afforded a brown solution. On work-up by TLC on silica two products were observed. The slower moving green band **1** and faster moving red-purple band **2** were isolated in moderate yields (Figure 2.2.1.1).

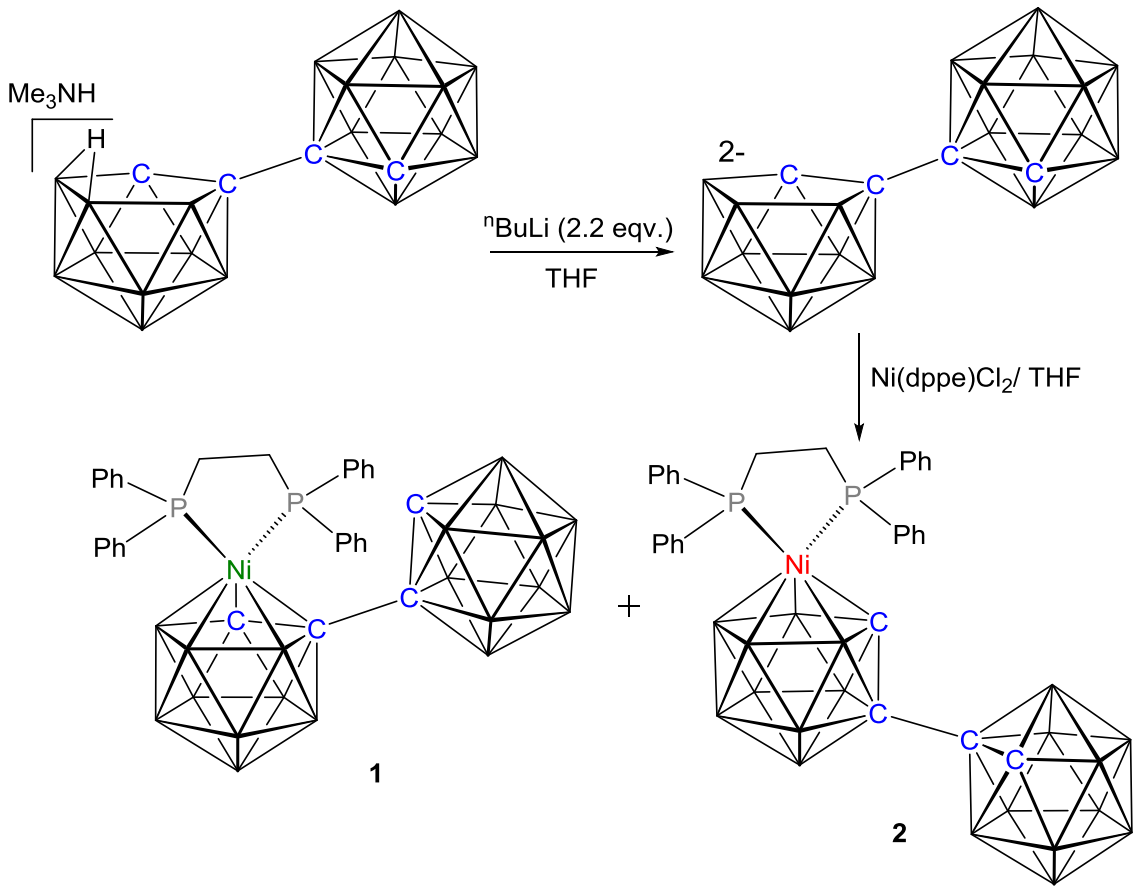

Figure 2.2.1.1 Metallation of [$HNMe_3$]**I** with $Ni(dppe)Cl_2$.

The EIMS of **1** contains an envelope centred on *m/z* 731.5 (M^+) (MW of **1** = 731.74 g mol^{-1}), and the elemental analysis is consistent with that expected for $C_{30}H_{45}B_{19}NiP_2{\cdot}CH_2Cl_2$ [crystals grown from DCM and 40-60 petroleum ether contain one molecule of DCM of solvation per molecule of nickelacarborane].

The $^{11}B\{^1H\}$ NMR spectrum of **1** consists of multiple overlapping resonances between δ 5.9 and -18.3 ppm with a total integral of 19B. It is not possible to deconvolute the entire spectrum due to multiple overlapping resonances, hence identification of the exact isomer is not achievable.

In the ^1H NMR spectrum there are, in addition to resonances arising from the dppe ligand, two broad resonances typical of C*H*$_{cage}$ signals, one at relatively high frequency (δ 3.08 ppm, assigned to the carborane cage) and the other at relatively low frequency (δ 1.74 ppm, assigned to the nickelacarborane). The latter appears as a doublet, J = 10.0 Hz, confirmed as arising from coupling to phosphorus since it collapses to a singlet on broad-band ^{31}P decoupling.

The $^{31}P\{^1H\}$ NMR spectrum of compound **1** reveals two mutual doublets, with coupling $^2J_{PP}$ = 25.5. Hz, at δ 51.8 and 41.0 ppm which indicates that two phosphorus atoms are magnetically inequivalent. This suggests an asymmetric nature within the metallacarborane cage.

Although these data are fully consistent with **1** being composed of $\{C_2B_{10}H_{11}\}$ and $\{(NiC_2B_9H_{10})(dppe)\}$ icosahedral fragments joined by a C–C bond, as expected, they do not define the isomeric nature of the nickelacarborane and consequently a structural study was undertaken.

Initially crystals of **1**, grown by diffusion of petroleum ether 40-60 and a DCM solution of **1** at 5 °C, did not provide publishable quality data. In a further attempt, good quality crystals of **1** were grown by diffusion of petroleum ether 40-60 and a THF solution of **1** at 5 °C. *X*-ray diffraction analysis explains all these spectroscopic findings of **1**. Although the crystallographic analysis revealed evidence for both disordered THF and disordered hexane in the lattice, the molecule of **1** is fully ordered. The nickelacarborane has a 3,1,2-NiC_2B_9 architecture arising from simple metallation of the open face of the precursor dianion $[\mathbf{I}]^{2-}$ by the $\{Ni(dppe)\}^{2+}$ fragment. Thus compound **1** is [1-(1′-1′,2′-

closo-$C_2B_{10}H_{11}$)-3-dppe-3,1,2-*closo*-$NiC_2B_9H_{10}$] or, in short form, 1-C_2B_{10}-3,1,2-NiC_2B_9.

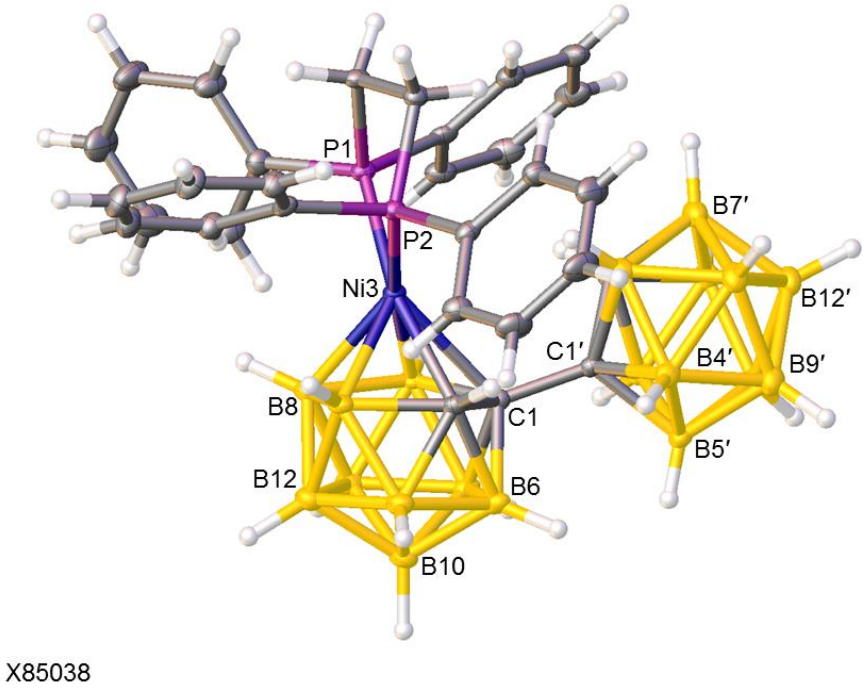

Figure 2.2.1.2 Molecular structure of [1-(1′-1′,2′-*closo*-$C_2B_{10}H_{11}$)-3-dppe-3,1,2-*closo*-$NiC_2B_9H_{10}$] (**1**)

A perspective view of a single molecule of **1** is shown in Figure 2.2.1.2. The presence of the bulky carborane substituent on C1 restricts rotation of the {Ni(dppe)} fragment about the Ni3…B10 axis rendering the phosphorus atoms inequivalent in solution at room temperature, as evidenced by the $^{31}P\{^1H\}$ NMR spectrum. Moreover, the carborane substituent clearly has an influence on the orientation of the {NiPP} unit. It is well-established that the electronically-controlled orientation of {ML_2} fragments in *M*C_2B_9 icosahedra is a function of the number and positions of the cage C atoms in the carborane ligand face;[10] for two adjacent C atoms (as in **1**) the plane through the {ML_2} fragment should lie perpendicular to the vertical mirror plane through the C_2B_9 unit. In **1** the dihedral angle, θ, between the plane through Ni3P1P2 and the plane through B6B8B10 is 61.87(9)º, not the electronically-preferred 90º. In fact, as Figure 2.2.1.2 shows, the NiPP plane in **1** lies effectively perpendicular to the plane through C1B10B12 so as to minimise steric congestion between the dppe ligand and the carborane substituent on C1. Even then a degree of steric crowding is still observed in that the NiPP plane is bent back

from perpendicular to the plane through atoms B5B6B11B12B9 [dihedral angle 10.76(6)º] and Ni3–C1 is significantly longer than Ni3–C2 [2.338(2) *versus* 2.112(2) Å].

Moving to compound **2**, from the mass spectrum and elemental analysis [EIMS: contains an envelope centred on *m/z* 731.5 (M^+) (MW = 731.74 g mol^{-1}); CHN analysis: consistent with that expected for $C_{30}H_{45}B_{19}NiP_2{\cdot}CH_2Cl_2$] compound **2**, a co-product of **1**, was assumed to be a geometrical isomer.

The ^1H spectrum of **2** is similar to that of compound **1**, the main difference being the CH_{cage} resonance at low frequency δ 1.90 ppm corresponding to the nickelacarborane cage is a simple singlet.

The $^{11}B\{^1H\}$ NMR spectrum of **2** is different to that of **1** and consists of multiple overlapping resonances between δ 4.7 and -15.8 ppm with a total integral of 19B. Due to multiple overlapping resonances, identification of the exact isomer is not possible.

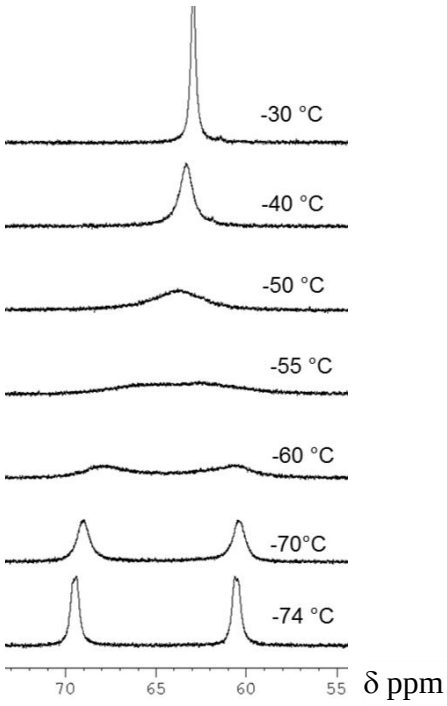

Figure 2.2.1.3 Variable temperature $^{31}P\{^1H\}$ NMR spectra of compound **2** in CD_2Cl_2.

A single (singlet) resonance is observed in the room temperature $^{31}P\{^1H\}$ spectrum, suggesting rotation of the {Ni(dppe)} fragment about the metal-cage axis that is rapid on the NMR timescale. Cooling a solution of **2** in CD_2Cl_2 freezes out this rotation with the

singlet at room temperature giving way to mutual doublets, $^{2}J_{PP}$ = 33.2 Hz, at δ 69.6 and 60.6 ppm, at 199 K, the lowest temperature reached (Figure 2.2.1.3). Using the standard coalescence temperature method [11] ($T_{coalescence}$ = 221 K) the activation energy for rotation of the {Ni(dppe)} fragment is estimated to be *ca*. 35 kJ mol^{-1}.

Crystals of **2** were grown by diffusion of petroleum ether 40-60 and a CH_2Cl_2 solution of **2** at 5 °C. Analysis by *X*-ray diffraction shows **2** to be [2-(1′-1′,2′-*closo*-$C_2B_{10}H_{11}$)-4-dppe-4,1,2-*closo*-$NiC_2B_9H_{10}$].

A perspective view of a single molecule of **2** is shown in Figure 2.2.1.4. In 4,1,2-*M*C_2B_9 species C2 occupies the lower pentagonal belt of the icosahedron (working down from the metal vertex) and is not directly bonded to the metal atom but the direct C1–C2 connectivity is retained. Such isomers are relatively rare; there are only ten examples [9a,12] of this isomeric form in the Cambridge Structural Database [13] and all but one of these [12e] are formed by isomerisation of an initial 3,1,2-*M*C_2B_9 isomer. Factors contributing to the reason for this isomerisation will be discussed in section 2.2.6.

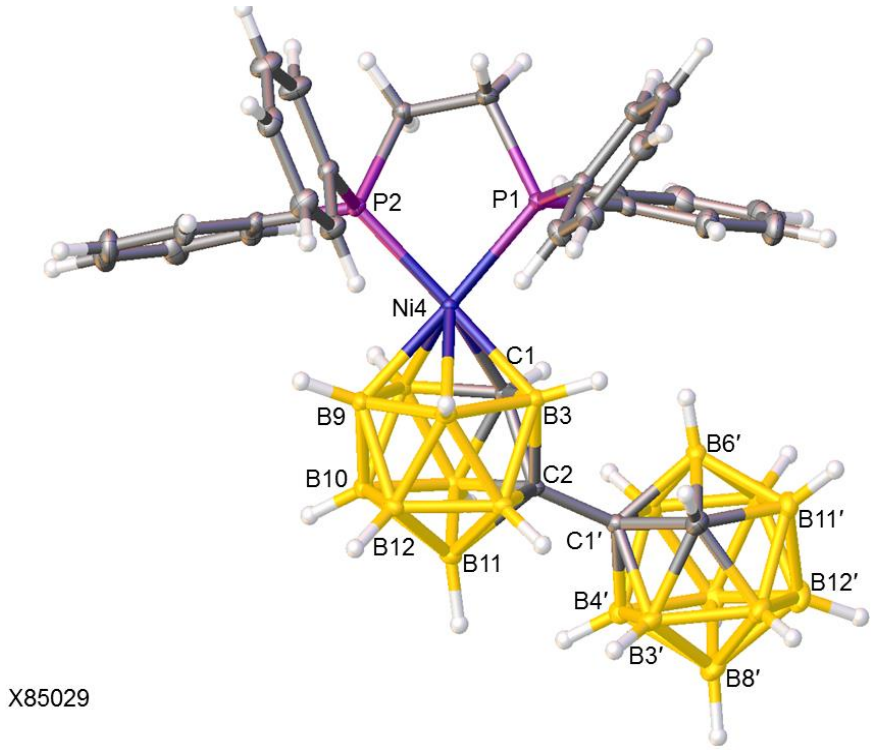

Figure 2.2.1.4 Molecular structure of [2-(1′-1′,2′-*closo*-$C_2B_{10}H_{11}$)-4-dppe-4,1,2-*closo*-$NiC_2B_9H_{10}$] (**2**).

In **2** the {NiPP} fragment is now bound to a CB_4 face. The expected orientation of the metal-phosphine unit is that in which the dihedral angle, θ, between the NiPP and C1B11B12 planes is 90º,[10] whilst in **2** θ is found experimentally to be only 56.67(5)º. Note however that calculations were based on a $[L_2MCB_{10}]^-$ anion and it may be that in **2** the C atom in the lower belt has some influence on the orientation observed.

For the compounds **1**, **2** the location of the second C atom (first one is linkage C atoms of two cages) is very crucial since it defines the exact isomer and in both cases the positions of second C atoms were established unambiguously by using both the VCD method [14] and BHD analysis.[15] To get the *Prostructure* all cage atoms (except Ni) are described as boron and H atoms are allowed positional refinement. Vertex-to-Centroid distances were compared within each cage of the Prostructure. For compound **1**, this clearly shows (Table 2.2.1.1) that the second C atom (where C1 is linkage carbon atom) is at vertex 2 as VCD from 2 is shorter than VCD from 9 or others by >0.138 Å for the nickelacarborane cage and VCD from 2′ (C1′ is linkage carbon atom) is shorter than VCD from 9 or others by >0.137 Å for the carborane cage. This is consistent with BHD analysis; the shortest BHD is at 2 and 2′ for the nickelacarborane and carborane respectively (Table 2.2.1.2). On the other hand for compound **2** the second C atom (C4 linkage carbon atom) is at vertex 1 as VCD from 1 is shorter than VCD from 10 or others by >0.074 Å for the nickelacarborane cage and VCD from 2′ (C1′ linkage carbon atom) is shorter than VCD from 6 or others by >0.048 Å for the carborane cage (Table 2.2.1.1). This is consistent with BHD analysis; the shortest BHD is at 1 and 2′ for nickelacarborane and carborane respectively (Table 2.2.1.2). Both VCD and BHD analysis have been used routinely for all compounds discussed in this Chapter. Additionally, Table 2.2.1.1 summarizes some key structural parameters of compound **1** and **2**.

Table 2.2.1.1 Vertex-to-centroid distances (Å) in Prostructures of [1-(1′-1′,2′-*closo*-$C_2B_{10}H_{11}$)-3-dppe-3,1,2-*closo*-$NiC_2B_9H_{10}$] (**1**) and [2-(1′-1′,2′-*closo*-$C_2B_{10}H_{11}$)-4-dppe-4,1,2-*closo*-$NiC_2B_9H_{10}$] (**2**).

Vertex	Compound **1**		Compound **2**	
	Metallated cage	Carborane cage	Metallated cage	Carborane cage
1	1.623(3)	1.615(7)	1.5980(19)	1.6010(19)
2	1.521(3)	1.534(4)	2.2054(6)	1.6045(17)
3	2.3330(9)	1.706(4)	1.705(2)	1.703(2)
4	1.673(3)	1.703(3)	1.5383(18)	1.692(3)
5	1.694(4)	1.686(3)	1.6929(17)	1.698(2)
6	1.726(4)	1.708(3)	1.7341(16)	1.6487(18)
7	1.701(4)	1.693(3)	1.6837(17)	1.689(2)
8	1.732(4)	1.690(3)	1.7330(16)	1.6831(19)
9	1.659(3)	1.671(4)	1.687(2)	1.6717(19)
10	1.697(3)	1.686(4)	1.672(2)	1.694(2)
11	1.671(3)	1.698(3)	1.7030(17)	1.695(3)
12	1.676(4)	1.682(4)	1.673(2)	1.681(3)

Table 2.2.1.2 Boron-hydrogen distances (Å) in Prostructures [1-(1′-1′,2′-*closo*-$C_2B_{10}H_{11}$)-3-dppe-3,1,2-*closo*-$NiC_2B_9H_{10}$] (**1**) and [2-(1′-1′,2′-*closo*-$C_2B_{10}H_{11}$)-4-dppe-4,1,2-*closo*-$NiC_2B_9H_{10}$] (**2**)

Vertex	Compound **1**		Compound **2**	
	Metallated cage	Carborane cage	Metallated cage	Carborane cage
1	-	-	0.35(3)	-
2	0.45(4)	0.39(4)	-	0.68(2)
3	-	1.09(4)	1.14(3)	1.06(2)
4	1.07(3)	1.17(3)	-	1.05(3)
5	1.09(3)	0.98(3)	1.11(2)	1.06(2)
6	1.14(3)	1.09(3)	1.07(2)	0.895(19)
7	1.13(3)	1.11(3)	1.09(2)	1.06(2)
8	1.11(8)	1.12(3)	1.12(2)	1.109(19)
9	1.09(3)	1.12(4)	1.03(3)	1.08(2)
10	1.14(3)	1.08(3)	1.08(3)	1.05(2)
11	1.15(3)	1.10(3)	1.112(19)	1.05(3)
12	1.08(3)	1.12(3)	1.08(2)	1.07(3)

Table 2.2.1.3 Selected geometric parameters (Å, º) for [1-(1′-1′,2′-*closo*-$C_2B_{10}H_{11}$)-3-dppe-3,1,2-*closo*-$NiC_2B_9H_{10}$] (**1**) and [2-(1′-1′,2′-*closo*-$C_2B_{10}H_{11}$)-4-dppe-4,1,2-*closo*-$NiC_2B_9H_{10}$] (**2**).

Compound **1**		Compound **2**	
Ni3—C1	2.337(3)	Ni4—C1	2.0983(13)
Ni3—C2	2.112(2)	Ni4—B3	2.0373(16)
Ni3—B4	2.129(3)	Ni4—B8	2.1688(14)
Ni3—B7	2.090(3)	Ni4—B9	2.085(9)
Ni3—B8	2.124(3)	Ni4—B5	2.0826(17)
Ni3—P1	2.2008(7)	Ni4—P1	2.1802(5)
Ni3—P2	2.1947(7)	Ni4—P2	2.1461(5)
P—C_{Ph}	1.815(3) –1.830(3)	P—C_{Ph}	1.8248(13) –1.8258(15)
P1—C_{113}	1.849(2)	P1—C_{101}	1.8651(14)
P2—C_{213}	1.824(2)	P2—C_{201}	1.8390(16)
P1—Ni3—P2	86.60(3)	P1—Ni4—P2	86.233(17)
C_{113}—C_{213}	1.528(4)	C_{101}—C_{201}	1.534(3)
C1—C2	1.592(4)	C1—C2	1.6382(17)
C1—B4	1.716(4)	C1—B3	1.7747(19)
C1—B5	1.703(3)	C1—B5	1.660(3)
C1—B6	1.715(3)	C1—B6	1.728(2)
C2—B6	1.765(4)	C2—B3	1.7914(19)
C2—B7	1.747(4)	C2—B6	1.722(2)
C2—B11	1.723(3)	C2—B7	1.7280(19)
C1—C1′	1.529(4)	C2—B11	1.729(3)
C1′—C2′	1.650(3)	C2—C1′	1.526(2)
C1′—B3′	1.740(3)	C1′—C2′	1.680(3)
C1′—B4′	1.732(4)	C1′—B3′	1.7328(19)
C1′—B5′	1.732(2)	C1′—B4′	1.724(2)
C1′—B6′	1.745(4)	C1′—B5′	1.732(2)
C2′—B3′	1.712(4)	C1′—B6′	1.705(3)
C2′—B6′	1.709(4)	C2′—B3′	1.738(3)
C2′—B7′	1.704(4)	C2′—B6′	1.714(2)
C2′—B11′	1.700(4)	C2′—B7′	1.718(2)
-	-	C2′—B11′	1.730(3)

2.2.1.1 Thermal isomerisation of compound 1 to compound 2

Heating compound **1** in refluxing THF for two hours, during which the green solution changed to red purple, followed by chromatography gave a red-purple product in 70% yield.

After spectroscopic characterisations ($^{11}B\{^1H\}$, $^{31}P\{^1H\}$, ^1H), the red-purple product was shown to be compound **2**.

We assume that the metal-phosphine fragment in **2** is able to undergo unrestricted rotation at room temperature because the nickelacarborane cage had isomerised with the carborane substituent moving away from the Ni-bonded face, and a crystallographic study (Figure 2.2.1.4) confirmed this to be the case. In short form, compound **2** is 2-C_2B_{10}-4,1,2-NiC_2B_9, *i.e.* the nickelacarborane portion of crowded molecule **1** has undergone a 3,1,2- to a 4,1,2-NiC_2B_9 isomerisation to relieve that crowding (note that the conventional numbering system for metallacarboranes requires the substituted cage C atom to be at vertex 1 in the 3,1,2- isomer **1** but at vertex 2 in the 4,1,2- isomer **2**). That it is likely that compound **2** forms from the initial compound **1** in the synthesis is supported by the fact that repeated chromatography of green **1** always shows a small amount of a faster-moving red-purple band and freshly prepared NMR samples of **1** always show **2** as a minor impurity.

2.2.2 Synthesis of [8-(1′-1′,2′-*closo*-$C_2B_{10}H_{11}$)-2-dmpe-2,1,8-*closo*-$NiC_2B_9H_{10}$] (3)

Compound **3** is synthesised by the same procedure as **1**, but metalation was carried out using $\{Ni(dmpe)\}^{2+}$ fragment. After chromatographic analysis a yellow-orange compound **3** was observed in 35% yield.

The mass spectrum of **3** contains an envelope centred on *m/z* 483.4 (M^+) (MW = 483.45 g mol^{-1}), and elemental analysis is in good agreement with that expected for $C_{10}H_{37}B_{19}NiP_2$. From microanalysis and mass spectrometry it was evident that the $\{Ni(dmpe)\}^{2+}$ fragment had added to the $[\mathbf{I}\text{-}H]^{2-}$ dianion as expected.

The $^{11}B\{^1H\}$ NMR spectrum of **3** was clearly different to that for **1**and **2** and consists of a 2:1:1:1:8:2:1:1:2 pattern from high frequency to low frequency between δ -3.6 and -20.3 ppm, but spectroscopy alone does not define the isomer type to which **3** belongs.

Both CH_{cage} resonances appear as singlets in the ^1H spectrum with that for the carborane (δ *ca*. 2.2 ppm) overlapping the signals from the -CH_2-CH_2- bridge of the dmpe ligand. There are two resonances for the CH_3 groups (overlapping doublets in the ^1H spectrum and singlets in the $^1H\{^{31}P\}$ spectrum) and a singlet in the $^{31}P\{^1H\}$ spectrum, together suggesting that at room temperature the Ni(dmpe) unit is undergoing rapid rotation about an asymmetric carborane cage. As was the case with compound **2**, cooling the sample arrested that rotation ($T_{coalescence}$ = 241 K) affording, for **3**, mutual doublets in the $^{31}P\{^1H\}$ spectrum at δ 48.9 and 45.8 ppm, $^2J_{PP}$ = 48.6 Hz (Figure 2.2.2.1). The activation energy for rotation was estimated as *ca*. 38 kJ mol^{-1}.

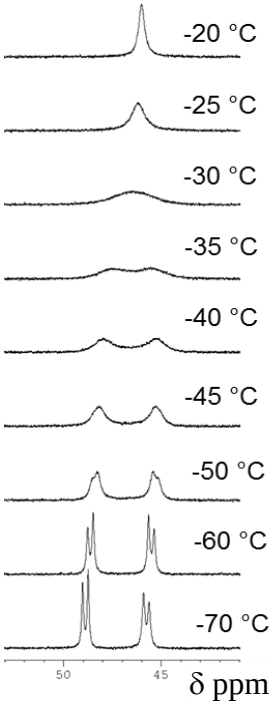

Figure 2.2.2.1 Variable temperature $^{31}P\{^{1}H\}$ NMR spectra of compound **3** in CD_2Cl_2.

Crystals of **3** were grown by diffusion of petroleum ether 40-60 and a CH_2Cl_2 solution of **3** at 5 °C. Analysis by *X*-ray diffraction shows **3** to be [8-(1′-1′,2′-*closo*-$C_2B_{10}H_{11}$)-2-dmpe-2,1,8-*closo*-$NiC_2B_9H_{10}$].

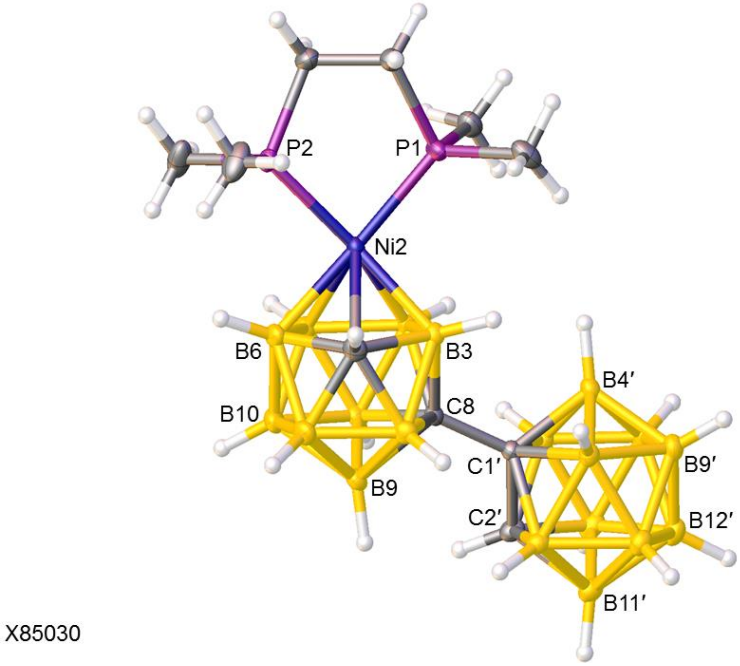

Figure 2.2.2.2 Molecular structure of [8-(1′-1′,2′-*closo*-$C_2B_{10}H_{11}$)-2-dmpe-2,1,8-*closo*-$NiC_2B_9H_{10}$] (**3**).

From both VCD and BHD analysis of the Prostructure of compound **3**, the positions of C atoms were identified. From the VCD method, for the nickelacarborane cage, having C8 as linkage carbon atom, the C1 atom is at vertex 1 as VCD from 1 is shorter than VCD from 6 or others by >0.047 Å and for the carborane cage with C1′ as linkage carbon atom, VCD from 2′ is shorter than VCD from 3 or others by >0.28 Å. Note that VCD from 3 in the carborane cage is also short as there is partial disorder of the carbon atom between vertices 2 and 3. This is consistent with BHD analysis; the shortest BHD is at 1 and 2′, 3′ for nickelacarborane and carborane respectively (Table 2.2.2.3).

Although the molecule is partly disordered (only the major occupancies are shown in Figure 2.2.2.2) the key result of the study is clear; the nickelacarborane cage has isomerised into a 2,1,8-NiC_2B_9 icosahedron, making compound **3** overall 8-C_2B_{10}-2,1,8-NiC_2B_9 in short form. In the metallacarborane the {NiPP} fragment adopts an orientation with θ, the dihedral angle between NiP1P2 and C1B9B12 planes, being 78.97(7)º, close to the expected [10] 90º.

Table 2.2.2.3 Vertex-to-centroid and boron-hydrogen distances (Å) in Prostructure of [8-(1′-1′,2′-*closo*-$C_2B_{10}H_{11}$)-2-dmpe-2,1,8-*closo*-$NiC_2B_9H_{10}$] (**3**).

Vertex	VCD distances		BHD distances	
	Metallated cage	Carborane cage	Metallated cage	Carborane cage
1	1.601(3)	1.6022(19)	0.47(3)	-
2	2.2191(11)	1.608(3)	-	0.66(2)
3	1.687(3)	1.636(2)	1.11(2)	0.81(4)
4	1.707(4)	1.695(3)	1.10(2)	1.16(3)
5	1.696(3)	1.685(3)	1.12(3)	1.04(3)
6	1.647(2)	1.696(3)	1.06(2)	1.07(3)
7	1.718(3)	1.696(3)	1.06(3)	1.09(3)
8	1.5635(19)	1.688(3)	-	1.05(3)
9	1.696(3)	1.674(3)	1.12(3)	1.09(3)
10	1.668(3)	1.680(2)	1.09(3)	1.12(2)
11	1.707(2)	1.688(3)	1.07(2)	1.05(3)
12	1.690(3)	1.675(2)	1.11(3)	1.09(2)

2.2.3 Synthesis of [1-(1′-1′,2′-*closo*-$C_2B_{10}H_{11}$)-3,3-$(PMe_3)_2$-3,1,2-*closo*-$NiC_2B_9H_{10}$] (4), [7-(1′-1′,2′-*closo*-$C_2B_{10}H_{11}$)-10-(PMe_3)-7,8-*nido*-$C_2B_9H_{10}$] (5) and [1-(1′-1′,2′-*closo*-$C_2B_{10}H_{11}$)-3-Cl-3-PMe_3-8-PMe_3-3,1,2-*closo*-$NiC_2B_9H_9$] (6)

Compound **4** is synthesised by the same procedure as **1**, but metalation was carried out using $\{Ni(PMe_3)_2\}^{2+}$ fragment as shown in Figure 2.2.3.1. After chromatographic analysis a green product **4** in 23% yield and a trace amount lavender purple product were observed.

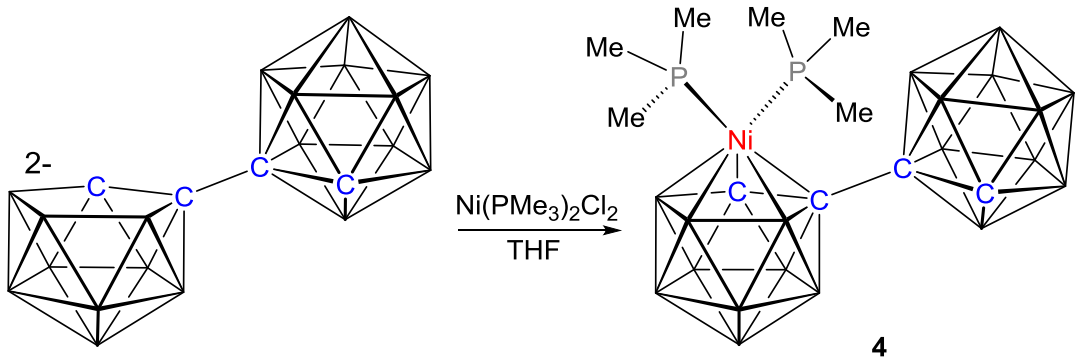

Figure 2.2.3.1 Metallation of [$HNMe_3$]**I** with *cis*-$Ni(PMe_3)_2Cl_2$.

The MS of **4** contains an envelope centred on *m/z* 485.3 (M^+) (MW = 485.47 g mol^{-1}), and the elemental analysis is in good agreement with that expected for $C_{10}H_{39}B_{19}NiP_2$.

In the ^1H spectrum of compound **4** there are two broad resonances with the integral of one each at δ 3.99 ppm assigned to the CH_{cage} carborane and δ 1.55 ppm corresponding to the CH_{cage} nickelacarborane which appears as doublet ($^3J_{PH}$ = 10.8 Hz) along with two sets of doublets at δ 1.55 ($^2J_{PH}$ = 9.6 Hz), 1.49 ($^2J_{PH}$ = 8.4 Hz) ppm. The CH_{cage} nickelacarborane appears as doublet due to coupling with P nucleus and this collapses to a singlet in the $^1H\{^{31}P\}$ NMR spectrum. Similarly methyl resonances give two singlets in the $^1H\{^{31}P\}$ NMR spectrum confirming coupling of methyl protons with phosphorus.

The $^{31}P\{^1H\}$ NMR spectrum of compound **4** reveals two mutual doublets with coupling constant $^2J_{PP}$ = 43.3 Hz which indicates that two phosphorus atoms are magnetically

inequivalent. Therefore it implies no isomerisation and the carborane moiety remains in the top belt at C1 position.

Crystals of **4** were grown by diffusion of petroleum ether 40-60 and a CH_2Cl_2 solution of **4** at 5 °C. Single crystal by *X*-ray diffraction shows **4** to be the expected [1-(1′-1′,2′-*closo*-$C_2B_{10}H_{11}$)-3,3-(PMe_3)$_2$-3,1,2-*closo*-$NiC_2B_9H_{10}$] (Figure 2.2.3.2).

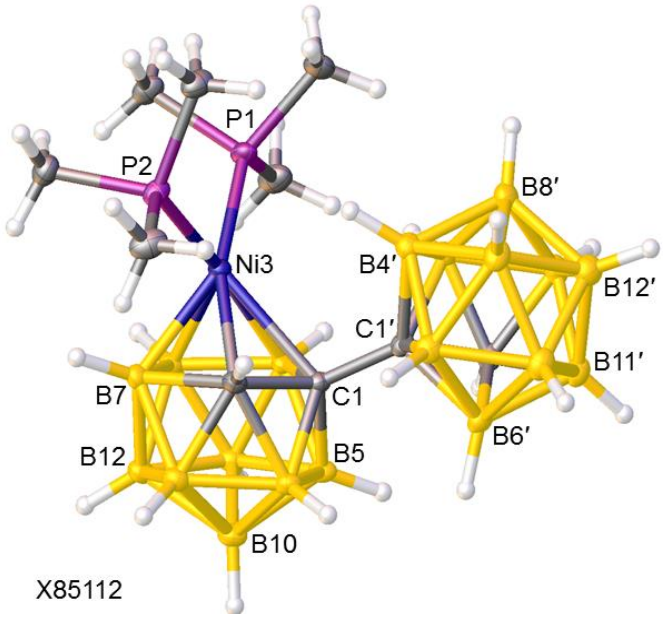

Figure 2.2.3.2 Solid state structure of [1-(1′-1′,2′-*closo*-$C_2B_{10}H_{11}$)-3,3-(PMe_3)$_2$-3,1,2-*closo*-$NiC_2B_9H_{10}$] (**4**).

In the solid state structure there is disorder between vertices 2 and 4 of the nickelacarborane cage [that shown is (just) the major component] but this does not alter the isomer type. The plane through Ni3P1P2 is inclined at 11.74(6)º to that through B5B6B11B12B9 (similar to the situation in **1**) reflecting the crowding between the carborane substituent on C1 and the PMe_3 ligands which prevents {NiP_2} rotation at room temperature.

Crystallisation of the lavender purple product revealed both lavender purple and colourless crystals. The colourless material (**5**) was recovered in insufficient quantity for full characterisations. Subsequent multiple batches of the same reaction gave enough material for spectroscopic and crystallographic characterisations of **5**. The lavender purple material, compound **6**, however, was analysed by mass spectrometry, NMR spectroscopy and *X*-ray diffraction.

The MS of compound **5** shows an envelope centered on *m/z* 350.3 (M^+) [MW = 350.7 g mol^{-1}] but elemental analysis was not possible due to trace amount.

In the $^{11}B\{^1H\}$ spectrum of **5** the two distinct lowest frequency resonances at δ -27.9 and -29.2 ppm are characteristic resonances arising from B10 and B1 of a {*nido*-C_2B_9} cage.[16] Additionally, there are multiple overlapping resonances arising from a {*closo*-C_2B_{10}} cage.

In the ^1H spectrum of compound **5** is a doublet $^2J_{PH}$ = 12.0 Hz assigned to methyl protons which collapses to a singlet in the $^1H\{^{31}P\}$ spectrum indicating coupling of methyl protons with ^{31}P nucleus. There are also two broad singlets characteristics of CH_{cage} resonances, one at high frequency δ 4.51 ppm corresponding to CH_{cage} *closo*-carborane and the other at δ 2.43 ppm assigning to CH_{cage} *nido*-carborane, consistent with the $^{11}B\{^1H\}$ spectrum. Additionally a broad singlet at δ -1.80 ppm is assigned to the bridging hydrogen of the nido cage.

The $^{31}P\{^1H\}$ spectrum reveals a quartet resonance at δ -6.9 ppm with coupling constant $^1J_{PB}$ = 151.2 Hz.

Colourless crystals of **5** were developed by diffusion of petroleum ether 40-60 and a CH_2Cl_2 solution of purple product at 5 °C. Single crystal *X*-ray diffraction reveals **5** as [7-(1′-1′,2′-*closo*-$C_2B_{10}H_{11}$)-10-(PMe_3)-7,8-*nido*-$C_2B_9H_{10}$].

The crystallographic analysis justifies all these spectroscopic features and the colourless nature of the species. The molecule is partly disordered, only the major component is shown in Figure 2.2.3.3 and the key result of the study is obvious, metallation has not occurred. At B10 position is a PMe_3 group linked to a {7,8-*nido*-C_2B_9} cage which is joined to another {*closo*-C_2B_{10}} unit by a C–C linkage. A μ-H is positioned at B10 and B11 in the nido cage.

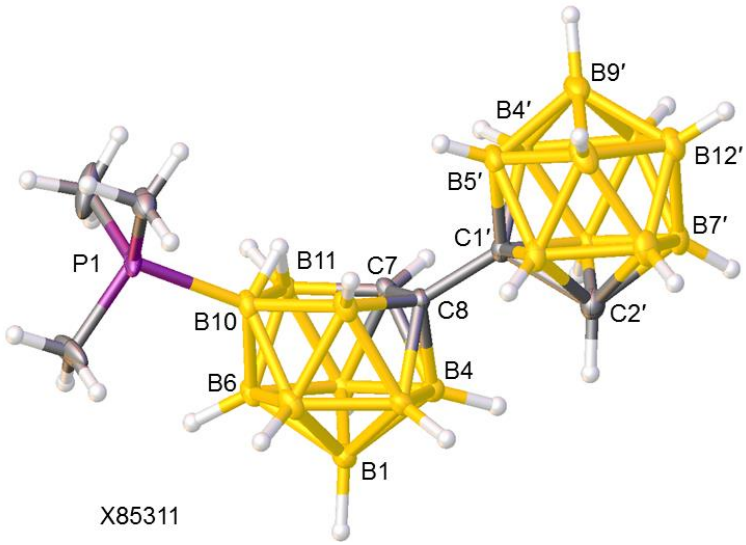

Figure 2.2.3.3 Solid state structure of [7-(1′-1′,2′-*closo*-$C_2B_{10}H_{11}$)-10-(PMe_3)-7,8-*nido*-$C_2B_9H_{10}$] (**5**).

Moving on from colourless to lavender purple species, the mass spectrum of **6** displays a parent ion centered on *m/z* 519.9 (M^+) [MW = 519.91 g mol^{-1}] which is higher mass compared to **4**. This gives an idea this may be a derivative of compound **4** but elemental analysis was not possible due to trace amount.

In the ^1H spectrum are two broad singlets characteristic of CH_{cage} resonances, one of which is at unusually high frequency, δ 6.13 ppm, along with two sets of doublets at δ 1.74 ppm with coupling constant $^2J_{PH}$ = 12.0 Hz and at δ 1.36 ppm with coupling constant $^2J_{PH}$ = 15.6 Hz assigning to two methyl groups; these collapses to two singlets in the $^1H\{^{31}P\}$ spectrum.

In the $^{31}P\{^1H\}$ spectrum is a 1:1:1:1 quartet characteristic of P bound to B ($^1J_{PB}$ = 145.8 Hz) and a singlet. A ^1H-^{31}P HMBC experiment allowed the CH_3 resonance at δ 1.74 ppm to be associated with the quartet ^{31}P resonance, and that at δ 1.36 ppm to be associated with the singlet ^{31}P resonance.

Single crystals of **6** were grown by diffusion of petroleum ether 40-60 and a $CDCl_3$ solution of purple product at 5 °C. Solid state crystallographic analysis shows **6** as [1-(1′-1′,2′-*closo*-$C_2B_{10}H_{11}$)-3-Cl-3-PMe_3-8-PMe_3-3,1,2-*closo*-$NiC_2B_9H_9$].

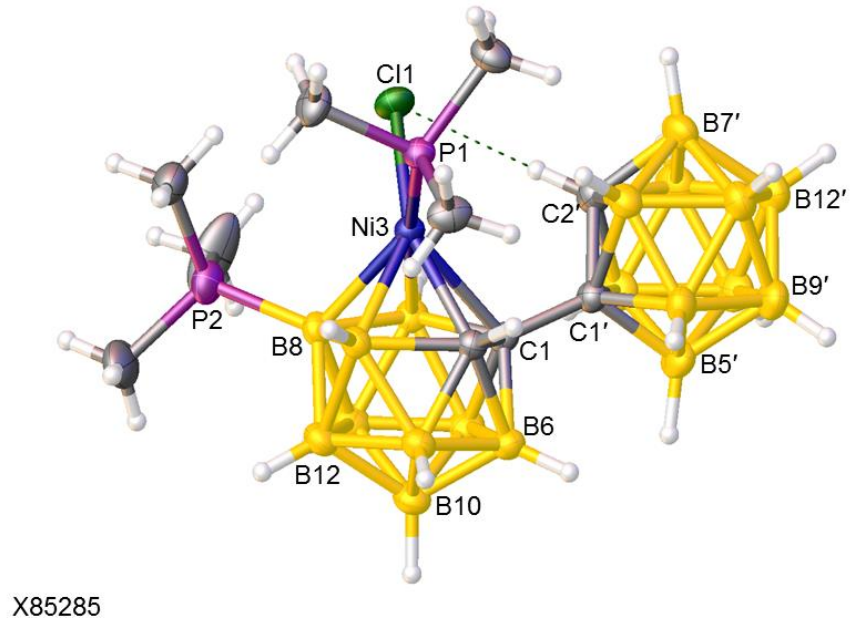

Figure 2.2.3.4 Molecular structure of [1-(1′-1′,2′-*closo*-$C_2B_{10}H_{11}$)-3-Cl-3-PMe_3-8-PMe_3-3,1,2-*closo*-$NiC_2B_9H_9$] (**6**).

The diffraction study (Figure 2.2.3.4) rationalises the spectroscopic findings. In the nickelacarborane cage (which is of 3,1,2-NiC_2B_9 architecture) the metal is ligated by one PMe_3 group and one Cl atom, the latter showing H-bonding to the C*H* atom of the carborane substituent on C1 [H2′…Cl, 2.60(2) Å; C2′–H2′…Cl 147.6(15)º; H2′…Cl–Ni3 77.9(4)º], the origin of the high-frequency resonance of the C*H* atom. A PMe_3 group on B8 completes the molecule and thus the trace compound **6** is identified as [1-(1′-1′,2′-*closo*-$C_2B_{10}H_{11}$)-3-Cl-3,8-$(PMe_3)_2$-3,1,2-*closo*-$NiC_2B_9H_9$]. A similar single-cage compound, [3-Cl-3,8-$(PPh_3)_2$-3,1,2-*closo*-$NiC_2B_9H_{10}$], afforded by the reaction between [10-PPh_3-7,8-*nido*-$C_2B_9H_{11}$]$^-$ and *cis*-[$NiCl_2(PPh_3)_2$], has been reported by Hawthorne.[2a] We believe that a similar reaction is the origin of compound **6** involving a phosphacarborane anion which is the deprotonated form of the colourless co-product (Figure 2.2.3.5).

One interesting point is that in **6** the nickelacarborane CH_{cage} atom appears as a singlet in the ^{1}H NMR spectrum, whereas in the other 3,1,2- species **1** and **4** it couples to one of the P atoms. The fact that in **6** the sole phosphine is *cis* to the CH_{cage} suggests that in **1** and **4** the coupling is to the *trans* phosphine.

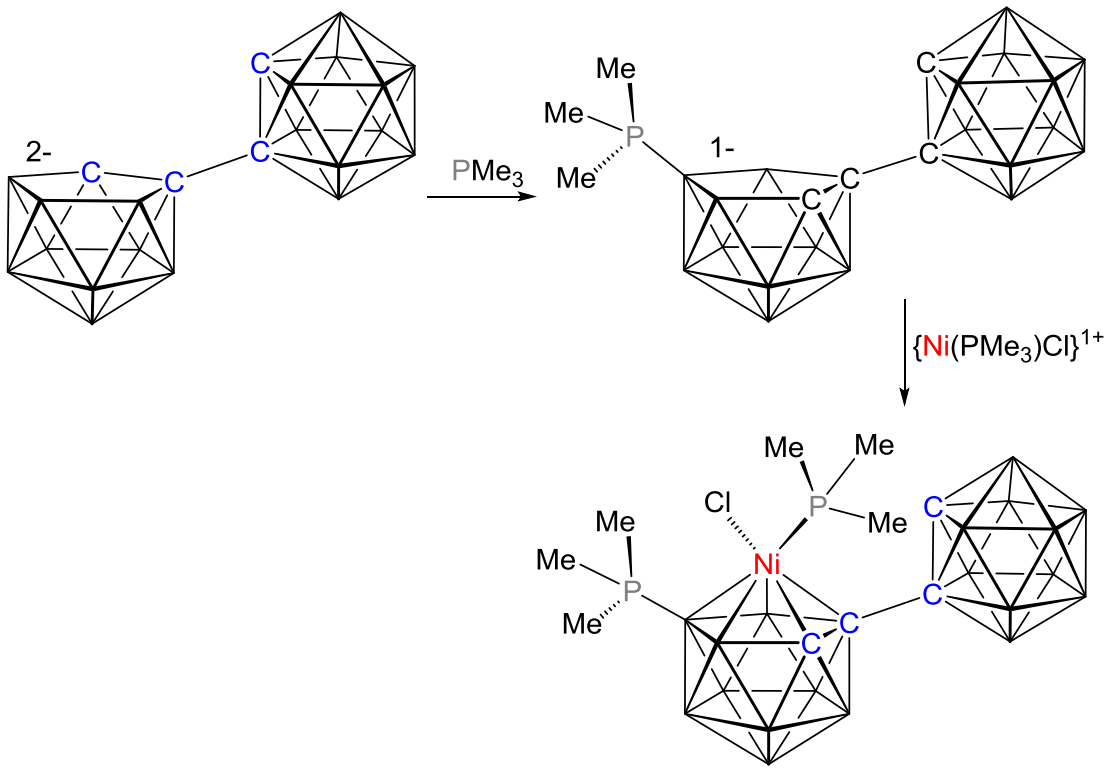

Figure 2.2.3.5 Possible mechanism of formation of **6**.

2.2.4 Synthesis of [1-(1′-1′,2′-*closo*-$C_2B_{10}H_{11}$)-3,3-$(PMe_2Ph)_2$-3,1,2-*closo*-$NiC_2B_9H_{10}$] (7) and [7-(1′-1′,2′-*closo*-$C_2B_{10}H_{11}$)-10-(PMe_2Ph)-7,8-*nido*-$C_2B_9H_{10}$] (8)

Compound **7** was synthesised by the same procedure as **1**, but metalation was carried out using *cis*-$[Ni(PMe_2Ph)_2Cl_2]$. After chromatographic separation a green product, **7** in 25% yield and a trace amount lavender purple product were isolated.

The EIMS of **7** contains an envelope centred on *m/z* 609.3 (M^+) (MW = 609.61 g mol^{-1}), and the elemental analysis is in good agreement with that expected for $C_{20}H_{43}B_{19}NiP_2$.

In the ^1H spectrum of compound **7** there are, in addition to resonances arising from phenyl moieties, two broad resonances one of which is a singlet assigned to the CH_{cage} carborane and the other due to CH_{cage} nickelcarborane a doublet ($^3J_{PH}$ = 14.0 Hz), presumably due to coupling to the *trans*-phosphine. Furthermore, there are four sets of doublets of integral-3 for the methyl protons defining asymmetry in the cage environment. All of these last resonances (CH_{cage} nickelacarborane and 4 CH_3) give corresponding singlets in the $^1H\{^{31}P\}$ NMR spectrum confirming coupling with P nucleus.

The $^{31}P\{^1H\}$ NMR spectrum of compound **7** reveals two mutual doublets with coupling constant $^2J_{PP}$ = 39.7 Hz which correspond to two inequivalent phosphorus environments. This implies the no isomerisation occurred in the nickelacarborane cage.

Crystals of **7** were grown by diffusion of petroleum ether 40-60 and a THF solution of green product at 5 °C. Crystallographic analysis shows **7** to be the expected [1-(1′-1′,2′-*closo*-$C_2B_{10}H_{11}$)-3,3-$(PMe_2Ph)_2$-3,1,2-*closo*-$NiC_2B_9H_{10}$].

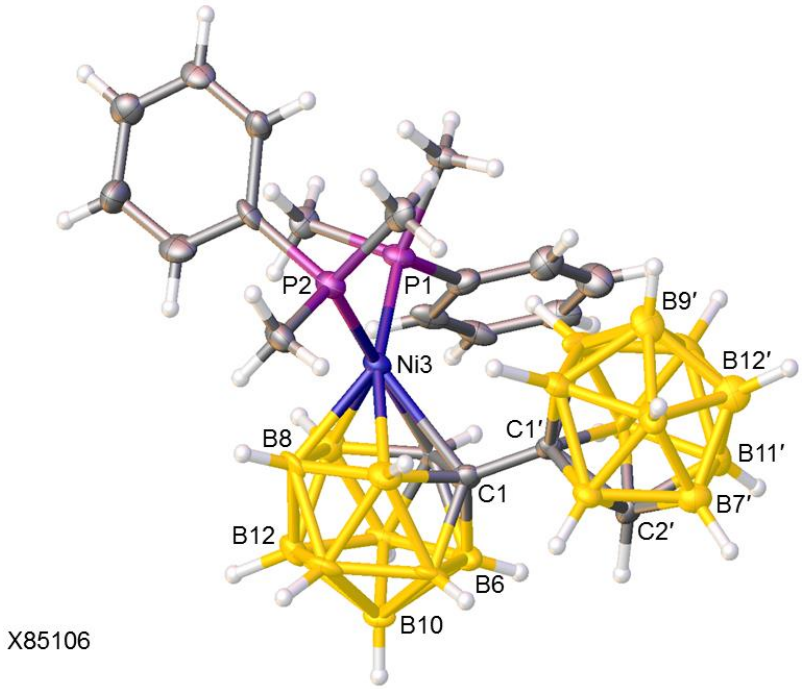

Figure 2.2.4.1 Molecular structure of [1-(1′-1′,2′-*closo*-$C_2B_{10}H_{11}$)-3,3-$(PMe_2Ph)_2$-3,1,2-*closo*-$NiC_2B_9H_{10}$] (**7**).

The crystallographic study of **7** (Figure 2.2.4.1) is fully consistent with the spectral analysis. There is some disorder between vertices 2 and 4 of the nickelacarborane cage with the major component shown in the Figure. The key features of the structure resemble those of compounds **1** and **4**; the NiP1P2 plane is twisted away from its expected [10] orientation perpendicular to the plane through B6B8B10 [θ = 55.0(2)º] by the steric demands of the carborane substituent bonded to C1 and also bent back from perpendicular to the plane through B5B6B11B12B9 [by 12.2(2)º] for the same reason.

Crystallisation of the lavender purple product gave both lavender purple and colourless crystals. The colourless material (**8**) was recovered in sufficient quantity for complete characterisation.

Initial characterisation, mass spectrum with an envelope centred on *m/z* 412.7 (M^+) [MW = 412.77 g mol^{-1}] and elemental analysis of **8** is in good agreement for $C_{12}H_{32}B_{19}P$ being a similar nido-phosphine species to compound **5**.

The $^{11}B\{^1H\}$ spectrum of **8** consists of two separate low frequency resonances at δ -33.4 and -34.2 ppm which corresponds to the B1 and B10 of the {*nido*-C_2B_9} cage similar to

compound **5**. In addition, there are several overlapping resonances arising from the {*closo*-C_2B_{10}} unit.

The ^{1}H spectrum of compound **8** consists of, in addition to resonances arising from phenyl ring and methyl protons, two broad singlets characteristic of CH_{cage} *closo*-carborane and *nido*-carborane which is consistent with the $^{11}B\{^{1}H\}$ spectrum. The doublet resonances of methyl protons gives two singlets with integral-3 in the $^{1}H\{^{31}P\}$ spectrum. Additionally a broad singlet at δ -1.93 ppm in $^{1}H\{^{11}B\}$ spectrum identifies the bridging hydrogen of the nido cage.

The $^{31}P\{^{1}H\}$ spectrum reveals a 1:1:1:1 pattern resonances at δ -8.8 ppm with coupling constant, $^{1}J_{PB}$ = 148.5 Hz defining phosphorus connected to a boron in the nido cage.

Colourless crystals of **8** were developed by diffusion of petroleum ether 40-60 and a $CDCl_3$ solution of the purple mixture at 5 °C. Analysis by *X*-ray diffraction shows **8** to be the expected [7-(1′-1′,2′-*closo*-$C_2B_{10}H_{11}$)-10-(PMe_2Ph)-7,8-*nido*-$C_2B_9H_{10}$] (Figure 2.2.4.2).

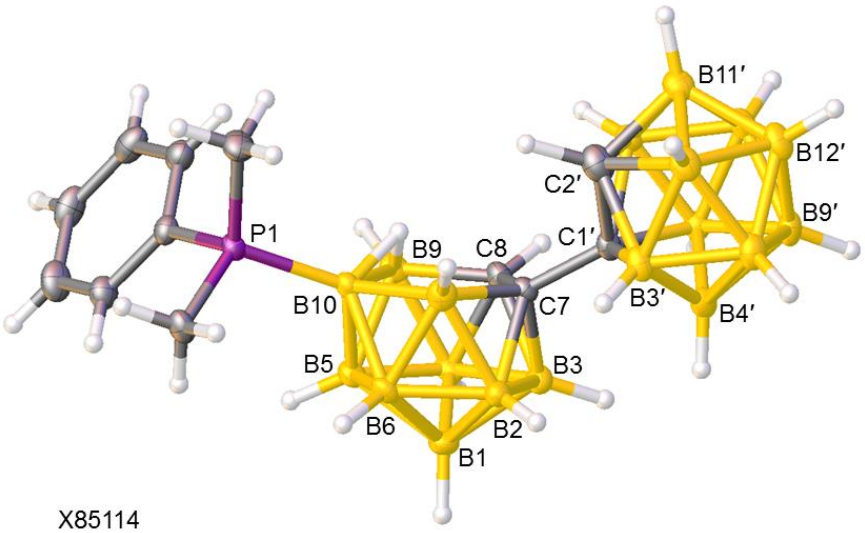

Figure 2.2.4.2 Molecular structure of [7-(1′-1′,2′-*closo*-$C_2B_{10}H_{11}$)-10-(PMe_2Ph)-7,8-*nido*-$C_2B_9H_{10}$] (**8**).

The single crystal XRD analysis confirms that compound **8** is analogous to nido-phosphine derivative **5**. The unprimed cage has not been metallated, rather it has a PMe_2Ph group bound at B10 and a μ-H atom between B9 and B10.

Following crystallisation of the lavender purple mixture, not enough lavender purple material was recovered for complete analysis. However, the $^{31}P\{^{1}H\}$ spectrum of the mixture of purple and colourless material consists of a quartet (δ -5.3 ppm, 1:1:1:1 ratio, $^{1}J_{PB}$ = 137.3 Hz) and singlet (δ -15.7 ppm), both of integral-1, plus another quartet (δ -8.8 ppm, 1:1:1:1 ratio) of integral-3 (Figure 2.2.4.3). The latter quartet corresponds to compound **8**. Thus, the spectroscopic evidence strongly suggests that the lavender material is analogous to compound **6**.

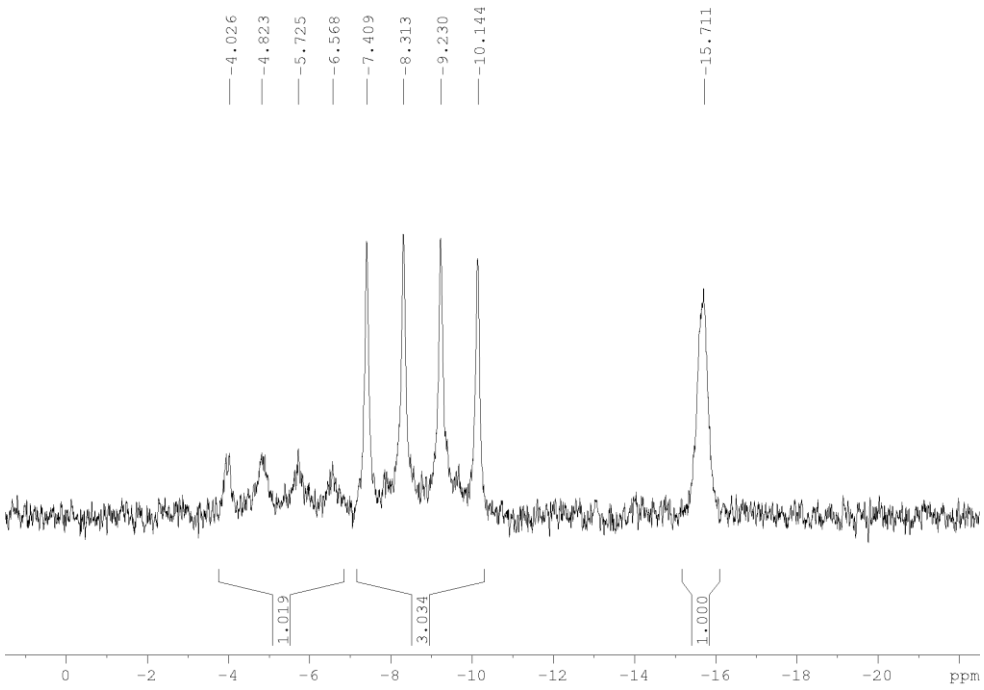

Figure 2.2.4.3 $^{31}P\{^{1}H\}$ NMR ($CDCl_3$) spectrum of the mixture of purple and colourless products.

2.2.5 Synthesis of [2-(1′-1′,2′-*closo*-$C_2B_{10}H_{11}$)-4,4-$(PMePh_2)_2$-4,1,2-*closo*-$NiC_2B_9H_{10}$] (9)

Compound **9** was made in the same way as **1**, where metallation was performed using *cis*-[$Ni(PMePh_2)_2Cl_2$]. After the usual workup and TLC only olive green **9** in 20% yield was isolated.

The mass spectrum of **9** consists an envelope centred on *m/z* 733.4 (M^+) (MW = 733.76 g mol^{-1}), and the elemental analysis fits well for $C_{30}H_{45}B_{19}NiP_2 \cdot 0.5CH_2Cl_2$, for which there is evidence from the ^1H NMR spectrum recorded in [$(CD_3)_2CO$].

The ^1H NMR spectrum of **9** shows two broad singlet resonances with the integral-1 (CH_{cage} carborane, CH_{cage} nickelacarborane). There are also resonances arising from phenyl rings and an apparent triplet (overlapping of two doublets) corresponding to methyl protons. The latter one gives two single integral-3 singlets in the $^1H\{^{31}P\}$ spectrum confirming proton coupling with P nucleus.

The $^{31}P\{^1H\}$ NMR spectrum of compound **9** reveals a single singlet resonance which implies isomerisation of the nickelacarborane has occurred.

Unfortunately *X*-ray quality crystals of **9** could not be obtained despite trying several different solvent combinations, however the isomer was determined by comparing $^{11}B\{^1H\}$ NMR spectra of compounds **2** (4,1,2-isomer) and **3** (2,1,8-isomer) with **9**. The nickelacarborane cage is the 4,1,2- isomer and not the 2,1,8- isomer from the similarity of the $^{11}B\{^1H\}$ NMR spectra of **9** and **2** and the dissimilarity of the spectra of **9** and **3** (Figure 2.2.5.1).

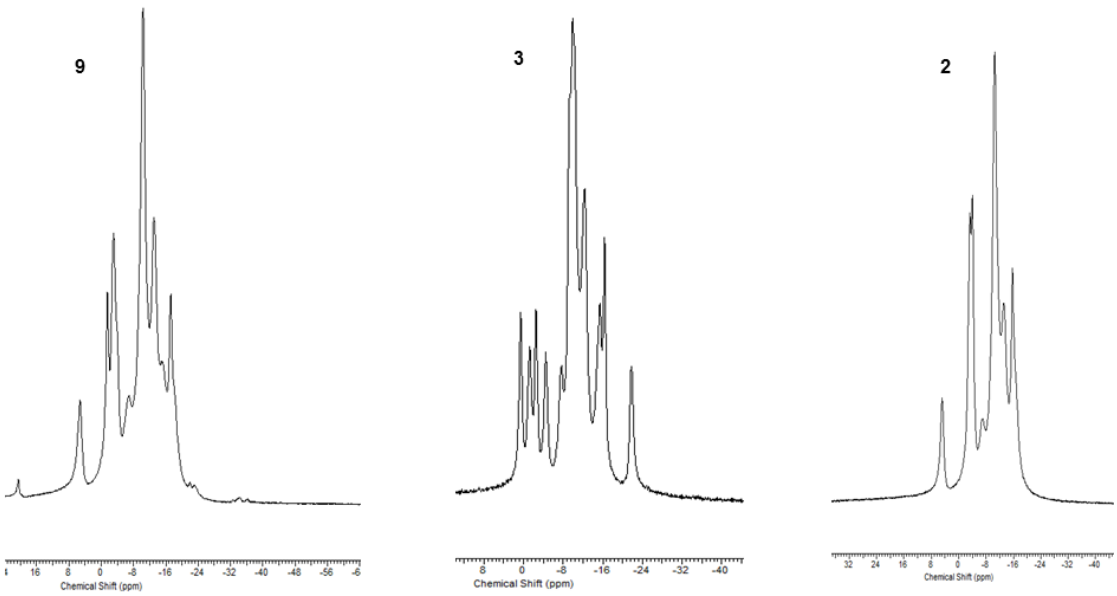

Figure 2.2.5.1 Comparison of $^{11}B\{^{1}H\}$ NMR spectra of **9** with **2**, **3**.

2.2.6 Isomerisation behaviour for chelating phosphines and unidentate phosphines

Summarising the results so far, addition of $\{Ni(dppe)\}^{2+}$ to $[\mathbf{I}]^{2-}$ results in both unisomerised, 1-C_2B_{10}-3,1,2-NiC_2B_9 (**1**) and isomerised, 2-C_2B_{10}-4,1,2-NiC_2B_9 (**2**) products, and **1** is easily converted into **2** with gentle heat, whilst in contrast addition of $\{Ni(dmpe)\}^{2+}$ to $[\mathbf{I}\text{-H}]^{2-}$ results in the differently isomerised 8-C_2B_{10}-2,1,8-NiC_2B_9 (**3**) as the only isolated product. What causes these isomerisations and why do the different chelating diphosphine result in different isomerised products?

Clearly steric crowding between the $C_2B_{10}H_{11}$ substituent on C1 and the diphosphine ligand on Ni3 of an unisomerised 3,1,2-NiC_2B_9 species is likely to contribute to the isomerisation (we have already noted the steric crowding in compound **1**), since the isomerisation moves the carborane substituent down to the lower pentagonal belt. But relief from steric crowding alone cannot account for our results since an unisomerised product (**1**) was isolated with the larger diphosphine dppe (albeit that **1** could readily be isomerised) whereas no such unisomerised species was found with the smaller dmpe. Moreover, since alleviating steric crowding is as effective in a 3,1,2- to 4,1,2- isomerisation as it is for a 3,1,2- to 2,1,8- isomerisation what is it that determines which isomerisation path is followed?

A relevant factor may be the differeing donor/acceptor abilities of the diphosphines. The relatively electron-withdrawing dppe ligand will reduce the electron density at the metal centre and a 3,1,2- to 4,1,2- isomerisation of the nickelacarborane would help stabilise that since a CB_4 carborane face is expected to be a better donor than a C_2B_3 face. There are precedents for 3,1,2- to 4,1,2- isomerisations driven by *reducing* the metal electron density; Hawthorne and co-workers showed that 1-e oxidation of the anion [3,3′-Ni-{1,2-μ-$(CH_2)_3$-1,2-$C_2B_9H_9$}$_2$]$^-$ caused a 3,1,2- to 4,1,2- isomerisation in one cage,[9a] and Stone *et al* have suggested that the dissociation of labile ligands from 3,1,2-PdC_2B_9 species may facilitate an isomerisation to the 4,1,2- form.[12c] On the other hand the dmpe ligand will be relatively electron-donating, and there is literature precedence for an *increase* in electron density at the metal centre facilitating the 3,1,2- to 2,1,8- isomerisation process; Hanusa and Todd [9b] found that 1-e reduction of 3-Cp-3,1,2-*closo*-$CoC_2B_9H_{11}$ (Cp = η-C_5H_5) resulted in a 3,1,2- to 2,1,8- isomerisation at relatively low temperature, and we recently demonstrated a similar phenomenon with a 1,1′-bis(*o*-carborane) analogue of this

simple cobaltacarborane.[7] We therefore conclude that the electronic properties of the diphosphines play some part in determining the nature of the isomerisation process. That the effect of the net addition of electron density to a 1,2-*closo*-C_2 icosahedral heteroborane should result in C1–C2 breaking (as observed in the 3,1,2- to 2,1,8-isomerisation) is fully consistent with the LUMO of 1,2-*closo*-$C_2B_{10}H_{12}$ being antibonding between the cage C atoms.[17]

Compounds **4**, **7** and **9** represent a series of molecules in which the phosphine ligands are varied from PMe_3 to PMe_2Ph to $PMePh_2$. Compounds **4** and **7** are unisomerised (3,1,2-NiC_2B_9) whilst in **9** the nickelacarborane cage is putatively isomerised to a 4,1,2-NiC_2B_9 form. Clearly, as the series PMe_3, PMe_2Ph, $PMePh_2$ is progressed there is an increase in both the electron-withdrawing capability and the size of the phosphine and this makes it difficult, if not impossible, to know which of these factors is primarily responsible for the isomerisation.

In the context of completing the phosphine series, we have also attempted metallation of $[\mathbf{I}]^{2-}$ with *cis*-$[Ni(PPh_3)_2Cl_2]$ and upon metallation we observed a mobile orange band by preparative TLC analysis. Unfortunately we were not able to isolate the desired compound in a pure form. The impure $^{31}P\{^1H\}$ spectrum of the orange species shows singlet and quartet resonances, implying it is analogous to compound **6**.

Further, another attempt, the metallation of $[\mathbf{I}]^{2-}$ with *cis*-$[Ni(P(p\text{-tol})_3)_2Cl_2]$ was not successful. After completing the reaction and usual work up, spot TLC reveals no coloured mobile band. The failed metallation might be related to bulkiness of the P(*p*-tol)$_3$. The capitation reaction of $[\mathbf{I}]^{2-}$ with $\{Ni(P(i\text{Pr})_3)_2\}^{2+}$ was also ineffective and unfortunately we were unable to isolate the desired product.

In view of this we have targeted trimethylphosphite, $P(OMe)_3$, as an important ligand in this work. Since $P(OMe)_3$ is smaller than PMe_3 but more electron-withdrawing than $PMePh_2$ [18] its use may help delineate the relative importance of the steric and electronic properties of the exopolyhedral ligand in the isomerisation process.

2.2.7 Investigation of phosphite based metallacarborane

After literature research, we could not find as appropriate dihalonickel(II) species as the source of the $\{Ni(P(OMe)_3)_2\}^{2+}$ fragment. $[NiX_2(P(OMe)_3)_2]$ (X = Cl, Br, I) does not exist in the literature. There is a crystal structure report of tris(trimethylphosphite) nickel(II)iodide species but not any synthetic method.[19] However we have attempted to synthesise $[NiCl_2(P(OMe)_3)_2]$ by the treatment of hydrated $NiCl_2$ in ethanol with $P(OMe)_3$ followed by reflux for 2 hrs (Figure 2.2.7.1). After work up this gave a brown-red liquid but $^{31}P\{^1H\}$ spectroscopic analysis was inconclusive due to multiple resonances.

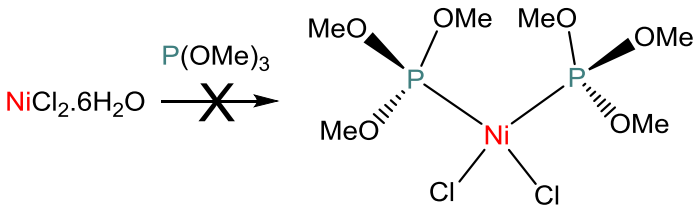

Figure 2.2.7.1 Attempted synthesis of $[NiCl_2(P(OMe)_3)_2]$.

Having been unsuccessful in the synthesis of $[Ni(P(OMe)_3)_2Cl_2]$, we found an analogous compound of palladium, *cis*-$[Pd(P(OMe)_3)_2Cl_2]$ which has been synthesised in the literature.[20] To provide a link with bisphosphine-nickelacarborane, *cis*-$[PdCl_2(PMe_3)_2]$ was considered and also synthesised by literature method.[21]

Metallation of [7-(1′-1′,2′-*closo*-$C_2B_{10}H_{11}$)-7,8-*nido*-$C_2B_9H_{11}]^{2-}$ with the $\{Pd(PMe_3)_2\}^{2+}$ fragment gave [1-(1′-1′,2′-*closo*-$C_2B_{10}H_{11}$)-3-Cl-3-PMe_3-8-PMe_3-3,1,2-*closo*-$PdC_2B_9H_9$] (**10**) which was not expected and is discussed in detail in section 2.2.8. Further metallation of ([$HNMe_3$]**I**) with $\{Pd(P(OMe)_3)_2\}^{2+}$ was carried out by following the same procedure used for **1 (**Figure 2.2.7.2). Spot TLC analysis revealed no coloured mobile band and only a colourless one. The spectroscopic ($^{31}P\{^1H\}$, $^{11}B\{^1H\}$) characterisations, a quartet resonance in the $^{31}P\{^1H\}$ spectrum and two distinct characteristic nido peaks in the $^{11}B\{^1H\}$ spectrum of the crude reaction mixture, suggest possible formation of a nido-phosphite derivative similar to **5** and **8**. However this derivative was not desired and hence was not fully characterised. Thus metallation has not occurred and this might be due to very labile P–Pd bond cleavage giving free $P(OMe)_3$ which adds to the deprotonated nido species.

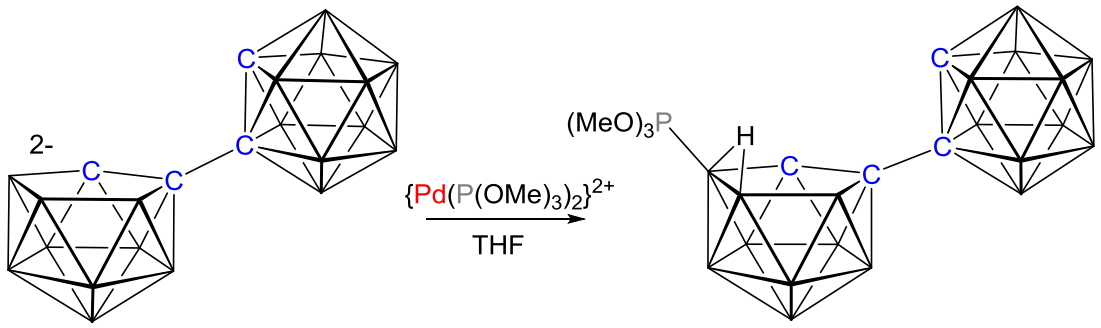

Figure 2.2.7.2 Metallation of [HNMe$_3$]**I** with [PdCl$_2$(P(OMe)$_3$)$_2$].

In other approach, we have also attempted the metallation of nido/closo-carborane, ([HNMe$_3$]**I**), with [PdCl$_2$(NCPh)$_2$] and *in situ* addition of PMe$_3$ where [PdCl$_2$(NCPh)$_2$] was prepared by following the reported method.[22] The reaction of deprotonated nido/closo carborane with [PdCl$_2$(NCPh)$_2$] followed by addition of PMe$_3$ and subsequent usual work-up was not successful in isolating any palladacarborane species (Figure 2.2.7.3). The spectroscopic analysis of the resultant crude material after addition of [PdCl$_2$(NCPh)$_2$] showed no evidence of closo species, only characteristic nido resonances were present in the ^{11}B{^{1}H} spectrum.

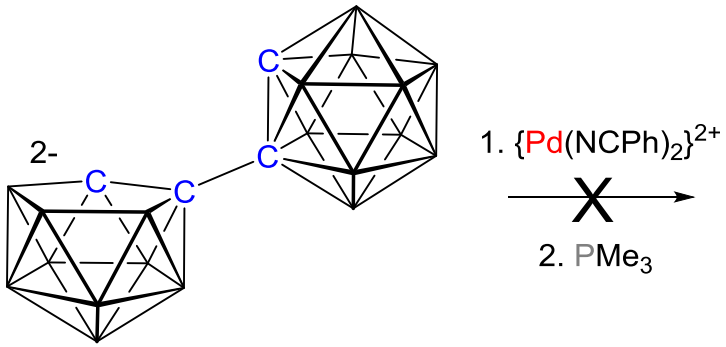

Figure 2.2.7.3 Attempted metallation of [**I**]$^{2-}$ by {Pd(NCPh)$_2$}$^{2+}$ and *in situ* addition of PMe$_3$.

Having been unsuccessful in the metallation reaction with {Pd(P(OMe)$_3$)$_2$}$^{2+}$ fragment, further delving into the literature found precedence of a 3,3-{P(OMe)$_3$}$_2$-3,1,2-PdC$_2$B$_9$ species. Wallbridge *et al* reported the facile syntheses of 3,3-{P(OMe)$_3$}$_2$-3,1,2-PdC$_2$B$_9$H$_{11}$ and 3,3-(PMe$_3$)$_2$-3,1,2-PdC$_2$B$_9$H$_{11}$ by the P(OMe)$_3$ and PMe$_3$ displacement of tmeda from a 3-tmeda-3,1,2-PdC$_2$B$_9$H$_{11}$ species.[23] This suggested the synthesis of our targeted trimethylphosphite based metallacarborane species. Thus single decapitation

and metallation of 1,1′-bis(*o*-carborane) with [$PdCl_2$(tmeda)] and subsequently ligand displacement with $P(OMe)_3$ and PMe_3 of the resultant amine-palladacarborane species were targeted and further discussion is in section 2.2.10.

2.2.8 Synthesis of 1-(1′-1′,2′-*closo*-$C_2B_{10}H_{11}$)-3-Cl-3-PMe_3-8-PMe_3-3,1,2-*closo*-$PdC_2B_9H_9$] (10)

Compound **10** was prepared by following the same method as for **1**, but metallation was performed using *cis*-[$PdCl_2(PMe_3)_2$]. After usual workup and preparative TLC analysis only greenish yellow **10** in 20.5% yield was isolated.

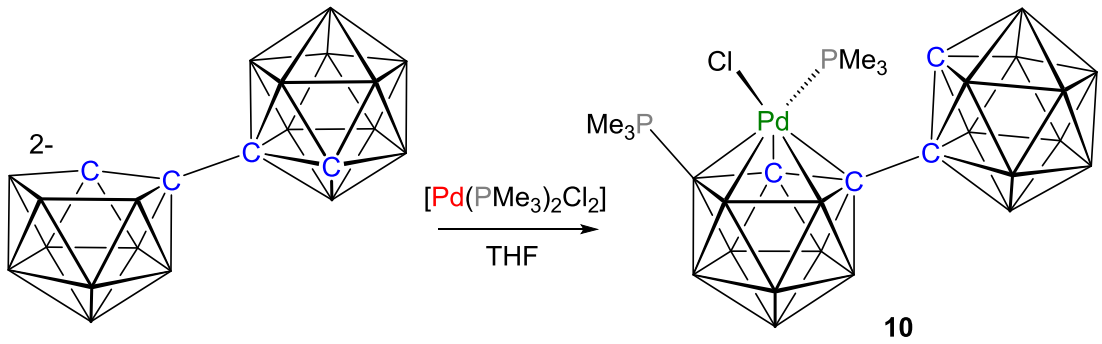

Figure 2.2.8.2 Metallation of [$HNMe_3$]**I** with [$PdCl_2(PMe_3)_2$]

The mass spectrum of **10** displays an envelope centered on *m/z* 567.2 (M^+) [MW = 567.62 g mol^{-1}] which is higher mass than expected for $(PMe_3)_2PdC_2B_9H_{10}$-$C_2B_{10}H_{11}$ [MW = 533.18 g mol^{-1} for $C_{10}H_{39}B_{19}P_2Pd$] and indicates a derivative of the target molecule.

In the ^1H spectrum are two broad singlets characteristic of CH_{cage} resonances, one of which is at unusually high frequency, δ 5.74 ppm, along with two sets of doublets at δ 1.73 ppm with coupling constant $^2J_{PH}$ = 12.0 Hz and at δ 1.61 ppm with coupling constant $^2J_{PH}$ = 11.2 Hz assigned to two methyl groups which collapse to two singlets in the $^1H\{^{31}P\}$ spectrum.

In the $^{31}P\{^1H\}$ spectrum is a 1:1:1:1 quartet characteristic of P bound to B ($^1J_{PB}$ = 144.6 Hz) and a singlet.

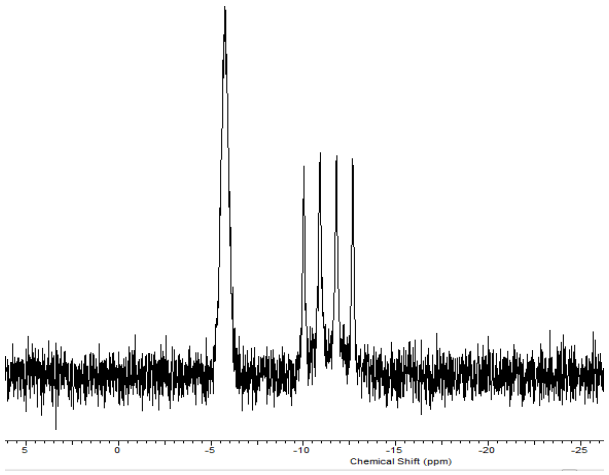

Figure 2.2.8.2 $^{31}P\{^{1}H\}$ NMR spectrum of compound **10** in $CDCl_3$.

Solvent evaporation of a $CDCl_3$ solution of **10** at room temperature (16 ^{o}C) resulted in suitable quality crystals for *X*-ray diffraction and unit cell determination reveals that this is isomorphous to compound **6** and so must be [1-(1′-1′,2′-*closo*-$C_2B_{10}H_{11}$)-3-Cl-3-PMe_3-8-PMe_3-3,1,2-*closo*-$PdC_2B_9H_9$] (**10**).

2.2.9 Synthesis of [1-(1′-1′,2′-*closo*-$C_2B_{10}H_{11}$)-3-tmeda-3,1,2-*closo*-$PdC_2B_9H_{10}$] (11) and [8-(1′-1′,2′-*closo*-$C_2B_{10}H_{11}$)-2-tmeda-2,1,8-*closo*-$PdC_2B_9H_{10}$] (12)

The reaction between [7-(1′-1′,2′-*closo*-$C_2B_{10}H_{11}$)-7,8-*nido*-$C_2B_9H_{11}]^{2-}$, prepared by deprotonation of ([$HNMe_3$]**I**) with two equiv. *n*BuLi in THF and addition of [$PdCl_2$(tmeda)] in THF gave two yellow compounds **11** and **12** in modest yields following work-up involving preparative TLC.

The mass spectra of **11** and **12** (EIMS: an envelope centered *m/z* 497.3 (M^+), MW = 497.23 g mol^{-1} for **11**; an envelope centered *m/z* 497.3 (M^+), MW = 497.23 g mol^{-1} for **12**) reveals these are isomeric in nature.

The ^{1}H NMR spectra of both compounds are of relatively similar pattern. In the ^{1}H NMR spectrum of a freshly-prepared $CDCl_3$ solution of **11** are CH_{cage} resonances, one at relatively high frequency (δ 3.96 ppm, assigned to the carborane cage) and the other at relatively low frequency (δ 3.07 ppm, assigned to the palladacarborane) along with the signals (δ 2.95-2.75 ppm) from the -CH_2-CH_2- bridge of the tmeda ligand. There are four singlet resonances with integral-3 for the methyl protons which confirms the asymmetry of the cage environment in the palladacarborane.

The ^{11}B{^{1}H} NMR spectrum of **11** is different compared to previously characterised nickelacarboranes (3,1,2-1′,2′; 4,1,2-1′,2′; 2,1,8-1′,2′) and consists of multiple overlapping resonances between δ -2.9 and -27.2 ppm with a total integral of 19B. It was not possible to deconvolute the entire spectrum due to multiple overlapping resonances.

Crystals of **11** were grown by diffusion of petroleum ether 40-60 and a $CDCl_3$ solution of **11** at 5 °C. Single crystal *X*-ray diffraction reveals **11** as [1-(1′-1′,2′-*closo*-$C_2B_{10}H_{11}$)-3-tmeda-3,1,2-*closo*-$PdC_2B_9H_{10}$].

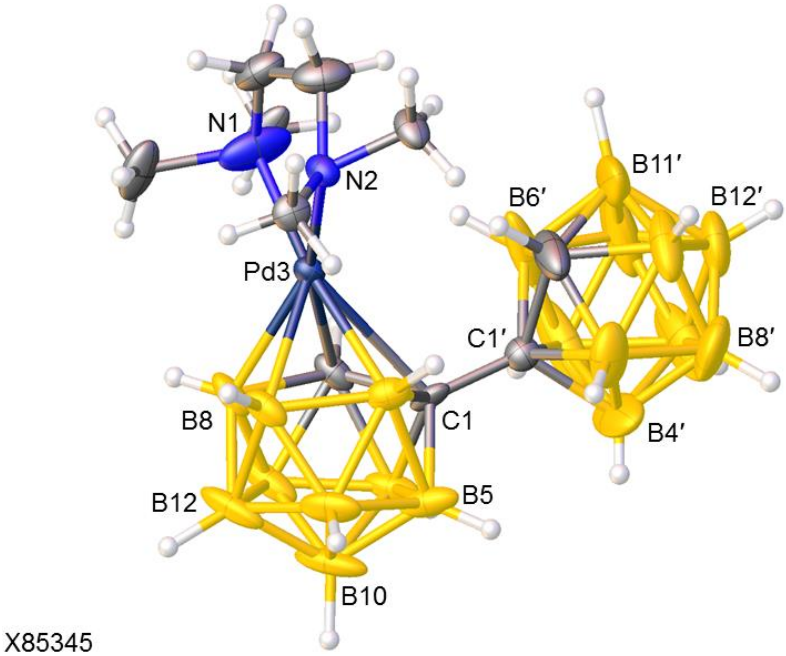

Figure 2.2.9.1 Molecular structure of [1-(1′-1′,2′-*closo*-$C_2B_{10}H_{11}$)-3-tmeda-3,1,2-*closo*-$PdC_2B_9H_{10}$] (**11**).

Although the molecule is partly disordered (only the major occupancies are shown in Figure 2.2.9.1) the key result of the study is clear; the palladacarborane cage is an unisomerised 3,1,2-PdC_2B_9 icosahedron, making compound **11** overall 1-C_2B_{10}-3,1,2-PdC_2B_9 in short form. In the metallacarborane, the metal atom is bound to a C_2B_3 face which is folded into usual envelope conformation (dihedral angle between C2C1B4 and C2B7B8B4 planes 19.4°), and moreover, the Pd atom is slipped away from C1 (slipped parameter,[10] Δ = 0.303 Å) resulting in a long Pd3-C1 distance, 2.647(3) Å. The reasons underlying these slipping and folding distortions are mainly electronic. The presence of purely sigma donor tmeda ligand causes this distortion.

Moving to **12**, the ^{1}H NMR spectrum contains two C*H*$_{cage}$ resonances, δ 3.73 ppm due to the carborane cage, δ 2.52 ppm corresponding to the palladacarborane, with multiple signals (δ 2.90-2.75 ppm) from the -CH_2-CH_2- bridge of the tmeda ligand. There are also four singlet resonances with integral-3 for the methyl protons which signifies again the asymmetric nature of the metallacarborane cage.

The ^{11}B{^{1}H} NMR spectrum of **12** has a different pattern compared to **11** and consists of multiple overlapping resonances between δ -3.1 and -22.4 ppm with the total integral of 19B. It was not possible to determine the exact isomer.

Crystals of **11** were developed by diffusion of petroleum ether 40-60 and a $CDCl_3$ solution of **12** at 5 °C. Analysis by *X*-ray diffraction shows **12** as [8-(1′-1′,2′-*closo*-$C_2B_{10}H_{11}$)-2-tmeda-2,1,8-*closo*-$PdC_2B_9H_{10}$].

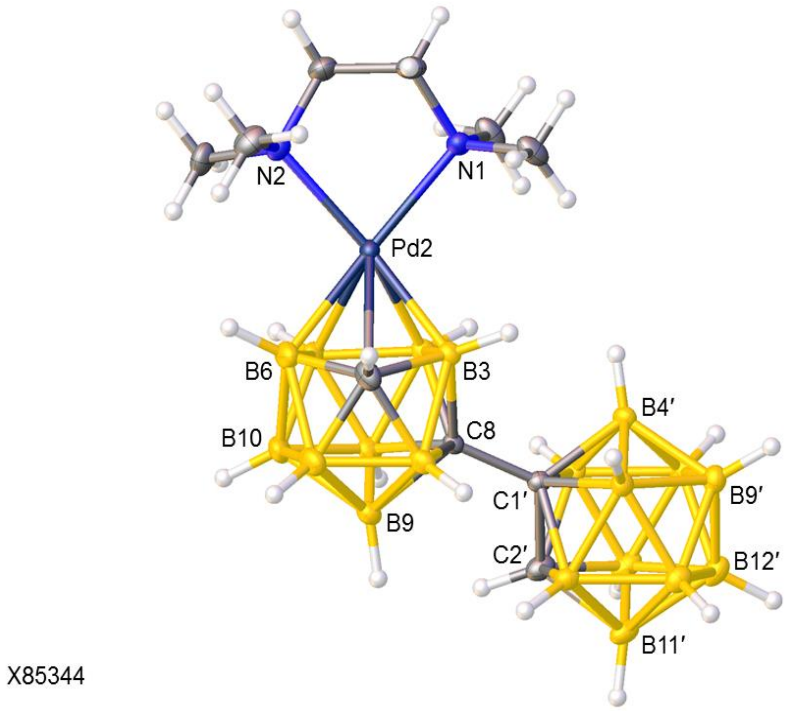

Figure 2.2.9.2 Molecular structure of [8-(1′-1′,2′-*closo*-$C_2B_{10}H_{11}$)-2-tmeda-2,1,8-*closo*-$PdC_2B_9H_{10}$] (**12**).

The crystallographic analysis reveals that the palladacarborane cage is isomerised to a 2,1,8-PdC_2B_9 icosahedron connected to a C_2B_{10} moiety, making compound **12** overall 8-C_2B_{10}-2,1,8-PdC_2B_9 in short form (Figure 2.2.9.2). In the metallacarborane, the metal atom is bound to a CB_4 face which is folded into usual envelope conformation (dihedral angle between B3C1B6 and B3B7B11B6 planes 17.8°), and moreover, the Pd atom is slipped away from C1 (Δ = 0.320 Å) resulting in a long Pd2-C1 distance, 2.5674(3) Å. The reasons underlying these slipping and folding distortions are again mainly the presence of the sigma donor tmeda ligand.[10] Selected geometric parameters for **11** and **12** are listed in Table 2.2.9.1.

Table 2.2.9.1 Selected bond lengths (Å) [1-(1′-1′,2′-*closo*-$C_2B_{10}H_{11}$)-3-tmeda-3,1,2-*closo*-$PdC_2B_9H_{10}$] (**11**) and [8-(1′-1′,2′-*closo*-$C_2B_{10}H_{11}$)-2-tmeda-2,1,8-*closo*-$PdC_2B_9H_{10}$] (**12**).

Compound **11**		Compound **12**	
Pd3—C1	2.647(3)	Pd2—C1	2.558(3)
Pd3—C2	2.243(2)	Pd2—B3	2.167(3)
Pd3—B4	2.231(4)	Pd2—B6	2.192(4)
Pd3—B7	2.221(4)	Pd2—B7	2.165(3)
Pd3—B8	2.223(4)	Pd2—B11	2.258(4)
Pd3—N1	2.182(4)	Pd2—N1	2.199(3)
Pd3—N2	2.192(3)	Pd2—N2	2.185(3)
N—C_{Me}	1.374(9) –1.726(11)*	N—C_{Me}	1.477(3) –1.483(3)
C1—C2	1.680(5)	C1—B3	1.657(3)
C1—B4	1.695(5)	C1—B4	1.651(4)
C1—B5	1.664(5)	C1—B5	1.671(5)
C1—B6	1.675(5)	C1—B6	1.695(3)
C2—B11	1.820(5)	C8—B3	1.772(4)
C2—B6	1.842(6)	C8—B4	1.745(3)
C2—B7	1.809(6)	C8—B7	1.726(4)
		C8—B9	1.763(4)
C1—C1′	1.521(5)	C8—C1′	1.536(3)
C1′—C2′	1.663(6)	C1′—C2′	1.689(4)
C1′—B3′	1.728(6)	C1′—B3′	1.718(3)
C1′—B4′	1.701(7)	C1′—B4′	1.727(3)
C1′—B5′	1.704(7)	C1′—B5′	1.718(3)
C1′—B6′	1.687(8)	C1′—B6′	1.739(4)
C2′—B3′	1.694(9)	C2′—B3′	1.712(4)
C2′—B6′	1.653(11)	C2′—B6′	1.740(4)
C2′—B7′	1.691(7)	C2′—B7′	1.720(4)
C2′—B11′	1.697(10)	C2′—B11′	1.719(3)

* The tmeda ligand is disordered including the methyl groups, and the distances are given from part 1 of the structure.

2.2.10 Attempted synthesis of bis(phosphite) nickelacarboranes

With the eventual aim of making PMe_3 and $P(OMe)_3$ based palladacarboranes, addition of a $\{Pd(tmeda)\}^{2+}$ fragment to [7-(1′-1′,2′-*closo*-$C_2B_{10}H_{11}$)-7,8-*nido*-$C_2B_9H_{11}]^{2-}$, prepared by lithiation using exactly two equiv. *n*BuLi, affords both the unisomerised species [1-(1′-1′,2′-*closo*-$C_2B_{10}H_{11}$)-3-tmeda-3,1,2-*closo*-$PdC_2B_9H_{10}$] (**11**) and the isomerised [8-(1′-1′,2′-*closo*-$C_2B_{10}H_{11}$)-2-tmeda-2,1,8-*closo*-$PdC_2B_9H_{10}$] (**12**). We note the isomerisation of 1-C_2B_{10}-3,1,2-PdC_2B_9 to 8-C_2B_{10}-2,1,8-PdC_2B_9 where the carborane unit moves to the lower belt at C8 position. With time, solutions of **11** show clear evidence for a slow transformation of **11** to **12** as a minor component **12** was always observed during preparative TLC purification of **11**. The isomerisation might be related to the electron richness of tmeda ligand. A similar type of phenomenon has been observed for compound **3,** where basic but small chelating dmpe causes isomerisation to a 2,1,8 species.

In light of this isomerisation, using tmeda for 1-C_2B_{10}-3,1,2-PdC_2B_9 (**11**) to 8-C_2B_{10}-2,1,8-PdC_2B_9 (**12**), we have considered the relatively less basic en ligand instead of tmeda. [$PdCl_2$(en)] was synthesised by literature preparation [24] and metallation has been attempted in the standard way (Figure 2.2.13.1). Unfortunately, we were not able to isolate any closo metallacarborane species.

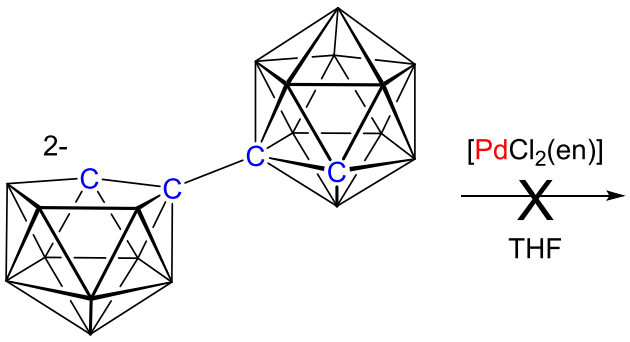

Figure 2.2.10.1 Attempted metallation of $\mathbf{I}^{2-}$ with [$PdCl_2$(en)].

However, having characterised crystallographically and spectroscopically compounds **11** and **12**, we attempted ligand displacement reaction of compound **11** with $P(OMe)_3$ and PMe_3 in NMR scale reactions. The 2 hrs stirring of a solution of **11** in DCM in the presence of excess $P(OMe)_3$ or PMe_3 at room temperature [23] resulted in no colour change

in the reaction mixture (starting material **11** with a minor amount of **12** recovered) and prolong stirring effected partial decomposition of the starting material.

Having these inconclusive results, we then considered introducing the same idea into the Ni-system *i.e.* preparation of 3-(tmeda)-3,1,2-NiC_2B_9-1′,2′-C_2B_{10} followed by a ligand displacement reaction using $P(OMe)_3$. Further literature research, revealed a Ni-tmeda complex, $[Ni_3(tmeda)_3Cl_5]Cl$. This was synthesised by the literature method [25] and further discussion has been continued in section 2.2.14.

2.2.11 Synthesis of [1-(1′-1′,2′-*closo*-$C_2B_{10}H_{11}$)-3,3-{$P(OMe)_3$}$_2$-3,1,2-*closo*-$NiC_2B_9H_{10}$] (13) and [1-(1′-1′,2′-*closo*-$C_2B_{10}H_{11}$)-2,2-{$P(OMe)_3$}$_2$-2,1,8-*closo*-$NiC_2B_9H_{10}$] (14)

The reaction between dianion [7-(1′-1′,2′-*closo*-$C_2B_{10}H_{11}$)-7,8-*nido*-$C_2B_9H_{11}$]$^{2-}$, prepared by deprotonation of ([$HNMe_3$]**I**) with 2 equiv. *n*BuLi in THF, and stoichiometric [$Ni_3(tmeda)_3Cl_5$]Cl in THF gave a bluish-green solution after warming to room temperature. Addition of $P(OMe)_3$ in excess followed by stirring for 18 h afforded a brown solution. On work-up by TLC a purple compound, **13** was isolated in moderate yields. By performing the same reaction using 0.5 equiv. of [$Ni_3(tmeda)_3Cl_5$]Cl used for metallation, we have isolated a yellow compound, **14** and a trace amount of purple compound **13** (Figure 2.2.11.1).

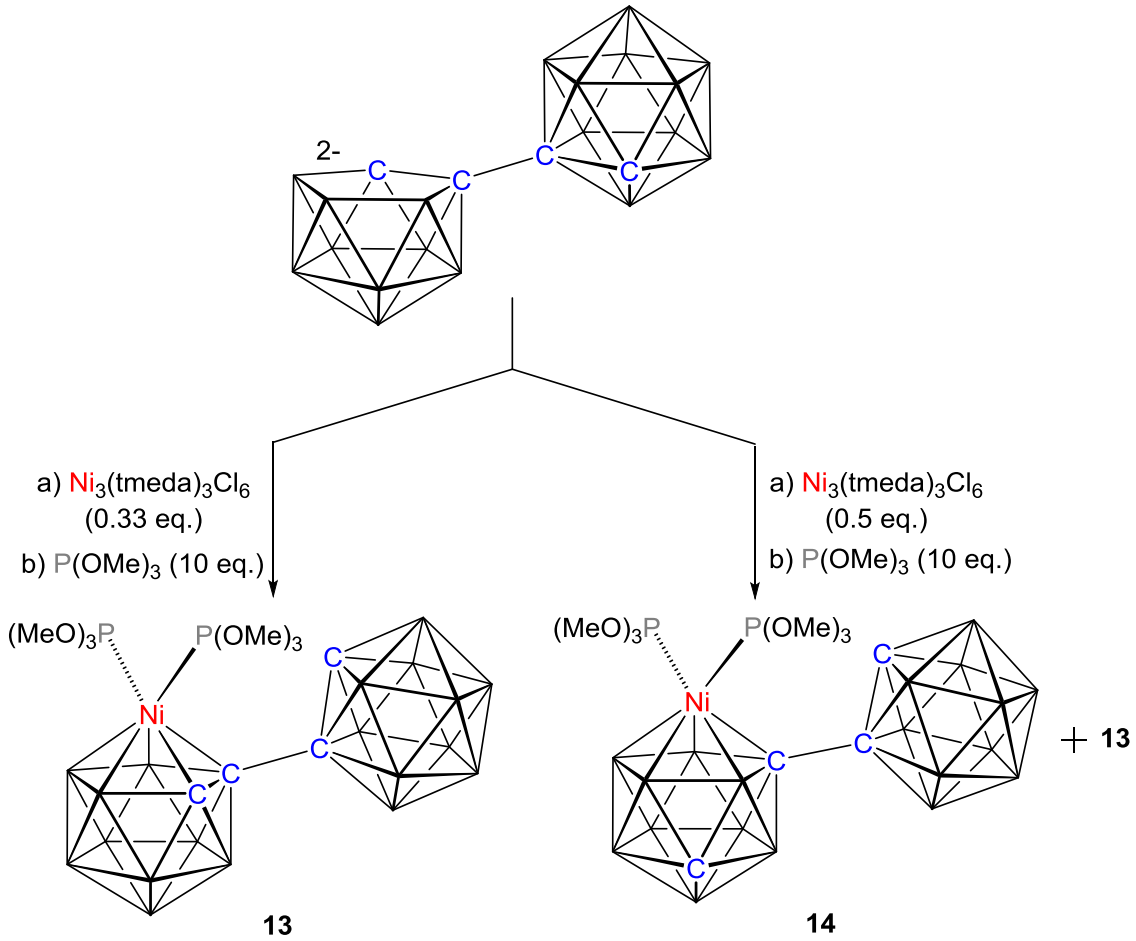

Figure 2.2.11.1 Metallation of $\mathbf{I}^{2-}$ with $\{Ni(tmeda)\}^{2+}$ and *in situ* addition of $P(OMe)_3$.

The mass spectrum of **13** contains an envelope centered on *m/z* 581.3 (M^+), MW = 581.47 g mol^{-1} for **13**, and the elemental analysis is in excellent agreement with that expected for $C_{10}H_{39}B_{19}NiO_6P_2$.

In the ^1H NMR spectrum of **13**, there are signals arising from methyl protons with integral-18 at δ 3.85 ppm giving an apparent triplet $^3J_{PH}$ = *ca*. 11.0 Hz, *i.e*. coincidence of two single doublets. Additionally there are also CH_{cage} resonances at unusually high frequency at δ 4.59 ppm (which is comparable to C*H*cage carborane resonances of compounds **6**, **10**) and at relatively low frequency (δ 2.52 ppm) a doublet ($^3J_{PH}$ = 10.0 Hz), assigned to the metallated cage. Similar splittings were observed for compounds **2**, **4** and **8**. These coupled resonances collapse to two integral-9 singlets for methyl protons and a singlet with integral-1 for CH_{cage} of the nickelacarborane in the $^1H\{^{31}P\}$ NMR spectrum confirming the coupling of protons with a P nucleus.

The $^{31}P\{^1H\}$ NMR spectrum of compound **13** reveals two mutually coupled doublets with $^2J_{PP}$ = 118.2 Hz which indicates that two phosphorus atoms are magnetically inequivalent. Therefore it implies no isomerisation and that the carborane moiety remains in the top belt at C1 position.

The $^{11}B\{^1H\}$ NMR spectrum of **13** consists of multiple overlapping resonances between δ 1.3 and -18.7 ppm with a total integral of 19B. It was not possible to deconvolute the entire spectrum due to multiple overlapping resonances. However we are confident this is a closo species as no characteristic nido signals were observed.

Crystals of **13** were developed by diffusion of petroleum ether 40-60 and a $CDCl_3$ solution of **13** at 5 °C. Analysis of single crystals by *X*-ray diffraction shows **13** as to be expected [1-(1′-1′,2′-*closo*-$C_2B_{10}H_{11}$)-3,3-{$P(OMe)_3$}$_2$-3,1,2-*closo*-$NiC_2B_9H_{10}$].

The single crystal diffraction study (Figure 2.2.11.2) explains these spectroscopic results and reveals that a C_2B_{10} moiety is connected to a unisomerised 3,1,2-NiC_2B_9 unit. In the nickelacarborane cage the orientation of {$Ni(P(OMe)_3)_2$} fragment is not lying perpendicular to the mirror plane through the C_2B_9 unit. The dihedral angle, θ, between the plane through P1P2Ni3 and the plane through B6B8B10 is 55.13(12)°. Effectively, the NiPP plane in **13** lies perpendicular to the plane through C1B10B12 [θ = 90.50(9)°]

to minimise steric congestion between the two phosphite ligands and the carborane substituent on C1.

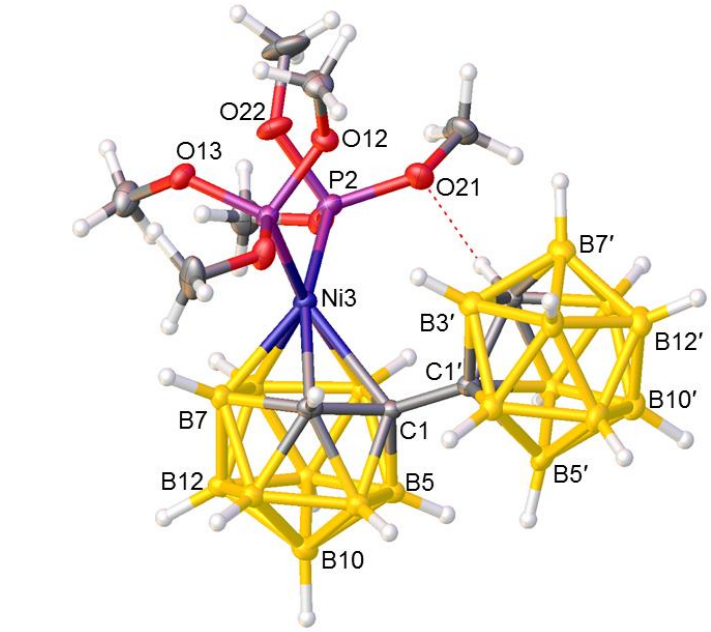

Figure 2.2.11.2 Molecular structure [1-(1′-1′,2′-*closo*-$C_2B_{10}H_{11}$)-3,3-{$P(OMe)_3$}$_2$-3,1,2-*closo*-$NiC_2B_9H_{10}$] (**13**).

In the nickelacarborane cage the metal is ligated by two $P(OMe)_3$ ligands as expected, but one methoxy group is shows H-bonding to the C*H* of the carborane substituent on C1 [H2′…O21, 2.19(4) Å; C2′–H2′…O21 170(3)º; H2′…O21–P2 106.5(9)º; H2′…O21-C21 120.3(9)º; torsion angle: H2′…O21-P2-Ni3 10.2(8)º], this causing the high-frequency resonance of the C*H* atom.

From the mass spectrum (an envelope centered on *m/z* 581.3 (M^+), MW = 581.47 g mol^{-1}) and elemental analysis (excellent agreement with that expected for $C_{10}H_{39}B_{19}NiO_6P_2$), compound **14** is confirmed as an isomer of **13**.

The ^{1}H NMR spectrum of **14** contains two CH_{cage} resonances, one at high frequency, similar to **13** (δ 4.32 ppm, singlet, integral-1, assigned to the carborane cage) and the other a low frequency integral-1 singlet (δ 3.07 ppm, assigned to the nickelacarborane), but no coupling compared to **13**. For the methyl protons, there are also two integral-9 doublet resonances at δ 3.83, 3.79 ppm with additional structure. Both couplings result from

coupling of a P nucleus as we see two integral-9 singlet resonances at δ 3.83, 3.79 ppm in the $^{1}H\{^{31}P\}$ spectrum.

The $^{31}P\{^{1}H\}$ NMR spectrum of **14** reveals two overlapping doublets at δ 125.2, 123.5 ppm, the close proximity preventing the measurement of their coupling constants. These spectra do not define the isomer.

Similarly the $^{11}B\{^{1}H\}$ NMR spectrum of **14** has a different pattern compared to **13** and consists of multiple overlapping resonances between δ -2.5 and -18.4 ppm with the total integral of 19B. It is not possible to deconvolute the entire spectrum due to multiple overlapping resonances, precluding identification of the exact isomer present, and crystallographic study is required.

Crystals of **14** were grown by diffusion of petroleum ether 40-60 and a $CDCl_3$ solution of **14** at 5 °C. Analysis by *X*-ray diffraction shows **14** as [1-(1′-1′,2′-*closo*-$C_2B_{10}H_{11}$)-2,2-{$P(OMe)_3$}$_2$-2,1,8-*closo*-$NiC_2B_9H_{10}$].

Solid state structural analysis (Figure 2.2.11.3) shows that a C_2B_{10} unit is connected at C1 position of a isomerised 2,1,8-NiC_2B_9 architecture where CH is isomerised to a 8 position. This is a rare example where a bulky (carborane) unit remains at top belt and CH moves away to the bottom belt.[26] In the nickelacarborane cage the orientation of the {$Ni(P(OMe)_3)_2$} fragment is not perpendicular to the mirror plane through the C_2B_9 unit. The dihedral angle, θ, between the plane through P1P2Ni3 and the plane through B6B8B10 is 55.13(12)°. Practically, the NiPP plane in **13** lies perpendicular to the plane through C1B10B12 [θ = 90.50(9)°] to minimise steric congestion between the two phosphite ligands and the carborane substituent on C1.

In the nickelacarborane cage the metal is ligated by two $P(OMe)_3$ ligands as expected but one of the methoxy groups shows H-bonding to the C*H* atom of the carborane substituent on C1 [H2′…O23, 2.351(19) Å; C2′–H2′…O23 158(15)º; H2′…O23–P2 99.5(5)º; H2′…O23-C23 128.0(5)º; torsion angle: H2′…O23-P2-Ni2 18.9(5)º], the origin of the high-frequency resonance of the C*H* atom.

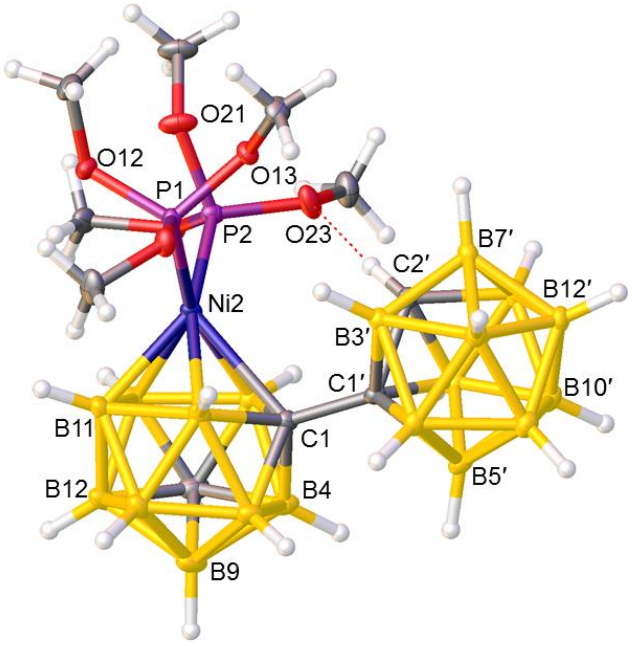

Figure 2.2.11.3 Molecular structure of [1-(1′-1′,2′-*closo*-$C_2B_{10}H_{11}$)-2,2-{$P(OMe)_3$}$_2$-2,1,8-*closo*-$NiC_2B_9H_{10}$] (**14**).

For compound **14**, CH moves to the bottom belt and the carborane unit remains at the top belt in the nickelacarborane cage, therefore it is necessary to confirm the second C atom positions for both **13** and **14** correctly. Thus we have used both VCD and BHD analysis of the *Prostructure*s for **13**, **14**. For compound **13**, VCD clearly shows (Table 2.2.11.1) that the second C atom (C1 linkage carbon atom) is at vertex 2 (VCD from 2 is shorter than VCD from 9 or others by >0.124 Å) for the nickelacarborane cage and the second C atom for carborane cage is at vertex 2′ (C1′ is linkage carbon atom). This is consistent with BHD analysis; the shortest BHD at 2 and 2′ for nickelacarborane and carborane respectively (Table 2.2.11.2). In contrast for compound **14**, VCD shows (Table 2.2.11.1) that the second C atom (C2 linkage carbon atom) is at vertex 8 as the VCD from 8 is shorter than VCD from 10 or others by >0.115 Å for the nickelacarborane cage and the second C atom is at 2′ (C1′ linkage carbon atom) for the carborane cage. This also is consistent with BHD analysis, with the shortest BHDs at 8 and 2′ for nickelacarborane and carborane respectively (Table 2.2.11.2). Additionally, Table 2.2.11.3 summarises some key structural parameters of compound **13** and **14**.

Table 2.2.11.1 Vertex-to-centroid (VCD) distances (Å) in Prostructures of [1-(1′-1′,2′-*closo*-$C_2B_{10}H_{11}$)-3,3-{$P(OMe)_3$}$_2$-3,1,2-*closo*-$NiC_2B_9H_{10}$] (**13**) and [1-(1′-1′,2′-*closo*-$C_2B_{10}H_{11}$)-2,2-{$P(OMe)_3$}$_2$-2,1,8-*closo*-$NiC_2B_9H_{10}$] (**14**).

Vertex	Compound **13**		Compound **14**	
	Metallated cage	Carborane cage	Metallated cage	Carborane cage
1	1.615(3)	1.603(3)	1.6442(19)	1.6159(19)
2	1.526(3)	1.541(4)	2.2866(3)	1.548(3)
3	2.3011(5)	1.691(4)	1.6692(2)	1.706(2)
4	1.674(4)	1.694(4)	1.714(3)	1.693(2)
5	1.693(4)	1.689(4)	1.697(2)	1.701(3)
6	1.725(4)	1.711(4)	1.645(2)	1.710(2)
7	1.703(4)	1.698(4)	1.735(2)	1.697(2)
8	1.728(4)	1.685(4)	1.535(2)	1.694(2)
9	1.650(4)	1.666(4)	1.704(3)	1.680(2)
10	1.681(4)	1.684(4)	1.650(2)	1.689(3)
11	1.669(4)	1.693(4)	1.737(3)	1.692(2)
12	1.675(4)	1.676(4)	1.701(3)	1.686(2)

Table 2.2.11.2 Boron-hydrogen distances (Å) in Prostructures of [1-(1′-1′,2′-*closo*-$C_2B_{10}H_{11}$)-3,3-{$P(OMe)_3$}$_2$-3,1,2-*closo*-$NiC_2B_9H_{10}$] (**13**) and [1-(1′-1′,2′-*closo*-$C_2B_{10}H_{11}$)-2,2-{$P(OMe)_3$}$_2$-2,1,8-*closo*-$NiC_2B_9H_{10}$] (**14**).

Vertex	Compound **13**		Compound **14**	
	Metallated cage	Carborane cage	Metallated cage	Carborane cage
1	-	-	-	-
2	0.43(4)	0.33(5)	-	0.20(4)
3	-	0.99(4)	1.09(2)	1.10(2)
4	1.10(4)	1.14(4)	1.15(3)	1.01(2)
5	1.07(4)	1.09(4)	1.09(3)	1.13(3)
6	1.10(4)	1.09(4)	1.05(3)	1.07(3)
7	1.10(4)	1.04(3)	1.15(3)	1.10(3)
8	1.17(4)	1.15(4)	0.50(3)	1.06(3)
9	1.17(4)	1.05(4)	1.19(3)	1.09(3)
10	1.19(4)	1.08(4)	1.10(3)	1.10(2)
11	1.12(4)	1.13(4)	1.04(3)	1.08(3)
12	1.13(4)	1.07(4)	1.11(3)	1.03(3)

Table 2.2.11.3 Selected geometric parameters (Å, º) [1-(1′-1′,2′-*closo*-$C_2B_{10}H_{11}$)-3,3-{$P(OMe)_3$}$_2$-3,1,2-*closo*-$NiC_2B_9H_{10}$] (**13**) and [1-(1′-1′,2′-*closo*-$C_2B_{10}H_{11}$)-2,2-{$P(OMe)_3$}$_2$-2,1,8-*closo*-$NiC_2B_9H_{10}$] (**14**).

Compound **13**		Compound **14**	
Ni3—C1	2.279(3)	Ni2—C1	2.3337(16)
Ni3—C2	2.094(3)	Ni2—B3	2.0794(19)
Ni3—B4	1.718(4)	Ni2—B6	2.1256(19)
Ni3—B7	2.100(3)	Ni2—B7	2.093(2)
Ni3—B8	2.107(3)	Ni2—B11	2.1314(19)
Ni3—P1	2.1678(8)	Ni2—P1	2.1648(5)
Ni3—P2	2.1326(8)	Ni2—P2	2.1687(5)
P1—O_{Me}	1.584(2) –1.594(2)	P1—O_{Me}	1.5949(12) –1.6011(12)
P2—O_{Me}	1.583(2) –1.588(2)	P2—O_{Me}	1.5885(13) –1.5972(12)
C1—C2	1.592(4)	C1—B3	1.700(3)
C1—B4	1.718(4)	C1—B4	1.698(3)
C1—B5	1.704(4)	C1—B5	1.702(3)
C1—B6	1.719(4)	C1—B6	1.714(3)
C2—B6	1.774(4)	C8—B3	1.735(3)
C2—B7	1.745(4)	C8—B4	1.713(3)
C2—B11	1.731(4)	C8—B7	1.719(3)
		C8—B9	1.730(2)
		C8—B12	1.725(3)
C1—C1′	1.538(4)	C1—C1′	1.540(2)
C1′—C2′	1.646(4)	C1′—C2′	1.654(2)
C1′—B3′	1.734(4)	C1′—B3′	1.751(2)
C1′—B4′	1.725(4)	C1′—B4′	1.733(2)
C1′—B5′	1.727(4)	C1′—B5′	1.733(2)
C1′—B6′	1.739(4)	C1′—B6′	1.737(2)
C2′—B3′	1.700(4)	C2′—B3′	1.715(3)
C2′—B6′	1.722(4)	C2′—B6′	1.719(2)
C2′—B7′	1.706(4)	C2′—B7′	1.699(2)
C2′—B11′	1.695(4)	C2′—B11′	1.704(2)
Ni3-C1-C1′-C2′	36.9(2)	Ni2-C1-C1′-C2′	25.60(17)

2.2.12 Alternative synthesis of [1-(1′-1′,2′-*closo*-$C_2B_{10}H_{11}$)-3,3-{$P(OMe)_3$}$_2$-3,1,2-*closo*-$NiC_2B_9H_{10}$] (13)

Cis-[$NiBr_2(P(OMe)_3)_2$] (**15**) was prepared *via* analogous methods to the preparation of *cis*-[$NiBr_2(P(OEt)_3)_2$].[27] The preparation involves the treatment of anhydrous $NiBr_2$ with appropriate equivalent of trimethylphosphite in anhydrous THF afforded a dark purple solution. After 2 hrs stirring, removal of solvent yielded a brown powder in a high yield.

Compound **15** was characterised by spectroscopically. The elemental analysis is in agreement with that expected for $C_6H_{18}Br_2NiO_6P_2$. In the ^1H NMR spectrum consists a singlet resonance and in the ^{31}P spectrum it gives a broad weak signal. These results confirm purity of the compound **15**. Having pure compound **15**, metallation of [7-(1′-1′,2′-*closo*-$C_2B_{10}H_{11}$)-7,8-*nido*-$C_2B_9H_{11}]^{2-}$ has been carried out by the same procedure as **11** using one equivalent of *cis*-[$NiBr_2(P(OMe)_3)_2$]. After spot TLC analysis followed by chromatographic purification, a purple compound **13** was isolated in reasonable yields and identified by NMR spectroscopies.

2.2.13 Synthesis of [1-(1′-1′,2′-*closo*-$C_2B_{10}H_{11}$)-3,3-{$P(OEt)_3$}$_2$-3,1,2-*closo*-$NiC_2B_9H_{10}$] (16)

Compound **16** was prepared by following the same procedure as for **13**, but metallation was done using the $\{Ni(P(OEt)_3)_2\}^{2+}$ fragment in a stoichiometric ratio. After usual work-up and prep TLC purification, a purple product was isolated in moderate yields. Compound **16** was characterised by microanalysis, mass spectrometry and ^1H, ^{11}B, ^{31}P NMR spectroscopies.

The mass spectrum of **16** contains an envelope centred on *m/z* 665.6 (M^+) (MW = 665.63 g mol^{-1}). The elemental analysis of compound **16** is in good agreement with that expected for $C_{16}H_{51}B_{19}NiO_6P_2$.

In the ^1H NMR spectrum of **16**, there is a C*H*$_{cage}$ resonance at relatively high frequency at δ 5.00 ppm, comparable to C*H*$_{cage}$ carborane resonances of compound **13**. There is also a low frequency C*H*$_{cage}$ doublet (δ 2.44 ppm) with J = 13.0 Hz resonance assigned to the metallated cage. These spectroscopic features suggest, the compound **16** must be analogous to **13**. Additionally, multiple overlapping resonances arising from two doublets of quartets at δ 4.30-4.05 ppm with integral-12 corresponding to ethoxy methylene protons and a triplet of doublets $^3J_{HH}$ = 7.2 Hz, $^4J_{PH}$ = <1 Hz at δ 1.34 ppm with integral-18 assigned to methyl hydrogens were also observed. In the $^1H\{^{31}P\}$ NMR spectrum the nickelacarborane cage C*H*$_{cage}$ and methyl protons give singlet and triplet resonances respectively. There are also multiplets arising from ethoxy methylene protons.

The $^{31}P\{^1H\}$ NMR spectrum of compound **16** reveals two mutual doublets with $^2J_{PP}$ = 116.1 Hz. Therefore it indicates that the nickelacarborane cage must remain in an unisomerised form.

The $^{11}B\{^1H\}$ NMR spectrum of **16** is similar to that of compound **13** (Figure 2.2.13.1) and consists of multiple overlapping resonances between δ 1.3 and -18.9 ppm with a total integral of 19B. This strongly suggests, therefore, that compound **16** must be 3,1,2-1′,2′ architecture.

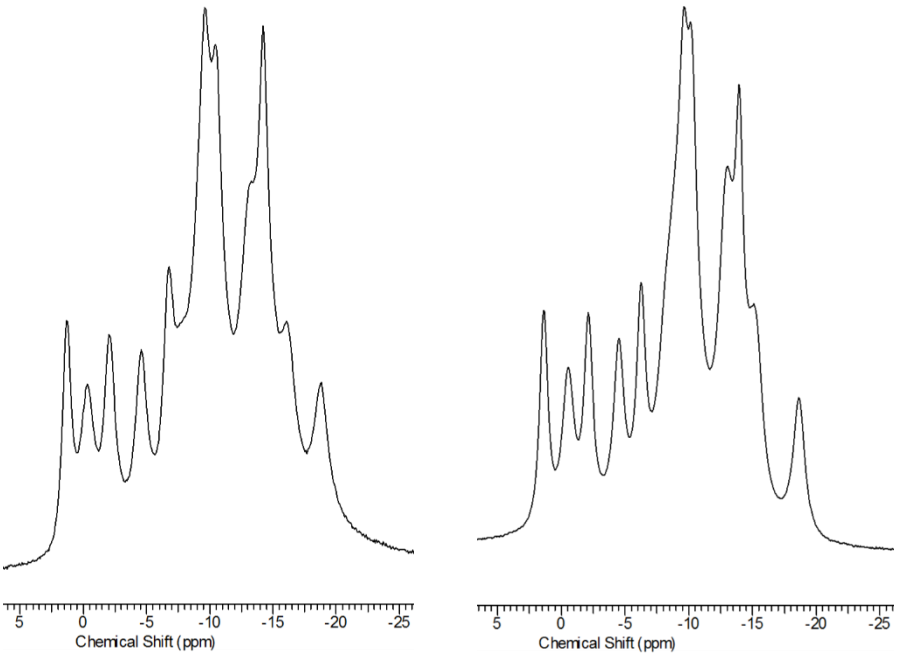

Figure 2.2.13.1 Comparison of the $^{11}B\{^{1}H\}$ NMR spectra of compound **16** (left) and **13** (right) between +5 and –25 ppm.

From the spectroscopic data we confirm that compound **16** must be [1-(1′-1′,2′-*closo*-$C_2B_{10}H_{11}$)-3,3-{$P(OEt)_3$}$_2$-3,1,2-*closo*-$NiC_2B_9H_{10}$] (Figure 2.2.13.2), therefore crystallographic analysis was not performed.

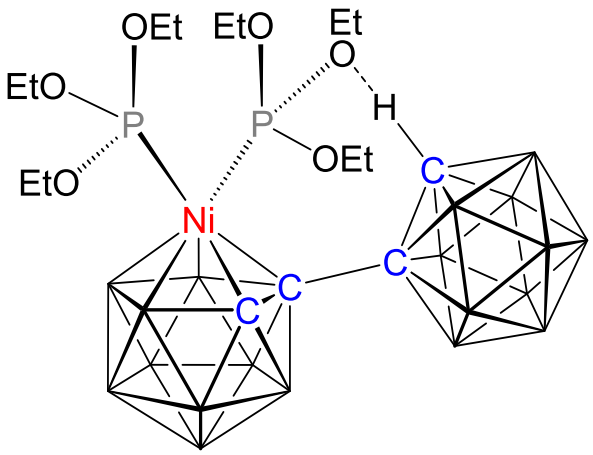

Figure 2.2.13.2 Molecular structure [1-(1′-1′,2′-*closo*-$C_2B_{10}H_{11}$)-3,3-{$P(OEt)_3$}$_2$-3,1,2-*closo*-$NiC_2B_9H_{10}$] (**16**)

2.2.14 Isomerisation of bis(phosphite) nickelacarboranes

A metallation reaction was carried out by following the same procedure used for **11** but using a $\{Ni(tmeda)\}^{2+}$ fragment (Figure 2.2.14.1). Unfortunately, we were unable to isolate any 3-(tmeda)-3,1,2-NiC_2B_9-1′,2′-C_2B_{10} species.

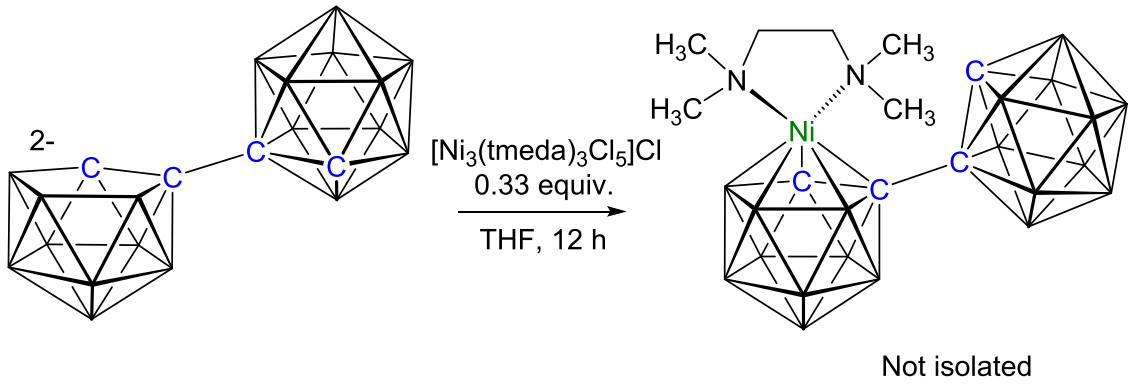

Figure 2.2.14.1 Metallation of $\mathbf{I}^{2-}$ with $[Ni_3(tmeda)_3Cl_5]Cl$.

However, in another approach, metallation of the dianion $\mathbf{I}^{2-}$ with 0.33 equiv. $[Ni_3(tmeda)_3Cl_5]Cl$ followed by *in situ* addition of excess $P(OMe)_3$ affords only unisomerised [1-(1′-1′,2′-*closo*-$C_2B_{10}H_{11}$)-3,3-$\{P(OMe)_3\}_2$-3,1,2-*closo*-$NiC_2B_9H_{10}$] (**13**) whereas metallation with 0.5 equiv. $[Ni_3(tmeda)_3Cl_5]Cl$ followed by *in situ* addition of excess $P(OMe)_3$ results in both isomerised [1-(1′-1′,2′-*closo*-$C_2B_{10}H_{11}$)-2,2-$\{P(OMe)_3\}_2$-2,1,8-*closo*-$NiC_2B_9H_{10}$] (**14**) as the major component and unisomerised **13** as the minor product. The isomerisation might be related to the isomerisation of the 3,1,2-1′,2′ isomer (**11**) to 2,1,8-1′,2′ (**12**) caused by the basic nature of the tmeda ligand. Therefore the 2,1,8-1′,2′ phosphite species **14** is the result of isomerisation before the $P(OMe)_3$ was added and not because of it.

From crystallographic analysis and the ^1H NMR spectrum, a short contact H-bonding of one of the oxygen atoms of methoxy groups to the C*H* atom of the carborane substituent on C1 was observed. We have attempted to break this H-bonding by supplying gentle heating. Thus compound **13** was dissolved in THF and the temperature gradually increased from 30 °C to 60 °C and finally up to reflux. The reaction was monitored by $^{31}P\{^1H\}$ NMR spectroscopy at each increment of 10 °C. However no isomerisation was observed at higher temperature and the compound partially decomposes at 50 °C.

We have concluded our study by performing the synthesis of compound **13** by direct metallation using the $\{Ni(P(OMe)_3)_2\}^{2+}$ fragment instead of *in situ* addition of $P(OMe)_3$. Metallation of nido/closo carborane using c*is*-$[NiBr_2(P(OMe)_3)_2]$ yields only compound **13** with the synthetic procedure discussed in section 2.2.12. Thus, metallation of the dianion $\mathbf{I}^{2-}$ with $\{Ni(P(OMe)_3)_2\}^{2+}$ generates only the 3,1,2-1′,2′ isomer with no 2,1,8-1′,2′ isomer isolated.

We have also extended this to triethylphosphite, metallation of [7-(1′-1′,2′-*closo*-$C_2B_{10}H_{11}$)-7,8-*nido*-$C_2B_9H_{11}]^{2-}$ with a $\{Ni(P(OEt)_3)_2\}^{2+}$ fragment affording [1-(1′-1′,2′-*closo*-$C_2B_{10}H_{11}$)-3,3-$\{P(OEt)_3\}_2$-3,1,2-*closo*-$NiC_2B_9H_{10}$] (**16**), the synthesis of which is described in section 2.2.13. Here also we have observed only the 3,1,2-1′,2′ product and no 2,1,8-1′,2′ or 4,1,2-1′,2′ isomers. From the ^1H NMR spectrum, a short H-bonding contact of one of the ethoxy oxygen atoms to the C*H* atom of the carborane substituent on C1 was observed. We have also attempted to cleave this H-bonding by applying gentle heating. Thus, compound **16** was taken in THF and heated initially at 30 °C with gradual increments of 10 °C and finally up to 65 °C. The reaction was also monitored using $^{31}P\{^1H\}$ NMR spectroscopy. However no change was observed with respect to the starting isomer and it also slightly decomposes at 50 °C. Thus the experiment again confirms that formation of H-bonding does not play significant role for the formation of 3,1,2-NiC_2B_9-1′,2′-C_2B_{10}.

In summary the studies on phosphite based nickelacarboranes suggest the electron withdrawing capability of the phosphites do not effect in the isomerisation process *i.e.* 3,1,2-1′,2′ to 4,1,2-1′,2′ isomerisation. Therefore, in the case of chelating and monodentate bulky phosphines (dppe, PPh_2Me) the isomerisation 3,1,2- to 4,1,2- must be related to steric and not electronic factors.

2.3 Summary

Examples of mono-metallated derivatives of 1,1′-bis(*o*-carborane) have been prepared and spectroscopically characterised and where relevant structurally characterised. Mono-metallated nickelacarboranes have been synthesised with the fragments $\{Ni(dppe)\}^{2+}$, $\{Ni(dmpe)\}^{2+}$, $\{Ni(PMe_3)_2\}^{2+}$, $\{Ni(PMe_2Ph)_2\}^{2+}$, $\{Ni(PPh_2Me)\}^{2+}$, $\{Ni(P(OMe)_3)_2\}^{2+}$ and $\{Ni(P(OEt)_3)_2\}^{2+}$. With the metal fragments $\{Ni(PPh_3)_2\}^{2+}$, $\{Ni(P\textit{i}Pr_3)_2\}^{2+}$, $\{Ni(P(\textit{p}\text{-tol})_3)_2\}^{2+}$ and $\{Ni(tmeda)\}^{2+}$ metallation was also attempted. Single capitation was also performed with the palladium fragments $\{Pd(NCPh)_2\}^{2+}$, $\{Pd(PMe_3)_2\}^{2+}$, $\{Pd(P(OMe)_3)_2\}^{2+}$, $\{Pd(tmeda)\}^{2+}$ and $\{Pd(en)\}^{2+}$. The nature of any isomerisations of these metallacarboranes are also explored.

The metallation of [7-(1′-1′,2′-*closo*-$C_2B_{10}H_{11}$)-7,8-*nido*-$C_2B_9H_{11}$]$^{2-}$ with $\{Ni(dppe)\}^{2+}$ results in both unisomerised [1-(1′-1′,2′-*closo*-$C_2B_{10}H_{11}$)-3-dppe-3,1,2-*closo*-$NiC_2B_9H_{10}$] (**1**) and isomerised [2-(1′-1′,2′-*closo*-$C_2B_{10}H_{11}$)-4-dppe-4,1,2-*closo*-$NiC_2B_9H_{10}$] (**2**) products. Compound **1** is readily isomerised to **2** by heating to reflux in THF. Compound **2** is fluxional at room temperature confirmed by variable temperature $^{31}P\{^1H\}$ NMR experiments. However metallation with the $\{Ni(dmpe)\}^{2+}$ fragment gives only [8-(1′-1′,2′-*closo*-$C_2B_{10}H_{11}$)-2-dmpe-2,1,8-*closo*-$NiC_2B_9H_{10}$] (**3**), and no 3,1,2-1′,2′ or 4,1,2-1′,2′ isomer. Compound **3** is also fluxional at room temperature.

In the case of $\{Ni(dppe)\}^{2+}$ with the bulky phosphine dppe, the isomerisation from the 3,1,2-1′,2′ isomer to the 4,1,2-1′,2′ isomer occurs to relieve steric crowding whereas in the case of dmpe, isomerisation occurs from a less stable 3,1,2-1′,2′ precursor to more stable 2,1,8-1′,2′ isomer. As dmpe is smaller in size but a more basic phosphine, this must be an obvious factor for the isomerisation process. From literature precedent, we initially believed that the electron withdrawing nature of dppe causes 3,1,2- to 4,1,2-isomerisation. To investigate this we have tested other monodentate phosphines such as PMe_3, PMe_2Ph, $PMePh_2$ and PPh_3.

The reaction of the dianion [7-(1′-1′,2′-*closo*-$C_2B_{10}H_{11}$)-7,8-*nido*-$C_2B_9H_{11}$]$^{2-}$ with the $\{Ni(PMe_3)_2\}^{2+}$ fragment affords, as the major product, unisomerised [1-(1′-1′,2′-*closo*-$C_2B_{10}H_{11}$)-3,3-$(PMe_3)_2$-3,1,2-*closo*-$NiC_2B_9H_{10}$] (**4**) and a trace amount of [7-(1′-1′,2′-*closo*-$C_2B_{10}H_{11}$)-10-(PMe_3)-7,8-*nido*-$C_2B_9H_{10}$] (**5**) and [1-(1′-1′,2′-*closo*-$C_2B_{10}H_{11}$)-3-Cl-3-PMe_3-8-PMe_3-3,1,2-*closo*-$NiC_2B_9H_9$] (**6**). All these were fully characterised by

NMR spectroscopy, mass spectrometry and *X*-ray crystallography. Compound **5** is a nido-phosphine derivative whereas compounds **4** and **6** are metallcarboranes. A possible mechanism of formation of these compounds is provided. Similarly, the treatment of nido/closo bis(carborane) with $\{Ni(PMe_2Ph)\}^{2+}$ yields compound **7** as the major product, unisomerised [1-(1′-1′,2′-*closo*-$C_2B_{10}H_{11}$)-3,3-$(PMe_2Ph)_2$-3,1,2-*closo*-$NiC_2B_9H_{10}$] *i.e.* in the 3,1,2-1′,2′ form. From this reaction we have also observed products analogous to compounds of **5** and **6**. However we are able to isolate only [7-(1′-1′,2′-*closo*-$C_2B_{10}H_{11}$)-10-(PMe_2Ph)-7,8-*nido*-$C_2B_9H_{10}$] (**8**) analogous to **5**. But the spectroscopic evidence shows there is also a species analogous to compound **6**. Further metallation of the dianion [7-(1′-1′,2′-*closo*-$C_2B_{10}H_{11}$)-7,8-*nido*-$C_2B_9H_{11}]^{2-}$ with the metal fragment $\{Ni(PPh_2Me)\}^{2+}$ gives only isomerised [2-(1′-1′,2′-*closo*-$C_2B_{10}H_{11}$)-4,4-$(PMePh_2)_2$-4,1,2-*closo*-$NiC_2B_9H_{10}$] (**9**) and no 3,1,2-1′,2′ precursor was observed. Compound **9** is characterised only by spectroscopic methods with all attempts to crystallise this species unsuccessful. Hence the isomer was confirmed by comparing the $^{11}B\{^1H\}$ NMR spectra of compounds **2** (4,1,2-1′,2′ isomer) and **3** (2,1,8-1′,2′ isomer) with **9**. Again the metallation reaction with $\{Ni(PPh_3)_2\}^{2+}$ was tried, although unsuccessful in isolating the desired compound. But the spectroscopic evidence indicate that the species must be analogous to compound **6**. The capitation reaction of nido/closo bis(carborane) with $\{Ni(P(p\text{-tol})_3)_2\}^{2+}$ and $\{Ni(P\textit{i}Pr_3)_2\}^{2+}$ fragments were also attempted where $P(p\text{-tol})_3$ (cone angle = 145°) and $P\textit{i}Pr_3$ (cone angle = 160°) have similar cone angles to PPh_3 (cone angle = 145°). However metallation reactions were unsuccessful in both cases, and we have not observed any desired closo metallacarborane species.

As there is an increase in the number of phenyl rings in the phosphine series from PMe_3 to PMe_2Ph to $PMePh_2$, a trend of formation of the products is observed from unisomerised compounds **4** (3,1,2-1′,2′ for PMe_3) and **7** (3,1,2-1′,2′ for PMe_2Ph) to isomerised compound **9** (4,1,2-1′,2′ for $PMePh_2$). This might be a result of either electron withdrawing capability or size of the phosphine as increasing number of phenyl rings in the phosphine series changes both steric and electronic factors. To investigate if this isomerisation is driven by steric or electronic effects, we have studied metallation reactions using $P(OMe)_3$.

From the literature, we could not find any suitable source of the $\{Ni(P(OMe)_3)_2\}^{2+}$ fragment except a palladium analogue *i.e.* *cis*-$[PdCl_2(P(OMe)_3)_2]$. We have also used *cis*-$[PdCl_2(PMe_3)_2]$ to connect the palladacarboranes with nickelacarboranes. Thus

treatment of the dianion [7-(1′-1′,2′-*closo*-$C_2B_{10}H_{11}$)-7,8-*nido*-$C_2B_9H_{11}]^{2-}$ with $\{Pd(PMe_3)_2\}^{2+}$ yields only [1-(1′-1′,2′-*closo*-$C_2B_{10}H_{11}$)-3-Cl-3-PMe_3-8-PMe_3-3,1,2-*closo*-$PdC_2B_9H_9$] (**10**) with no other products of interest. Compound **10** was characterised spectroscopically and crystallographically. It is isomorphous to compound **6**. In contrast, doing the metallation of the nido/closo bis(carborane) with $\{Pd(P(OMe)_3)_2\}^{2+}$ no closo species were observed and, from the spectroscopic evidence, a phosphine-nido species is formed. This may be due to a labile Pd-P bond. However we have also tried metallation of the dianion [7-(1′-1′,2′-*closo*-$C_2B_{10}H_{11}$)-7,8-*nido*-$C_2B_9H_{11}]^{2-}$ with $\{Pd(NCPh)_2\}^{2+}$ and *in situ* addition of PMe_3. Unfortunately this approach was also not successful as we have not observed any closo metallacarborane.

Eventually we targeted 3,3-$\{P(OMe)_3\}_2$-3,1,2-PdC_2B_9-1′,2′-C_2B_{10} by the $P(OMe)_3$ displacement of tmeda from 3,3-(tmeda)-3,1,2-PdC_2B_9-1′,2′-C_2B_{10}. Treatment of [7-(1′-1′,2′-*closo*-$C_2B_{10}H_{11}$)-7,8-*nido*-$C_2B_9H_{11}]^{2-}$ with $\{Pd(tmeda)\}^{2+}$ gives both the unisomerised [1-(1′-1′,2′-*closo*-$C_2B_{10}H_{11}$)-3-tmeda-3,1,2-*closo*-$PdC_2B_9H_{10}$] (**11**) and isomerised [8-(1′-1′,2′-*closo*-$C_2B_{10}H_{11}$)-2-tmeda-2,1,8-*closo*-$PdC_2B_9H_{10}$] (**12**). The isomerisation of the 3,1,2- isomer to the 2,1,8- isomer is related to the basicity of the tmeda ligand. Compound **11** always converts to **12** at room temperature. However the tmeda displacement of compound **11** in the presence of excess $P(OMe)_3$ is not successful. Having this isomerisation from 3,1,2-PdC_2B_9-1,2-C_2B_{10} to 2,1,8-PdC_2B_9-1,2-C_2B_{10}, we have used the less basic en ligand. Unfortunately attempted metallation results in no closo species.

Nevertheless we have successfully applied the same idea in the nickel system *i.e*. the targeted synthesis of 3,3-(tmeda)-3,1,2-NiC_2B_9-1′,2′-C_2B_{10} followed by tmeda displacement by $P(OMe)_3$. We have isolated rare examples of phosphite based nickelcarboranes by metallation of [7-(1′-1′,2′-*closo*-$C_2B_{10}H_{11}$)-7,8-*nido*-$C_2B_9H_{11}]^{2-}$ with $\{Ni(tmeda)\}^{2+}$ and *in situ* addition of $P(OMe)_3$. The stoichiometric addition of $[Ni_3(tmeda)_3Cl_5]Cl$ to the dianion [7-(1′-1′,2′-*closo*-$C_2B_{10}H_{11}$)-7,8-*nido*-$C_2B_9H_{11}]^{2-}$ followed by excess $P(OMe)_3$ yields unisomerised [1-(1′-1′,2′-*closo*-$C_2B_{10}H_{11}$)-3,3-$\{P(OMe)_3\}_2$-3,1,2-*closo*-$NiC_2B_9H_{10}$] (**13**) whereas using excess $\{Ni(tmeda)\}^{2+}$ results in both the isomerised major product, [1-(1′-1′,2′-*closo*-$C_2B_{10}H_{11}$)-2,2-$\{P(OMe)_3\}_2$-2,1,8-*closo*-$NiC_2B_9H_{10}$] (**14**) and the unisomerised **13**. Here the 3,1,2 to 2,1,8 isomerisation is driven by the electron-donating character of the tmeda ligand. This isomerisation happens before subsequent displacement of the tmeda by phosphite. Further direct metallation

studies confirm this. The reaction of nido/closo carborane with c*is*-[$NiBr_2(P(OMe)_3)_2$] gives only compound **13** *i.e.* the 3,1,2-NiC_2B_9-1′,2′-C_2B_{10} isomer. Controlled heating of compound **13** does not produce a new isomer, suggesting that H-bonding does not play any role in preventing the isomerisation process. We have also used another example of an electron withdrawing phosphite, triethylphosphite. Upon metallation of monodecapitated bis(carborane) with the $\{Ni(P(OEt)_3)_2\}^{2+}$ fragment, we isolated a 3,1,2-NiC_2B_9-1,2-C_2B_{10} isomer *i.e.* [1-(1′-1′,2′-*closo*-$C_2B_{10}H_{11}$)-3,3-$\{P(OEt)_3\}_2$-3,1,2-*closo*-$NiC_2B_9H_{10}$] (**16**).

Thus the studies on trimethylphosphite and triethylphosphite strongly suggest that the electron withdrawing nature of the phosphite does not play any role in the isomerisation. The bulkiness of chelating phosphine (dppe) and monodentate phosphine ($PMePh_2$) causes the isomerisation of 3,1,2-1′,2′ to 4,1,2-1′,2′. Electron-rich dmpe or tmeda ligands induce isomerisation of 3,1,2-1′,2′ to 2,1,8-1′,2′.

2.4 References

1 (a) R. A. Wiesboeck and M. F.Hawthorne, *J. Am. Chem. Soc.*, 1964, **86**, 1642; (b) M. F. Hawthorne, D. C. Young, T. D. Andrews, D. V. Howe, R. L. Pilling, A. D. Pitts, M. Reintjes, L. F. Warren, Jr., and P. A. Wegner, *J. Am. Chem. Soc.*, 1968, **90**, 879.

2 (a) S. B. Miller and M. F. Hawthorne, *J. Chem. Soc., Chem. Commun.*, 1976, 786; (b) R. E. King III, S. B. Miller, C. B. Knobler and M. F. Hawthorne, *Inorg. Chem.*, 1983, **22**, 3548.

3 A. A. Erdaman, Z. P. Zubreichuk, V. A. Knizhnikov, A. A. Maier, G. G. Aleksandrov, S. E. Nefedov and I. L. Eremenko, *Russ. Chem. Bull. Int. Ed.*, 2001, **50**, 2248.

4 X. Yang, W. Jiang, C. B. Knobler, M. D. Mortimer and M. F. Hawthorne, *Inorg. Chim. Acta*, 1995, **240**, 371.

5 S. Ren and Z. Xie, *Organometallics*, 2008, **27**, 5167.

6 M. F. Hawthorne, D. A. Owen and J. W. Wiggins, *Inorg. Chem.*, 1971, **10**, 1304.

7 G. Thiripuranathar, W. Y. Man, C. Palmero, A. P. Y. Chan, B. T. Leube, D. Ellis, D. McKay, S. A. Macgregor, L. Jourdan, G. M. Rosair and A. J. Welch, *Dalton Trans.*, 2015, **44**, 5628.

8 G. S. Kazakov, I. B. Sivaev, K. Y. Suponitsky, A. D. Kirilin, V. I. Bregadze, and A. J. Welch, *J. Organomet. Chem.*, 2016, **805**, 1.

9 (a) T. E. Paxson, M. K. Kaloustian, G. M. Tom, R. J. Wiersema and M. F. Hawthorne, *J. Am. Chem. Soc.*, 1972, **94**, 4882; (b) T. P. Hanusa and L. J. Todd, *Polyhedron*, 1985, **4**, 2063.

10 (a) D. M. P. Mingos, M. I. Forsyth and A. J. Welch, *J. Chem. Soc., Chem. Commun.*, 1977, 605; (b) *idem, J. Chem. Soc., Dalton Trans.*, 1978, 1363; (c) P. D. Abram, D. McKay, D. Ellis, S. A. Macgregor, G. M. Rosair and A. J. Welch, *Dalton Trans.*, 2010, **39**, 2412.

11 E. W. Abel, J. K. Bhargava and K. G. Orrell, *Prog. Inorg. Chem.*, 1984, **32**, 1.

12 (a) M. R. Churchill and K. Gold, *J. Am. Chem. Soc.*, 1970, **92**, 1180; (b) N. Carr, D. F. Mullica, E. L. Sappenfield and F. G. A. Stone, *Inorg. Chem.*, 1994, **33**, 1666; (c) K. Fallis, D. F. Mullica, E. L. Sappenfield and F. G. A. Stone, *Inorg. Chem.*, 1994, **33**, 4927; (d) R. M. Garrioch, P. Kuballa, K. S. Low, G. M. Rosair and A. J. Welch, *J. Organomet. Chem.*, 1999, **575**, 57; (e) M. A. Fox, J. A. K.

Howard, A. K. Hughes, J. M. Malget and D. S. Yufit, *J. Chem. Soc., Dalton Trans*., 2001, 2263; (f) S. Robertson, D. Ellis, G. M. Rosair and A. J. Welch, *Appl. Organomet. Chem*., 2003, **17**, 518; (g) S. Robertson, R. M. Garrioch, D. Ellis, T. D. McGrath, B. E. Hodson, G. M. Rosair and A. J. Welch, *Inorg. Chim. Acta*, 2005, **358**, 1485; (h) W. Y. Man, G. M. Rosair and A. J. Welch, *Dalton Trans*., 2015, **44**, 15417.

13 C. R. Groom and F. H. Allen, *Angew. Chem. Int. Ed*., 2014, **53**, 662.

14 A. McAnaw, G. Scott, L. Elrick, G. M. Rosair and A. J. Welch, *Dalton Trans*., 2013, **42**, 645.

15 A. McAnaw, M. E. Lopez, D. Ellis, G. M. Rosair and A. J. Welch, *Dalton Trans*., 2014, **43**, 5095.

16 J. Buchanan, E. J. M. Hamilton, D. Reed and A. J. Welch, *J. Chem. Soc. Dalton Trans*. 1990, 677.

17 *e.g*. D. McKay, S. A. Macgregor and A. J. Welch, *Chem. Sci*., 2015, **6**, 3117.

18 C. A. Tolman, *Chem. Rev*., 1977, **77**, 313.

19 L. J. V. Griend, J. C. Clardy and J. G. Verkade, *Inorg. Chem*., 1975, **14**, 710.

20 A. M. Z. Slawin, P. G. Waddell and J. D. Woollins, *Acta Cryst*., 2009, **E65**, m1391.

21 G. Schultz, N. Yu. Subbotina, C. M. Jensen, J. A. Golen and I. Hargittai, *Inorg. Chim. Acta*, 1992, **191**, 85.

22 M. S. Kharasch, R. C. Seyler and F. R. Mayo, *J. Am. Chem. Soc*., 1938, **60**, 882.

23 (a) H. M. Colquhoun, T. J. Greenhough and M. G. H. Wallbridge, *J. Chem. Soc., Chem. Comm*., 1978, 322; (b) H. M. Colquhoun, T. J. Greenhough and M. G. H. Wallbridge, *J. Chem. Soc., Dalton. Trans*., 1985, 761.

24 P. A. K. Alla, M. M. Shoukry and R. v. Eldik, *J. Coord. Chem*., 2015, **68**, 2041.

25 D. A. Handly, P. B. Hitchcock and G. J. Leigh, *Inorg. Chim. Acta*, 2001, **314**, 1.

26 D. R. Baghurst, R. C. B. Copley, H. Fleischer, D. M. P. Mingos, G. O. Kyd, L. J. Yellowlees, A. J. Welch, T. R. Spalding and D. O'Connell, *J. Organomet. Chem*., 1993, **447**, C14.

27 M. M. Lindner, U. Beckmann, W. Frank and W. Kläui, *ISRN Inorg. Chem*., 2013, **2013**, 1.

Chapter 3

Nickelacarboranes: double dec/met of 1,1′-bis(*o*-carborane)

3.1 Introduction

Monodeboronation of 1,1′-bis(*o*-carborane) was initially reported by Hawthorne *et al* [1a] in 1971 and complete characterisations of the decapitated derivative has been recently reported by Welch *et al*.[1b] Single decapitation of 1,1′-bis(*o*-carborane) can be achieved using one equivalent of EtO^-. A major limitation of this method is that using more than one equivalent (*e.g.* 1.1 equivalent KOH in ethannol) both single and double decapitated products of bis(carborane) are observed as noted in Chapter 2. Double deboronation of 1,1′-bis(*o*-carborane) is more complex than that of mododeboronation because the product is formed as two diastereoisomers. In 1971, Hawthorne reported a procedure for the synthesis of the double decapitated species, [7-(7′-7′,8′-*nido*-$C_2B_9H_{10}$)-7,8-*nido*-$C_2B_9H_{10}$]$^{4-}$ by treatment of [7-(1′-1′,2′-*closo*-$C_2B_{10}H_{11}$)-7,8-*nido*-$C_2B_9H_{11}$]$^-$ with 2.5 equivalents of KOH and heating under reflux for 120 hrs (Figure 3.1.1).[1a] Our group has also recently shown, however, that degradation of both cages of 1,1′-bis(*o*-carborane) can also be achieved using 30 equivalent of KOH in EtOH reflux for 48 hrs.[2]

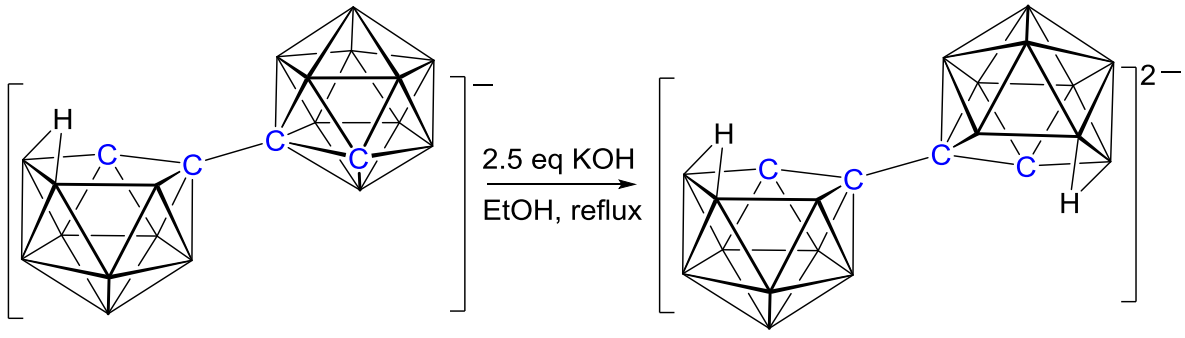

Figure 3.1.1 Decapitation of the closo cage in [7-(1′-1′,2′-*closo*-$C_2B_{10}H_{11}$)-7,8-*nido*-$C_2B_9H_{11}$]$^-$. Only the racemic product is arbitrarily shown.

Metallation of [7-(7′-7′,8′-*nido*-$C_2B_9H_{10}$)-7,8-*nido*-$C_2B_9H_{10}$]$^{4-}$ has been little explored. In 1985 Hawthorne reported capitation of Cs_2[7-(7′-7′,8′-*nido*-$C_2B_9H_{11}$)-7,8-*nido*-$C_2B_9H_{11}$] with [Rh(COD)(PEt_3)Cl] to form bis(rhodacarboranes) (Figure 3.1.2).[3] In

3,1,2-RhC_2B_{10}-3′,1′,2′-RhC_2B_{10} species, two icosahedral RhC_2B_9 units are joined by a C-C bond and a Rh-Rh bond with two Rh-H-B interactions between Rh3′, H7, B7 and Rh3, H7′, B7′. From the same reaction another isomer of bis(metallacarborane) 2,1,8-RhC_2B_{10}-3′,1′,2′-RhC_2B_{10} was also reported. In 2,1,8-RhC_2B_{11}-3′,1′,2′-RhC_2B_{11} one Rh centre is involved in a three centre Rh-H-B interaction.

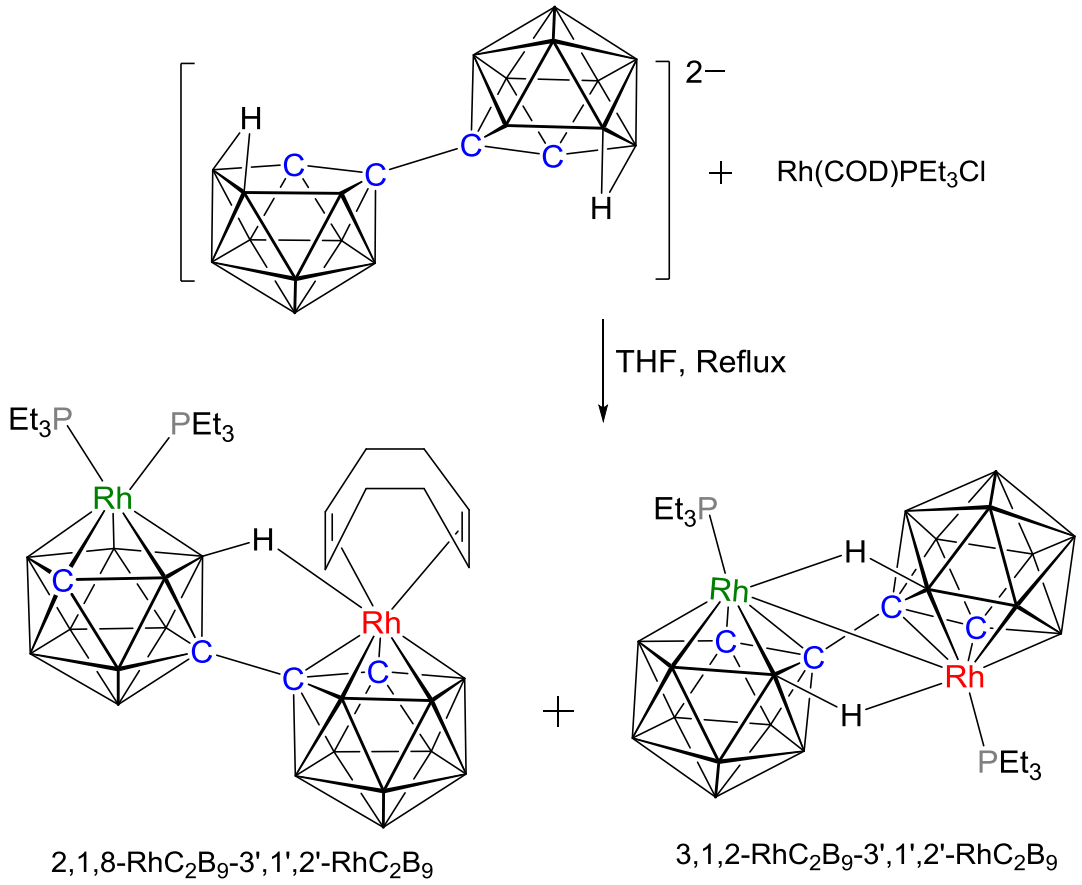

Figure 3.1.2 Synthesis of rhodacarboranes from [7-(7′-7′,8′-*nido*-$C_2B_9H_{11}$)-7,8-*nido*-$C_2B_9H_{11}$]$^{2-}$.

In 2006, Teixidor *et al* reported a B8-B9′ linked species [8-(9′-3′-Cp-3′,1′,2′-*closo*-$CoC_2B_9H_{10}$)-3-Cp-3,1,2-*closo*-$CoC_2B_9H_{10}$] but this was prepared from the reaction between [3-Cp-3,1,2-*closo*-$CoC_2B_9H_{11}$] and $S_8/AlCl_3$, [4] not from [7-(7′-7′,8′-*nido*-$C_2B_9H_{11}$)-7,8-*nido*-$C_2B_9H_{11}$]$^{2-}$. We have also explored metallation chemistry of [7-(7′-7′,8′-*nido*-$C_2B_9H_{11}$)-7,8-*nido*-$C_2B_9H_{11}$]$^{2-}$ using $\{CpCo\}^+$ (oxidised to $\{CpCo\}^{2+}$) or $\{(arene)Ru\}^{2+}$ fragments.[2] Metallation of [7-(7′-7′,8′-*nido*-$C_2B_9H_{10}$)-7,8-*nido*-$C_2B_9H_{10}$]$^{4-}$ with a $\{CpCo\}^{2+}$ fragment, generated *in situ* from $CoCl_2$/NaCp, followed by aerial oxidation produced bis(cobaltacarboranes) *i.e.* isomers of 2′,1′,8′-CoC_2B_9-3,1,2-

CoC_2B_9 (Figure 3.1.3) and a trace amount of 2′,1′,8′-CoC_2B_9-2,1,8-CoC_2B_9. In addition to this, bis(ruthenacarborane) were also synthesised upon metallation of doubly decapitated bis(carborane) using the {(*p*-cym)Ru}$^{2+}$ fragment. Treatment of [$HNMe_3$]$_2$[7-(7′-7′,8′-*nido*-$C_2B_9H_{11}$)-7,8-*nido*-$C_2B_9H_{11}$] with four equivalents of *n*BuLi followed by metallation with {(*p*-cym)Ru}$^{2+}$ gave isomers of 2′,1′,8′-*closo*-RuC_2B_9-3,1,2-RuC_2B_9 species (Figure 3.1.4). All of these isomers contain an unisomerised cage and an isomerised cage. There are no reported examples in which both cages are of 3,1,2-architecture.

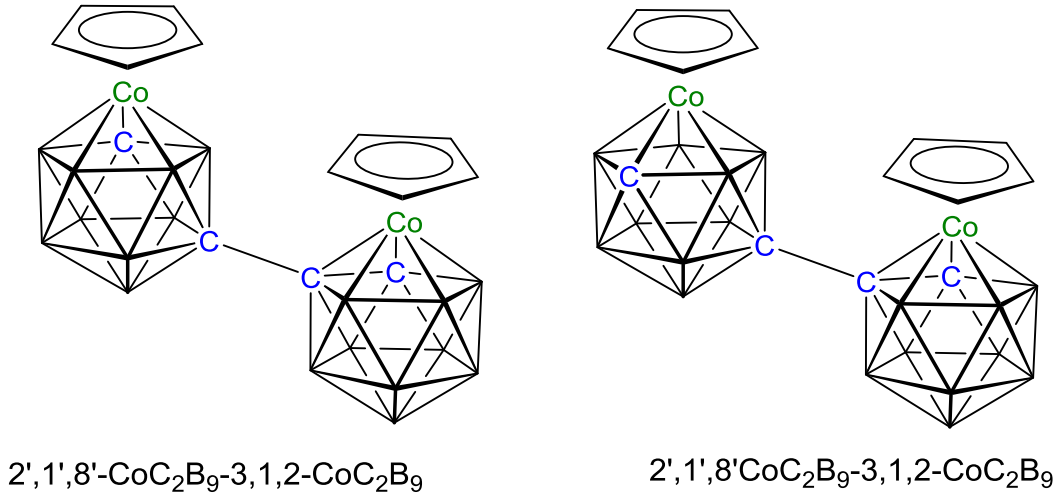

Figure 3.1.3 Isomers of bis(cobaltacarboranes).

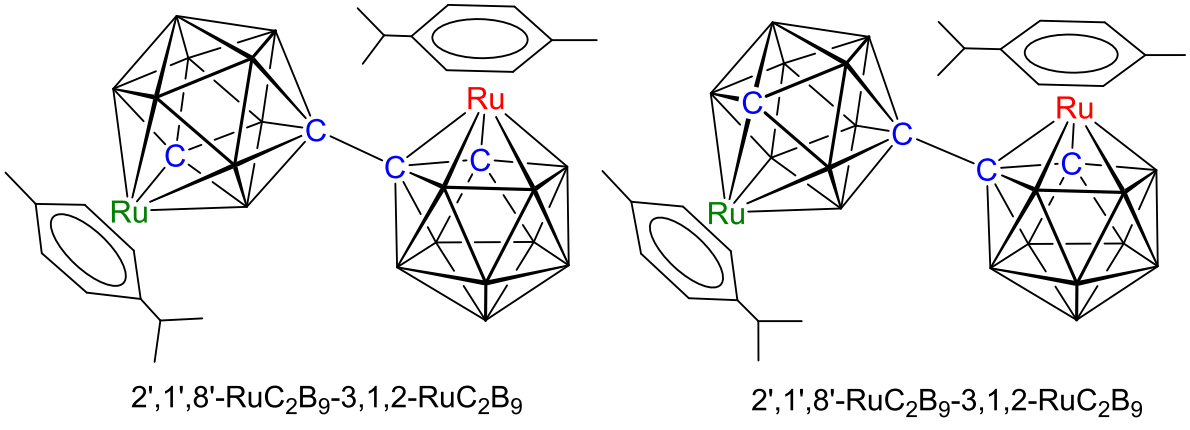

Figure 3.1.4 Isomers of bis(ruthenacarboranes).

To date, there are no reports of bis(nickellacarboranes) derived from double deboronations and metallation of 1,1′-bis(*o*-carborane). Therefore this chapter will focus

upon the syntheses of icosahedral bis(nickelacarboranes) and their isomerisation behaviour. We have used both $[HNMe_3]_2$[7-(7′-7′,8′-*nido*-$C_2B_9H_{11}$)-7,8-*nido*-$C_2B_9H_{11}$] and Tl_4[7-(7′-7′,8′-*nido*-$C_2B_9H_{10}$)-7,8-*nido*-$C_2B_9H_{10}$] for the capitations reactions where appropriate. Metallation with $\{Ni(dmpe)\}^{2+}$ and $\{Ni(dppe)\}^{2+}$ fragments led to the synthesis of new 12-vertex metallacarborane/12-vertex metallcarborane compounds. Thermal isomerisation of these derivatives has also been studied. Detailed spectroscopic and structural studies of these products are discussed and investigation of the isomerisation between them is considered. As part of the isomerisation studies of bis(nickelacarboranes), we have also explored the capitation chemistry of [7-(7′-7′,8′-*nido*-$C_2B_9H_{10}$)-7,8-*nido*-$C_2B_9H_{10}$]$^{4-}$ with $\{BI\}^{2+}$, $\{BBr\}^{2+}$ and $\{BPh\}^{2+}$ fragments.

3.2 Results and discussion

3.2.1 Synthesis $[Tl]_2[1\text{-}(1'\text{-}3',1',2'\text{-}TlC_2B_9H_{10})\text{-}3,1,2\text{-}TlC_2B_9H_{10}]$ (17) and discussion of double decapitation

Double deboronation of 1,1′-bis(*o*-carborane) was achieved using a large excess of KOH (24 equiv.) in refluxing EtOH overnight to afford $K_4[7\text{-}(7'\text{-}7',8'\text{-}nido\text{-}C_2B_9H_{10})\text{-}7,8\text{-}nido\text{-}C_2B_9H_{10}]$. Subsequent workup and cation metathesis with Tl^+ (basic medium) afforded $[Tl]_2[1\text{-}(1'\text{-}3',1',2'\text{-}closo\text{-}TlC_2B_9H_{10})\text{-}3,1,2\text{-}closo\text{-}TlC_2B_9H_{10}]$ (**17**) as a fine yellow powder in near-quantitative yields.

Due to the limited solubility of **17**, microanalysis was the only possible characterisation tool providing excellent agreement with that expected for $C_4H_{20}B_{18}Tl_4$ (theoretical: C 4.5, H 1.87%, experimental: C 4.4, H 1.78%).

$[Tl]_2[1\text{-}(1'\text{-}3',1',2'\text{-}closo\text{-}TlC_2B_9H_{10})\text{-}3,1,2\text{-}closo\text{-}TlC_2B_9H_{10}]$ (**17**) was prepared by following the same method as for $Tl[TlC_2B_9H_{11}]$ [5] although the decapitation was carried out in the presence of a large excess of KOH with overnight reflux. On closer inspection, the double decapitation of 1,1′-bis(*o*-carborane) (removal of one $\{BH\}^{2+}$ fragment from each C_2B_{10} unit) is significantly different compared to the decapitation of *o*-carborane based on the reaction time, reaction conditions and the decapitated species. The alcoholic base degradation of 1,1′-bis(*o*-carborane) proceeds in the same manner as in the case of *o*-carborane [6] albeit at a greatly reduced rate. The lower reaction rate can be rationalised on the basis of electronic factors. Initially monodeboronation of $[1',2'\text{-}C_2B_{10}\text{-}1,2\text{-}C_2B_{10}]$ (where the $\{1',2'\text{-}C_2B_{10}\}$ unit is electron withdrawing) affords $[1',2'\text{-}C_2B_{10}\text{-}7,8\text{-}C_2B_9]^{2-}$. The presence of a negative charge on the nido cage effectively reduces the electron withdrawing effect of the second carborane unit through charge dispersion. Therefore, the electrophilic character of B3′ and B6′ is reduced at the second carborane unit. As a result, the removal of a second B atoms from the dianion $[7\text{-}(1'\text{-}1',2'\text{-}closo\text{-}C_2B_{10}H_{11})\text{-}7,8\text{-}nido\text{-}C_2B_9H_{10}]^{2-}$ to afford the tetraanion $[7\text{-}(7'\text{-}7',8'\text{-}nido\text{-}C_2B_9H_{10})\text{-}7,8\text{-}nido\text{-}C_2B_9H_{10}]^{4-}$ species is not facile, and demands harsh condition (excess EtO^-) and overnight reflux.

Decapitation of both cages involves the possibility of deboronation of vertices B3, B6, B3′ and B6′ with an equal probability, and thus the possibility of two isomers. Upon

decapitation of B3, B3′ or B6, B6′ the *rac*-isomer is generated, whilst loss of B3, B6′ or B6, B3′ creates the *meso*-isomer (Figure 3.2.1.1). Therefore $[Tl]_2[1\text{-}(1'\text{-}3',1',2'\text{-}TlC_2B_9H_{10})\text{-}3,1,2\text{-}TlC_2B_9H_{10}]$ (**17**) or $[HNMe_3]_2[7\text{-}(7'\text{-}7',8'\text{-}nido\text{-}C_2B_9H_{11})\text{-}7,8\text{-}nido\text{-}C_2B_9H_{11}]$ is a mixture of two components or more precisely a mixture of diastereoisomers.

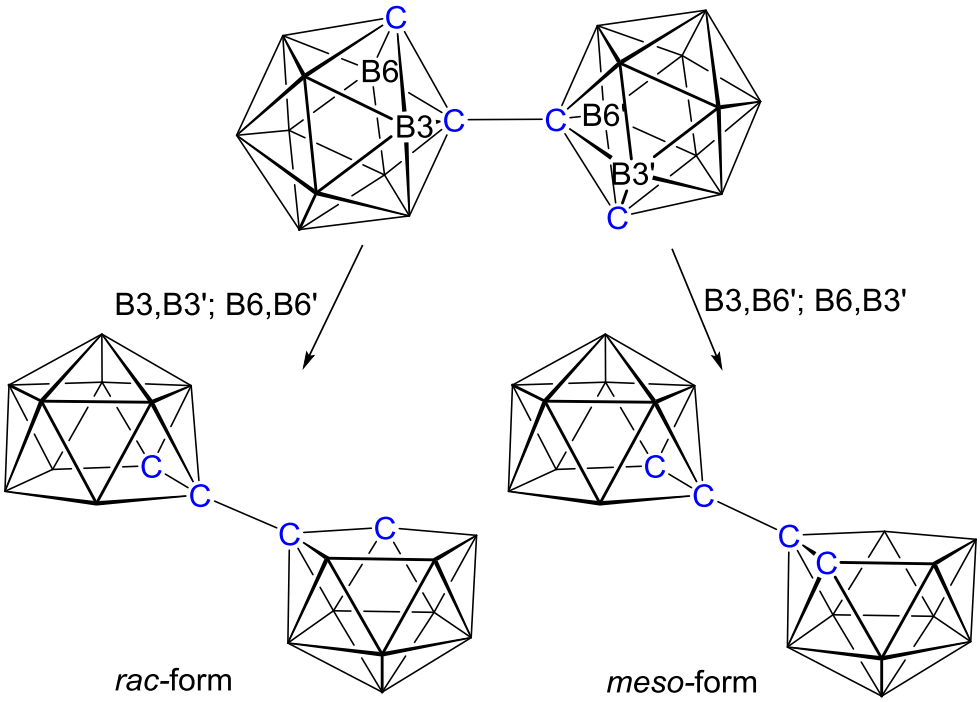

Figure 3.2.1.1 Formation of rac and meso isomers on double decapitation of 1,1′-bis(*o*-carborane).

3.2.2 Synthesis of *rac*-[1-(1′-3′-(dmpe)-3′,1′,2′-*closo*$^{\circlearrowleft}$-$NiC_2B_9H_{10}$)-3-(dmpe)-3,1,2-*closo*$^{\circlearrowleft}$-$NiC_2B_9H_{10}$] (18) and *meso*-[1-(1′-3′-(dmpe)-3′,1′,2′-*closo*$^{\circlearrowleft}$-$NiC_2B_9H_{10}$)-3-(dmpe)-3,1,2-*closo*$^{\circlearrowleft}$-$NiC_2B_9H_{10}$] (19)

The Tl_4-salt of [7-(7′-7′,8′-*nido*-$C_2B_9H_{10}$)-7,8-*nido*-$C_2B_9H_{10}$]$^{4-}$ was preferred for the metallation with {Ni(dmpe)}$^{2+}$ fragment. Compound **17** was suspended in THF. Addition of [$NiCl_2$(dmpe)] to the Tl_4-salt at –196 °C followed by warming to room temperature and stirring for 12 h afforded a dark green suspension. Filtration through silica of the crude reaction mixture followed by chromatographic purification afforded two dark green bands to give compounds **18** and **19** in moderate yield (Figure 3.2.2.1).

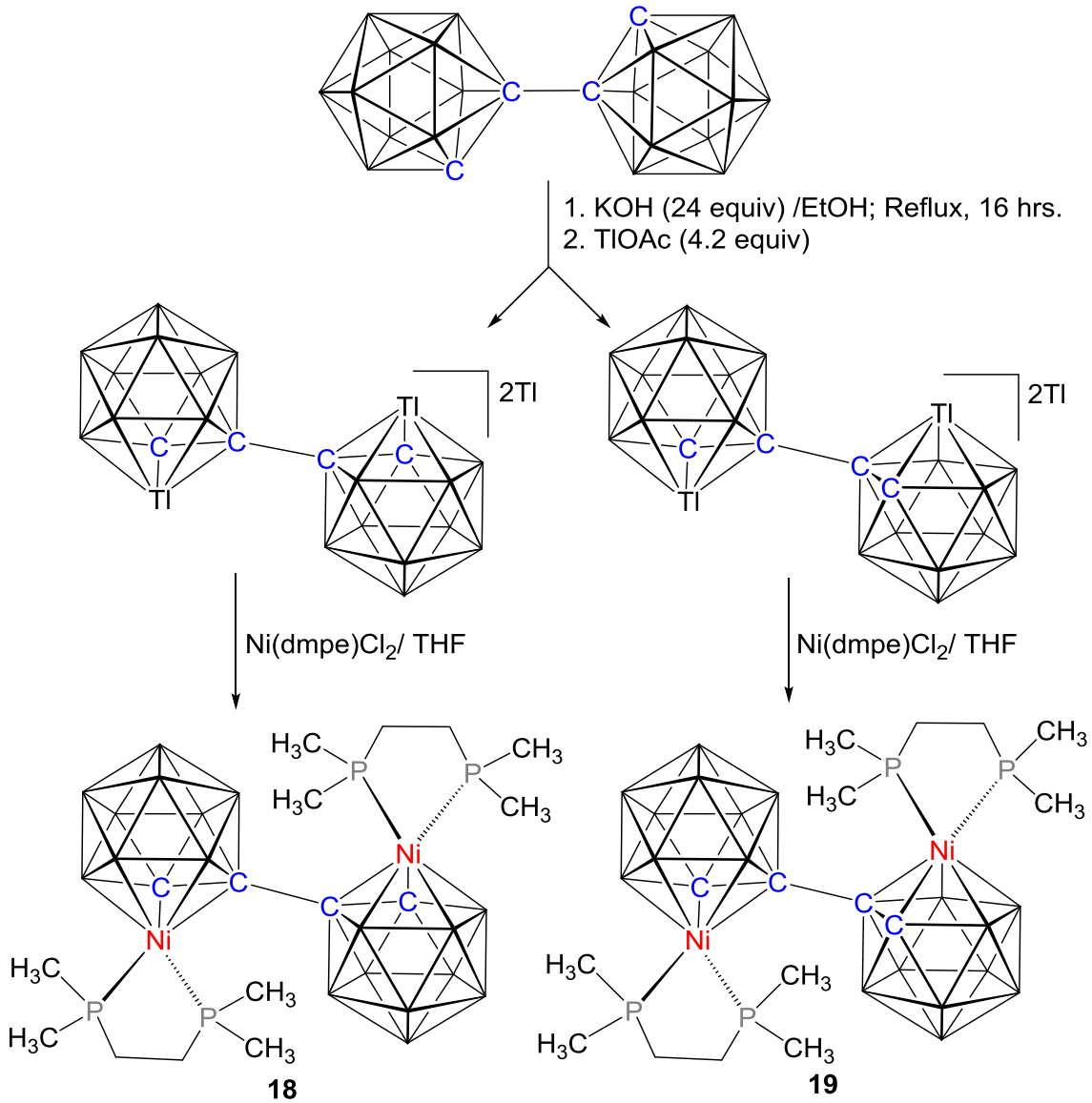

Figure 3.2.2.1 Metallation of **17** with Ni(dmpe)Cl_2.

For compound **18**, elemental analysis was in good agreement with the calculated values for $C_{16}H_{52}B_{18}Ni_2P_4 \cdot 0.5CH_2Cl_2$ (the ^1H NMR spectrum of compound **18** contains a DCM signal, even after pumping on the material for several hrs). The mass spectrum showed a sharp peak at *m/z* 681.0 (M^+) (MW = 680.47 g mol^{-1}), corresponding to the parent molecular ion. From the mass spectrum and elemental analysis, it appeared that both cages of the bis(carborane) were metallated with $\{Ni(dmpe)\}^{2+}$ fragments. For further confirmation other spectroscopic techniques were necessary.

The $^{11}B\{^1H\}$ NMR spectrum of compound **18** consists of seven resonances with relative integrals 2:2:2:2:2:4:4 from high frequency to low frequency and the spectrum is relatively simple and symmetric in nature compared to the $^{11}B\{^1H\}$ NMR spectra of mono metallated nickelacarboranes (discussed in Chapter 3). We have also attempted to identify correlations between the seven resonances. However, due to low resolution, it is not possible to fully correlate those resonances (Figure 3.2.2.2).

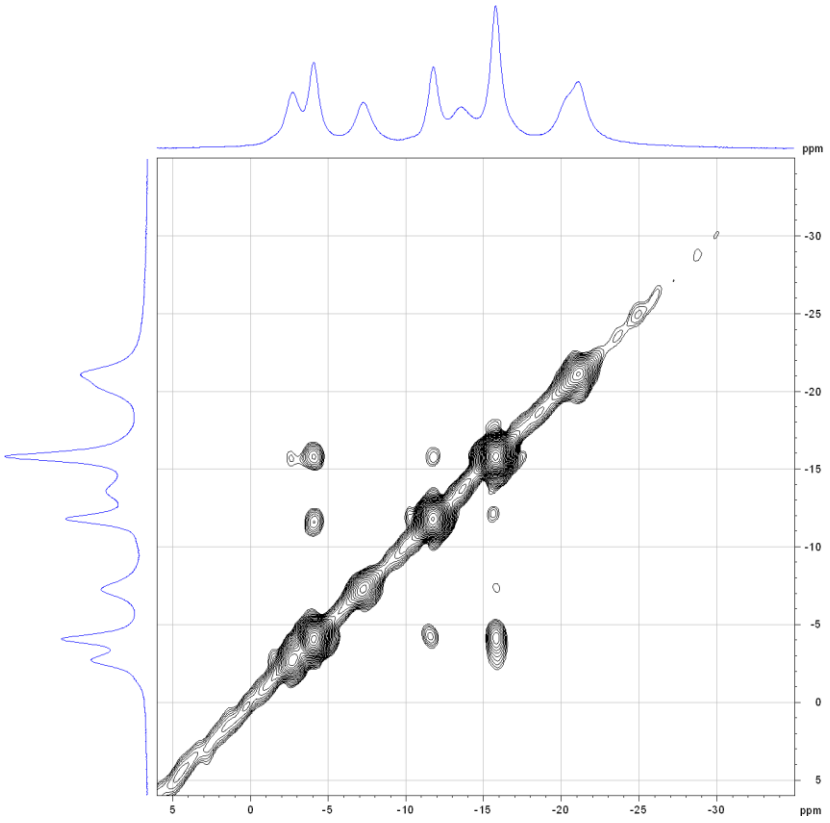

Figure 3.2.2.2 $^{11}B\{^1H\}$-$^{11}B\{^1H\}$ COSY NMR spectrum of compound **18** in CD_2Cl_2.

In the ^1H NMR spectrum there are resonances arising from the -CH_2-CH_2- bridge of the two dmpe ligands. The methyl groups of the dmpe ligands produce three doublet

resonances. The first two are of integral-6 at δ 1.83, 1.67 ppm with coupling $^{2}J_{PH}$ = 10.0 Hz and last is of integral-12 at δ 1.55, $^{2}J_{PH}$ = 10.0 Hz. These resonances collapse to the corresponding singlets in the $^{1}H\{^{31}P\}$ spectrum. There is also a single CH_{cage} resonance (δ 2.43 ppm) which appears as a doublet, J = 14.0 Hz, confirmed as arising from coupling to phosphorus since it collapses to a singlet on broad-band ^{31}P decoupling.

The $^{31}P\{^{1}H\}$ NMR spectrum of compound **18** reveals that two mutual doublets with integral four in total at δ 43.1 and 33.0 ppm and coupling constant $^{2}J_{PP}$ = 29.2 Hz (Figure 3.2.2.3). This indicates that in each cage the two phosphorus atoms are magnetically inequivalent. However out of four phosphorus atoms, two pairs in different cages are magnetically equivalent. Compound **18** is therefore, *closo*-metallated species in which the two phosphorus are in different environment and must be 3,1,2-NiC_2B_9-3′,1′,2′-NiC_2B_9 architecture.

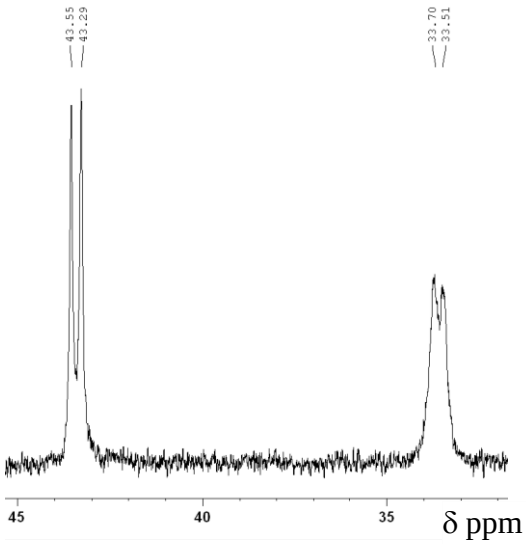

Figure 3.2.2.3 $^{31}P\{^{1}H\}$ NMR spectrum of compound **18** in CD_2Cl_2.

From the ^{1}H-^{31}P HMBC experiment (Figure 3.2.2.4), the splitting of the CH_{cage} arises from coupling with the phosphorus at δ 33.0 ppm. From the Chapter 2 we have seen that this type of coupling occurs with the phosphorus *trans* to the CH_{cage}. Therefore the resonance at δ 33.0 ppm is assigned to the *trans*-phosphorus to the CH_{cage} and that of δ 43.1 ppm corresponds to the *cis* phosphorus. Additionally the splitting of methyl protons is reflected in the spectrum.

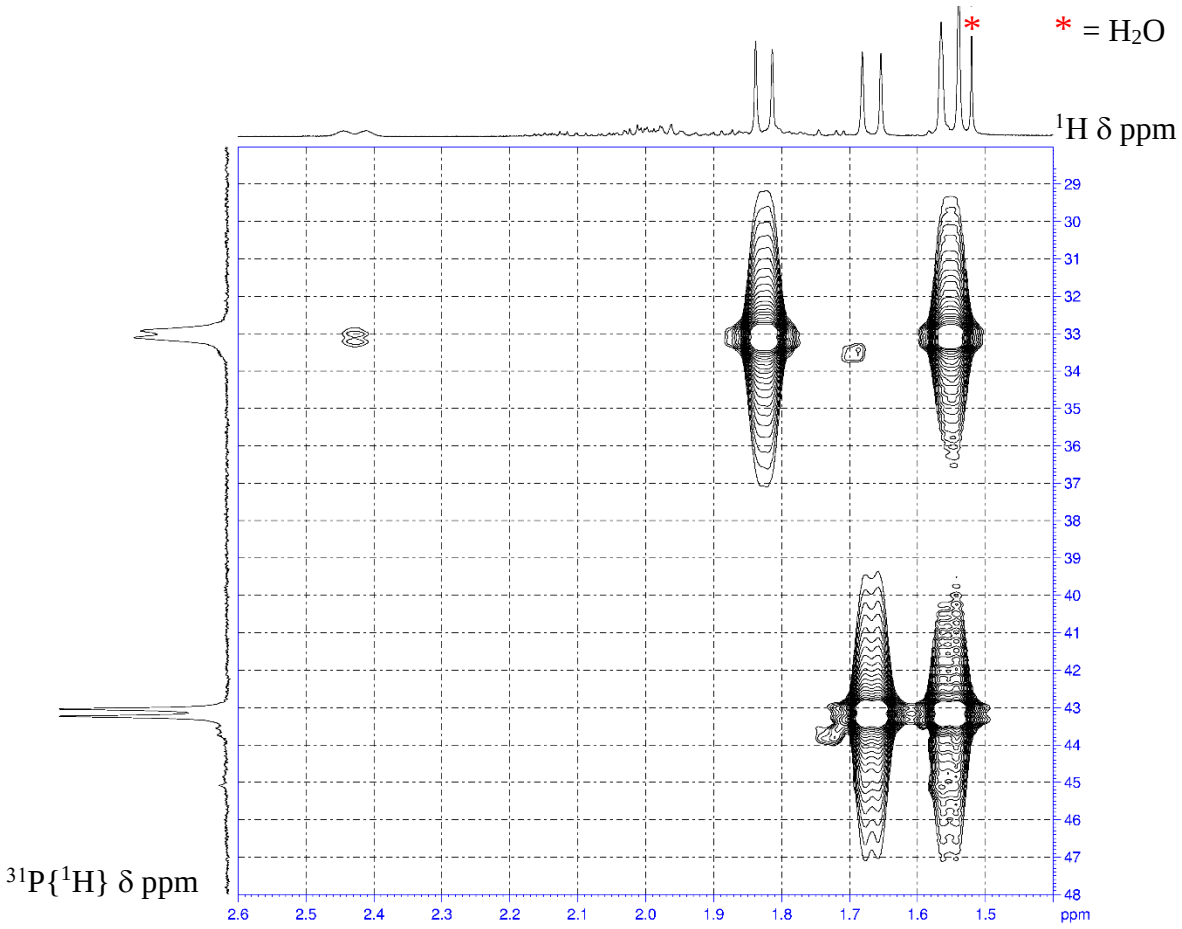

Figure 3.2.2.4 ^{1}H-$^{31}P\{^{1}H\}$ HMBC NMR spectrum of compound **18** in CD_2Cl_2.

These spectroscopic results are fully consistent with **18** being composed of two {(dmpe)(3,1,2-NiC_2B_9)} icosahedral fragments joined by a C–C bond, as expected. However, it is impossible to conclude the overall isomeric nature of the bis-nickelacarborane and consequently a structural analysis was performed.

X-ray quality crystals of compound **18** were grown by solvent diffusion of 40-60 petroleum ether into a DCM solution **18**. Single crystal *X*-ray diffraction analysis (Figure 3.2.2.5) is correlated with all these spectroscopic results on **18**. The nickelacarborane has a 3,1,2-NiC_2B_9-3′,1′,2′-NiC_2B_9 architecture arising from metallation of the tetraanion [7-(7′-7′,8′-*nido*-$C_2B_9H_{10}$)-7,8-*nido*-$C_2B_9H_{10}$]$^{4-}$ by two {Ni(dmpe)$^{2+}$} fragments. Thus compound **18** is *rac*-[1-(1′-3′-(dmpe)-3′,1′,2′-*closo*$^{\circlearrowleft}$-$NiC_2B_9H_{10}$)-3-(dmpe)-3,1,2-*closo*$^{\circlearrowleft}$-$NiC_2B_9H_{10}$].

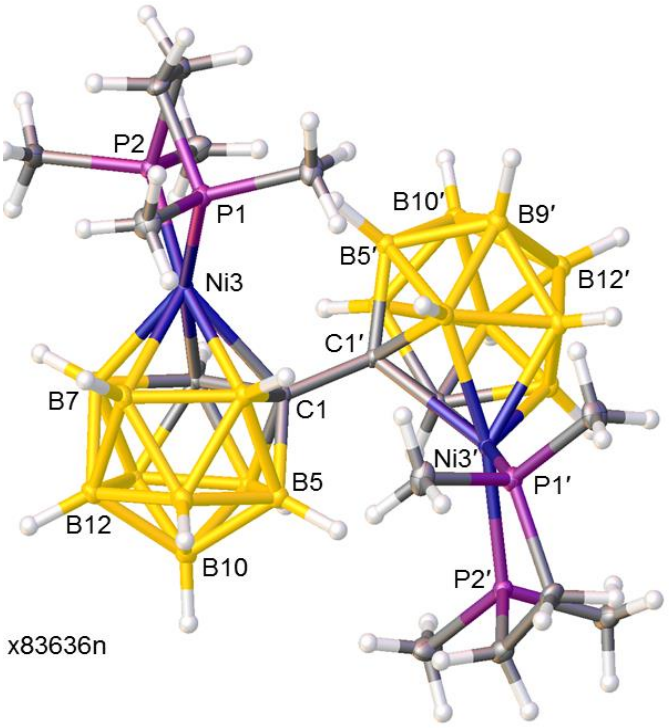

Figure 3.2.2.5 Molecular structure of [1-(1′-3′-(dmpe)-3′,1′,2′-*closo*^{5}-$NiC_2B_9H_{10}$)-3-(dmpe)-3,1,2-*closo*^{5}-$NiC_2B_9H_{10}$] *rac* (**18**).

A perspective view of a single molecule of **18** is shown in Figure 2.2.1.5. The structure is of considerable interest and show clear indications of internal crowding. In the unit cell, the structure can be grown fully by C_2 symmetry as it belongs to the *P*2/*n* space group (monoclinic) with Z′ = 0.5. Ideally the preferred orientation of the {NiP1P2} fragment in NiC_2B_9 icosahedra is lying perpendicular to the vertical mirror plane through the C_2B_9 unit.[7] In **18**, the dihedral angle, θ, between the plane through Ni3P1P2 and the plane through B6B8B10 is 55.36(8)º, a significant deviation from the electronically-preferred 90º. Practically, the NiP1P2 plane in **18** remains perpendicular to the plane of C1B10B12 vertices to reduce steric crowding between the dmpe ligand and bulky {(dmpe)(3′,1′,2′-NiC_2B_9)} substituent on C1. This is also necessarily true for the prime cage by symmetry. The plane of the {NiP1P2} fragment is somewhat bent from perpendicular to the bottom pentagonal plane through B5B6B11B12B9 vertices with the bend angle 7.4(8)º. This further indicates some steric congestion present in the molecule. This is further supported by the longer Ni3–C1 distance compared to Ni3–C2 [2.2977(19) *versus* 2.0657(18) Å].

A modified naming convention for icosahedral bis(metallcarboranes)

To identify and distinguish the chiral environments of two icosahedral MC_2B_9 units in a bis(metallacarborane), a new convention has been devised. By following the IUPAC numbering system for the icosahedral metallacarborane, if the first triangle 1→2→3 is either clockwise or anticlockwise, the chirality will be denoted by ↻ or ↺ symbols. The symbol will be added to the name following 'closo' in superscript. Additionally, if the elements in the order 1→2→3 in MC_2B_9-MC_2B_9 species are CCM/CCM or CCB/CCB, rac or meso will also be used (Figure 1). For example, for compound **18**, in both the non-prime and prime cages the first triangle in the order 1→2→3 is clockwise. Therefore the final naming will be *rac*-[1-(1′-3′-(dmpe)-3′,1′,2′-*closo*$^{↻}$-$NiC_2B_9H_{10}$)-3-(dmpe)-3,1,2-*closo*$^{↻}$-$NiC_2B_9H_{10}$] for compound **18**. All the bis(nickelcarboranes) in this Chapter have been named by following this new convention. Although possibly redundant for rac and meso species where the metallacarborane cages are both of the same isomer form, the new system is required when different metallacarborane isomers are joined.

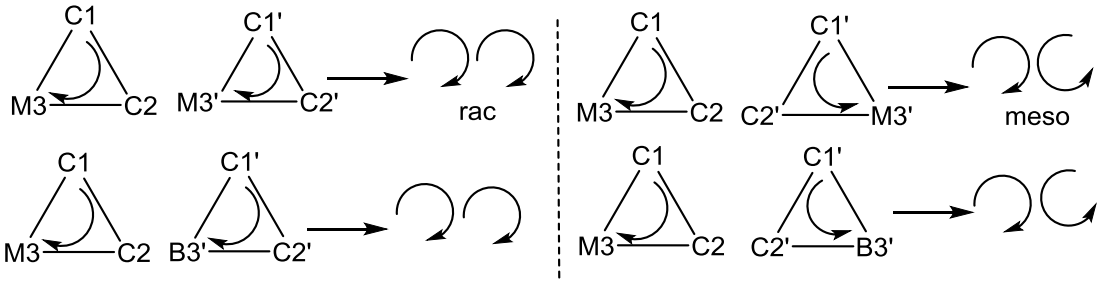

Figure 1. Naming for 12-vertex-12-vertex bis(metallacarborane).

Continuing section 3.2.2…

Moving on to compound **19**, the EI mass spectrum it shows a sharp peak at 679.6 (MW = 680.47 g mol^{-1}) corresponding to the molecular parent ion. Additionally microanalysis is in agreement with that expected for $C_{16}H_{52}B_{18}Ni_2P_4 \cdot 3CH_2Cl_2$ (the ^{1}H NMR spectrum of compound **19** always retains a DCM signal and crystals grown from DCM and 40-60 petroleum ether contain three molecules of DCM of solvation per molecule of nickelacarborane). From the mass spectrum and microanalysis, compound **19**, a co-product of **18**, was postulated to be a geometrical isomer.

The $^{11}B\{^{1}H\}$ NMR spectrum of compound **19** comprises seven resonances in the integral ratio 2:2:2:2:3:5:2 from high frequency to low frequency, a distinct pattern to that of compound **18**. From this data is impossible to identify the exact isomer of bis(nickelacarborane). Further, we have also tried to correlate the connectivity of the 18 boron atoms using a $^{11}B\{^{1}H\}$-$^{11}B\{^{1}H\}$ COSY spectrum to identify the isomer. However once more due to a very weak spectrum with multiple overlapping signals, it is not possible to fully correlate the resonances (Figure 3.2.2.6).

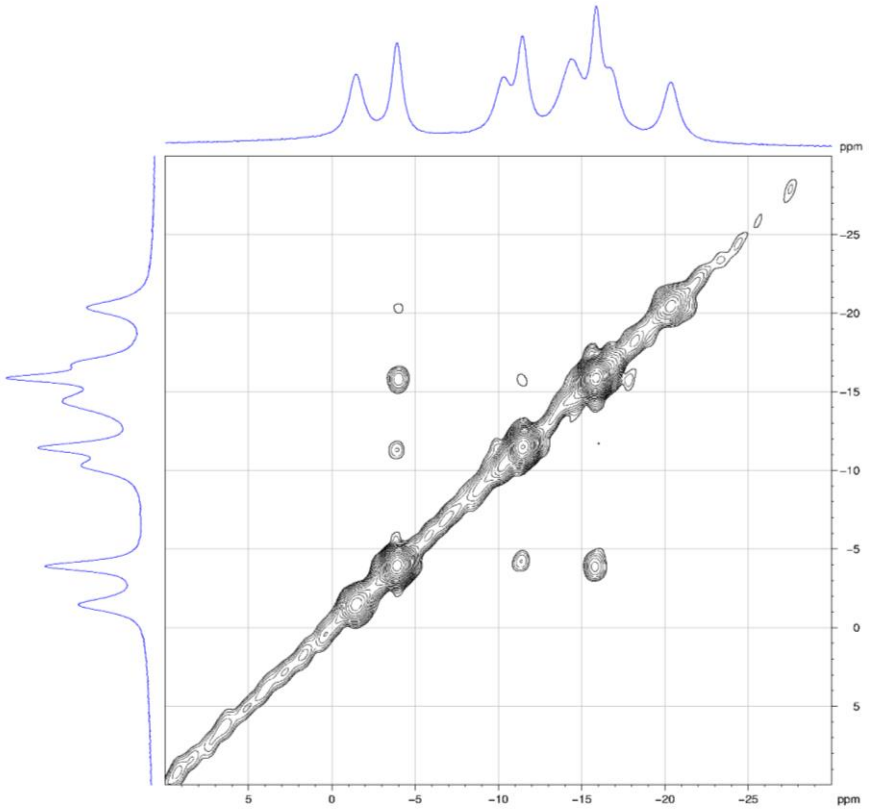

Figure 3.2.2.6 $^{11}B\{^{1}H\}$-$^{11}B\{^{1}H\}$ COSY NMR spectrum of compound **19** in CD_2Cl_2.

The ^{1}H NMR spectrum of **19** is significantly different to that of **18**. It consists, in addition the signals for -C*H*$_2$-C*H*$_2$- bridge of the both dmpe ligands, four doublets at δ 1.73 ($^{2}J_{PH}$ = 10.0 Hz), 1.70 ($^{2}J_{PH}$ = 8.0 Hz), 1.57 ($^{2}J_{PH}$ = 10.0 Hz) and 1.55 ($^{2}J_{PH}$ = 8.0 Hz) ppm each of integral-6. These are assigned to the methyl protons of the dmpe fragments. These resonances collapse to singlets by removing ^{31}P coupling in the $^{1}H\{^{31}P\}$ NMR spectrum. Additionally, there is a C*H*$_{cage}$ signal of integral two corresponding to the nickelacarborane at higher frequency, at δ 2.48 ppm, $^{3}J_{PH}$ = 10.0 Hz, which also gives a

singlet in the $^{1}H\{^{31}P\}$ NMR spectrum. Similar splittings were observed for compound **18**, and indicate that the metallacarborane environment must be of 3,1,2-architecture.

The $^{31}P\{^{1}H\}$ NMR spectrum of compound **19** reveals two mutually coupled doublets of integral two at δ 43.7 and 33.4 ppm with coupling $^{2}J_{PP}$ = 28.4 Hz, not significantly different to the $^{31}P\{^{1}H\}$ NMR spectrum of compound **18** (Figure 3.2.2.7). Hence this spectroscopic information is not conclusive in determining the exact architecture.

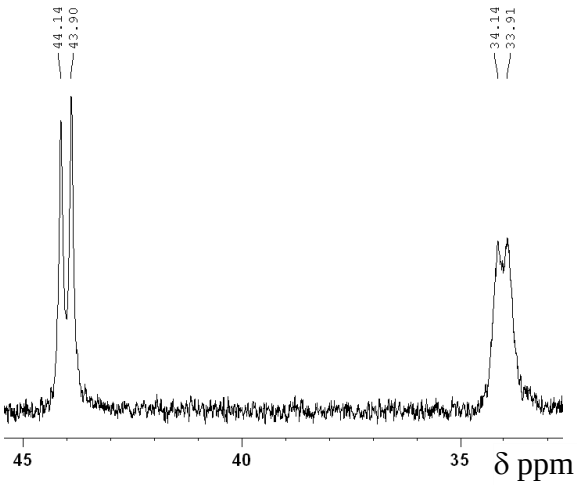

Figure 3.2.2.7 $^{31}P\{^{1}H\}$ NMR spectrum of compound **19** in CD_2Cl_2.

In the ^{1}H-^{31}P HMBC spectrum, the C*H*$_{cage}$ doublet arises from the coupling of the proton with the *trans*-phosphorus at δ 33.4 ppm. The resonances at δ 43.7 ppm is therefore assigned to the phosphorus *cis* to the CH_{cage}. Additionally the splitting of methyl protons is reflected in the spectrum (Figure 3.2.2.8). A point worthy of mentioning is that the magnitude of the coupling constant for the methyl protons depends on the degree of coupling from phosphorus. The phosphorus which is *cis* to the CH_{cage} couples more strongly (10.0 Hz) to the methyl protons compared to that *trans* to the CH_{cage} (8.0 Hz).

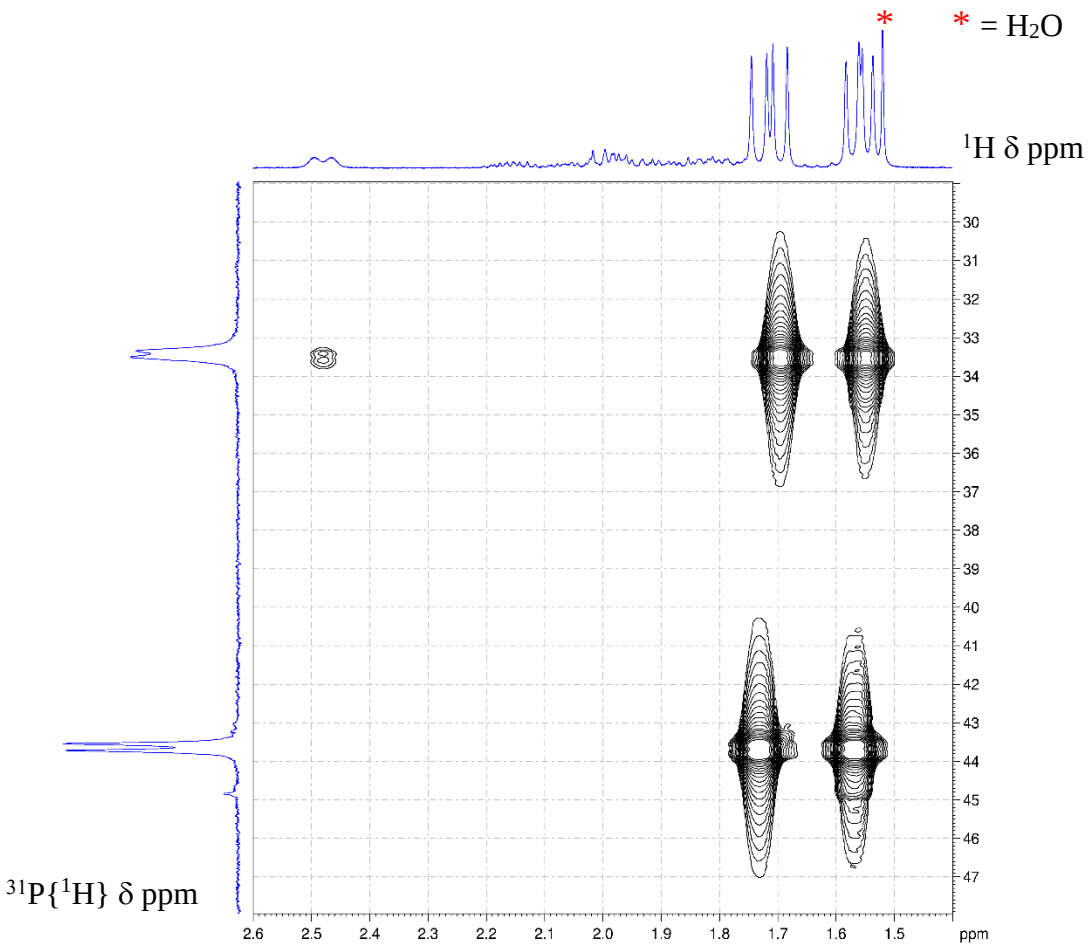

Figure 3.2.2.8 ^{1}H-$^{31}P\{^{1}H\}$ HMBC NMR spectrum of compound **19** in CD_2Cl_2.

Unfortunately, the available spectroscopic data were not conclusive with respect to determining the exact molecular geometry and crystallographic analysis of **19** was therefore performed.

X-ray quality crystals of compound **19** were grown by solvent diffusion of a 40-60 petroleum ether into a DCM solution and the result of the diffraction study were consistent with all the spectroscopic data for **19**. The nickelacarborane has a 3,1,2-NiC_2B_9-3′,1′,2′-NiC_2B_9 architecture which is very similar to that of compound **18** aside from the positions of the carbon atoms. Thus compound **19** is *meso*-[1-(1′-3′-(dmpe)-3′,1′,2′-*closo*$^{\circlearrowleft}$-$NiC_2B_9H_{10}$)-3-(dmpe)-3,1,2-*closo*$^{\circlearrowleft}$-$NiC_2B_9H_{10}$].

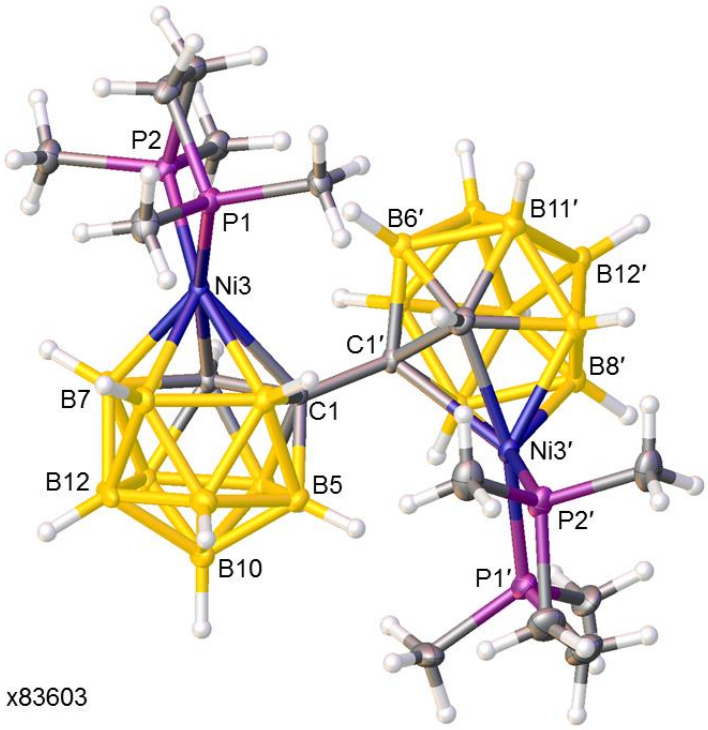

Figure 3.2.2.9 Molecular structure of *meso*-[1-(1′-3′-(dmpe)-3′,1′,2′-*closo*$^{\circlearrowleft}$-$NiC_2B_9H_{10}$)-3-(dmpe)-3,1,2-*closo*$^{\circlearrowleft}$-$NiC_2B_9H_{10}$] (**19**) (all solvents were omitted for clarity).

The molecular structure of compound **19** is shown in Figure 3.2.2.9. Two nickelcarboranes are joined by a C-C single bond with the Ni3-C1-C1′-Ni3′ torsion angle 142.65(16)º. The molecule is the meso diastereoisomer. The unit cell consists of two molecules of nickelacarborane in the *Pbar1* (triclinic) space group. There are also two fully ordered and one disordered DCM molecule in the lattice, although the molecule of **19** is fully ordered. The molecule shows clear indications of steric crowding. The expected orientation of the metal-phosphine unit is that in which the dihedral angle, θ, between the Ni3P1P2 and B6B8B10 planes is 90º,[7] whilst in **19** θ is found experimentally to be only 49.58(18)º for the nonprime cage and 57.59(15)º for the prime cage. In fact, the {NiPP} plane in **19** subtends a dihedral angle of 84.83(15)° to the plane through C1B10B12 for the nonprime cage and 87.63(12)° for the prime cage to minimise steric congestion. The plane of the {NiPP} fragment is bent from perpendicularity to the bottom pentagonal plane with a bend angle 6.1(12)º for the nonprime cage and 21.5(15)º for the prime cage. These indicate that there is steric congestion present in the molecule. This is reflected in the longer distances Ni3-C1: 2.326(4) [Ni2-C2: 2.066(4)]; Ni3′-C1′: 2.299(4) [Ni2′-C2′: 2.103(3)].

For compounds **18** and **19** the C atoms, except the linkage C atoms, were definitively identified by using both the VCD [8] and BHD [9] methods. The analysis was performed by following the procedure as discussed in Chapter 1. For compound **18**, it clearly indicates (Table 3.2.2.1) that the second C atom (where C1 is a linkage carbon atom) is at vertex 2 as the VCD from 2 is shorter than VCD from 9 or others by >0.131 Å for Ni3 (same reason is applicable for Ni3′ cage). This is consistent with BHD analysis, with the shortest BHDs found at 2 and 2′ for Ni3 cage and Ni3′ cage respectively (Table 3.2.2.2). For compound **19**, it shows (Table 3.2.2.1) that the second C atom (C1 linkage carbon atom) is at vertex 2 as the VCD from 2 is shorter than VCD from 9 or others by >0.110 Å for Ni3 cage and the VCD from 2′ (C1′ linkage carbon atom) is shorter than the VCD from 4 or others by >0.092 Å for Ni3′ cage. This is consistent with the BHD analysis; the shortest BHDs are found at 2 and 2′ for Ni3 cage and Ni3′ cage respectively (Table 3.2.2.2). Both VCD and BHD methods have been used regularly for all bis(carboranes) and bis(nickelacarboranes) discussed in this Chapter.

Table 3.2.2.1 Vertex-to-centroid distances (Å) in Prostructures of *rac*-[1-(1′-3′-(dmpe)-3′,1′,2′-*closo*^{5}-$NiC_2B_9H_{10}$)-3-(dmpe)-3,1,2-*closo*^{5}-$NiC_2B_9H_{10}$] (**18**) and *meso*-[1-(1′-3′-(dmpe)-3′,1′,2′-*closo*^{5}-$NiC_2B_9H_{10}$)-3-(dmpe)-3,1,2-*closo*^{5}-$NiC_2B_9H_{10}$] (**19**).

Vertex	Compound **18**		Compound **19**	
	Ni3 cage	Ni3′ cage	Ni3 cage	Ni3′ cage
1	1.652(2)	1.652(2)	1.648(4)	1.648(4)
2	1.523(3)	1.523(3)	1.529(5)	1.542(5)
3	2.2966(8)	2.2966(8)	2.3079(15)	2.2960(14)
4	1.665(3)	1.665(3)	1.649(5)	1.634(5)
5	1.680(3)	1.680(3)	1.683(5)	1.685(5)
6	1.718(3)	1.718(3)	1.701(5)	1.699(5)
7	1.710(3)	1.710(3)	1.710(5)	1.703(5)
8	1.730(3)	1.730(3)	1.721(5)	1.724(5)
9	1.654(3)	1.654(3)	1.639(5)	1.653(5)
10	1.700(2)	1.700(2)	1.694(5)	1.687(5)
11	1.673(3)	1.673(3)	1.664(5)	1.664(5)
12	1.692(2)	1.692(2)	1.679(5)	1.679(5)

Table 3.2.2.2 Boron-hydrogen distances (Å) in Prostructures *rac*-[1-(1′-3′-(dmpe)-3′,1′,2′-*closo*^{5}-$NiC_2B_9H_{10}$)-3-(dmpe)-3,1,2-*closo*^{5}-$NiC_2B_9H_{10}$] (**18**) and *meso*-[1-(1′-3′-(dmpe)-3′,1′,2′-*closo*^{5}-$NiC_2B_9H_{10}$)-3-(dmpe)-3,1,2-*closo*^{5}-$NiC_2B_9H_{10}$] (**19**).

Vertex	Compound **18**		Compound **19**	
	Ni3 cage	Ni3′ cage	Ni3 cage	Ni3′ cage
1	-	-	-	-
2	0.47(3)	0.47(3)	0.50(5)	0.58(5)
3	-	-	-	-
4	1.09(3)	1.09(3)	1.11(4)	0.94(4)
5	1.09(3)	1.09(3)	1.03(4)	1.120(6)
6	1.07(3)	1.07(3)	0.99(4)	1.02(4)
7	1.06(3)	1.06(3)	1.07(4)	1.05(4)
8	1.07(3)	1.07(3)	1.16(4)	1.08(4)
9	1.11(2)	1.11(2)	1.08(5)	1.10(4)
10	1.05(2)	1.05(2)	1.11(4)	1.08(4)
11	1.13(3)	1.13(3)	1.09(4)	1.05(4)
12	1.11(2)	1.11(2)	1.06(4)	1.12(4)

3.2.3 Thermal isomerisation of compounds 18 and 19 in THF reflux

Thermolysis of compound **18** was carried out in refluxing THF over 2.5 hrs, with the solution remaining dark green in colour throughout. Removal of solvent and spot TLC analysis followed by chromatographic purification gave two dark green products in 45% (top band) and 43% (bottom band) yields.

Similarly, compound **19** was thermolysed in THF at 65 °C over 2.5 hrs. Spot TLC analysis followed by chromatographic purification yielded two dark green products in 44% (upper band) and 47% (lower band) yields.

After spectroscopic characterisation ($^{11}B\{^1H\}$, $^{31}P\{^1H\}$ and ^1H NMR), the two dark green products in both cases were identified as compounds **18** (top band, *rac* form) and **19** (bottom band, *meso* form) (Figure 3.2.3.1).

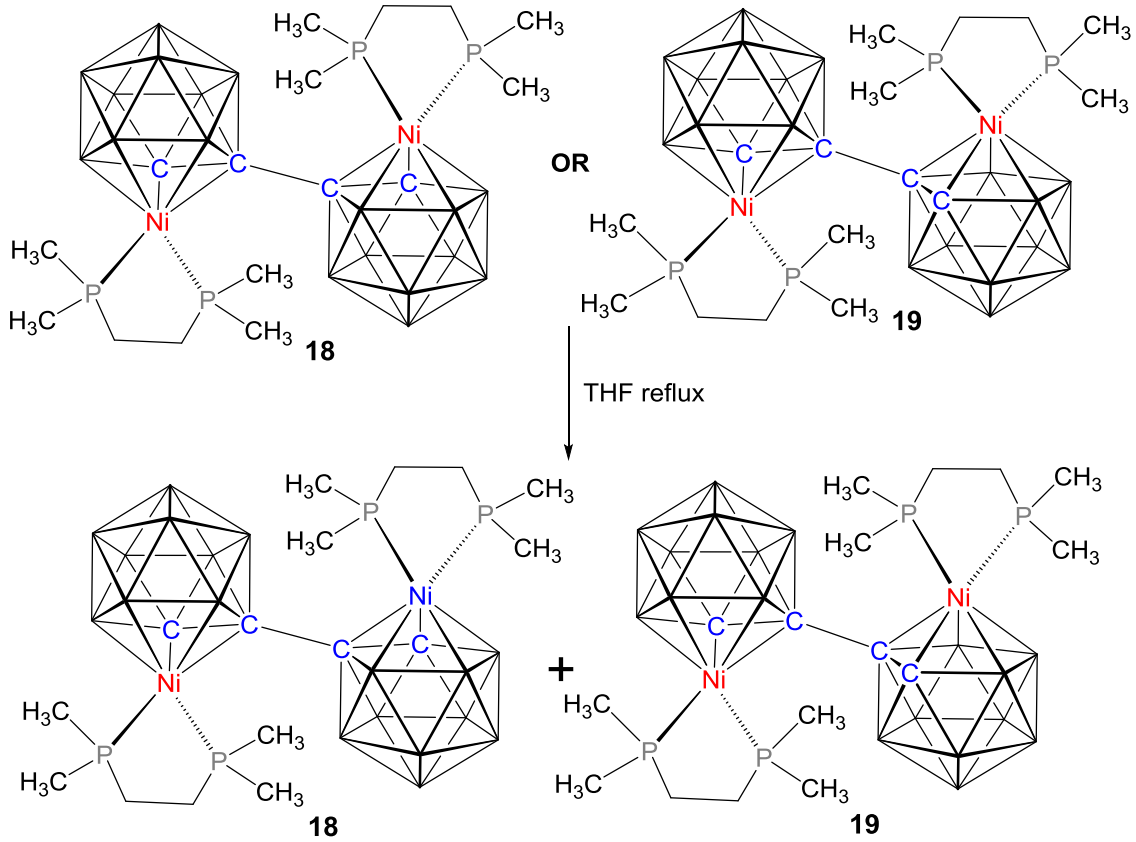

Figure 3.2.3.1 Thermolysis of compound **18** or **19** at 65 °C.

3.2.4 Discussion: interconversion of rac (18) and meso (19) in a 1:1 ratio

From the molecular structure of *rac*-3,1,2-NiC_2B_9-3′,1′,2′-NiC_2B_9 (**18**) and *meso*-3,1,2-NiC_2B_9-3′,1′,2′-NiC_2B_9 (**19**), both cages are in the 3,1,2- architecture. We know that 3,1,2- can be isomerised to either 4,1,2- or 2,1,8-species. So, in order to investigate isomerisation behaviour, pure compound **18** has been heated to reflux in THF for 2.5 hrs and from TLC purification two mobile bands were observed in a 1:1 ratio. From $^{31}P\{^1H\}$, ^1H and $^{11}B\{^1H\}$ NMR spectroscopies these two products are **18** and **19** as a 1:1 mixture. One would imagine both cages would isomerise to different architectures but we observed serendipitously upon heating to reflux in THF that compound **18** gives a mixture of *rac*-[1-(1′-3′-(dmpe)-3′,1′,2′-*closo*$^{\circlearrowleft}$-$NiC_2B_9H_{10}$)-3-(dmpe)-3,1,2-*closo*$^{\circlearrowleft}$-$NiC_2B_9H_{10}$] (**18**) and *meso*-[1-(1′-3′-(dmpe)-3′,1′,2′-*closo*$^{\circlearrowleft}$-$NiC_2B_9H_{10}$)-3-(dmpe)-3,1,2-*closo*$^{\circlearrowleft}$-$NiC_2B_9H_{10}$] (**19**) in a 1:1 ratio. Similarly thermolysis of pure compound **19** in THF also results in two green bands. After chromatographic separation and multinuclear spectroscopic characterisation these bands were identified as *rac*-3,1,2-NiC_2B_9-3′,1′,2′-NiC_2B_9 (**18**) and *meso*-3,1,2-NiC_2B_9-3′,1′,2′-NiC_2B_9 (**19**) again in a 1:1 ratio. This interconversion between *rac* and *meso* is very surprising at low temperature (65 ºC) and unprecedented in metallacarborane chemistry. The possible mechanism of the observed interconversion is discussed below.

We have proposed two possible mechanisms for the isomerisation process. For simplicity, a single metallacarborane cage has been considered instead of both metallacarborane cages. The first mechanism is as follows: the initial stage of the isomerisation of a 3,1,2-NiC_2B_9 cage is the formation of an intermediate (I) through rotation of the {HC1–C2H} unit (Figure 3.2.4.1). In the intermediate the C-C unit lies in the mirror plane passing through Ni3, B8 and B10. Then, in the final step, the C–C bond rotates further to afford the alternative isomer. This process may occur at either or both the {3,1,2-NiC_2B_9} or the {3′,1′,2′-NiC_2B_9} cages and it changes one diastereoisomer into the other. From the DFT analysis [10] the activation energy for the formation of the intermediate was far too high to achieve this intermediate at this temperature. For simplicity, the calculations were performed using a single 3,1,2-NiC_2B_9 cage where the dmpe ligand was replaced by two units of PMe_3, rather than 3,1,2-NiC_2B_9-3′,1′,2′-NiC_2B_9 species itself.

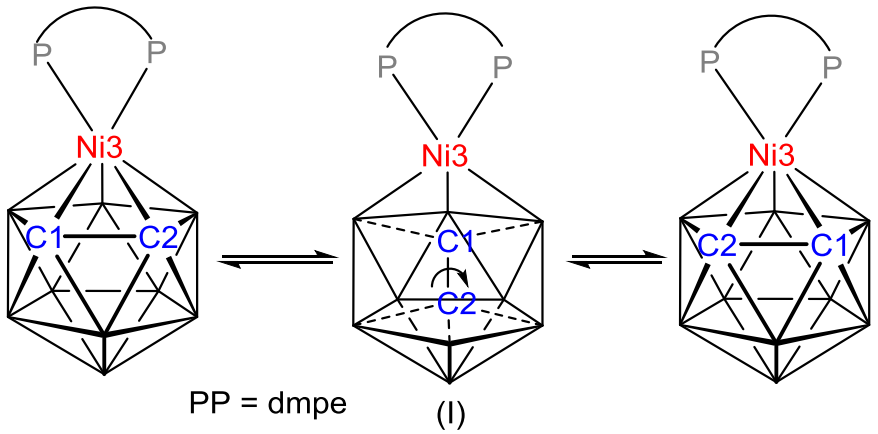

Figure 3.2.4.1 First mechanism: interconversion *via* rotation of the C1–C2 unit.

With this mechanism appearing to be unfeasible another pathway has been proposed for this rac and meso isomerisation. Here also a single cage has been considered for simplicity. Initially a TFR rearrangement of the C2B6B11 face of a {3,1,2-NiC_2B_9} species results an intermediate which undergoes a second TFR rearrangement of the C2C1B11 face to give the second isomer as shown in Figure 3.2.4.2. To support this mechanism experimentally we targeted labelling of the B6, B6′ positions in a 3,1,2-NiC_2B_9-3′,1′,2′-NiC_2B_9 species. If the isomerisation does follow this mechanism, the label will move from the B6 (B6′) position to B11 (B11′) or B5 (B5′) (Figure 3.2.4.2). For the synthesis of B6, B6′ substituted bis(heteroborane), one needs to synthesise initially a B3, B3′ substituted bis(carborane), and our attempts at doing this are described in the following section.

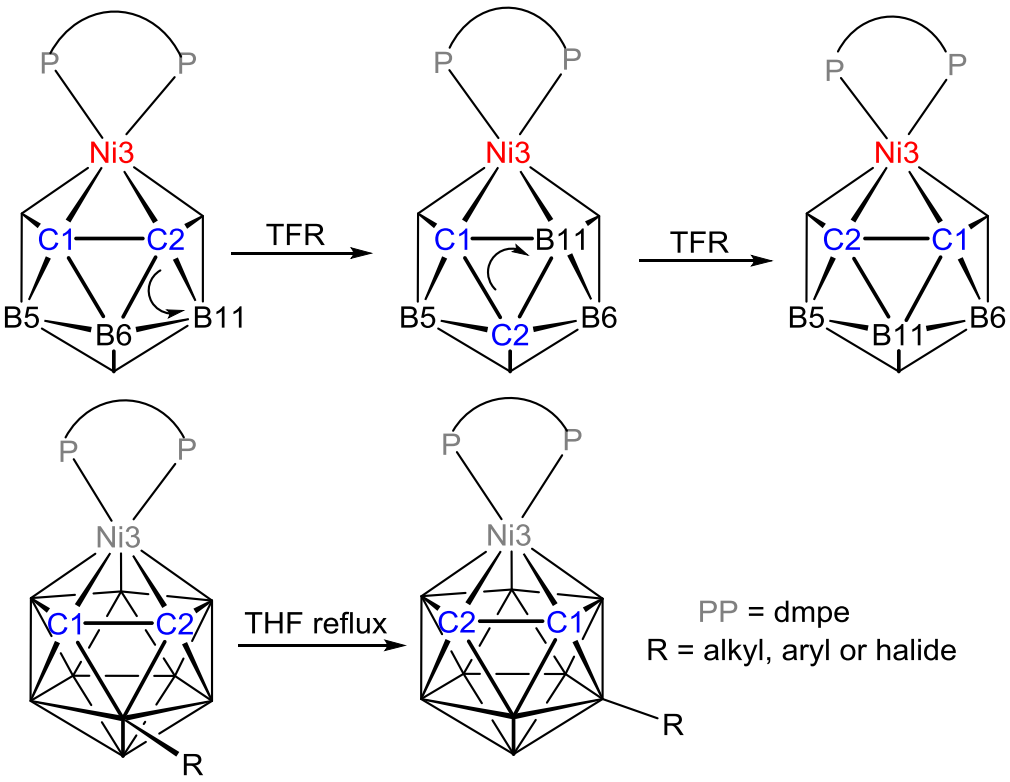

Figure 3.2.4.2 Second mechanism: two sequential TFRs.

3.2.5 Synthesis of [7-(7′-7′,8′-*nido*-$C_2B_9H_{12}$)-7,8-*nido*-$C_2B_9H_{12}$] (20)

$[Tl]_2$[1-(1′-3′,1′,2′-*closo*-$TlC_2B_9H_{10}$)-3,1,2-*closo*-$TlC_2B_9H_{10}$] (**17**) was suspended in petrol and frozen to -196 °C. A stoichiometric quantity of BI_3 or BBr_3 was added followed by warming to room temperature and stirring for 12 h affording a bright orange suspension. Filtration through silica of the crude reaction mixture followed by evaporation of all volatiles afforded compound **20** in moderate yield.

The $^{11}B\{^1H\}$ NMR spectrum of compound **20** consists of nine resonances with relative integrals 1:1:2:4:2:2:2:2:2 from high frequency to low frequency. In the ^1H NMR spectrum there is an integral-2 resonance at δ 3.73 ppm assigned to CH_{cage}.

Single crystals of compound **20** were grown by solvent diffusion of 40-60 petroleum ether into a DCM solution of **20**. Single crystal *X*-ray analysis reveals that compound **20** is [7-(7′-7′,8′-*nido*-$C_2B_9H_{12}$)-7,8-*nido*-$C_2B_9H_{12}$] the molecular structure of which is shown in Figure 3.2.5.1.

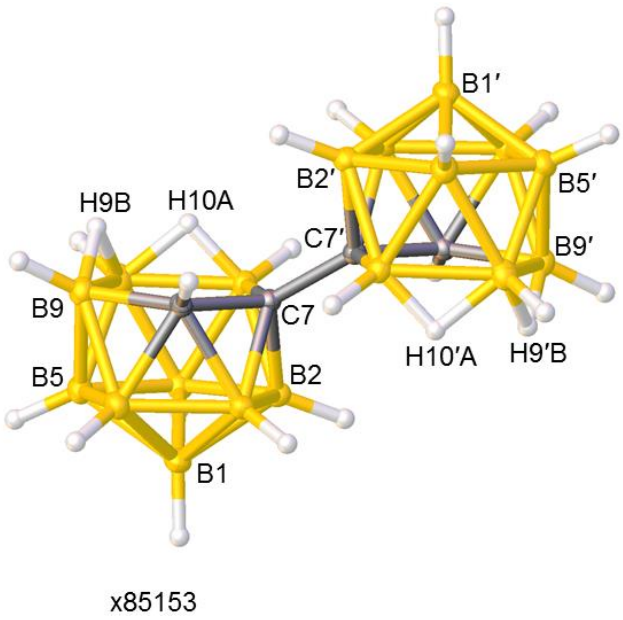

Figure 3.2.5.1 A perspective view of [7-(7′-7′,8′-*nido*-$C_2B_9H_{12}$)-7,8-*nido*-$C_2B_9H_{12}$] (**20**).

The reaction of **17** with a stoichiometric equivalent of BI_3 or BBr_3 yielded as the only isolable product **20**. The unexpected formation of **20** is associated with Lewis acid assisted protonation and it is discussed in section 3.2.8.

3.2.6 Synthesis of *rac*-[1-(1′-3′-Ph-1′,2′-*closo*$^{\circlearrowleft}$-$C_2B_{10}H_{10}$)-3-Ph-1,2-*closo*$^{\circlearrowleft}$-$C_2B_{10}H_{10}$] (21) and *meso*-[1-(1′-3′-Ph-1′,2′-*closo*$^{\circlearrowleft}$-$C_2B_{10}H_{10}$)-3-Ph-1,2-*closo*$^{\circlearrowleft}$-$C_2B_{10}H_{10}$] (22)

The tetraanion **II**$^{4-}$ was prepared by lithiation of $[HNMe_3]_2$[7-(7′-7′,8′-*nido*-$C_2B_9H_{11}$)-7,8-*nido*-$C_2B_9H_{11}$] in ether with nBuLi. Then capitation of tetraanion **II**$^{4-}$ with two equivalents of $\{PhB\}^{2+}$ in petrol gave a light purple suspension after 4 hrs stirring at room temperature. Work up followed by chromatographic separation afforded two colourless materials compounds **21** and **22** in 22% and 17% yields respectively (Figure 3.2.6.1).

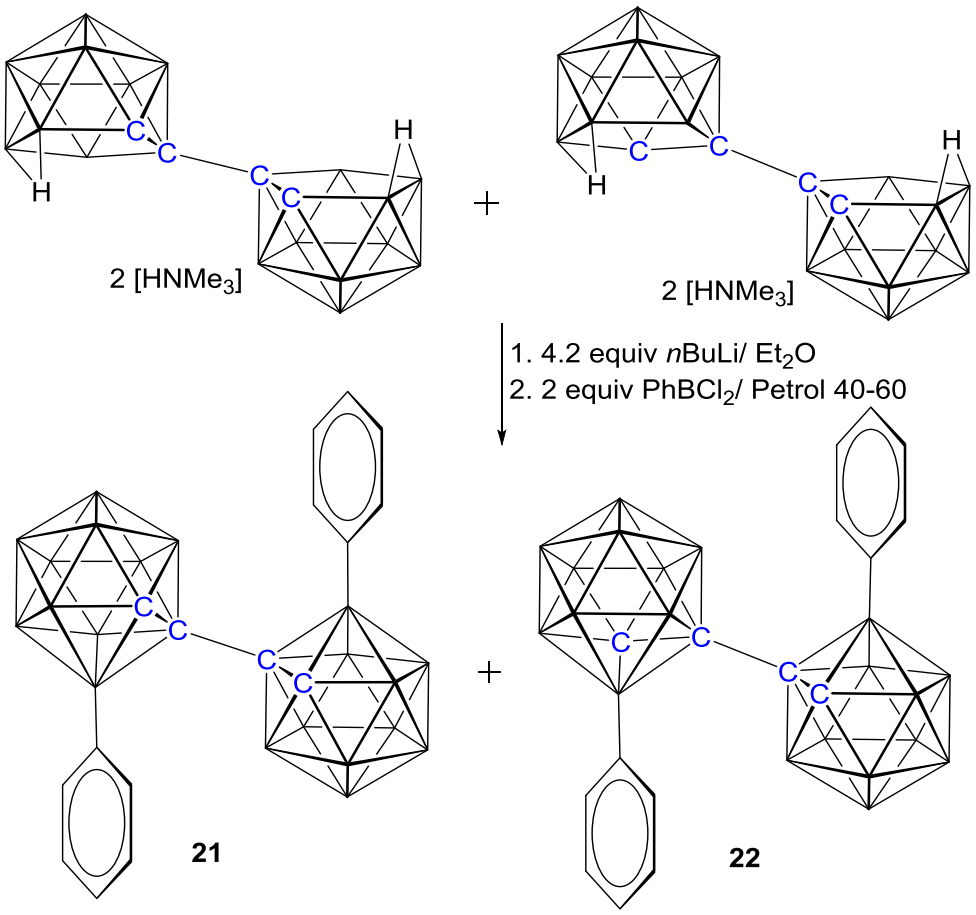

Figure 3.2.6.1 Capitation of **II**$[HNMe_3]_2$ with $PhBCl_2$.

The mass spectrum of compound **21** showed an envelope centred peak at *m/z* 438.4 (M^+) (MW = 438.64 g mol^{-1}). The CHN analysis was in agreement with the predicted values for $C_{16}H_{30}B_{20}$. From the mass spectrum and elemental analysis, it was evident that both cages of the bis(carborane) had been capitated successfully with $\{BPh\}^{2+}$ fragments. For further confirmation other spectroscopic techniques were also, however, necessary.

The $^{11}B\{^{1}H\}$ NMR spectrum of compound **21** reveals multiple overlapping resonances with a total integral of 20B and sheds a little light on the isomeric nature.

The ^{1}H NMR spectrum of compound **21** consists of a CH_{cage} resonance assigned to carborane cages at δ 3.69 ppm with integral-2. In addition, there are also phenyl protons of integral-10 in the spectrum. However the exact nature of **21** was determined by crystallography.

Crystals of compound **21** were developed by solvent diffusion of 40-60 petroleum ether into a DCM solution of **21**. Single crystal *X*-ray analysis reveals that compound **21** is *rac*-[1-(1′-3′-Ph-1′,2′-*closo*$^{\circlearrowleft}$-$C_2B_{10}H_{10}$)-3-Ph-1,2-*closo*$^{\circlearrowleft}$-$C_2B_{10}H_{10}$]. A perspective view of **21** is shown in Figure 3.2.6.2.

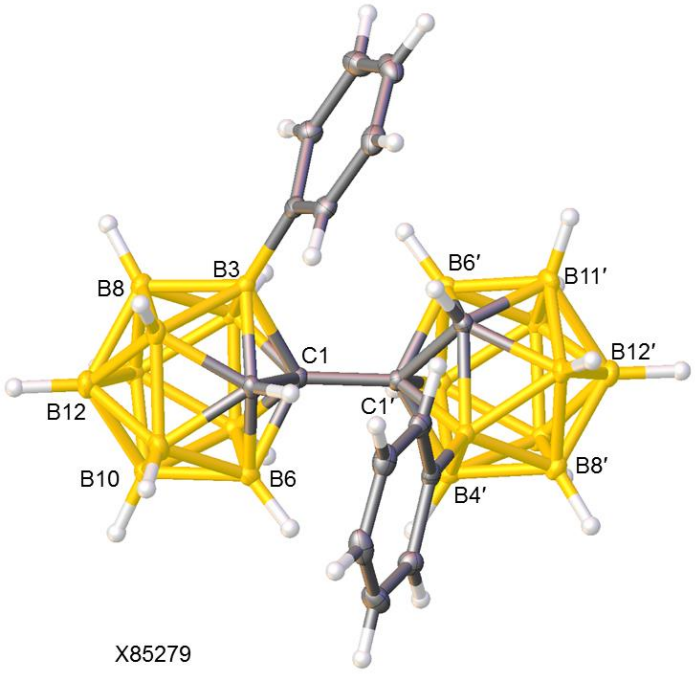

Figure 3.2.6.2 A perspective view of *rac*-[1-(1′-3′-Ph-1′,2′-*closo*$^{\circlearrowleft}$-$C_2B_{10}H_{10}$)-3-Ph-1,2-*closo*$^{\circlearrowleft}$-$C_2B_{10}H_{10}$] (**21**).

Having established that the upper colourless product is rac isomer (**21**), one would anticipate that the lower band must be another isomer. Indeed, from the mass spectrum (an envelope centred peak at *m/z* 438.4 (M^+), MW = 438.64 g mol^{-1}) and elemental analysis, it was evident that compound **22** was an isomer of compound **21**.

The $^{11}B\{^{1}H\}$ NMR spectrum of compound **22** is distinct to that of compound **21**, but also, however, it consists of multiple overlapping resonances of total integral 20B.

The ^{1}H NMR spectrum of compound **22** consists, in addition to phenyl protons, an integral-2 resonance at δ 4.19 ppm assigned as CH_{cage}.

Crystals of compound **22** were developed by solvent diffusion of 40-60 petroleum ether into a DCM solution of **22**. Single crystal *X*-ray analysis reveals that compound **22** is *meso*-[1-(1′-3′-Ph-1′,2′-*closo*$^{\circlearrowleft}$-$C_2B_{10}H_{10}$)-3-Ph-1,2-*closo*$^{\circlearrowleft}$-$C_2B_{10}H_{10}$], the molecular structure of which is shown in Figure 3.2.6.3.

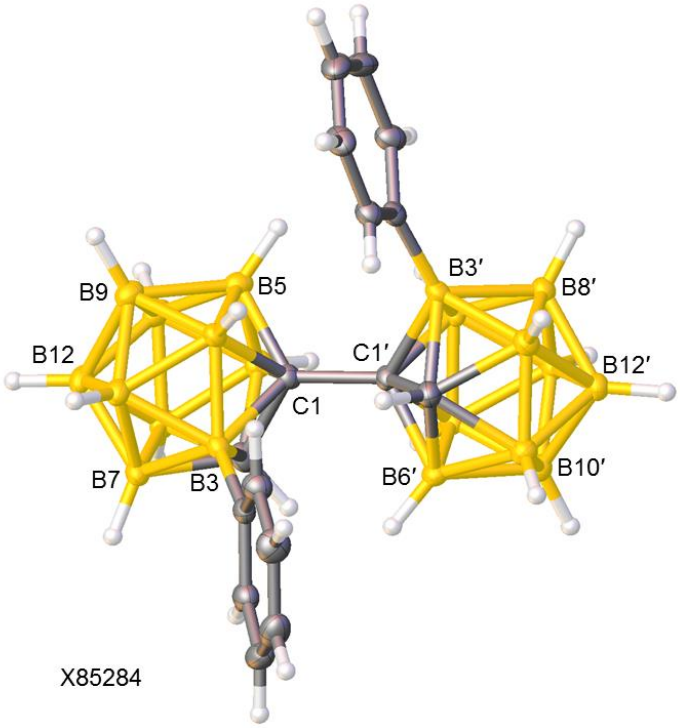

Figure 3.2.6.3 A perspective view of *meso*-[1-(1′-3′-Ph-1′,2′-*closo*$^{\circlearrowleft}$-$C_2B_{10}H_{10}$)-3-Ph-1,2-*closo*$^{\circlearrowleft}$-$C_2B_{10}H_{10}$] (**22**).

3.2.7 Synthesis of $[HNMe_3]_2$[7-(7′-3′-Ph-7′,8′-*nido*-$C_2B_9H_{10}$)-3-Ph-7,8-*nido*-$C_2B_9H_{10}$] ($[HNMe_3]_2$[23]) and $[BTMA]_2$[7-(7′-3′-Ph-7′,8′-*nido*-$C_2B_9H_{10}$)-3-Ph-7,8-*nido*-$C_2B_9H_{10}$] ($[BTMA]_2$[23]) as *rac* and *meso* mixtures

Double deboronations of 3′-Ph-1′,2′-C_2B_{10}-3-Ph-1,2-C_2B_{10} (**21** and **22** mixture) were achieved by following the same method for the double decapitations of 1,1′-bis(*o*-carborane). A mixture of **21** and **22** was treated excess KOH in refluxing EtOH overnight. Work-up followed by cation metathesis afforded the dianion [7-(7′-3′-Ph-7′,8′-*nido*-$C_2B_9H_{10}$)-3-Ph-7,8-*nido*-$C_2B_9H_{10}$]$^{2-}$(**23**), as either the $[HNMe_3]^+$ or $[BTMA]^+$ salt in moderate yields.

As the material was composed of two different decapitated derivatives *i.e*. two bis(*nido*-carboranes) species resulting from the decapitation of rac and meso isomers, the NMR spectra of the ($[HNMe_3]_2$[**23**]) species were complicated but contained all the expected resonances. However the elemental analysis of ($[HNMe_3]_2$[**23**]) is in agreement with that expected for $C_{22}H_{50}B_{18}N_2 \cdot 0.5CH_2Cl_2$ (Theoretical: C 46.6, H 8.87, N 4.83%; experimental: C 46.8, H 9.08, N 4.80%). Similarly the elemental analysis of ($[BTMA]_2$[**23**]), though its ^1H, $^{11}B\{^1H\}$ NMR spectra were complex, fitted with that predicted for $C_{36}H_{62}B_{18}N_2 \cdot 0.5CH_2Cl_2$.

Crystals of the meso-isomer of ($[BTMA]_2$[**23**]) salt were grown by solvent diffusion of 40-60 petroleum ether into a DCM solution of ($[BTMA]_2$[**23**]). Single crystal *X*-ray analysis identifies the compound as $[BTMA]_2$[7-(7′-3′-Ph-7′,8′-*nido*-$C_2B_9H_{10}$)-3-Ph-7,8-*nido*-$C_2B_9H_{10}$]. The structure of the anion is shown in the Figure 3.2.7.1. In the crystal structure, there are a partly disordered BTMA molecule, an ordered bis(carborane) and a DCM molecule. Crucially, it is obvious that both cages have been decapitated to yield two nido cages.

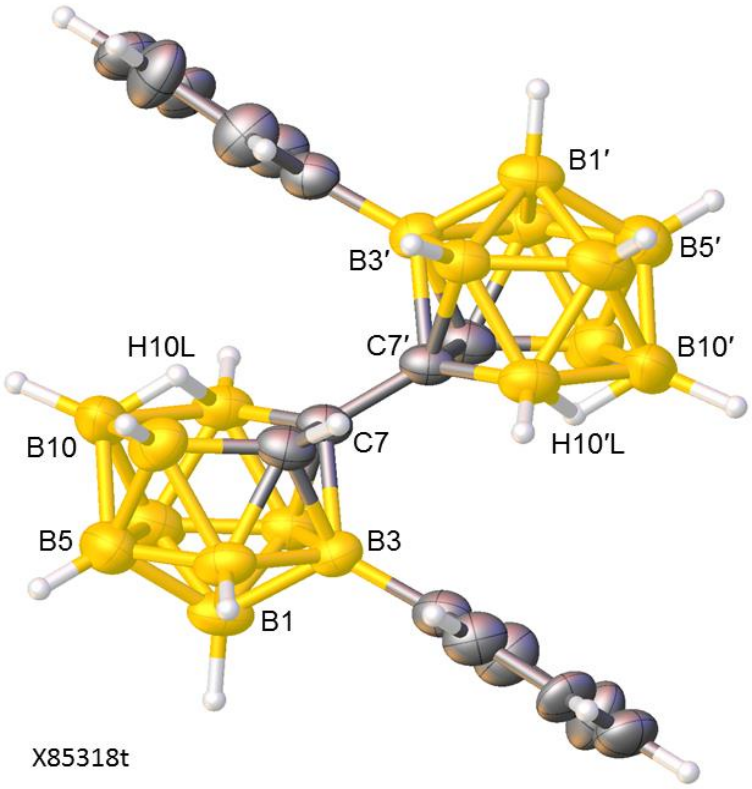

Figure 3.2.7.1 A perspective view of the anion of $[BTMA]_2$[7-(7′-3′-Ph-7′,8′-*nido*-$C_2B_9H_{10}$)-3-Ph-7,8-*nido*-$C_2B_9H_{10}$] (meso isomer of $[BTMA]_2$[**23**]) (counter cation, solvents are omitted for clarity).

3.2.8 Targeted synthesis of B3,B3′-substituted bis(carborane) and its metallation

Initially we attempted to synthesise the 3,3′-ethyl derivative of bis(carborane) by first making the 3-ethyl derivative of [1,2-*closo*-carborane]. In 1991, Jones *et al*. reported [3-Et-1,2-*closo*-$C_2B_{10}H_{11}$] *via* the synthesis of [3-I-1,2-*closo*-$C_2B_{10}H_{11}$] starting from [*nido*-$C_2B_9H_{11}]^{2-}$.[11] By following this protocol [3-I-1,2-*closo*-$C_2B_{10}H_{11}$] has been synthesised from the capitation of $Li_2[C_2B_9H_{11}]$ with boron triiodide (BI_3) in petrol in 50% yield. The product has been characterised by multinuclear NMR spectroscopy. However [3-EtO-1,2-*closo*-$C_2B_{10}H_{11}$] was also formed in substantial quantity as a side product. An alternative high yielding and convenient route to [3-I-1,2-*closo*-$C_2B_{10}H_{11}$] was also reported by Hawthorne *et al*. in 2011 [12] starting from thallium *o*-dicarbollide, $Tl[TlC_2B_9H_{11}]$. Thallium dicarbollide readily reacted with BI_3 in petrol to give [3-I-1,2-*closo*-$C_2B_{10}H_{11}$] in 70–80% yield with no evidence of significant by-products. Thus the dithallum salt of decapitated *o*-carborane has been chosen as starting material for the synthesis of [3-I-1,2-*closo*-$C_2B_{10}H_{11}$] in good yields.

Having sufficient amount of [3-I-1,2-*closo*-$C_2B_{10}H_{11}$], the 3 position of the carborane can be alkylated by Grignard reagents in a reaction catalysed by $[PdCl_2(PPh_3)_2]$.[11] Therefore, [3-I-1,2-*closo*-$C_2B_{10}H_{11}$] was treated with excess EtMgBr in the presence of Pd(II) catalyst as shown in Figure 3.2.8.1 to afford [3-Et-1,2-*closo*-$C_2B_{10}H_{11}$]. The compound was confirmed by ^1H, $^{11}B\{^1H\}$ NMR spectroscopies and purity confirmed by elemental analysis. With pure [3-Et-1,2-*closo*-$C_2B_{10}H_{11}$], the synthesis of 3,3′-ethyl substituted bis(carborane) was targeted by following the synthesis of 1,1′-bis(*o*-carborane).[13] Lithiation of 3-Et-1,2-*closo*-$C_2B_{10}H_{11}$ with ^{n}BuLi in toluene followed by addition of CuCl(I) results a dark red mixture after 48 hrs stirring at room temperature. Workup followed by purification by column chromatography results in a mixture of products, as indicated by ^1H NMR spectroscopy. A second purification with column chromatography affords a colourless oily substance.

Although the EI mass spectrum of the product reveals an envelope centred peak at *m/z* 342.4 (M^+) (MW = 342.55 g mol^{-1}), CHN analysis (calculated for $C_8H_{30}B_{20}$: C 28.1, H 8.83%; experimental values: C 25.5, H 8.85%) and ^1H NMR spectroscopy analysis (several $C_{cage}H$ resonances) of the oily substance were not convincing with respect to the suggested synthesis of the desired material.

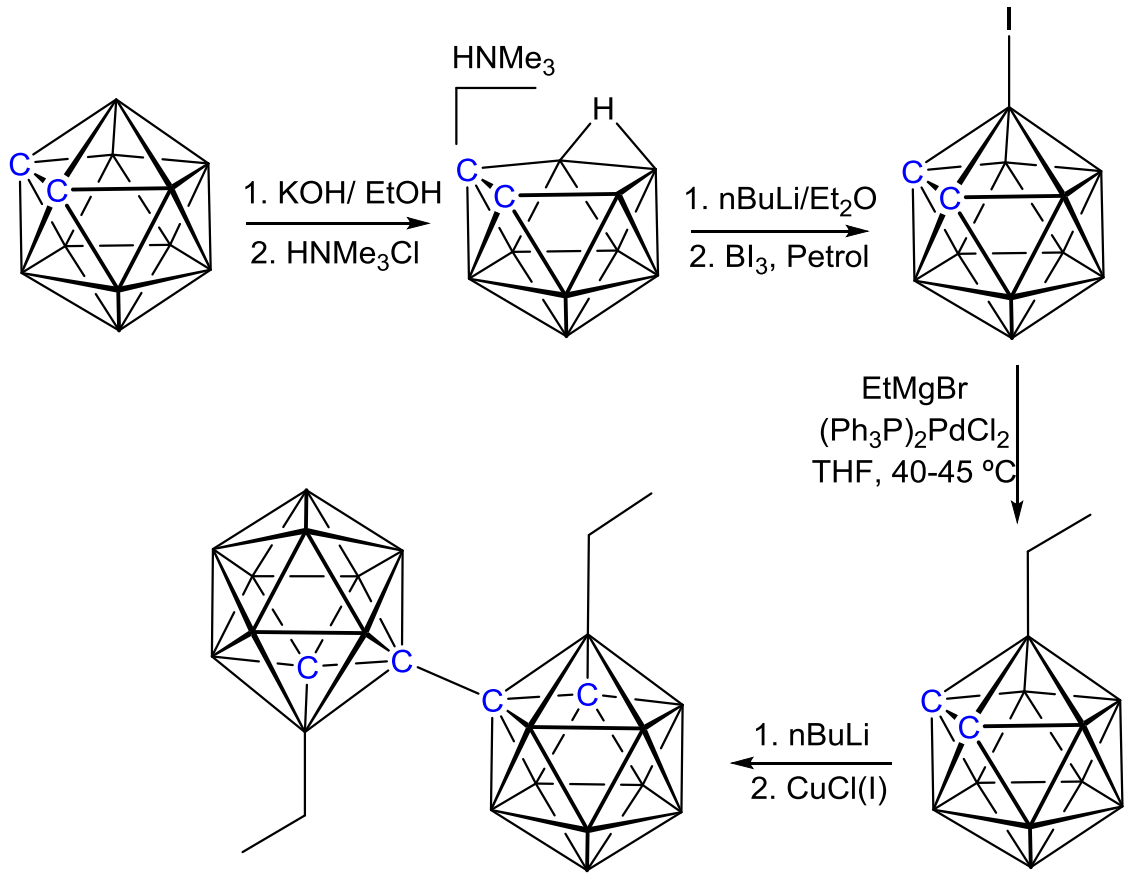

Figure 3.2.8.1 Attempted synthesis of 3,3′-ethyl substituted bis(carborane).

Having been unsuccessful in the synthesis of 3′-Et-1′,2′-C_2B_{10}-3-Et-1,2-C_2B_{10} by the coupling of two lithiated 3-Et-1,2-C_2B_{10} derivatives, we targeted capitation of the tetrathallium salt of bis(*o*-carborane) with BI_3. However treatment of a suspension of $[Tl]_2$[1-(1′-3′,1′,2′-*closo*-$TlC_2B_9H_{10}$)-3,1,2-*closo*-$TlC_2B_9H_{10}$] (**17**) with two equivalents of BI_3 or BBr_3 unexpectedly afforded [7-(7′-7′,8′-*nido*-$C_2B_9H_{12}$)-7,8-*nido*-$C_2B_9H_{12}$] (**20**). The synthesis of compound **20** has been discussed in section 3.2.5. Instead of capping [7-(7′-7′,8′-*nido*-$C_2B_9H_{10}$)-7,8-*nido*-$C_2B_9H_{10}$]$^{4-}$ with $\{BX\}^{2+}$ (X = I, Br) fragments, the reaction leads to protonation of both nido cages to afford a neutral diacid derivative of bis(carborane). A similar derivative of *ortho*-carborane, [$C_2B_9H_{13}$] was reported by Hawthorne and produced by protonation of [$C_2B_9H_{11}$]$^{2-}$ with HCl, [14] a strong acid. In contrast formation of **20** can be achieved by using the Lewis acid BBr_3 or BI_3 in petrol. The rationale for the formation of **20** can be explained by Lewis acid (BBr_3 or BI_3) assisted protonation. Reaction of BBr_3 or BI_3 with petrol may lead to the formation of H^+ which then protonates the nido-cages of bis(carborane).

Having been unsuccessful in the capitation of [7-(7′-7′,8′-*nido*-$C_2B_9H_{10}$)-7,8-*nido*-$C_2B_9H_{10}$]$^{4-}$ with {BX}$^{2+}$ (X = I, Br) fragments, we subsequently chose {BPh}$^{2+}$ as an alternative capping fragment. The first synthesis of [3-Ph-1,2-*closo*-$C_2B_{10}H_{11}$] was reported by Hawthorne and Wegner,[15] and involved the capitation of [*nido*-$C_2B_9H_{11}$]$^{2-}$ with a {PhB}$^{2+}$ fragment provided by $PhBCl_2$ in THF. By following the same procedure lithiation of [$HNMe_3$]$_2$[7-(7′-7′,8′-*nido*-$C_2B_9H_{11}$)-7,8-*nido*-$C_2B_9H_{11}$] ([$HNMe_3$]$_2$**II**) with *n*BuLi in THF followed by removal of amines afforded the tetralithium salt Li_4[7-(7′-7′,8′-*nido*-$C_2B_9H_{11}$)-7,8-*nido*-$C_2B_9H_{11}$]. Attempted capitation of [**II**]$^{4-}$ with $PhBCl_2$ in THF is not successful following chromatographic separation and spectroscopy analysis. We have also tested several variations on this capitation reaction using different salts of decapitated species and reaction media as shown in Table 3.2.8.1.

Table 3.2.8.1 Various attempts at capitation of [7-(7′-7′,8′-*nido*-$C_2B_9H_{10}$)-7,8-*nido*-$C_2B_9H_{10}$]$^{4-}$ or [7-(7′-7′,8′-*nido*-$C_2B_9H_{11}$)-7,8-*nido*-$C_2B_9H_{11}$]$^{2-}$ with $PhBCl_2$.

Decapitated species	Lithiation solvent	Capitation solvent	Results
Tetrathallium salt (**17**)	-	THF	Negative
Tetrathallium salt (**17**)	-	Petrol 40-60	Negative
Trimethylammonium salt ([$HNMe_3$]$_2$(**II**))	THF	THF	Negative
Trimethylammonium salt ([$HNMe_3$]$_2$(**II**))	THF	Petrol 40-60	Negative
Trimethylammonium salt ([$HNMe_3$]$_2$(**II**))	Et_2O	Petrol 40-60	Positive

From the Table the successful synthesis is the last one. Lithiation of [$HNMe_3$]$_2$[7-(7′-7′,8′-*nido*-$C_2B_9H_{11}$)-7,8-*nido*-$C_2B_9H_{11}$] in Et_2O afforded [7-(7′-7′,8′-*nido*-$C_2B_9H_{10}$)-7,8-*nido*-$C_2B_9H_{10}$]$^{4-}$, with subsequent treatment with $PhBX_2$ (X = Cl) yielding *rac*-[1-(1′-3′-Ph-1′,2′-*closo*$^{\circlearrowleft}$-$C_2B_{10}H_{10}$)-3-Ph-1,2-*closo*$^{\circlearrowleft}$-$C_2B_{10}H_{10}$] (**21**) and *meso*-[1-(1′-3′-Ph-1′,2′-*closo*$^{\circlearrowleft}$-$C_2B_{10}H_{10}$)-3-Ph-1,2-*closo*$^{\circlearrowleft}$-$C_2B_{10}H_{10}$] (**22**) in moderate yields. The preparation of these compounds has been discussed in section 3.2.6. Having fully characterised **21** and **22** by spectroscopic and crystallographic methods, their decapitation and metallation were then explored. Due to the tedious nature of separation of these isomers, a mixture of compounds **21** and **22** was employed in all subsequent reactions.

The treatment of a mixture of **21** and **22** with excess $[EtO]^-$ following the same methods as for the double deboronations of 1,1′-bis(*o*-carborane), afforded $[HNMe_3]_2$[7-(7′-3′-Ph-7′,8′-*nido*-$C_2B_9H_{10}$)-3-Ph-7,8-*nido*-$C_2B_9H_{10}$] ($[HNMe_3]_2$[**23**]) as a *rac* and *meso* mixture. The same anion was also isolated with BTMA as $[BTMA]_2$[7-(7′-3′-Ph-7′,8′-*nido*-$C_2B_9H_{10}$)-3-Ph-7,8-*nido*-$C_2B_9H_{10}$] ($[BTMA]_2$[**23**]) as a *rac* and *meso* mixture. The former derivative ($[HNMe_3]_2$[**23**]) was characterised by NMR spectroscopy whereas the latter one ($[BTMA]_2$[**23**]) by both spectroscopy and crystallography. Synthesis of theses species are described in section 3.2.7. After complete characterisation, metallation of ($[HNMe_3]_2$[**23**]) with $[NiCl_2(dmpe)]$ was also attempted.

By following the analogous procedure for ($[HNMe_3]_2$[**II**]), deprotonation of ($[HNMe_3]_2$[**23**]) in THF was carried out using *n*BuLi affording [7-(7′-3′-Ph-7′,8′-*nido*-$C_2B_9H_9$)-3-Ph-7,8-*nido*-$C_2B_9H_9$]$^{4-}$. Further treatment of [**23**]$^{4-}$ with two equivalents of $[NiCl_2(dmpe)]$ afforded a green solution (Figure 3.2.8.2). However, after work-up, spot TLC revealed no mobile bands. The EIMS of the crude reaction mixture does not contain the expected molecular ion peak. The unsuccessful metallation can be rationalised by the presence of bulky phenyl group at positions B3 and B3′ of [7-(7′-3′-Ph-7′,8′-*nido*-$C_2B_9H_9$)-3-Ph-7,8-*nido*-$C_2B_9H_9$]$^{4-}$ which may prevent coordination of the $\{Ni(dmpe)\}^{2+}$ fragments.

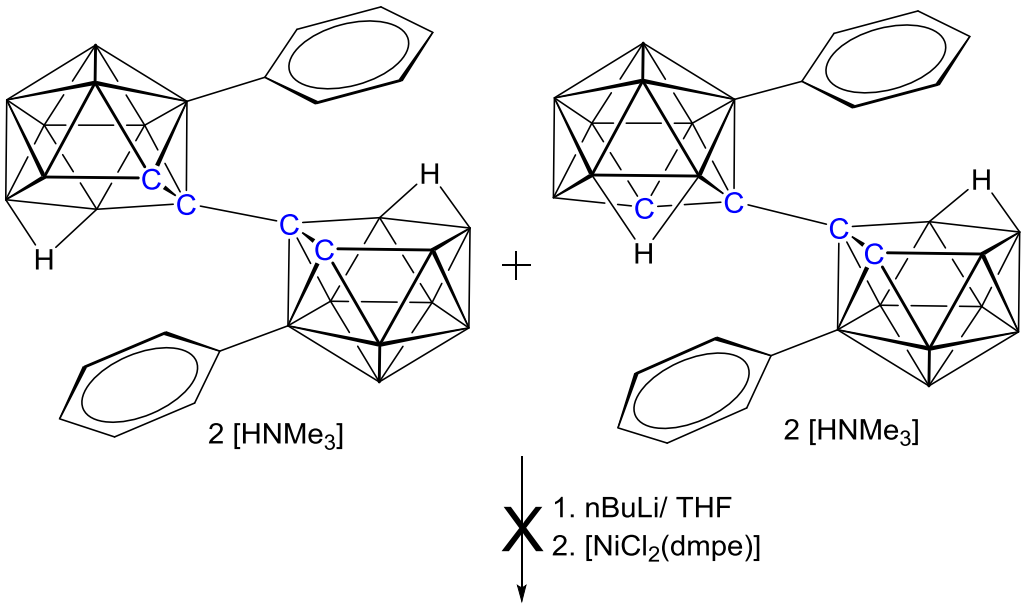

Figure 3.2.8.2 Attempted metallation of ($[HNMe_3]_2$[**23**]) with $[NiCl_2(dmpe)]$.

3.2.9 Synthesis of *rac*-[1-(1′-3′-(dppe)-3′,1′,2′-*closo*$^{\circlearrowleft}$-$NiC_2B_9H_{10}$)-3-(dppe)-3,1,2-*closo*$^{\circlearrowleft}$-$NiC_2B_9H_{10}$] (24) and [1-(2′-4′-(dppe)-4′,1′,2′-*closo*$^{\circlearrowleft}$-$NiC_2B_9H_{10}$)-3-(dppe)-3,1,2-*closo*$^{\circlearrowleft}$-$NiC_2B_9H_{10}$] (25)

By following a similar procedure as for compounds **18** and **19**, a suspension of $[Tl]_2$[1-(1′-3′,1′,2′-*closo*-$TlC_2B_9H_{10}$)-3,1,2-*closo*-$TlC_2B_9H_{10}$] (**17**) in THF was treated with [$NiCl_2$(dppe)]. An overnight stir of the reaction mixture afforded an army green suspension. Filtration through silica of the crude reaction mixture followed by chromatographic purification afforded two army green bands with trace amounts of a purple band, where the higher R_f army green band was subsequently defined as **24**. Crystallisation of the low R_f army green band gave compound **25** in pure form (Figure 3.2.9.1).

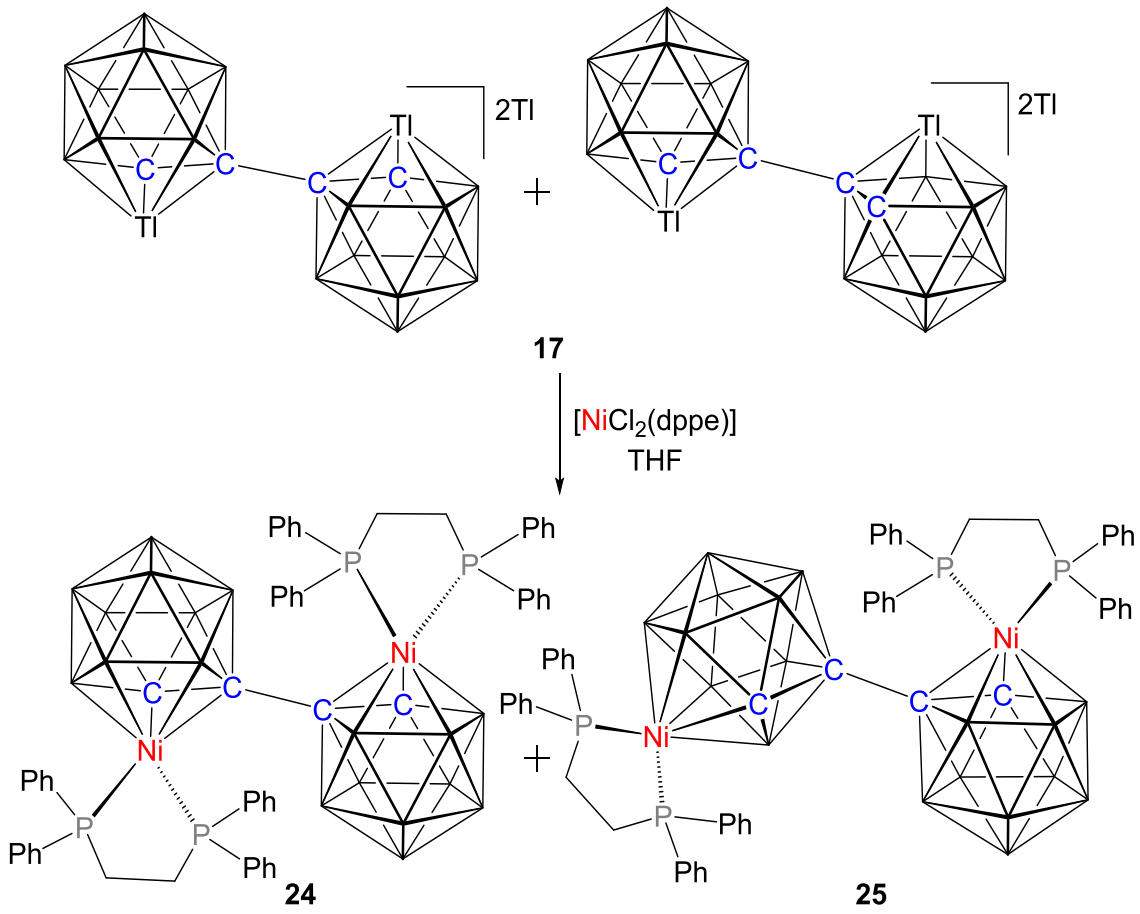

Figure 3.2.9.1 Metallation of **17** with [$NiCl_2$(dppe)].

Microanalysis of compound **24** is in agreement with that expected for $C_{56}H_{68}B_{18}Ni_2P_4$, and the mass spectrum illustrates an envelope centred at *m/z* 1176.6 (M^+) (MW = 1177.04 g mol^{-1}). From the mass spectrum and elemental analysis, it was evident that both cages of the bis(carborane) were metallated with $\{Ni(dppe)\}^{2+}$ fragments. For further confirmation of the exact isomer other spectroscopic techniques were necessary.

The $^{11}B\{^1H\}$ NMR spectrum of compound **24** reveals five resonances with the relative integrals 2:4:2:5:5 from high frequency to low frequency, a different pattern to that of compounds **18** or **19**. Therefore from this spectrum it is not possible to identify the isomer present in **24**.

In the ^1H NMR spectrum, there are resonances arising from phenyl protons and the $-CH_2-CH_2-$ bridge of the dppe ligands. In addition, there is also a CH_{cage} resonance assigned to nickelacarborane cages which appears at δ 1.84 ppm as a doublet J = 11.6 Hz of integral two. This resonance gives a singlet in the $^1H\{^{31}P\}$ spectrum confirming the coupling arises from *trans* phosphorus. Notably the CH_{cage} resonance of compound **24** appears at lower frequency than that of compounds **18** (δ 2.43 ppm) or **19** (δ 2.48 ppm).

The $^{31}P\{^1H\}$ NMR spectrum of compound **24** consists of two mutual doublets at δ 51.6 and 39.2 ppm with coupling J = 19.1 Hz with integral ratio 1:1. These indicate that in each cage the phosphorus atoms are magnetically inequivalent and each phosphorus is magnetically equivalent to the phosphorus of the biphosphine at the second cage. This justifies asymmetric nature in the each metallacarborane cage and symmetric nature in the whole. In summary at this stage, compound **24** identified as a *closo*-metallated species and must have a [3,1,2-NiC_2B_9-3′,1′,2′-NiC_2B_9] architecture.

Crystals of compound **24** were grown by solvent diffusion of a DCM solution and 40-60 petroleum ether. Study of the crystals by *X*-ray diffraction yielded a structure consistent with all the spectroscopic data for **24**. The nickelacarborane has a 3,1,2-NiC_2B_9-3′,1′,2′-NiC_2B_9 architecture arising from metallation of [7-(7′-7′,8′-*nido*-$C_2B_9H_{10}$)-7,8-*nido*-$C_2B_9H_{10}$]$^{4-}$ by two $\{Ni(dppe)\}^{2+}$ fragments. Thus compound **24** is *rac*-[1-(1′-3′-(dppe)-3′,1′,2′-*closo*$^{\cup}$-$NiC_2B_9H_{10}$)-3-(dppe)-3,1,2-*closo*$^{\cup}$-$NiC_2B_9H_{10}$] and has a similar architecture to compound **18**.

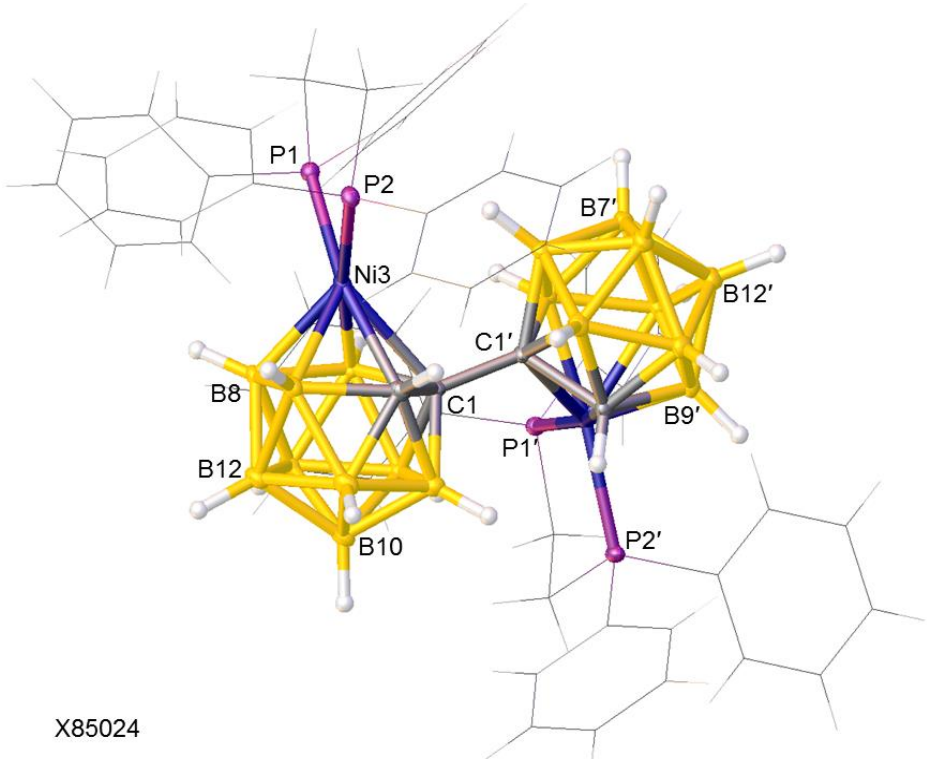

Figure 3.2.9.2 A perspective view of *rac*-[1-(1′-3′-(dppe)-3′,1′,2′-*closo*$^{\circlearrowleft}$-$NiC_2B_9H_{10}$)-3-(dppe)-3,1,2-*closo*$^{\circlearrowleft}$-$NiC_2B_9H_{10}$] (**24**) (all phenyl rings and the –CH_2-CH_2- bridge of dppe are presented in wireframe for clarity).

The molecular structure of **24** is displayed in Figure 3.2.9.2. The structure is of considerable interest and shows clear indications of internal crowding. In the unit cell, there are four molecules of **24** in space group *C*2/*c* giving the molecule crystallographically imposed of C_2 symmetry. The preferred orientation of the {NiP1P2} fragment in the NiC_2B_9 icosahedra would lie perpendicular to the vertical mirror plane through the C_2B_9 unit.[7] In **24** the dihedral angle, θ, between the plane containing Ni3P1P2 and the plane through B6B8B10 is 60.72(9)º, a significant deviation from the electronically-preferred 90º. Practically the NiP1P2 plane in **24** is essentially perpendicular (dihedral angle 84.48(7)º) to the plane of C1B10B12 vertices to reduce steric crowding between the dppe ligand and bulky {(dppe)(3′,1′,2′-NiC_2B_9)} substituent on C1. The plane of the {NiP1P2} fragment is bent away from the perpendicular to the bottom pentagonal plane through B5B6B11B12B9 vertices with a bend angle of 6.6(8)º, which indicates the presence of steric congestion in the molecule. This is further supported by the longer Ni3–C1 distance compared to Ni3–C2 [2.336(2) *versus* 2.124(2) Å]. The two nickelcarborane cages are joined by a C-C single bond with the Ni3-C1-C1′-Ni3′ torsion angle, 141.04(5)º and C2-C1-C1′-C2′ torsion angle 78.20(17)°.

Moving from **24** to compound **25**, the mass spectrum gives an envelope peak centred at *m/z* 1176.6 (M^+) (MW = 1177.04 g mol^{-1}), and microanalysis is in agreement with that expected for $C_{56}H_{68}B_{18}Ni_2P_4 \cdot CH_2Cl_2$ (crystals developed from DCM and 40-60 petroleum ether contain 3 DCM molecules per molecule of nickelacarborane). From the mass spectrum and elemental analysis data, compound **25** was anticipated to be a geometrical isomer of **24**.

The $^{11}B\{^1H\}$ NMR spectrum of **24** consists of multiple overlapping resonances with a total integral of 18B. The spectrum is different in pattern to that of compound **18**, **19** and **24**, thus preventing identification of the exact isomer present. Therefore other spectroscopic analysis is required.

In the ^1H NMR spectrum of **25** signals for the -C*H*$_2$-C*H*$_2$- bridge and phenyl protons of the dppe ligands are observed. There are also two C*H*$_{cage}$ resonances each of integral-1, one at δ 1.94 ppm appearing as a singlet and the other at δ 1.67 ppm appearing as a doublet J = 11.2 Hz which yields a singlet in the $^1H\{^{31}P\}$ NMR spectrum. The latter one must be related to the unisomerised $\{NiC_2B_9\}$ cage and the former to an isomerised $\{NiC_2B_9\}$ cage, which is supported by the $^{31}P\{^1H\}$ NMR spectrum.

The $^{31}P\{^1H\}$ NMR spectrum of **25** consists of a singlet of integral-2 at δ 62.9 ppm and two mutual doublets each with integral-1 at δ 49.4 and 47.5 ppm with coupling J = 16.6 Hz. In summary so far, compound **25** is identified as a *closo*-metallated species and must be a combination of a $\{(dppe)(3,1,2\text{-}NiC_2B_9)\}$ cage and either a $\{(dppe)(4,1,2\text{-}NiC_2B_9)\}$ or $\{(dppe)(2,1,8\text{-}NiC_2B_9)\}$ cage.

Crystals of **25** were grown by solvent diffusion of a DCM solution and 40-60 petroleum ether. Analysis of the crystals by *X*-ray diffraction yielded a structure consistent with all the spectroscopic data for **25**. The nickelacarborane has a 3,1,2-NiC_2B_9-4′,1′,2′-NiC_2B_9 architecture in contrast to compounds **18**, **19** and **24**. Thus compound **25** is [1-(2′-4′-(dppe)-4′,1′,2′-*closo*$^{\cup}$-$NiC_2B_9H_{10}$)-3-(dppe)-3,1,2-*closo*$^{\cup}$-$NiC_2B_9H_{10}$].

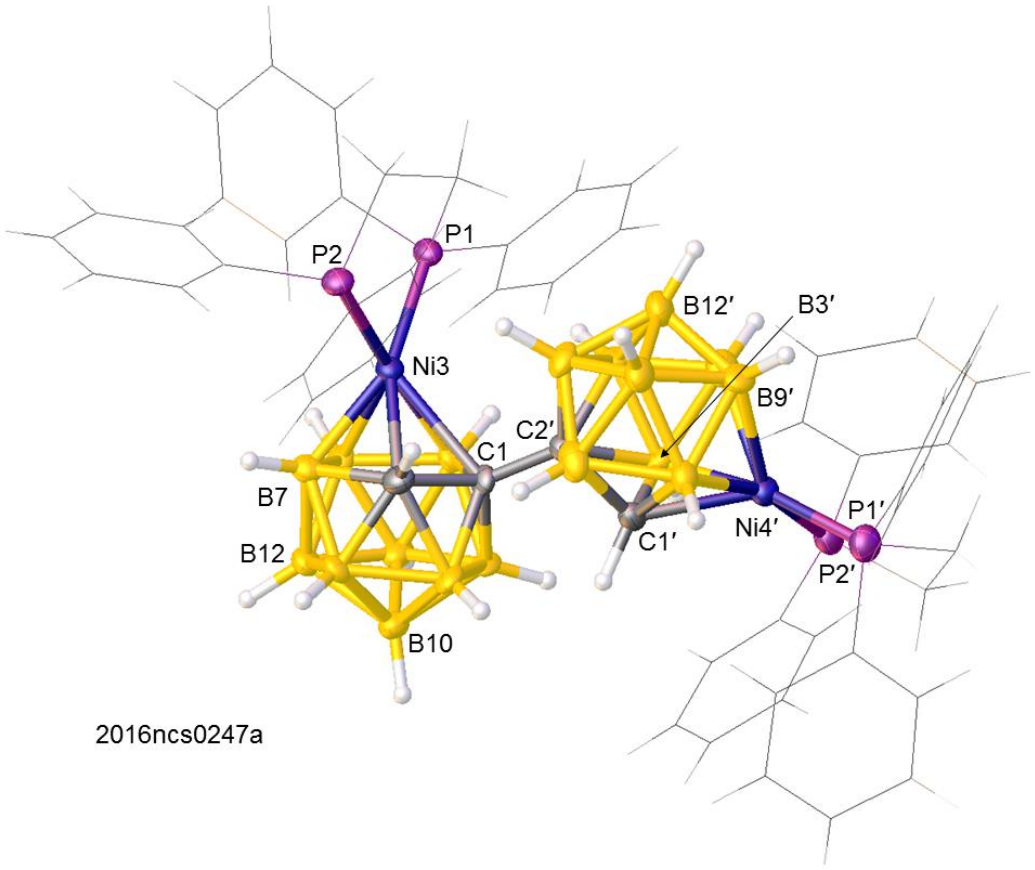

Figure 3.2.9.3 Molecular structure of [1-(2′-4′-(dppe)-4′,1′,2′-*closo*$^{\circlearrowleft}$-$NiC_2B_9H_{10}$)-3-(dppe)-3,1,2-*closo*$^{\circlearrowleft}$-$NiC_2B_9H_{10}$] (**29**) (all phenyl rings and the –CH_2-CH_2- bridge of dppe are presented in wireframe for clarity).

The molecular structure of **25** is shown in Figure 3.2.9.3. The unit cell consists of four molecules of nickelacarborane and twelve DCM molecules in the lattice in the $P2_12_12_1$ space group. The molecule of **25** is partly disordered. The atomic connectivity is nonetheless clear, and compound **9** consists of a {3,1,2-NiC_2B_9} cage and a {4′,1′,2′-NiC_2B_9} cage *i.e.* 3,1,2-NiC_2B_9-4′,1′,2′-NiC_2B_9. The orientation of the metal-phosphine unit in the {3,1,2-NiC_2B_9} cage is defined by the dihedral angle, θ, between the Ni3P1P2 and B6B8B10 planes 64.8(4)º not so far from 90º. For the {4′,1′,2′-NiC_2B_9} cage, the metal-phosphine unit is oriented with the dihedral angle 57.59(15)º between the Ni3′P1′P2′ and C1′B11′B12′ plane, not the electronically preferred 90º.[7] Both these distortions decrease steric crowding in the molecule. Residual steric congestion in the molecule is reflected in the longer distances Ni3-C1: 2.327(9) Å *versus* Ni2-C2: 2.129(9) Å. In the 4′,1′,2′-cage the distance Ni4′-C1′ is 2.167(8) Å. The two nickelcarboranes are joined by a C-C single bond with the C2-C1-C2′-C1′ torsion angle 101.1(8)º and Ni3-C1-C2′-C1′ torsion angle, 170.5(5)º.

3.2.10.1 Thermal isomerisation of compound 24 in toluene: synthesis of [2-(8′-2′-(dppe)-2′,1′,8′-*closo*$^{\circlearrowleft}$-$NiC_2B_9H_{10}$)-4-(dppe)-4,1,2-*closo*$^{\circlearrowleft}$-$NiC_2B_9H_{10}$] (26) and [2-(2′-4′-(dppe)-4′,1′,2′-*closo*$^{\circlearrowleft}$-$NiC_2B_9H_{10}$)-4-(dppe)-4,1,2-*closo*$^{\circlearrowleft}$-$NiC_2B_9H_{10}$] (27)

Thermolysis of compound **24** was carried out in refluxing toluene over 2.5 h during which time the army green colour solution became red-purple. Spot TLC followed by purification by prep TLC gave two red-purple products in yields of 27% for the higher R_f band (compound **27**) and 31% for the lower R_f band (compound **26**). In addition there was also a trace amount of red-purple product at very high R_f.

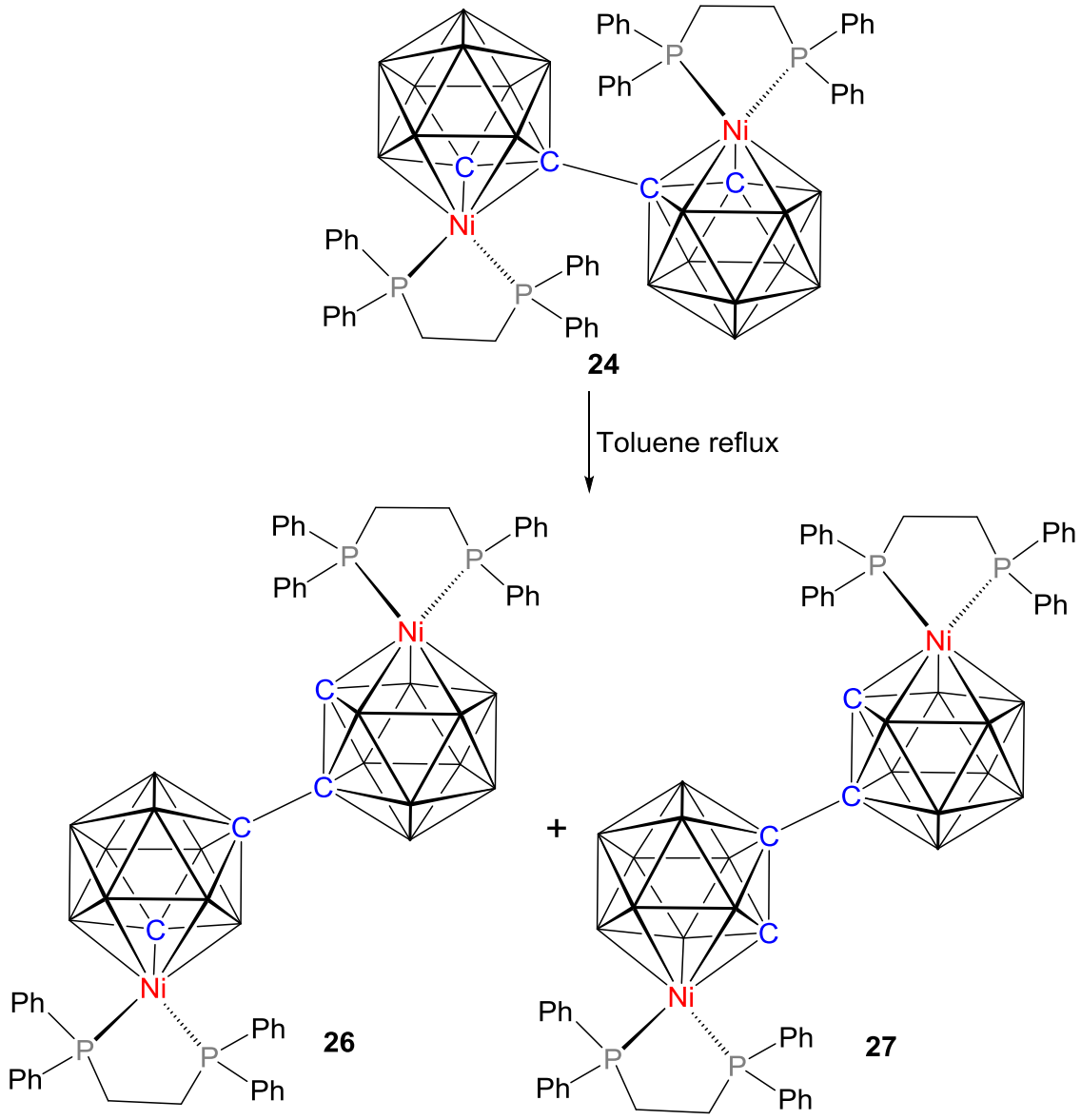

Figure 3.2.10.1.1 Thermolysis of compound **24** at 110 °C.

As these species are derived from the thermal isomerisation of **24**, compounds **26** and **27** were postulated isomeric analogues of compound **24**, with elemental analysis and mass spectrometry of both compounds in line with this suggestion.

The $^{11}B\{^{1}H\}$ NMR spectrum of **26** reveals overlapping resonances with a total integral of 18B. The spectrum is different in pattern to that of compounds **18**, **19**, **24** and **25**, and other spectroscopic analysis was therefore required to determine the exact isomeric nature of **26**.

The ^{1}H NMR spectrum of **26** is different to that of **24** and consists of signals for the -C*H*$_2$-C*H*$_2$- bridge and C$_6$*H*$_5$ of the dppe fragments. There are also two singlet C*H*$_{cage}$ resonances, each of integral-1, at δ 1.98, 1.81 ppm. This suggests both cages are isomerised and in different architectures.

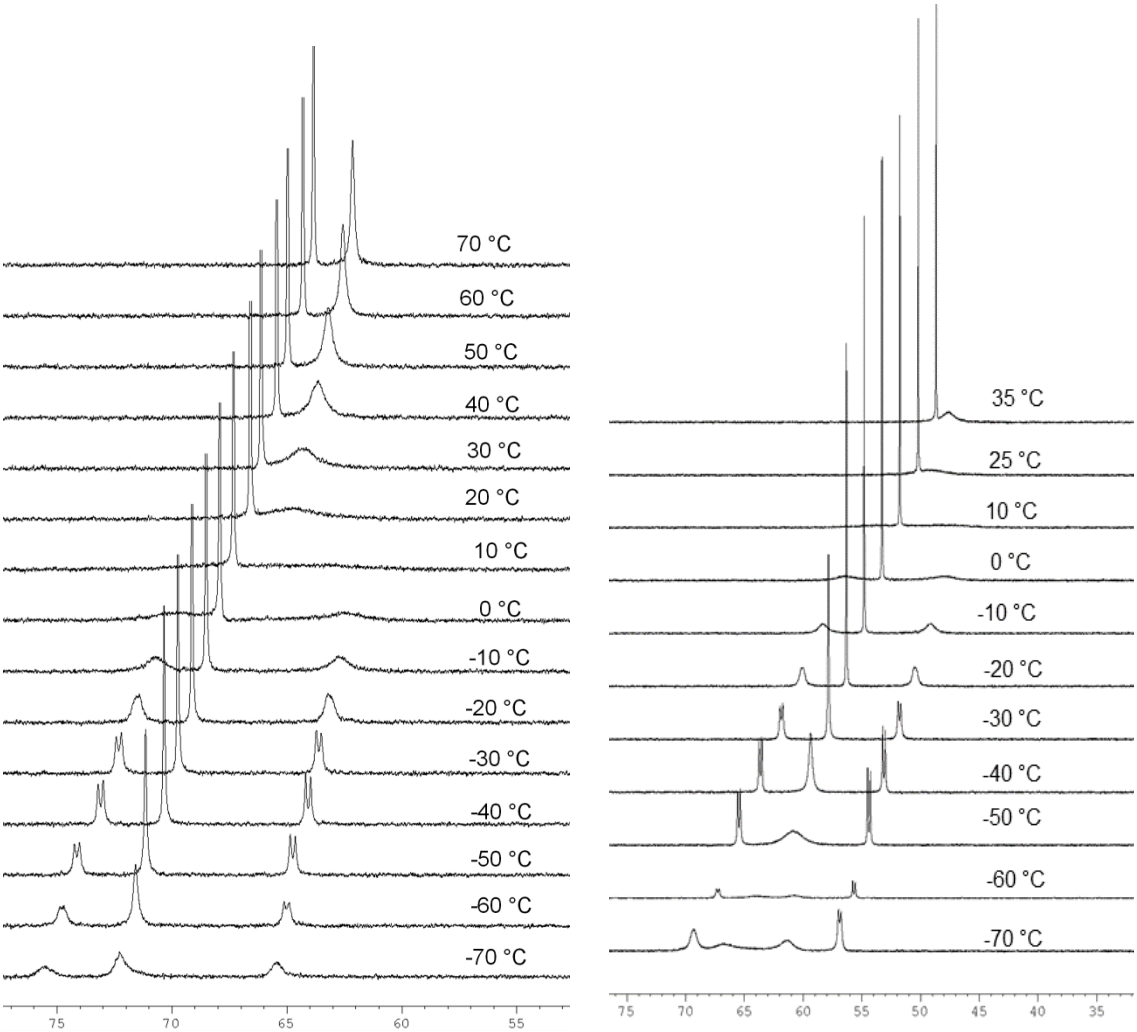

Figure 3.2.10.1.2 Variable temperature $^{31}P\{^{1}H\}$ NMR spectra of compound **26** in $CD_3C_6D_5$ (left) and in CD_2Cl_2 (right).

The $^{31}P\{^{1}H\}$ NMR spectrum of compound **26** in CD_2Cl_2 consists a singlet (δ 62.7 ppm) and a broad, very weak, resonance (δ 61.5 ppm) at room temperature (25 C°). Cooling a solution of **26** in CD_2Cl_2 to -70 °C gives four phosphorus resonances (Figure 3.2.10.1.2, right). The broad singlet at δ 68.7 ppm is resolved to mutual doublets $^{2}J_{PP}$ = 36.0 Hz, at δ 68.7 and 57.1 ppm whilst the singlet at δ 62.7 ppm gives way to two broad singlets δ 65.4 and 62.2 ppm at -70 °C (203 K), the lowest temperature reached. Further lowering temperature results in precipitation. Substantial heating of a solution of **26** in CD_2Cl_2 is not possible due to the low boiling point of the solvent and only reached 35 °C (308 K). However, heating a solution of compound **26** in $CD_3C_6D_5$ (d_6-toluene) gives two singlets, each of integral two (Figure 3.2.10.1.2, left). Therefore two different fluxional process are present in compound **26**. The activation energy for rotation of the {Ni(dppe)} fragment in one of the cages is calculated to be *ca*. 35 kJ mol^{-1} ($T_{coalescence}$ = 283 K) [16] based on the signal at δ 61.5 ppm, while the activation energy for rotation of the {Ni(dppe)} fragment in the other cage is estimated to be *ca*. 38 kJ mol^{-1} ($T_{coalescence}$ = 223 K). Notably, arresting the fluxionality of the species was not possible in $CD_3C_6D_5$ even at the lowest available temperature -70 °C (203 K) as shown in figure 3.2.10.1.2, left. Thus compound **26** must be a combination of {(dppe)(4,1,2-NiC_2B_9)} and {(dppe)(2,1,8-NiC_2B_9)} cages.

Crystals of compound **26** were developed by solvent diffusion of a THF solution and 40-60 petroleum ether, with analysis by *X*-ray diffraction resulting in a structure consistent with the spectroscopic data. The bis(nickelacarborane) has a 4,1,2-NiC_2B_9-2′,1′,8′-NiC_2B_9 architecture arising from thermal isomerisation of compound **24**. Thus **26** is [2-(8′-2′-(dppe)-2′,1′,8′-*closo*$^{\cup}$-$NiC_2B_9H_{10}$)-4-(dppe)-4,1,2-*closo*$^{\cup}$-$NiC_2B_9H_{10}$].

A perspective view of compound **26** is shown in Figure 3.2.10.1.3. The molecule belongs to the *C*2/*c* space group (monoclinic) with Z′ = 1 (where Z = 8). In **26** both {NiPP} fragments are now bound to CB_4 faces. In the {(dppe)(2′,1′,8′-NiC_2B_9)} cage, the dihedral angle, θ, between the plane through {NiPP} and the plane through C1′B9′B12′ is 58.11(14)º, far from the electronically-preferred 90º.[7] In fact {Ni2′P1′P2′} fragment lies almost perpendicular (θ = 87.07(11)°) to the plane passing through the B4′B7′B9′ vertices. In the case of the {(dppe)(4,1,2-NiC_2B_9)} cage, the expected orientation of the metal-phosphine unit is that in which the dihedral angle between the NiPP and C1B12B7 planes is 90º, [7] whilst θ is found experimentally to be only 54.89(15)º. Effectively the {NiPP} fragment lies perpendicular to the plane passing through the C2B7B10 vertices.

This clearly suggests steric congestion is present in the molecule. The isomerisation from a bis 3,1,2- precursor to a 4,1,2- and 2,1,8- species is likely to relieve steric crowding within the metallacarborane.

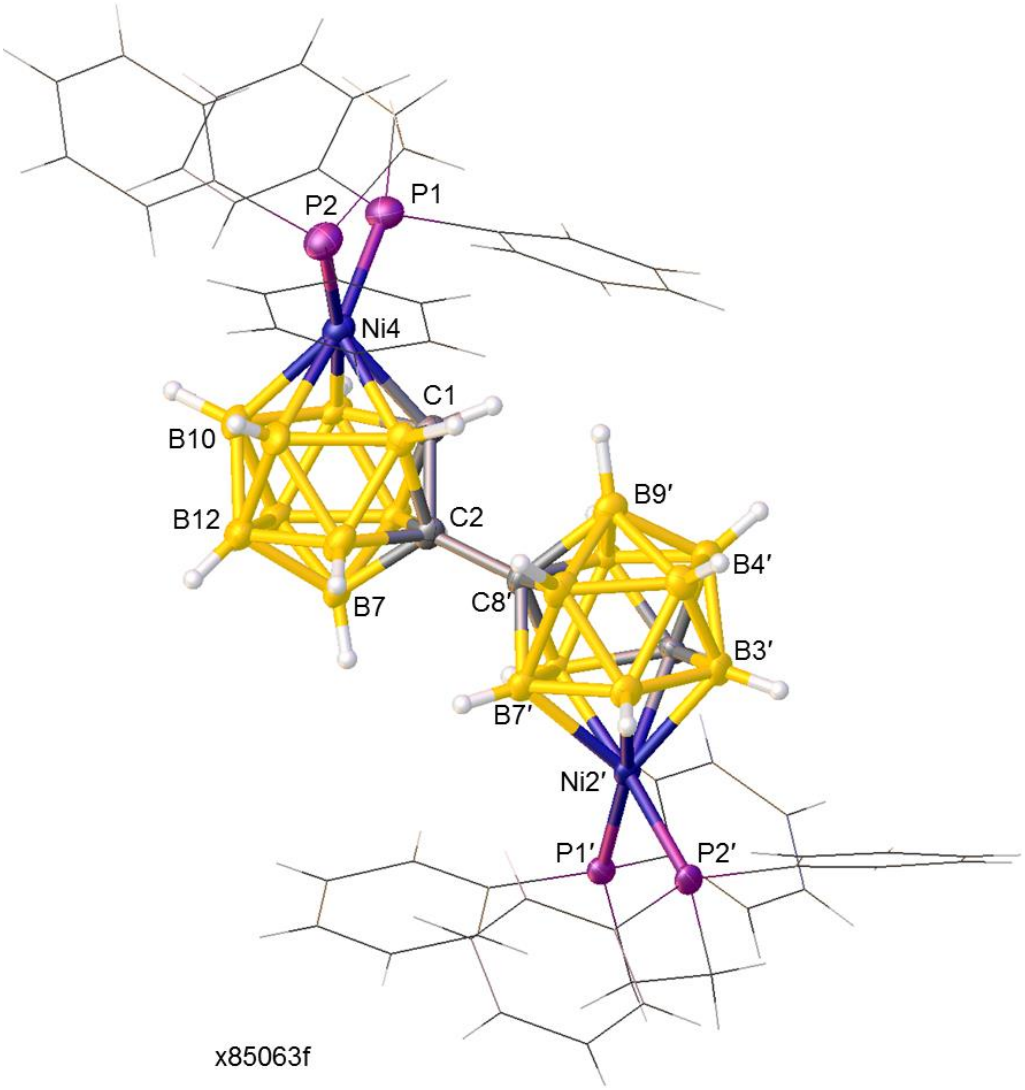

Figure 3.2.10.1.3 Molecular structure of [2-(8′-2′-(dppe)-2′,1′,8′-*closo*$^{\circlearrowleft}$-$NiC_2B_9H_{10}$)-4-(dppe)-4,1,2-*closo*$^{\circlearrowleft}$-$NiC_2B_9H_{10}$] (**26**) (all phenyl rings and the –CH_2-CH_2- bridge of dppe are presented in wireframe for clarity).

Moving from **26** to compound **27**, the $^{11}B\{^1H\}$ NMR spectrum of compound **27** consists of four overlapping signals with a total integral of 18B. The spectrum is different in pattern to that of compounds **24**, **25** and **26**, and as such was not conclusive for the identification of the exact isomer present.

The ^{1}H NMR spectrum of **27** consists of signals for the -C*H*$_2$-C*H*$_2$- bridge and aromatic protons of the dppe ligands. There is also a singlet C*H*$_{cage}$ resonance with integral-2 at δ 2.03 ppm. This suggests both cages are isomerised and of similar isomeric nature. The ^{31}P{^{1}H} NMR spectrum of compound **27** reveals only a singlet (δ 62.9 ppm) resonance at room temperature. This indicates rotation of the {Ni(dppe)} fragment about the metal-cage axis that is rapid on the NMR timescale. Thus compound **27** must be a combination of two {(dppe)(4,1,2-NiC_2B_9)} cages or two {(dppe)(2,1,8-NiC_2B_9)} cages.

X-ray quality crystals of compound **27** were grown by solvent diffusion of a DCM solution and 40-60 petroleum ether. Thus compound **27** was identified as [2-(2′-4′-(dppe)-4′,1′,2′-*closo*$^{\circlearrowleft}$-$NiC_2B_9H_{10}$)-4-(dppe)-4,1,2-*closo*$^{\circlearrowleft}$-$NiC_2B_9H_{10}$].

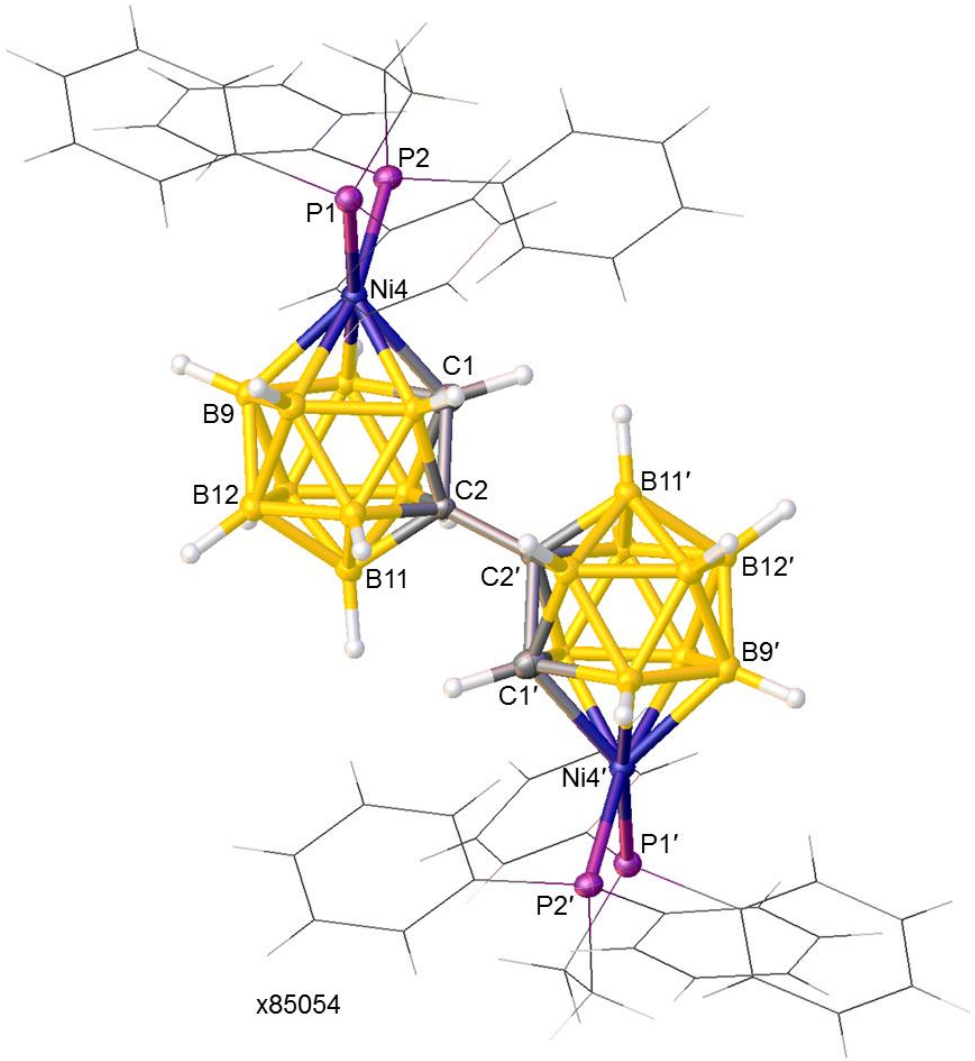

Figure 3.2.10.1.4 Molecular structure of [2-(2′-4′-(dppe)-4′,1′,2′-*closo*$^{\circlearrowleft}$-$NiC_2B_9H_{10}$)-4-(dppe)-4,1,2-*closo*$^{\circlearrowleft}$-$NiC_2B_9H_{10}$] (**27**) (all phenyl rings and the –CH_2-CH_2- bridge of dppe are presented in wireframe for clarity).

3.2.10.2 Thermal isomerisation of compound 25 in toluene: alternative synthesis of 26 and 27

Thermolysis of compound **25** was carried out in refluxing toluene for 2.5 h. During reflux the initial army green colour of the solution changed to red-purple. Purification by prep TLC gave two red-purple products in yields of 40% for the lower R_f and 38% for the higher R_f bands. After spectroscopic characterisations ($^{11}B\{^1H\}$, $^{31}P\{^1H\}$, ^1H NMR and EIMS), the two products were identified as compounds **26** (low R_f) and **27** (high R_f) (Figure 3.2.10.2.1).

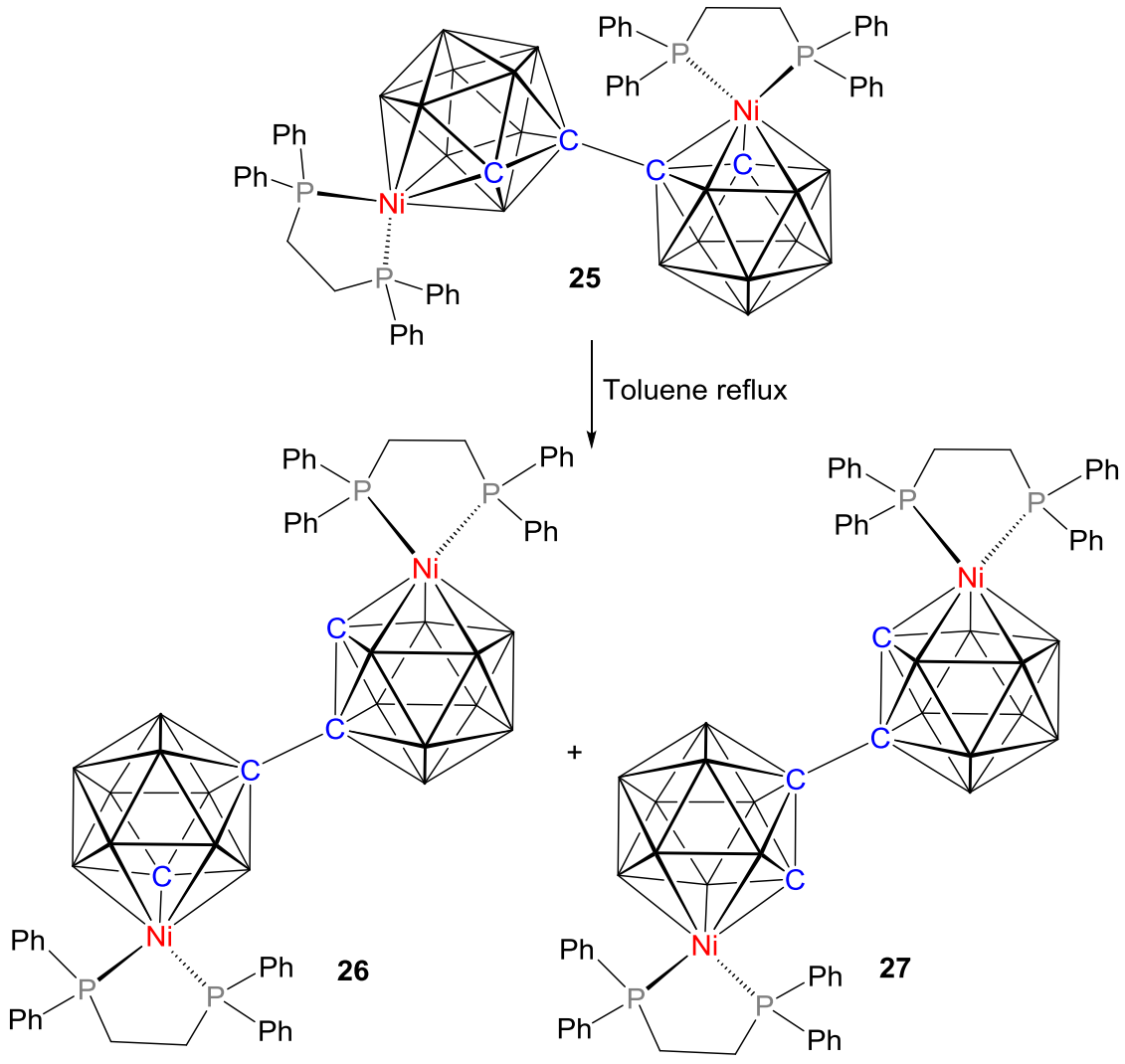

Figure 3.2.10.2.1 Thermolysis of compound **25** at 110 °C.

3.2.11 Discussion: metallation and isomerisation of double-decapitated bis(*o*-carborane) with $\{Ni(dppe)\}^{2+}$ and $\{Ni(dmpe)\}^{2+}$ fragments

For these metallation reactions, $[Tl]_2[1\text{-}(1'\text{-}3',1',2'\text{-}closo\text{-}TlC_2B_9H_{10})\text{-}3,1,2\text{-}closo\text{-}TlC_2B_9H_{10}]$ (**17**) has been chosen to enhance yields of the products compared to those obtained with ammonium salts. The Tl_4-salt is a convenient starting point for the synthesis of $MC_2B_9\text{-}MC_2B_9$ products by simple stirring with a source of the appropriate metal fragment at room temperature due to the halophilic nature of thallium. Addition of $\{Ni(dmpe)\}^{2+}$ to **17** results in both diastereoisomers *i.e*. *rac*-3,1,2-NiC_2B_9-3′,1′,2′-NiC_2B_9 (**18**) and *meso*-3,1,2-NiC_2B_9-3′,1′,2′-NiC_2B_9 (**19**). Both cages of compounds **18** and **19** remain in the unisomerised 3,1,2-architecture. Compound **18** is easily converted into a mixture of **18** and **19** by heating at 65 °C and similarly compound **19** results in the same components after THF reflux. We attempted to establish the mechanism of this rac and meso transformation by labelling studies. For the synthesis of B3, B3′ substituted bis(carborane), initially we attempted to couple two lithiated 3-Et-1,2-C_2B_{10} species *via* Cu(I). We also attempted to capitate $[Tl]_2[1\text{-}(1'\text{-}3',1',2'\text{-}closo\text{-}TlC_2B_9H_{10})\text{-}3,1,2\text{-}closo\text{-}TlC_2B_9H_{10}]$ (**17**) with $\{BX\}^{2+}$ (X = I, Br) fragments. Both were unsuccessful, however the latter yielded $[7\text{-}(7'\text{-}7',8'\text{-}nido\text{-}C_2B_9H_{12})\text{-}7,8\text{-}nido\text{-}C_2B_9H_{12}]$ (**20**) unexpectedly. The unexpected protonation of both cages might be caused by the presence of Lewis acid (BBr_3 or BI_3) in petrol. Again after several attempts, we have devised a successful synthetic route for the preparation of B3, B3′ phenyl substituted bis(carboranes). The capitation of $[7\text{-}(7'\text{-}7',8'\text{-}nido\text{-}C_2B_9H_{10})\text{-}7,8\text{-}nido\text{-}C_2B_9H_{10}]^{4-}$, prepared by lithiation of the corresponding precursor in ether, with $\{BPh\}^{2+}$ in petrol yielded *rac*-$[1\text{-}(1'\text{-}3'\text{-}Ph\text{-}1',2'\text{-}closo^{\cup}\text{-}C_2B_{10}H_{10})\text{-}3\text{-}Ph\text{-}1,2\text{-}closo^{\cup}\text{-}C_2B_{10}H_{10}]$ (**21**) and *meso*-$[1\text{-}(1'\text{-}3'\text{-}Ph\text{-}1',2'\text{-}closo^{\cup}\text{-}C_2B_{10}H_{10})\text{-}3\text{-}Ph\text{-}1,2\text{-}closo^{\cup}\text{-}C_2B_{10}H_{10}]$ (**22**). After complete characterisation of **21** and **22**, we have successfully decapitated both cages using excess $[EtO]^-$. The decapitated species was isolated as $[HNMe_3]_2[7\text{-}(7'\text{-}3'\text{-}Ph\text{-}7',8'\text{-}nido\text{-}C_2B_9H_{10})\text{-}3\text{-}Ph\text{-}7,8\text{-}nido\text{-}C_2B_9H_{10}]$ ($[HNMe_3]_2$[**23**]) as a *rac* and *meso* mixture and also as $[BTMA]_2[7\text{-}(7'\text{-}3'\text{-}Ph\text{-}7',8'\text{-}nido\text{-}C_2B_9H_{10})\text{-}3\text{-}Ph\text{-}7,8\text{-}nido\text{-}C_2B_9H_{10}]$ ($[BTMA]_2$[**23**]) in a *rac* and *meso* mixture. However metallation of $[7\text{-}(7'\text{-}3'\text{-}Ph\text{-}7',8'\text{-}nido\text{-}C_2B_9H_9)\text{-}3\text{-}Ph\text{-}7,8\text{-}nido\text{-}C_2B_9H_9]^{4-}$ with $\{Ni(dmpe)\}^{2+}$ was not successful. This might be related to the bulkiness of phenyl moieties which is clear from the molecular structure of the meso form of ($[BTMA]_2$[**23**]).

Thermolysis of compound **18** or **19** in refluxing toluene (110 °C) gave a red-orange product which has thus far been impossible to fully characterise due to its limited

solubility in common solvents. Surprisingly on metallation of **17** with $\{Ni(dmpe)\}^{2+}$ fragment, no isomerisation from 3,1,2- to 2,1,8- was observed at room temperature whereas for the same metal fragment the 3,1,2- to 2,1,8 isomerisation occurs for mono metallated nickelacarborane as discussed in Chapter 2. The isomerisation 3,1,2- to 2,1,8- is related to electronic factors. We will discuss this later in this section. Further, the treatment of **17** with $\{Ni(dppe)\}^{2+}$ yields *rac*-3,1,2-NiC_2B_9-3′,1′,2′-NiC_2B_9 (**24**) and 3,1,2-NiC_2B_9-4′,1′,2′-NiC_2B_9 (**25**). For compound **24**, both cages are unisomerised whilst in compound **25** one of the cages is isomerised to 4,1,2. Thus the metallation of **17** with $\{Ni(dppe)\}^{2+}$ results in only the rac unisomerised isomer, a stereospecific reaction, and another isomer where one of the cages of the bis(nickelcarborane) is isomerised.

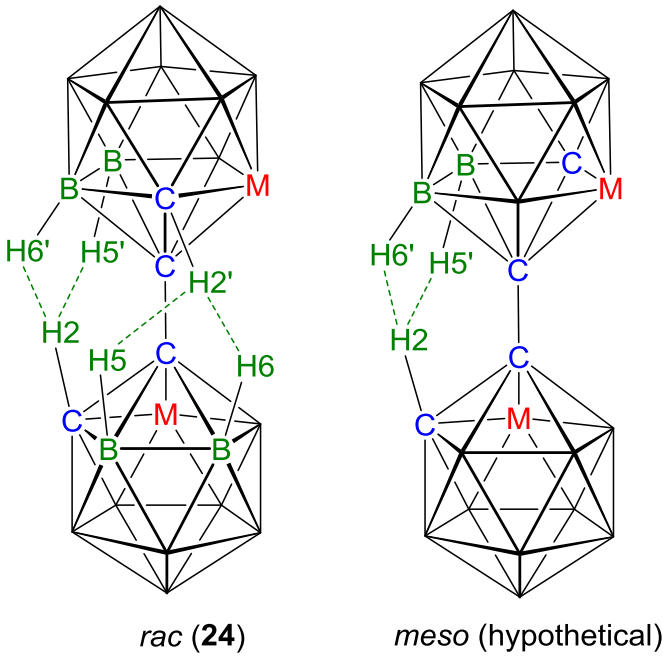

Figure 3.2.11.1 Pictorial presentations of DHB in dppe-bis(heteroborane).

The stereospecific nature of compound **24** can be explained by dihydrogen bonding (DHB) which is non-conventional hydrogen bonding involving H-centres as both the acceptor and donor. In the *rac* (**18**) and *meso* (**19**) forms of 3,1,2-NiC_2B_9-3′,1′,2′-NiC_2B_9 and *rac* 3,1,2-NiC_2B_9-3′,1′,2′-NiC_2B_9 (**24**), the formation of intramolecular DHBs involves H-atoms bound to the C atom of one cage and a B-atom of the other cage (C-H….H-B). In all these complexes a pair of DHBs exists. The strength of DHBs depends on the electron density on the H-atoms and is an electrostatic interaction. For a 3,1,2-MC_2B_9 species, the most δ- hydrogen atoms are positioned at vertices 5 and 6 based on the ^{11}B NMR chemical shifts as reported by Kennedy *et al*.[17] Thus the H atoms positioned

at 5, 6, 5' and 6' of compound **24** are most δ- in character whereas the hydrogen atoms positioned at 2 and 2' are most δ+ in character as C is more electronegative than B. The *rac* compound **24** has greater tendency to form intramolecular DHBs than the hypothetical *meso* isomer of compound **24**, since the *rac* isomer allows formation of two sets of DHBs whilst the hypothetic *meso* isomer only allows one, whatever the rotamer (Figure 3.2.11.1).

With this, the formation of compound **25** can be rationalised by steric factors. Steric crowding between the bulky {(dppe)(3,1,2-NiC_2B_9)} substituent on C1′ and dppe ligand on Ni3′ of an unisomerised (3′,1′,2′-NiC_2B_9)$_2$ species is most likely to contribute to the isomerisation (we have already noted the steric crowding in compound **24**), since the isomerisation moves the {(dppe)(3,1,2-NiC_2B_9)} substituent down to the lower pentagonal belt. Similar 3,1,2- to 4,1,2- isomerisation was observed for mono metallated nickelacarboranes with dppe and PPh_2Me ligands in Chapter 2. However we have already seen that some steric congestion remains in compound **25**.

Heating compounds **24** or **25** at THF reflux does not produce any isomerisation whereas thermolysis of *rac*-3,1,2-NiC_2B_9-3′,1′,2′-NiC_2B_9 (**24**) at higher temperature such as 110 °C (toluene reflux) yields different isomers of bis(nickelcarboranes) *i.e*. 4,1,2-NiC_2B_9-2′,1′,8′-NiC_2B_9 (**26**) and 4,1,2-NiC_2B_9-4′,1′,2′-NiC_2B_9 (**27**). Similarly refluxing in toluene of compound **25** also yields both compounds **26** and **27**. The high temperatures required for isomerisation indicates these compounds are thermally stable. The nature of isomerisation can be rationalised by crowding within the metallacarboranes. As compound **24** is in the 3,1,2-NiC_2B_9-3′,1′,2′-NiC_2B_9 architecture, there is a possibility of isomerisation from a 3,1,2- to either a 2,1,8- or a 4,1,2- isomer and this is true for both cages. Therefore the possible isomers from the isomerisation of compound **24** are 2,1,8-NiC_2B_9-2′,1′,8′-NiC_2B_9; 4,1,2-NiC_2B_9-2′,1′,8′-NiC_2B_9 and 4,1,2-NiC_2B_9-4′,1′,2′-NiC_2B_9. Only the latter two examples were, however, isolated. Additionally there is a small purple band observed during prep TLC at very high R_f and this may be the 2,1,8-NiC_2B_9-2′,1′,8′-NiC_2B_9 isomer. For compound **25**, only one cage remains unisomerised, the other already having isomerised to the 4,1,2- isomer. Thus possible isomers 2,1,8-NiC_2B_9-2′,1′,8′-NiC_2B_9, 4,1,2-NiC_2B_9-2′,1′,8′-NiC_2B_9 and 4,1,2-NiC_2B_9-4′,1′,2′-NiC_2B_9 can be derived from thermal isomerisation of compound **25**. In fact we observed only the last two *i.e*. compounds **26** and **27**. Thus formation of these isomers can also be explained by DHB. The observed isomers 4,1,2-NiC_2B_9-4′,1′,2′-NiC_2B_9 and

4,1,2-NiC_2B_9-2′,1′,8′-NiC_2B_9 are stabilised by two and one set of DHBs respectively whereas no DHB is possible theoretically for the 2,1,8-NiC_2B_9-2′,1′,8′-NiC_2B_9 isomer (Figure 3.2.11.2).

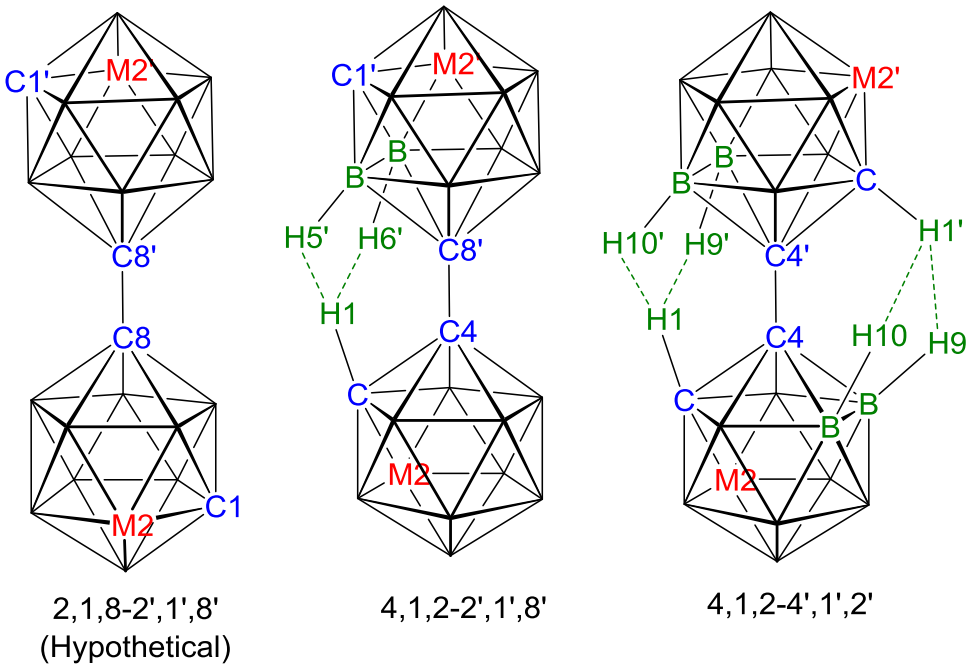

Figure 3.2.11.2 Pictorial presentations of DHB in dppe-bis(heteroborane).

Returning to the dmpe based bis(nickelcarboranes) **18** and **19**, no isomerisation was observed within the metallacarboranes at room temperature whereas an isomerisation was observed for the mono(dmpe)nickelcarborane, the latter related to electronic factors. Both compounds **18** and **19** remain in the 3,1,2-NiC_2B_9-3′,1′,2′-NiC_2B_9 form, even though there are two dmpe ligands present within the metallacarborane. We have already observed that steric congestion is present within the metallacarborane. The stability of the 3,1,2-NiC_2B_9-3′,1′,2′-NiC_2B_9 architecture can also be rationalised by DHB interactions. For the 3,1,2-NiC_2B_9-3′,1′,2′-NiC_2B_9 form there will be two set of DHBs whereas there will be no possible DHB in the hypothetical 2,1,8-NiC_2B_9-2′,1′,8′-NiC_2B_9 isomer (Figure 3.2.11.3).

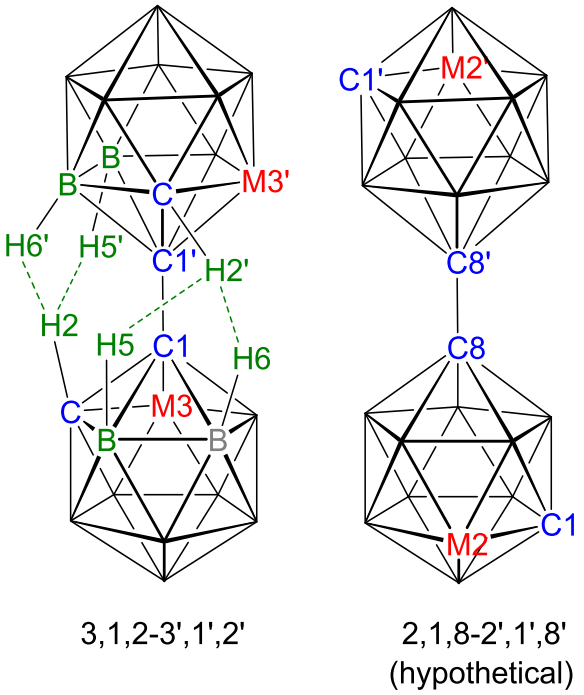

Figure 3.2.11.3 Pictorial presentations of DHB in dmpe-bis(heteroborane).

3.3 Summary

Double deboronation of 1,1′-bis(*o*-carborane) has been carried out and optimised and the decapitated species isolated as a Tl_4-salt. High yielding metallation reactions were observed using the Tl_4-salt. Thus examples of bis-metallated derivatives of 1,1′-bis(*o*-carborane) have been prepared and characterised both spectroscopically and structurally. Icosahedral bis(nickelacarboranes) have been synthesised with the fragments $\{Ni(dppe)\}^{2+}$ and $\{Ni(dmpe)\}^{2+}$. Thermal isomerisation of these bis(nickelcarboranes) has also been studied at moderate as well as high temperature. The mechanisms of the isomerisations, where applicable, have also been explored both theoretically and experimentally. The nature of isomerisations of these bis(nickelcarboranes) are explained with reference to DHB. Finally a new naming convention has been introduced for these 12-vertex-12vertex bis(nickelacarboranes) to distinguish the chiral nature of each cage.

The metallation of [7-(7′-7′,8′-*nido*-$C_2B_9H_{10}$)-7,8-*nido*-$C_2B_9H_{10}]^{4-}$ with $\{Ni(dmpe)\}^{2+}$ results in bis(nicklecarborane) diastereoisomers, *rac*-[1-(1′-3′-(dmpe)-3′,1′,2′-*closo*$^{\circlearrowleft}$-$NiC_2B_9H_{10}$)-3-(dmpe)-3,1,2-*closo*$^{\circlearrowleft}$-$NiC_2B_9H_{10}$] (**18**) and *meso*-[1-(1′-3′-(dmpe)-3′,1′,2′-*closo*$^{\circlearrowleft}$-$NiC_2B_9H_{10}$)-3-(dmpe)-3,1,2-*closo*$^{\circlearrowleft}$-$NiC_2B_9H_{10}$] (**19**). Compound **18** is readily converted to a mixture of **18** and **19** by refluxing in THF. Similar thermolysis of compound **19** yields an identical mixture of **18** and **19**.

This interconversion between **18** and **19** is unusual and two mechanisms for it have been proposed. The first mechanism involves interconversion between two diastereoisomers *via* an intermediate formed by C-C rotation. However, theoretical studies suggest this intermediate is not viable at this low temperature. The second mechanism involves two consecutive TFR rearrangements of a {3,1,2-NiC_2B_9} species. To prove this mechanism we have attempted to synthesise B6, B6′ substituted 3,1,2-NiC_2B_9-3′,1′,2′-NiC_2B_9 species. The synthesis of 3′-Et-1′,2′-C_2B_{10}-3-Et-1,2-C_2B_{10} by the coupling of two lithiated {3-Et-1,2-C_2B_{10}} units catalysed by Cu(I) was not successful. Capitation of [7-(7′-7′,8′-*nido*-$C_2B_9H_{10}$)-7,8-*nido*-$C_2B_9H_{10}]^{4-}$ with two equivalents of $\{BX\}^{2+}$ (X = I, Br) does not give the desired product, instead it yields [7-(7′-7′,8′-*nido*-$C_2B_9H_{12}$)-7,8-*nido*-$C_2B_9H_{12}$] (**20**). Further capitation of [7-(7′-7′,8′-*nido*-$C_2B_9H_{10}$)-7,8-*nido*-$C_2B_9H_{10}]^{4-}$ with $\{BPh\}^{2+}$ fragments was attempted under different reaction conditions. However the only successful route was *via* lithiation of $[HNMe_3]_2$[7-(7′-7′,8′-*nido*-$C_2B_9H_{11}$)-7,8-*nido*-$C_2B_9H_{11}$] in diethyl ether followed by addition of two equivalent

{BPh}$^{2+}$ fragments in 40-60 petrol. This results in two examples of 3,3′-ligated bis(carborane) *i.e.* *rac*-[1-(1′-3′-Ph-1′,2′-*closo*$^{\cup}$-$C_2B_{10}H_{10}$)-3-Ph-1,2-*closo*$^{\cup}$-$C_2B_{10}H_{10}$] (**21**) and *meso*-[1-(1′-3′-Ph-1′,2′-*closo*$^{\cup}$-$C_2B_{10}H_{10}$)-3-Ph-1,2-*closo*$^{\cup}$-$C_2B_{10}H_{10}$] (**22**). After complete characterisation of these species, double deboronations were carried out on a mixture of **21** and **22** affording [$HNMe_3$]$_2$[7-(7′-3′-Ph-7′,8′-*nido*-$C_2B_9H_{11}$)-3-Ph-7,8-*nido*-$C_2B_9H_{11}$] ([$HNMe_3$]$_2$[**23**]). Double degradation of both cages has been confirmed by crystallography as the BTMA salt of [7-(7′-3′-Ph-7′,8′-*nido*-$C_2B_9H_{10}$)-3-Ph-7,8-*nido*-$C_2B_9H_{10}$]$^{2-}$ ([BTMA]$_2$[**23**]). Then metallation of deprotonated ([$HNMe_3$][**23**]) with {Ni(dmpe)}$^{2+}$ was not successful. This might be due to the bulky phenyl moiety preventing the metallation process, as implied by the molecular structure of [7-(7′-3′-Ph-7′,8′-*nido*-$C_2B_9H_{10}$)-3-Ph-7,8-*nido*-$C_2B_9H_{10}$]$^{2-}$. Thus we have been unsuccessful in establishing the mechanism of interconversion between compounds **18** and **19**, resulting from THF reflux.

The isomerisation of compounds **18** and **19** was also studied at 110 °C (toluene reflux). After heating these compounds to reflux in toluene over 2.5 hrs, a red-orange material is obtained. Unfortunately characterisation of this material was not possible due to its insolubility in common solvents.

In contrast, reaction between [7-(7′-7′,8′-*nido*-$C_2B_9H_{10}$)-7,8-*nido*-$C_2B_9H_{10}$]$^{4-}$ and the metal fragment {Ni(dppe)}$^{2+}$ results in two major products, a stereospecific product *rac*-[1-(1′-3′-(dppe)-3′,1′,2′-*closo*$^{\cup}$-$NiC_2B_9H_{10}$)-3-(dppe)-3,1,2-*closo*$^{\cup}$-$NiC_2B_9H_{10}$] (**24**) and [1-(2′-4′-(dppe)-4′,1′,2′-*closo*$^{\cup}$-$NiC_2B_9H_{10}$)-3-(dppe)-3,1,2-*closo*$^{\cup}$-$NiC_2B_9H_{10}$] (**25**) in which one of the nicklecarborane cage is of 4,1,2- architecture. The formation of the stereospecific isomer **24** is rationalised by DHB. The most δ- H atoms positioned at 5, 6, 5' and 6' of compound **24** form DHBs with the most δ+ hydrogen atoms positioned at 2 and 2', in contrast to the hypothetical *meso* isomer which has only one DHB. The formation of coproduct **25** is related to steric congestion. The use of the bulky phosphine dppe causes the isomerisation from the 3,1,2-3′,1′,2′ isomer to the 3,1,2-4′,1′,2′ isomer to relieve steric crowding within the molecule.

Thermolysis of both compounds **24** and **25** at 65 °C (THF reflux) does not produce any new species. However, heating compound **24** at 110 °C (toluene reflux) produces [2-(8′-2′-(dppe)-2′,1′,8′-*closo*$^{\cup}$-$NiC_2B_9H_{10}$)-4-(dppe)-4,1,2-*closo*$^{\cup}$-$NiC_2B_9H_{10}$] (**26**), [2-(2′-4′-(dppe)-4′,1′,2′-*closo*$^{\cup}$-$NiC_2B_9H_{10}$)-4-(dppe)-4,1,2-*closo*$^{\cup}$-$NiC_2B_9H_{10}$] (**27**) and also a

trace amount of a purple product. Compound **26** is fluxional at room temperature confirmed by variable temperature $^{31}P\{^{1}H\}$ NMR experiments. The VT experiments reveal that there are two different fluxional processes present in compound **26**. Compound **27** is also fluxional at room temperature. Of the possible isomers resulting from isomerisation on heating **24** we have isolated 4,1,2-NiC_2B_9-2′,1′,8′-NiC_2B_9 (**26**) and 4,1,2-NiC_2B_9-4′,1′,2′-NiC_2B_9 (**27**). These two isomers are also isolated from the thermolysis of compound **25** in refluxing toluene. Formation of these two stable isomers is rationalised by DHB. Isomerisation from the 3,1,2- isomer to the 4,1,2- or 2,1,8-isomers occurs to relieve steric crowding between the bulky dppe fragment and the {(dppe)(NiC_2B_9)} cage.

We recall that no isomerisation was observed in the room temperature metallations of **17** with the $\{Ni(dmpe)\}^{2+}$ fragment and the bis-nickelcarboranes **18** and **19** can also be rationalised by DHB. The 3,1,2-NiC_2B_9-3′,1′,2′-NiC_2B_9 form is stabilised by two sets of DHB whereas in the hypothetical 2,1,8-NiC_2B_9-2′,1′,8′-NiC_2B_9 isomer no DHB is possible.

3.4 References

1 (a) M. F. Hawthorne, D. A. Owen and J. W. Wiggins, *Inorg. Chem*., 1971, **10**, 1304; (b) G. Thiripuranathar, W. Y. Man, C. Palmero, A. P. Y. Chan, B. T. Leube, D. Ellis, D. McKay, S. A. Macgregor, L. Jourdan, G. M. Rosair and A. J. Welch, *Dalton Trans*., 2015, **44**, 5628.

2 G. Sivasubramanian, PhD thesis, Heriot-Watt University, 2011.

3 P. E. Behnken, T. B. Marder, R. T. Baker, C. B. Knobler, M. R. Thompson and M. F. Hawthorne, *J. Am. Chem. Soc*., 1985, **107**, 933.

4 J. G. Planas, C. Viñas, F. Teixidor, M. E. Light and M. B. Hursthouse, *J. Organomet. Chem*., 2006, **691**, 3472.

5 (a) T. P. Hanusa, J. C. Huffman, and L. J. Todd, *Polyhedron*, 1982, **1**, 77, (b) M. P. Garcia, M. Green, F. G. A. Stone, R. G. Somerville, C. E. Briant, D. N. Cox, D. M. P. Mingos and A. J. Welch, *J. Chem. Soc. Dalton Trans*., 1985, 2343.

6 (a) R. A. Wiesboeck and M. F.Hawthorne, *J. Am. Chem. Soc*., 1964, **86**, 1642; (b) M. F. Hawthorne, D. C. Young, P. M. Garrett, D. A. Owen, S. G. Schwerin, F. N. Tebbe and P. A. Wegner, *J. Am. Chem. Soc*., 1968, **90**, 862.

7 (a) D. M. P. Mingos, M. I. Forsyth and A. J. Welch, *J. Chem. Soc., Chem. Commun*., 1977, 605; (b) *idem, J. Chem. Soc., Dalton Trans*., 1978, 1363; (c) P. D. Abram, D. McKay, D. Ellis, S. A. Macgregor, G. M. Rosair and A. J. Welch, *Dalton Trans*., 2010, **39**, 2412.

8 A. McAnaw, G. Scott, L. Elrick, G. M. Rosair and A. J. Welch, *Dalton Trans*., 2013, **42**, 645.

9 A. McAnaw, M. E. Lopez, D. Ellis, G. M. Rosair and A. J. Welch, *Dalton Trans*., 2014, **43**, 5095.

10 DFT calculations have been used to calculate activation energy of the intermediate (I), performed by Dr David McKay, Heriot-Watt University.

11 J. Li, C. F. Logan and M. Jones Jr., *Inorg. Chem*., 1991, **30**, 4866.

12 A. V. Safronov and M. F. Hawthorne, *Inorg. Chim. Acta*, 2011, **375**, 308.

13 S. Ren and Z. Xie, *Organometallics*, 2008, **27**, 5167.

14 J. A. Dupont and M. F. Hawthorne, *J. Am. Chem. Soc*., 1964, **86**, 1643.

15 M. F. Hawthorne and P. A. Wegner, *J. Am. Chem. Soc*., 1968, **90**, 896.

16 E. W. Abel, J. K. Bhargava and K. G. Orrell, *Prog. Inorg. Chem*., 1984, **32**, 1.

17 M. Bown, J. Plešek, K. Baše, B. Štíbr, X. L. R. Fontaine, N. N. Greenwood and J. D. Kennedy, *Magn. Reson. Chem.*, 1989, **27**, 947.

Chapter 4

Supraicosahedral bis(cobaltacarboranes)

4.1 Introduction

MC_2B_{10} 13-vertex metallacarboranes are generally prepared by the reduction of *closo*-C_2B_{10} carboranes followed by metallation of the resulting reduced species. Reduction of 1,2-*closo*-$C_2B_{10}H_{12}$ affords [7,9-*nido*-$C_2B_{10}H_{12}]^{2-}$ which has the cage C atoms separated by a B vertex. Metallation of the 7,9-*nido* dianion with a suitable metal fragment, for example $\{CpCo\}^{+/2+}$ or $\{(arene)Ru\}^{2+}$, generates 4,1,6-MC_2B_{10} compounds (Figure 4.1.1).[1,2]

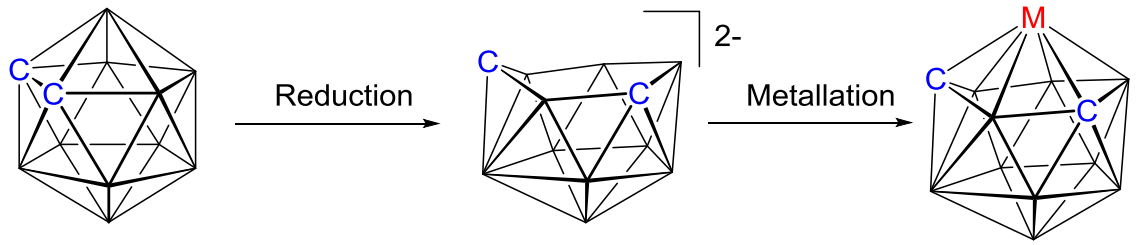

Figure 4.1.1 Synthesis of 4,1,6-MC_2B_{10}.

4,1,6-MC_2B_{10} compounds undergo thermal isomerisation to the progressively more thermodynamically stable 4,1,8- and 4,1,12- isomers (Figure 4.1.2). Isomerisation occurs much more readily in cobaltacarboranes [3,4] than in ruthenacarboranes.[2,5]

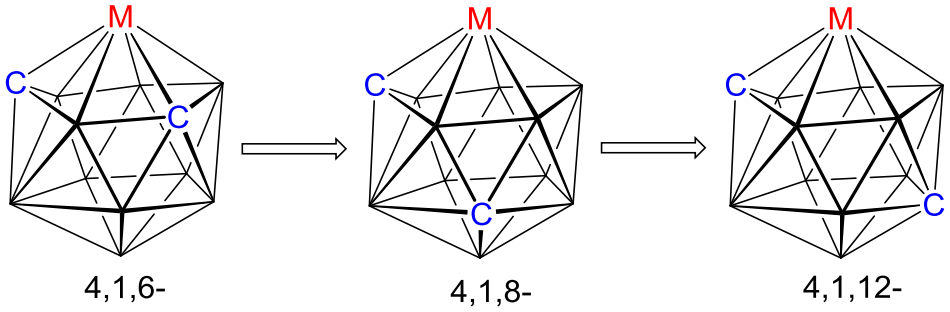

Figure 4.1.2 Thermal isomerisation 4,1,6- → 4,1,8- → 4,1,12-MC_2B_{10}.

Metallacarborane chemistry *via* reduction and metallation of bis(carborane) has been developed recently in our group.[6] In 2010 Welch *et al*. reported the expansion of both cages of 1,1′-bis(*o*-carborane) using $\{CoCp\}^{+}$ (subsequently oxidised to $\{CpCo\}^{2+}$) fragments to give 13-vertex metallacarborane/13-vertex metallacarborane species, the first supraicosahedral bis(cobaltacaborane).[7] Reduction of 1,1′-bis(*o*-carborane) with lithium naphthalenide (LN) followed by treatment with {CpCo} generated *in situ* afforded rac and meso diastereoisomers of [1-(1′-4′-Cp-4′,1′,6′-*closo*-$CoC_2B_{10}H_{11}$)-4-Cp-4,1,6-*closo*-$CoC_2B_{10}H_{11}$)] (Figure 4.1.3**)**. By following the thermal isomerisation analogy of 4,1,6-MC_2B_{10} to 4,1,8 to 4,1,12 isomers, this Chapter describes isomerisation of a rac and meso mixture of [1-(1′-4′-Cp-4′,1′,6′-*closo*-$CoC_2B_{10}H_{11}$)-4-Cp-4,1,6-*closo*-$CoC_2B_{10}H_{11}$)] at high temperature. Finally, reduction and metallation of the isomerised species has also been attempted using appropriate metal fragments.

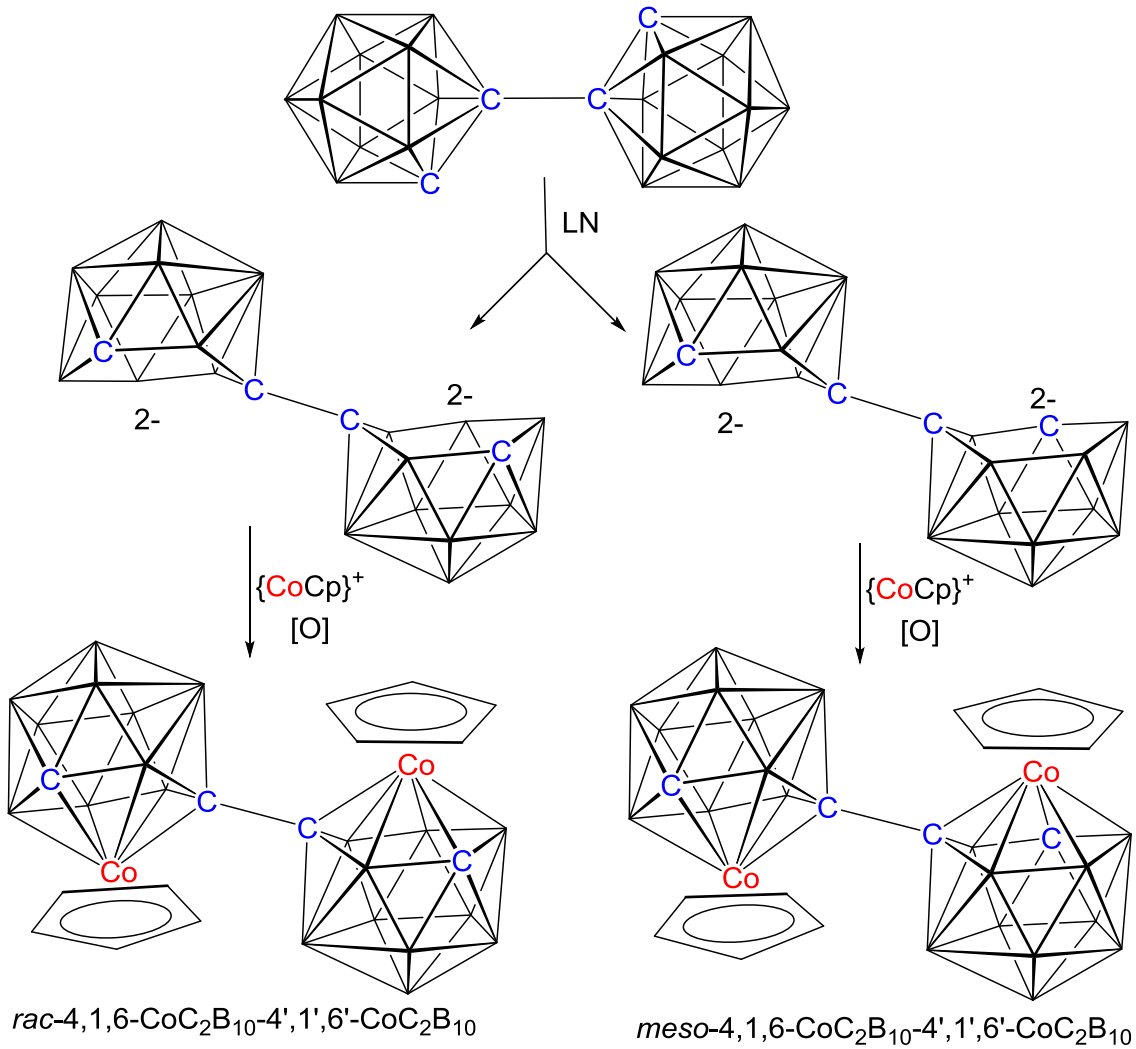

Figure 4.1.3 Synthesis of rac and meso diastereoisomers of 4,1,6-CoC_2B_{10}-4′,1′,6′-CoC_2B_{10}.

4.2 Results and discussion

4.2.1 Synthesis of *rac*-[1-(1′-4′-Cp-4′,1′,12′-*closo*-$CoC_2B_{10}H_{11}$)-4-Cp-4,1,12-*closo*-$CoC_2B_{10}H_{11}$)] (28) and *meso*-[1-(1′-4′-Cp-4′,1′,12′-*closo*-$CoC_2B_{10}H_{11}$)-4-Cp-4,1,12-*closo*-$CoC_2B_{10}H_{11}$)] (29)

Heating a rac and meso mixture of [1-(1′-4′-Cp-4′,1′,6′-*closo*-$CoC_2B_{10}H_{11}$)-4-Cp-4,1,6-*closo*-$CoC_2B_{10}H_{11}$)] at 180 °C for 4 hrs affords a rac and meso mixture of the isomerised species [1-(1′-4′-Cp-4′,1′,12′-*closo*-$CoC_2B_{10}H_{11}$)-4-Cp-4,1,12-*closo*-$CoC_2B_{10}H_{11}$)], from which the pure compounds **28** (rac form) and **29** (meso form) were isolated by TLC.

For compound **28**, elemental analysis was in excellent agreement with the calculated values for $C_{14}H_{32}B_{20}Co_2$. The mass spectrum showed an envelope centred peak at *m/z* 534.0 (M^+) (MW = 534.5 g mol^{-1}), corresponding to the molecular ion. The mass spectrum and elemental analysis strongly suggest that this species was an isomeric analogue of [1-(1′-4′-Cp-4′,1′,6′-*closo*-$CoC_2B_{10}H_{11}$)-4-Cp-4,1,6-*closo*-$CoC_2B_{10}H_{11}$)]. For further confirmation other spectroscopic techniques were necessary.

The $^{11}B\{^1H\}$ NMR spectrum of compound **28** consists of eight resonances with relative integrals 4:4:2:2:2:2:2:2 from high frequency to low frequency (integral-4 resonances representing 2+2 coincidence) and the spectrum is different from that of its precursor.

The ^1H NMR spectrum of compound **28** reveals a singlet assigned to cyclopentadienyl protons with integral-10 and a broad CH_{cage} with integral-2. This suggests that Cp protons in both cages are magnetically equivalent and similarly CH_{cage} protons as well. However, it is impossible to conclude the overall isomeric nature of the bis(cobaltacarborane) and consequently a structural analysis was performed.

X-ray quality crystals of compound **28** were grown by vapour diffusion of 40-60 petroleum ether into a THF solution of **28**. The cobaltacarborane has a 4,1,12-CoC_2B_{10}-4′,1′,12′-CoC_2B_{10} architecture arising from thermal isomerisation of a 4,1,6-CoC_2B_{10}-4′,1′,6′-CoC_2B_{10} isomer. Thus compound **28** is *rac*-[1-(1′-4′-Cp-4′,1′,12′-*closo*-$CoC_2B_{10}H_{11}$)-4-Cp-4,1,12-*closo*-$CoC_2B_{10}H_{11}$)] (Figure 4.2.1.1).

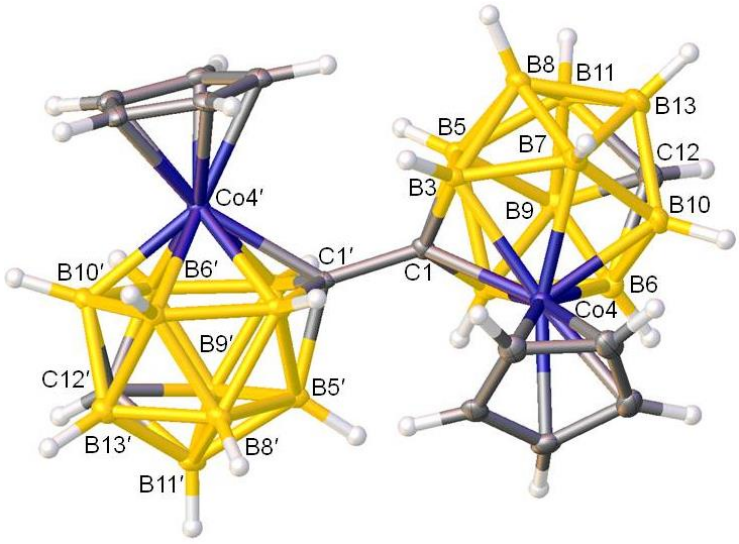

Figure 4.2.1.1 Molecular structure of *rac*-[1-(1′-4′-Cp-4′,1′,12′-*closo*-$CoC_2B_{10}H_{11}$)-4-Cp-4,1,12-*closo*-$CoC_2B_{10}H_{11}$)] (**28**).

Moving to compound **29**, elemental analysis was in good agreement with the calculated values for $C_{14}H_{32}B_{20}Co_2$. The mass spectrum of **29** reveals a molecular ion envelope centred peak at *m/z* 534.0 (M^+) (MW = 534.5 g mol^{-1}). These analyses show compound **29** is an isomeric analogue of **28**. For the determination of the exact isomeric nature, other spectroscopic analysis was carried out.

The $^{11}B\{^1H\}$ NMR spectrum of compound **29** consists of eight resonances with relative integrals 5:3:2:2:2:2:2:2 from high frequency to low frequency and the spectrum is different to that of compound **28**.

The ^1H NMR spectrum of compound **29** reveals two singlets assigned to cyclopentadienyl protons with each of integral-5. This suggests that the Cp protons in both cages are magnetically inequivalent. There are also two broad CH_{cage} singlets of integral-1 which indicates the CH_{cage} protons are also magnetically inequivalent. However, it was inconclusive with respect to molecular geometry and consequently a structural analysis was performed.

X-ray quality crystals of compound **29** were grown by vapour diffusion of a 40-60 petroleum ether into a THF solution of **29**. The single crystal analysis identifies the compound **29** as *meso*-[1-(1′-4′-Cp-4′,1′,12′-*closo*-$CoC_2B_{10}H_{11}$)-4-Cp-4,1,12-*closo*-$CoC_2B_{10}H_{11}$)] (Figure 4.2.1.2).

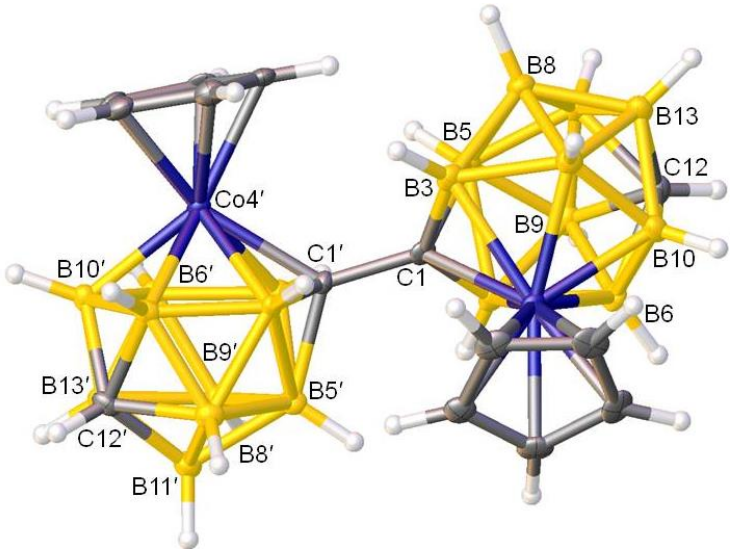

Figure 4.2.1.2 Molecular structure of *meso*-[1-(1′-4′-Cp-4′,1′,12′-*closo*-$CoC_2B_{10}H_{11}$)-4-Cp-4,1,12-*closo*-$CoC_2B_{10}H_{11}$)] (**29**).

Both compounds **28** and **29** comprise two 13-vertex CoC_2B_{10} cages which are in docosahedron geometry similar to the geometry of the archetypal 13-vertex metallacarborane [4-Cp-4,1,6-*closo*-$CoC_2B_{10}H_{12}$].[8] In both cases **28** and **29**, for the CoC_2B_{10} cage there is one degree-4 vertex occupied by C atoms at position 1 and two degree-6 vertices at positions 4 and 5, where the former (vertex 4) occupied by the Co atoms. Remaining vertices are degree-5 in the cage. Theoretically, the number of possible isomers are seven for a 4,1,*x*-MC_2B_{10} docosahedron where *x* = 2, 5, 6, 8, 10, 11 or 12. There are known example of all isomers except for the 4,1,5-isomer. As compounds **28** and **29** were prepared by thermal isomerisation of [1-(1′-4′-Cp-4′,1′,6′-*closo*-$CoC_2B_{10}H_{11}$)-4-Cp-4,1,6-*closo*-$CoC_2B_{10}H_{11}$)], it was anticipated that in each cage the second C atom would be at either positions 8 or 12 (or a combination thereof) from the literature evidence.[3] However we have confirmed the identification of the second C atom undoubtedly by using both the VCD method [9] and BHD analysis [10] and therefore the isomers were correctly identified. The analysis was performed by following the procedure discussed in Chapter 1. VCDs were analysed and compared for topologically-equivalent vertices with in each cage of the Prostructure. It reveals that the second C atom is at vertex 12 (or 12′) in all cases (VCD from 12 is shorter than VCD from 13 by >0.15 Å in all cases) (non-italicised entries in Table 4.2.1.1 for **28** and Table 4.2.1.2 for **29**). This was in agreement with the BHD analysis which shows short B-H distances at vertex 12 in all cages (Table 4.2.1.3). Notably in both **28** and **29**, a small difference exists in VCDs for topologically equivalent vertices B10 and B11 ($VCD_{10} - VCD_{11}$ = 0.05-0.06

Å). One would suggest the positions of C atoms at vertices 11 but it can be reliably eliminated by the BHDs and hence it implies the usefulness of using both methods as appropriate for the location of cage C atoms. However the short difference in VCDs from B10 and B11 raises further consideration for the calculation of polyhedral centroid. The polyhedral centroid for a docosahedral MC_2B_{10} species is generally calculated by excluding the metal at position 4 and the antipodal atom at position 11.[9] One would think this is just a speculation the way the polyhedral centroid is calculated. To confirm the propose method, the centroids in **28** and **29** have been redefined excluding not only the atoms vertices 4 and 11 but also those at 5 and 10. This is restoring the original symmetry C_{2v} of the remaining vertices (1, 2, 3, 6, 7, 8, 9, 12 and 13) for the docosahedron geometry. The results show that the change in the difference in VCDs from B10 and B11 is minor, only slight increasing (italicised entries in Table 4.2.1.1 for **28** and Table 4.2.1.2 for **29**). Therefore it is crucial to include appropriate vertices for centroid determination. From the CSD [11] search, twelve example were found for 4,1,12-MC_2B_{10} species and for seven of them the metallacarborane cage is ordered. VCD analysis of these ordered structures are shown in Table 4.2.1.4. In all cases we also observe that VCD_{11} is shorter than VCD_{10} (Δ *ca*. 0.06-0.08 Å). However for one case (YALKUS, [4-dppe-4,1,12-*closo*-$NiC_2B_{10}H_{12}$],[12]) the difference between VCDs from 10 and 11 is actually greater than that between VCDs from 12 and 13 (0.03 Å), which is because of some disorder of the degree-5 C atom between vertices 12 and 13.

Selected molecular parameters are summarised in Table 4.2.1.5. The overall structures of the rac (**28**) and meso (**29**) forms of [1-(1′-4′-Cp-4′,1′,12′-*closo*-$CoC_2B_{10}H_{11}$)-4-Cp-4,1,12-*closo*-$CoC_2B_{10}H_{11}$)] are similar both to each other and to their parent derivative as well *i.e.* [1-(1′-4′-Cp-4′,1′,6′-*closo*-$CoC_2B_{10}H_{11}$)-4-Cp-4,1,6-*closo*-$CoC_2B_{10}H_{11}$)].[7] Thus the gross conformation, defined by the torsion angle Co4–C1–C1′–Co4′, is 137.13(13)º in **28** and 134.9(3)º in **29** (144.8 and 137.9º in the respective precursors). Furthermore intramolecular congestion is evidenced by both Cp ligands tilting away from the other metallacarborane cluster, calculated by the dihedral angle θ between the Cp least-square plane and that through cage vertices 5,8,13,12 and 9. The same is also applicable for the prime cage. In **28** the θ values are 12.04(7) for non-primed and 11.72(9)º for primed cages, whereas in **29** the equivalent θ values are 12.1(2) and 11.4(2)º (11.0 – 11.4º in the precursor molecules).

Table **4.2.1.1** Vertex-to-centroid distances (Å) in Prostructures of *rac*-[1-(1′-4′-Cp-4′,1′,12′-*closo*-$CoC_2B_{10}H_{11}$)-4-Cp-4,1,12-*closo*-$CoC_2B_{10}H_{11}$)] (**28**).

Vertex	Co4 cage		Co4′cage	
1	2.019(2)	*1.984(2)*	2.018(2)	*1.983(2)*
2	1.884(3)	*1.863(3)*	1.885(2)	*1.864(2)*
3	1.878(3)	*1.852(3)*	1.876(3)	*1.850(3)*
4	2.0102(8)	*1.9965(9)*	2.0057(9)	*1.9922(10)*
5	1.596(3)	*1.575(3)*	1.595(3)	*1.574(3)*
6	1.778(3)	*1.789(3)*	1.772(3)	*1.784(3)*
7	1.776(3)	*1.781(3)*	1.770(3)	*1.775(3)*
8	1.734(3)	*1.735(3)*	1.740(3)	*1.740(3)*
9	1.756(3)	*1.763(3)*	1.753(3)	*1.759(3)*
10	1.801(3)	*1.826(3)*	1.798(3)	*1.822(3)*
11	1.742(3)	*1.759(3)*	1.734(3)	*1.750(3)*
12	1.724(3)	*1.756(3)*	1.723(3)	*1.755(3)*
13	1.878(3)	*1.908(3)*	1.883(3)	*1.912(3)*

Table 4.2.1.2 Vertex-to-centroid distances (Å) in Prostructures of of *meso*-[1-(1′-4′-Cp-4′,1′,12′-*closo*-$CoC_2B_{10}H_{11}$)-4-Cp-4,1,12-*closo*-$CoC_2B_{10}H_{11}$)] (**29**).

Vertex	Co4 cage		Co4′ cage	
1	2.041(5)	*2.007(5)*	2.044(5)	*2.009(5)*
2	1.895(6)	*1.876(6)*	1.884(6)	*1.861(6)*
3	1.905(6)	*1.877(6)*	1.919(6)	*1.894(6)*
4	2.0348(19)	*2.022(2)*	2.0313(18)	*2.017(2)*
5	1.608(6)	*1.587(6)*	1.606(3)	*1.583(6)*
6	1.793(6)	*1.807(6)*	1.783(6)	*1.794(6)*
7	1.796(6)	*1.799(6)*	1.803(6)	*1.808(6)*
8	1.762(6)	*1.759(6)*	1.765(6)	*1.767(6)*
9	1.782(6)	*1.790(6)*	1.771(6)	*1.777(6)*
10	1.815(6)	*1.840(6)*	1.806(6)	*1.830(6)*
11	1.751(6)	*1.767(7)*	1.757(6)	*1.775(6)*
12	1.742(7)	*1.775(7)*	1.740(7)	*1.770(7)*
13	1.895(7)	*1.923(7)*	1.911(6)	*1.944(6)*

Table 4.2.1.3 Boron-hydrogen distances (Å) in Prostructures *rac*- and *meso*-[1-(1′-4′-Cp-4′,1′,12′-*closo*-$CoC_2B_{10}H_{11}$)-4-Cp-4,1,12-*closo*-$CoC_2B_{10}H_{11}$)].

Vertex	Compound **28**		Compound **29**	
	Co4 cage	Co4′ cage	Co4 cage	Co4′ cage
2	1.13(3)	1.12(3)	1.11(5)	1.11(6)
3	1.15(4)	1.12(3)	1.16(5)	1.15(5)
5	1.07(3)	1.05(3)	1.15(5)	1.07(6)
6	1.07(3)	1.01(3)	1.14(5)	1.05(6)
7	1.12(3)	1.17(3)	1.12(6)	1.13(5)
8	1.12(3)	1.15(3)	1.19(6)	1.19(6)
9	1.20(3)	1.06(3)	1.11(6)	1.09(5)
10	1.06(3)	1.09(3)	1.05(6)	1.06(5)
11	1.10(3)	1.02(3)	1.02(6)	1.08(6)
12	0.35(3)	0.38(3)	0.33(7)	0.32(7)
13	1.07(3)	1.14(3)	1.10(6)	1.14(5)

Table 4.2.1.4 Vertex-to-centroid distances (Å) in literature 1,12-R_2-4-L-4,1,12-$MC_2B_{10}H_{10}$ structures.

CSD refcode	YALKUS	EDIMAG	EDIMIO	PUYHOH	GESZIP	TEGXOU	TEGXUA
R, *L*, *M*	H, dppe, Ni	Ph, Cp, Co	Ph, cym, Ru	Me, indy, Co	C_7F_7, Cp, Co	Me, Cp, Co	Me, cym, Ru
Reference	12	7	7	13	14	15	15
1	1.989(3)	2.013(3)	2.023(6)	2.004(2)	1.999(4)	1.968(4)	2.007(2)
2	1.876(3)	1.878(3)	1.881(9)	1.889(2)	1.899(4)	1.900(5)	1.896(3)
3	1.878(3)	1.878(3)	1.871(8)	1.868(2)	1.886(5)	1.848(7)	1.870(3)
4	2.0417(9)	2.0096(11)	2.177(2)	2.0056(8)	2.0015(14)	2.0012(16)	2.1661(7)
5	1.609(3)	1.597(3)	1.598(7)	1.598(3)	1.611(4)	1.598(6)	1.597(2)
6	1.767(2)	1.761(3)	1.767(7)	1.763(2)	1.780(4)	1.786(6)	1.777(3)
7	1.756(3)	1.760(3)	1.764(7)	1.772(2)	1.765(5)	1.769(4)	1.777(3)
8	1.744(3)	1.743(3)	1.739(8)	1.737(2)	1.744(4)	1.733(7)	1.743(3)
9	1.731(3)	1.749(3)	1.747(7)	1.754(3)	1.747(4)	1.739(5)	1.741(3)
10	1.808(3)	1.793(3)	1.797(7)	1.787(3)	1.785(4)	1.789(6)	1.798(2)
11	1.728(3)	1.723(4)	1.722(8)	1.726(3)	1.710(5)	1.718(4)	1.729(3)
12	1.785(3)	1.763(3)	1.762(6)	1.758(2)	1.783(4)	1.732(5)	1.756(2)
13	1.814(3)	1.870(4)	1.875(9)	1.873(3)	1.878(5)	1.886(6)	1.862(3)

Table 4.2.1.5 Selected geometric parameters (Å, º) *rac*- and *meso*-[1-(1′-4′-Cp-4′,1′,12′-*closo*-$CoC_2B_{10}H_{11}$)-4-Cp-4,1,12-*closo*-$CoC_2B_{10}H_{11}$)].

rac form **28**		meso form **29**	
Co4—C1	2.1099(17)	Co4—C1	2.129(4)
Co4—B2	2.210(2)	Co4—B2	2.227(5)
Co4—B6	2.139(2)	Co4—B6	2.168(5)
Co4—B10	2.128(2)	Co4—B10	2.144(6)
Co4—B7	2.176(2)	Co4—B7	2.208(5)
Co4—B3	2.202(2)	Co4—B3	2.233(5)
Co4′—C1′	2.1091(18)	Co4′—C1′	2.122(4)
Co4′—B2′	2.207(2)	Co4′—B2′	2.250(5)
Co4′—B6′	2.132(2)	Co4′—B6′	2.198(5)
Co4′—B10′	2.123(2)	Co4′—B10′	2.140(5)
Co4′—B7′	2.169(2)	Co4′—B7′	2.170(5)
Co4′—B3′	2.211(2)	Co4′—B3′	2.210(5)
C1—C1′	1.521(2)	C1—C1′	1.533(6)
Co4—C_{Cp}	2.043(2) – 2.100(2)	Co4—C_{Cp}	2.075(5) – 2.118(5)
Co4′—C_{Cp}	2.038(2) – 2.094(2)	Co4′—C_{Cp}	2.067(5) – 2.121(5)
Co4—C1—C1′—Co4′	137.13(13)	Co4—C1—C1′—Co4′	134.9(3)

4.2.2 Discussion: thermal isomerisation of 4,1,6-CoC_2B_{10}-4′,1′,6′-CoC_2B_{10} and attempted polyhedral expansion of 4,1,12-CoC_2B_{10}-4′,1′,12′-CoC_2B_{10} isomer

Four electron reduction of 1,1′-bis(*o*-carborane) was carried out with lithium naphthalenide (LN). Treatment of [7-(7′-7′,9′-*nido*-$C_2B_{10}H_{11}$)-7,9-*nido*-$C_2B_{10}H_{11}$]$^{4-}$ with the {CoCp}$^{+}$ fragment, followed by aerial oxidation, afforded the red bis(cobaltacarborane) [7] [1-(1′-4′-Cp-4′,1′,6′-*closo*-$CoC_2B_{10}H_{11}$)-4-Cp-4,1,6-*closo*-$CoC_2B_{10}H_{11}$)] as a racemic (*RR*/*SS*, *rac*) and meso (*RS*/*SR*, *meso*) mixture in a total yield of 48%. Initially we attempted to purify each isomer in good yields using Upside-Down Column Chromatography (USDCC). Anticipating better separation of the diastereoisomers, the USDCC was designed on the same principle as preparative TLC and a diagram is shown in Figure 4.2.2.1. Unfortunately USDCC was not appropriate for separation of rac and meso isomers due to their limited solubility. Each purification required 24-26 hrs to complete and the isolated diastereoisomers were insufficient in quantity for further study.

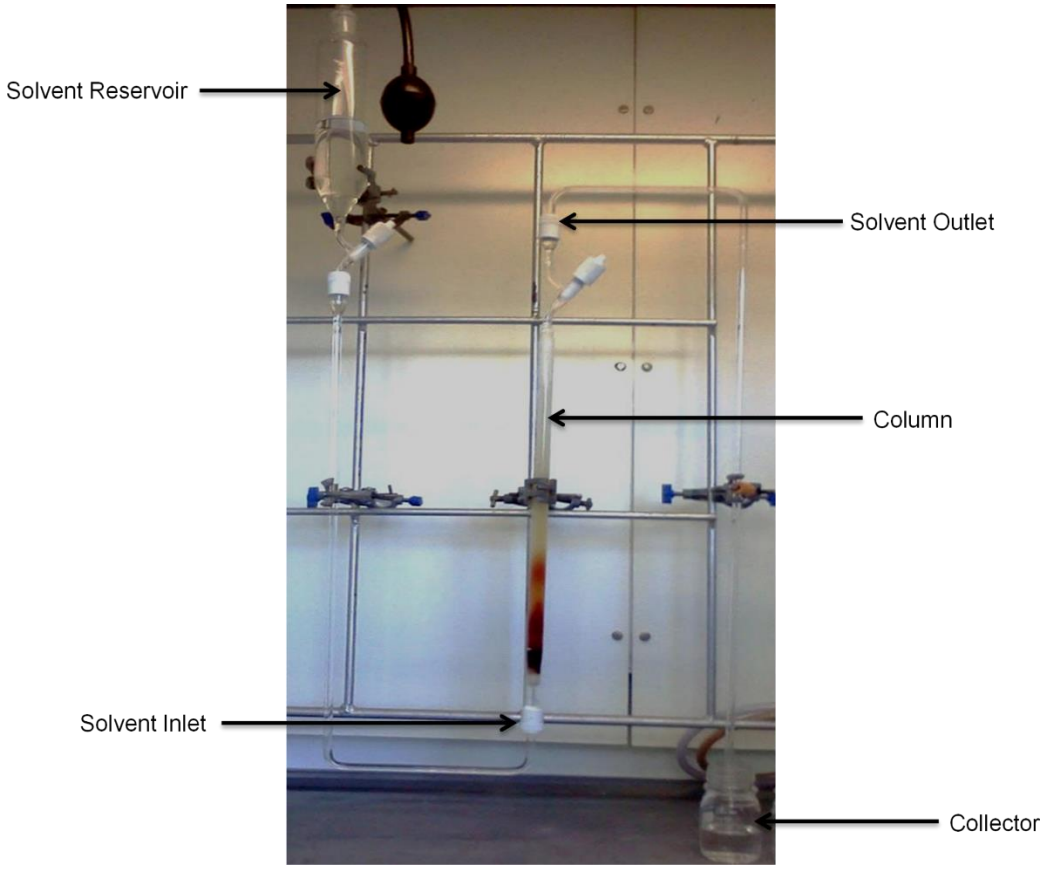

Figure 4.2.2.1 Pictorial presentations of USDCC.

Having been unsuccessful in separatating of each isomer, thermal isomerisations were performed by taking mixture of diastereoisomers. Initially we attempted thermolysis of a *rac* and *meso* mixture of [1-(1′-4′-Cp-4′,1′,6′-*closo*-$CoC_2B_{10}H_{11}$)-4-Cp-4,1,6-*closo*-$CoC_2B_{10}H_{11}$)] in toluene reflux by analogy with Hawthorne's established protocol. [3] After preparative TLC compounds **28** and **29** were afforded in trace amounts. Heating a *rac* and *meso* mixture of [1-(1′-4′-Cp-4′,1′,6′-*closo*-$CoC_2B_{10}H_{11}$)-4-Cp-4,1,6-*closo*-$CoC_2B_{10}H_{11}$)] to reflux in xylenes at 180 °C for 4 hrs then afforded a *rac* and *meso* mixture of the isomerised species [1-(1′-4′-Cp-4′,1′,12′-*closo*-$CoC_2B_{10}H_{11}$)-4-Cp-4,1,12-*closo*-$CoC_2B_{10}H_{11}$)], from which the pure compounds (**28**) (rac form) and (**29**) (meso form) were isolated by TLC in higher yields. Spectroscopic results have been described in section 4.2.1. Having fully characterised these species, we have also attempted polyhedral expansion reactions.

In 1974 Hawthorne reported the first 14-vertex metallacarborane [1,14-Cp_2-1,14,2,10-*closo*-$Co_2C_2B_{10}H_{12}$] prepared from the polyhedral expansion of [4-Cp-4,1,12-*closo*-$CoC_2B_{10}H_{12}$] (Figure 4.2.2.2).[16] The bicapped hexagonal antiprismatic structure of the 14-vertex 1,14,2,10- cluster was recently confirmed crystallographically by Welch.[17] Having good amounts of pure **28** with which to work, the first 14-vertex metallacarborane/14-vertex metallacarborane was targeted and reduction/metallation was performed by following the general procedure of polyhedral expansion using the {CoCp} fragment.

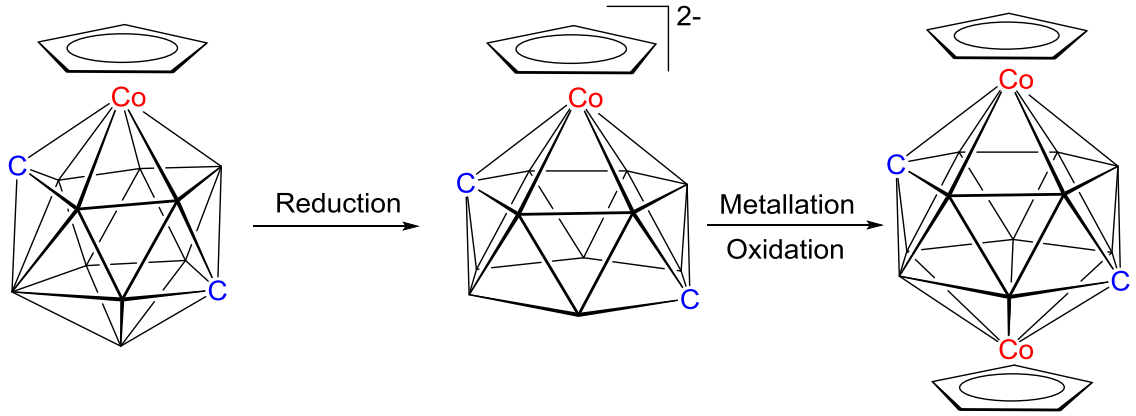

Figure 4.2.2.2 Synthesis of [1,14-Cp_2-1,14,2,10-*closo*-$Co_2C_2B_{10}H_{12}$].

In the first attempt compound **28** (rac form) was reduced in the presence of excess lithium naphthalenide and was then treated with the {CpCo} fragment generated *in situ* from

$CoCl_2$ and NaCp, followed by aerial oxidation. This yielded only a single purple product which was identified as the single cage 14-vertex bimetallic cobaltacarborane [1,14-Cp_2-1,14,2,10-*closo*-$Co_2C_2B_{10}H_{12}$] [14] (Figure 4.2.2.3), confirmed by ^1H and $^{11}B\{^1H\}$ NMR spectroscopies. Similarly, reduction of **29** (meso form) in the presence of excess LN and metallation using the {CpCo} fragment afforded the same 14-vertex bimetallic species *i.e.* [1,14-Cp_2-1,14,2,10-*closo*-$Co_2C_2B_{10}H_{12}$]. The cleaving of the C–C bond was assumed to be due to the presence of excess electrons. Subsequently we attempted reduction/metallation of **28** or **29** using stoichiometric amounts of lithium naphthalenide.

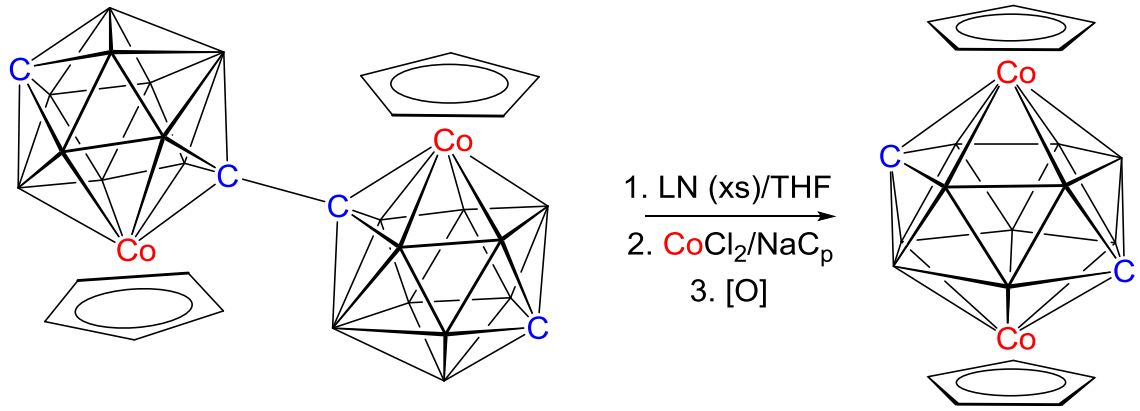

Figure 4.2.2.3 Excess reduction and metallation of compound **28**.

Compound **28** was reduced using 2-equivalents of LN, however metallation with $\{CpCo\}^+$, generated *in situ* from $CoCl_2$ and NaCp followed by oxidations, returned only the starting material. Reduction of **28** was carried out with 4-equivalents of lithium naphthalenide but after metallation with $\{CoCp\}^+$, then oxidation, only starting material and other minor products were observed. Unfortunately no desired product was isolated using stoichiometric reduction/metallation (Figure 4.2.2.4).

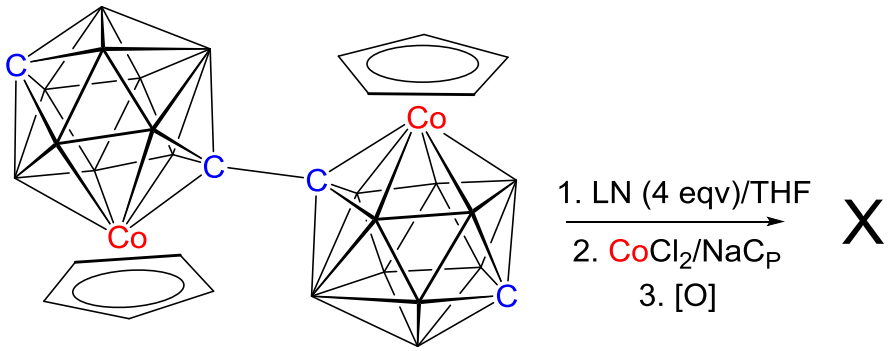

Figure 4.2.2.4 Attempted stoichiometric reduction and metallation of compound **28**.

4.3 Summary

Both *rac*-[1-(1′-4′-Cp-4′,1′,12′-*closo*-$CoC_2B_{10}H_{11}$)-4-Cp-4,1,12-*closo*-$CoC_2B_{10}H_{11}$] (**28**) and *meso*-[1-(1′-4′-Cp-4′,1′,12′-*closo*-$CoC_2B_{10}H_{11}$)-4-Cp-4,1,12-*closo*-$CoC_2B_{10}H_{11}$] (**29**) were prepared by thermolysis of a *rac*/*meso* mixture of the precursor species [1-(1′-4′-Cp-4′,1′,6′-*closo*-$CoC_2B_{10}H_{11}$)-4-Cp-4,1,6-*closo*-$CoC_2B_{10}H_{11}$] and were separated, spectroscopically characterised and studied crystallographically. Cage C-atom identification was accomplished by both the VCD and BHD methods, and, in both cases, the structure established crystallographically is fully consistent with the spectroscopic data. Both the *rac*-(**28**) and *meso*-(**29**) forms share the same overall conformation (Co–C–C′–Co′ *ca* 136°) and show clear evidence of intra-molecular steric crowding resulting in tilted cyclopentadienyl ligands. Further polyhedral expansion of these species has not been successful. Excess reduction and metallation of compounds **28** and **29** gives the single cage 14-vertex bimetallic species by cleaving C–C linkage of bis(cobaltacaborane). In contrast stoichiometric reduction and metallation of compound **28** did not result in any desired 14-vertex metallacarborane/14-vertex metallacarborane derivative.

4.4 References

1 G. B. Dunks, M. M. McKown and M. F. Hawthorne, *J. Am. Chem. Soc*., 1971, **93**, 2541.

2 A. Burke, D. Ellis, D. Ferrer, D. L. Ormsby, G. M. Rosair and A. J. Welch, *Dalton Trans*., 2005, 1716.

3 D. F. Dustin, G. B. Dunks and M. F. Hawthorne, *J. Am. Chem. Soc*., 1973, **95**, 1109.

4 A. Burke, R. McIntosh, D. Ellis, G. M. Rosair and A. J. Welch, *Collect. Czech. Chem. Commun*., 2002, **67**, 991.

5 S. Zlatogorsky, D. Ellis, G. M. Rosair and A. J. Welch, *Chem. Commun*., 2007, 2178.

6 (a) D. Ellis, D. McKay, S. A. Macgregor, G. M. Rosair and A. J. Welch, *Angew. Chem. Int. Ed*., 2010, **49**, 4943; (b) W. Y. Man, S. Zlatogorsky, H. Tricas, D. Ellis, G. M. Rosair and A. J. Welch, *Angew. Chem. Int. Ed*., 2014, **53**, 12222; (c) W. Y. Man, D. Ellis, G. M. Rosair and A. J. Welch, *Angew. Chem. Int. Ed*., 2016, **55**, 4596.

7 D. Ellis, G. M. Rosair and A. J. Welch, *Chem. Commun.*, 2010, **46**, 7394.

8 M. R. Churchill and B. G. Deboer, *J. Chem. Soc. Chem. Commun*., 1972, 1326.

9 A. McAnaw, G. Scott, L. Elrick, G. M. Rosair and A. J. Welch, *Dalton Trans*., 2013, **42**, 645.

10 A. McAnaw, M. E. Lopez, D. Ellis, G. M. Rosair and A. J. Welch, *Dalton Trans*., 2014, **43**, 5095.

11 C. R. Groom and F. H. Allen, *Angew. Chem. Int. Ed*., 2014, **53**, 662.

12 D. Ellis, M. E. Lopez, R. McIntosh, G. M. Rosair, A. J. Welch and R. Quenardelle, *Chem. Commun*., 2005, 1348.

13 G. Scott, A. McAnaw, D. McKay, A. S. F. Boyd, D. Ellis, G. M. Rosair, S. A. Macgregor, A. J. Welch, F. Laschi, F. Rossi and P. Zanello, *Dalton Trans*., 2010, **39**, 5286.

14 J. S. Ward, H. Tricas, G. Scott, D. Ellis, G. M. Rosair and A. J. Welch, *Organometallics*, 2012, **31**, 2523.

15 A. McAnaw, M. E. Lopez, G. Scott, D. Ellis, D. McKay, G. M. Rosair and A. J. Welch, *Dalton Trans.*, 2012, **41**, 10957.

16 W. J. Evans and M. F. Hawthorne, *J. Chem. Soc., Chem. Commun*., 1974, 38.

17 A. McAnaw, M. E. Lopez, D. Ellis, G. M. Rosair and A. J. Welch, *Dalton Trans*., 2013, **42**, 671.

Chapter 5

Experimental Section

5.1 General Experimental

Synthesis

All experiments were carried out under dry, oxygen-free N_2, using standard Schlenk techniques, with some subsequent manipulations in the open laboratory. All solvents were freshly distilled under N_2 from the appropriate drying agents CaH_2 (CH_2Cl_2, CH_3CN), Na/benzophenone (THF, diethylether) and Na wire (40-60 petroleum ether) or were stored over 4 Å molecular sieves immediately before use whilst toluene was dried in an MBRAUN SPS-800. All solvents were degassed (3×freeze-pump-thaw cycles) before use. Deuterated solvents were stored over 4 Å molecular sieves. Preparative TLC employed 20×20 cm Kieselgel F_{254} glass plates and column chromatography used 60 Å silica as the stationary phase. Where appropriate all crude reaction mixtures have been filtered through Celite or 60 Å silica.

Analysis

1D NMR spectra at 400.1 MHz (^{1}H, ^{1}H{^{31}P}, ^{1}H{^{11}B}), 162.0 MHz (^{31}P, ^{31}P{^{1}H}) or 128.4 MHz (^{11}B, ^{11}B{^{1}H}) and 2D NMR spectra (^{1}H-^{31}P HMBC, ^{11}B-^{11}B COSY) were recorded on AVIII-400 spectrometer from $CDCl_3$, CD_2Cl_2 or $(CD_3)_2CO$ solutions at room temperature unless otherwise stated. Electron impact mass spectrometry (EIMS) was carried out using a Finnigan (Thermo) LCQ Classic ion trap mass spectrometer at the University of Edinburgh. Elemental Analyses (CHN) were determined using an Exeter CE-440 elemental analyser.

Hazards

Standard principles of safe handling and good general laboratory practice were followed, including the wearing of protective clothing and safety glasses. All experiments were performed in a fume cupboard. Extra care and attention were employed when handling

flammable solvents, volatile compounds, moisture and air sensitive reagents, sodium, lithium, thallium acetate and liquid phosphines.

Standard Preparations

The starting materials 1,1′-bis(*o*-carborane),[1] its single decapitated derivative [HNMe$_3$][7-(1′-1′,2′-*closo*-$C_2B_{10}H_{11}$)-7,8-*nido*-$C_2B_9H_{11}$] ([HNMe$_3$]**I**),[2] its double decapitated species [HNMe$_3$]$_2$[7-(7′-7′,8′-*nido*-$C_2B_9H_{11}$)-7,8-*nido*-$C_2B_9H_{11}$] ([HNMe$_3$]$_2$[**II**]),[3] [NiCl$_2$(dmpe)],[4] *cis*-[NiCl$_2$(PMe$_3$)$_2$],[5] *cis*-[NiCl$_2$(PMe$_2$Ph)$_2$],[5] *cis*-[NiCl$_2$(PMePh$_2$)$_2$],[5] *cis*-[PdCl$_2$(PMe)$_3$],[6,7] *cis*-[PdCl$_2$(P(OMe)$_3$)$_2$],[6,8] [PdCl$_2$(tmeda)],[9] [Ni$_3$(tmeda)$_3$Cl$_5$]Cl,[10] *cis*-[NiBr$_2$(P(OEt)$_3$)$_2$],[11] and BI$_3$,[12] were prepared by literature methods or slight variations thereof. [NiCl$_2$(dppe)] and all other reagents were supplied commercially and used as received. A 2.5M solution of *n*BuLi, 1M BBr$_3$ in hexane, 2M solution of NaCp were used in the relevant syntheses.

Crystallography

Single crystals suitable for *X*-ray diffraction were grown by either solvent or vapour diffusion as appropriate for a particular compound using common solvent system such as CH_2Cl_2/40-60 petroleum ether or THF/40-60 petroleum ether either at room temperature (16 ^oC) or at 5 ^oC. Solvent evaporation was also adopted for compound **10**. The specific crystallisation approach has been described in '*X*-ray diffraction' section for each compound. Crystals were mounted in inert oil on a cryoloop and cooled to 100 K (200 K in the case of compound **6**) by an Oxford Cryosystems Cryostream. Intensity data were collected on a Bruker X8 APEXII diffractometer using graphite-monochromated Mo-K_α *X*-radiation. Indexing, data collection and absorption correction were performed using the APEXII suite of programs.[13] Using OLEX2 [14] structures were solved with the OLEX2.solve programme [15] and refined by full-matrix least-squares (SHELXL).[16] Refinement was completed with all non-hydrogen atoms assigned anisotropic displacement parameters.

Cage C atoms not involved in the intercage link were identified by a combination of (i) the examination of refined (as B) isotropic thermal parameters, (ii) the lengths of cage connectivities, (iii) the *Vertex-Centroid Distance Method* [17] and (iv) the *Boron-H Distance Method*,[18] with all four methods affording excellent mutual agreement.

5.2.1 Synthesis of [1-(1′-1′,2′-*closo*-$C_2B_{10}H_{11}$)-3-dppe-3,1,2-*closo*-$NiC_2B_9H_{10}$] (1) and [2-(1′-1′,2′-*closo*-$C_2B_{10}H_{11}$)-4-dppe-4,1,2-*closo*-$NiC_2B_9H_{10}$] (2)

Salt [$HNMe_3$]**I** (0.20 g, 0.59 mmol) was dissolved in dry THF (20 ml), *n*-BuLi (0.51 mL of 2.5M solution in hexanes, 1.29 mmol) was added dropwise at 0 °C and the solution was stirred at room temperature for 2 hrs. The pale yellow THF solution of Li_2[7-(1′-1′,2′-*closo*-$C_2B_{10}H_{11}$)-7,8-*nido*-$C_2B_9H_{10}$] was frozen at -196 °C, [$NiCl_2$(dppe)] (0.34 g, 0.64 mmol) was added and the reaction mixture stirred overnight at room temperature, during which time the solution changed to green-purple. THF was removed *in vacuo* and the crude mixture dissolved in DCM and filtered through Celite®. Preparative TLC using an eluent system of DCM and petrol (50:50) afforded two mobile bands which were collected as solids:

Green	R_f = 0.55	Yield = 89 mg, 23%	Compound **1**
Red purple	R_f = 0.66	Yield = 68 mg, 15%	Compound **2**

Compound 1:

[1-(1′-1′,2′-*closo*-$C_2B_{10}H_{11}$)-3-dppe-3,1,2-*closo*-$NiC_2B_9H_{10}$]

Elemental analysis (CHN) Required for $C_{30}H_{45}B_{19}NiP_2$: C 49.2, H 6.20%.
Required for $C_{30}H_{45}B_{19}NiP_2 \cdot CH_2Cl_2$: C 45.6, H 5.80%.
Found for **1**$\cdot CH_2Cl_2$: C 45.8, H 5.31%.

$^{11}B\{^1H\}$ NMR (CD_2Cl_2) δ 5.9 (1B), 2.6 (1B), -2.8 (1B), -5.3 to -18.3 multiple overlapping resonances with maxima at -5.3, -8.3, -10.2, -11.5, -12.9, -14.3, -15.8, -18.3 (total integral of last eight resonances 16B).

^1H NMR (CD_2Cl_2) δ 7.97-7.30 (m, 20H, C_6H_5), 3.08 (s, 1H, CH_{cage}), 2.52-2.22 (m, 4H, P{CH_2}$_2$P), 1.74 (d, $^3J_{PH}$ = 10.0 Hz, 1H, CH_{cage}).

$^1H\{^{31}P\}$ NMR (CD_2Cl_2) δ 7.97-7.30 (m, 20H, C_6H_5), 3.08 (s, 1H, CH_{cage}), 2.52-2.22 (m, 4H, P{CH_2}$_2$P), 1.75 (s, 1H, CH_{cage}).

$^{31}P\{^1H\}$ NMR (CD_2Cl_2) δ 51.8 (d, $^2J_{PP}$ = 25.5 Hz, 1P), 41.0 (d, $^2J_{PP}$ = 25.5 Hz, 1P).

Mass Spectrometry (EI) Envelope centred on *m/z* 731.5 (M^+).
[MW = 731.74 g mol^{-1}].

***X*-Ray Diffraction** First attempt solvent diffusion of 40-60 petroleum ether into a CH_2Cl_2 solution of **1** at 5 ^oC resulted poor quality crystals for *X*-ray diffraction Second attempt solvent diffusion of 40-60 petroleum ether into a THF solution of **1** at 5 ^oC resulted in suitable quality crystals for *X*-ray diffraction.

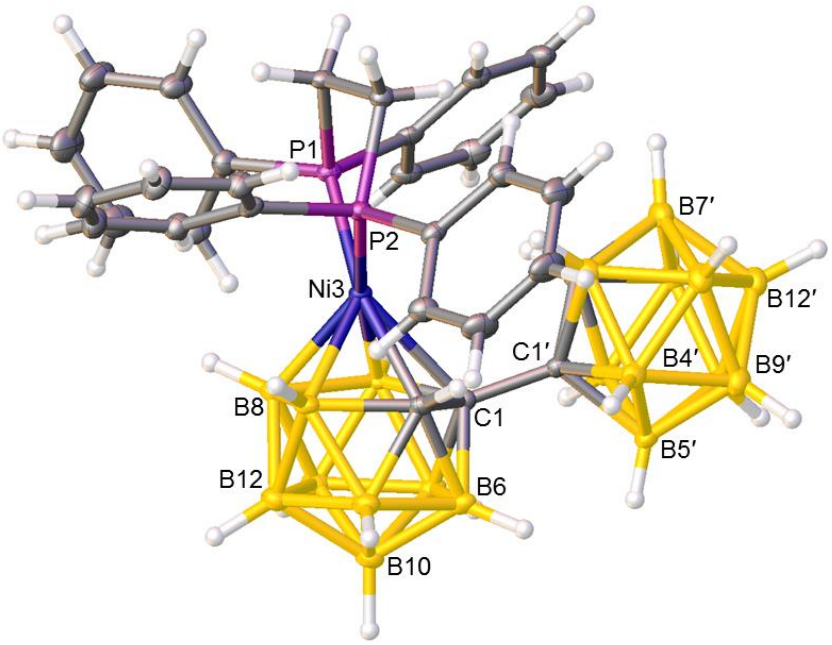

X85038

Compound 2:

[2-(1′-1′,2′-*closo*-$C_2B_{10}H_{11}$)-4-dppe-4,1,2-*closo*-$NiC_2B_9H_{10}$]

Elemental analysis (CHN) Required for $C_{30}H_{45}B_{19}NiP_2$: C 49.2, H 6.20%.
Required for $C_{30}H_{45}B_{19}NiP_2 \cdot CH_2Cl_2$: C 45.6, H 5.80%.
Found for **2**$\cdot CH_2Cl_2$: C 45.8, H 6.19%.

$^{11}B\{^1H\}$ NMR $[(CD_3)_2CO]$ δ 4.7 (1B), -3.4 to -15.8 multiple overlapping resonances with maxima at -3.4, -4.1, -6.9, -10.6, -13.2, -15.8 (total integral of last six resonances 18B).

^1H NMR $[(CD_3)_2CO]$ δ 7.92-7.78 (m, 8H, C_6H_5), 7.58-7.45 (m, 12H, C_6H_5), 3.95 (s, 1H, CH_{cage}), 2.85-2.70 (m, 4H, $P\{CH_2\}_2P$), 1.90 (s, 1H, CH_{cage}).

$^{31}P\{^1H\}$ NMR $[(CD_3)_2CO]$ δ 63.9 (s).

$^{31}P\{^1H\}$ NMR (CD_2Cl_2) δ 69.6 (d, $^2J_{PP}$ = 33.2 Hz, 1P), 60.6 (d, $^2J_{PP}$ = 33.2 Hz, 1P) at 199 K.

Mass Spectrometry (EI) Envelope centred on *m/z* 731.5 (M^+).
[MW = 731.74 g mol^{-1}].

***X*-Ray Diffraction** Solvent diffusion of 40-60 petroleum ether into a CH_2Cl_2 solution of **2** at 5 °C resulted in suitable quality crystals for *X*-ray diffraction.

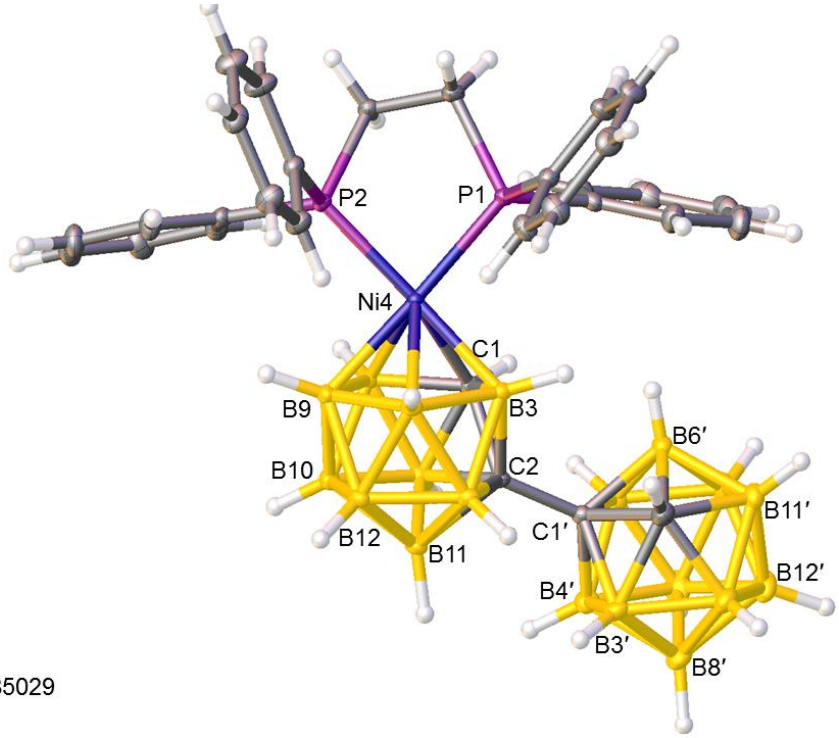

X85029

5.2.2 Thermal isomerisation of compound 1 to compound 2

Compound **1** (0.020 g, 0.027 mmol) was dissolved in THF (20 mL) and the solution heated at reflux for 2 hr. The solvent was removed and the product purified by preparative TLC using an eluent system of DCM:petrol 40-60 (50:50) to afford compound **2** characterised by ^{1}H, ^{31}P and ^{11}B NMR spectroscopies.

Red purple $R_f = 0.66$ Yield = 14 mg, 70% Compound **2**

5.2.3 Synthesis of [8-(1′-1′,2′-*closo*-$C_2B_{10}H_{11}$)-2-dmpe-2,1,8-*closo*-$NiC_2B_9H_{10}$] (3)

Salt [$HNMe_3$]**I** (0.20 g, 0.59 mmol) was deprotonated with *n*-BuLi (0.51 mL of 2.5M solution in hexanes, 1.29 mmol) as above and then frozen at -196 °C. [$NiCl_2$(dmpe)] (0.18 g, 0.64 mmol) added and the reaction mixture stirred overnight at room temperature during which time the solution changed to orange-yellow. All volatiles were removed *in vacuo* and the crude mixture dissolved in DCM and filtered through Celite®. Following spot TLC (DCM:petrol, 50:50) purification by preparative TLC using the same eluent gave a solid:

Yellow-orange R_f = 0.44 Yield = 90 mg, 35% Compound **3**

Compound 3:

[8-(1′-1′,2′-*closo*-$C_2B_{10}H_{11}$)-2-dmpe-2,1,8-*closo*-$NiC_2B_9H_{10}$]

Elemental analysis (CHN) Required for $C_{10}H_{37}B_{19}NiP_2$: C 24.8, H 7.71%.
Found for **3**: C 23.6, H 7.79%.

$^{11}B\{^1H\}$ NMR $[(CD_3)_2CO]$ δ -3.6 (2B), -4.7 (1B), -6.0 (1B), -7.6 (1B), -10.6 (8B), -13.5 (2B), -16.9 (1B), -18.7 (1B), -20.3 (2B).

^1H NMR $[(CD_3)_2CO]$ δ 4.29 (s, 1H, C*H*$_{cage}$), 2.39-2.12 (m, 4H, P{C*H*$_2$}$_2$P and s, 1H, C*H*$_{cage}$), 1.65-1.60 (m, 12H, C*H*$_3$).

$^1H\{^{31}P\}$ NMR $[(CD_3)_2CO]$ δ 4.28 (s, 1H, C*H*$_{cage}$), 2.28-2.14 (m, 4H, P{C*H*$_2$}$_2$P and s, 1H, C*H*$_{cage}$), 1.64 (s, 6H, C*H*$_3$), 1.63 (s, 6H, C*H*$_3$).

$^{31}P\{^1H\}$ NMR $[(CD_3)_2CO]$ δ 46.2 (s).

$^{31}P\{^1H\}$ NMR (CD_2Cl_2) δ 48.9 (d, $^2J_{PP}$ = 48.6 Hz, 1P), 45.8 (d, $^2J_{PP}$ = 48.6 Hz, 1P) at 203 K.

Mass Spectrometry (EI) Envelope centred on *m/z* 483.4 (M^+).
[MW = 483.45 g mol^{-1}].

***X*-Ray Diffraction** Solvent diffusion of 40-60 petroleum ether into a CH_2Cl_2 solution of **2** at 5 ^oC resulted in suitable quality crystals for *X*-ray diffraction.

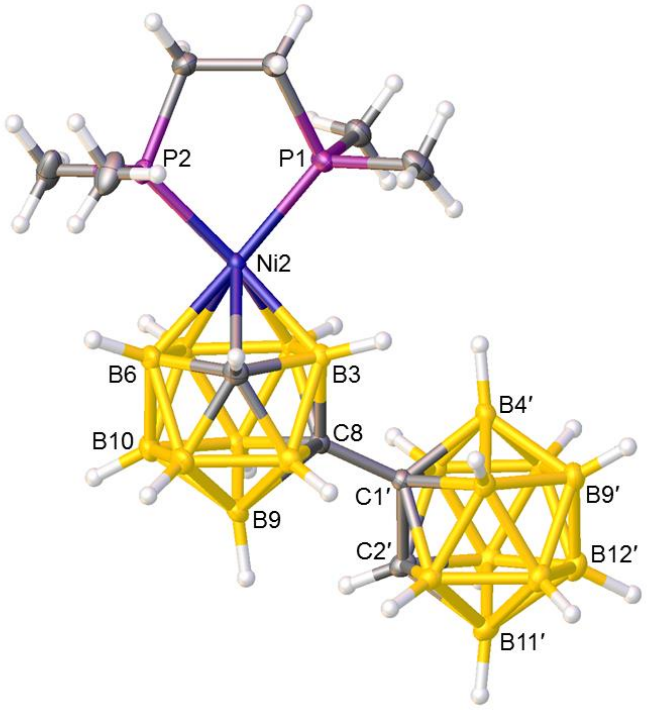

X85030

5.2.4 Synthesis of [1-(1′-1′,2′-*closo*-$C_2B_{10}H_{11}$)-3,3-$(PMe_3)_2$-3,1,2-*closo*-$NiC_2B_9H_{10}$] (4), [7-(1′-1′,2′-*closo*-$C_2B_{10}H_{11}$)-10-(PMe_3)-7,8-*nido*-$C_2B_9H_{10}$] (5) and [1-(1′-1′,2′-*closo*-$C_2B_{10}H_{11}$)-3-Cl-3-PMe_3-8-PMe_3-3,1,2-*closo*-$NiC_2B_9H_9$] (6)

Salt $[HNMe_3]$**I** (0.20 g, 0.59 mmol) was treated with *n*-BuLi (0.51 mL of 2.5M solution in hexanes, 1.29 mmol) as above and frozen at -196 °C. *Cis*-$[NiCl_2(PMe_3)_2]$ (0.18 g, 0.64 mmol) was added and the reaction mixture stirred overnight at room temperature, during which time the solution turned green. THF was removed *in vacuo* and the crude mixture was dissolved in DCM and filtered through Celite®. Preparative TLC using an eluent system of DCM and petrol, 50:50, afforded a major component green and a trace amount lavender purple bands.

Crystallisation of lavender purple band revealed both lavender purple and colourless solids which were subsequently characterised as compound **5** and compound **6** respectively.

Green $R_f = 0.55$ Yield = 89 mg, 23% Compound **4**

Lavender purple $R_f = 0.70$ Yield trace amount Compound **5** and **6**

Compound 4:

[1-(1′-1′,2′-*closo*-$C_2B_{10}H_{11}$)-3,3-$(PMe_3)_2$-3,1,2-*closo*-$NiC_2B_9H_{10}$]

Elemental analysis (CHN) Required for $C_{10}H_{39}B_{19}NiP_2$: C 24.7, H 8.10%.
Found for **4**: C 24.4, H 8.30%.

$^{11}B\{^1H\}$ NMR ($CDCl_3$) δ 0.5 (1B), -1.4 (1B), -2.6 (1B), -4.6 (1B), -7.7 to -16.4 multiple overlapping resonances with maxima at -7.7, -10.3, -12.4, -15.4, -16.4 (total integral of last five resonances 14B), -21.8 (1B).

^1H NMR ($CDCl_3$) δ 3.99 (s, 1H, C*H*$_{cage}$), 1.64 (d, $^3J_{PH}$ = 10.8 Hz, 1H, C*H*$_{cage}$), 1.55 (d, $^2J_{PH}$ = 9.6 Hz, 9H, C*H*$_3$), 1.49 (d, $^2J_{PH}$ = 8.4 Hz, 9H, C*H*$_3$).

$^1H\{^{31}P\}$ NMR ($CDCl_3$) δ 3.99 (s, 1H, C*H*$_{cage}$), 1.64 (s, 1H, C*H*$_{cage}$), 1.52 (s, 9H, C*H*$_3$), 1.47 (s, 9H, C*H*$_3$).

^{31}P NMR ($CDCl_3$) δ -9.9 (d, $^2J_{PP}$ = 43.3 Hz, 1P), -24.9 (d, $^2J_{PP}$ = 43.3 Hz, 1P).

Mass Spectrometry (EI) Envelope centred on *m/z* 485.3 (M^+).
[MW = 485.47 g mol^{-1}].

***X*-Ray Diffraction** Solvent diffusion of 40-60 petroleum ether into a CH_2Cl_2 solution of **4** at 5 °C resulted in suitable quality crystals for *X*-ray diffraction.

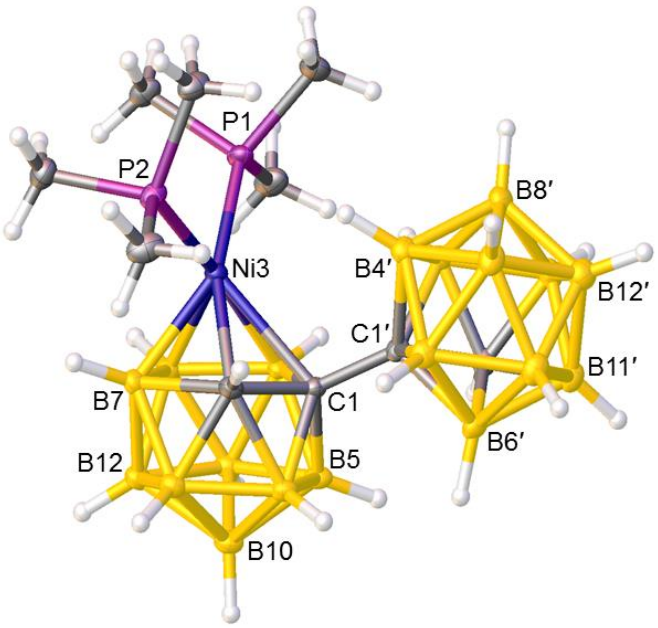

X85112

Compound 5:

[7-(1′-1′,2′-*closo*-$C_2B_{10}H_{11}$)-10-(PMe_3)-7,8-*nido*-$C_2B_9H_{10}$]

Elemental analysis (CHN) Required for $C_7H_{30}B_{19}P$: C 24.0, H 8.62%.
Found: No analysis due to trace amount.

$^{11}B\{^1H\}$ NMR [$(CD_3)_2CO$] δ 1.7 (1B), -0.2 (1B), -3.5 to -12.6 multiple overlapping resonances with maxima at -3.5, -5.0, -6.1, -8.1, -10.9, -12.6, -16.1 (total integral of last seven resonances 15B), -27.9 (1B), -29.2 (1B).

^1H NMR [$(CD_3)_2CO$] δ 4.51 (s, 1H, C*H*$_{cage}$), 2.43 (s, 1H, C*H*$_{cage}$), 1.65 (d, $^2J_{PH}$ = 12.0 Hz, 9H, C*H*$_3$).

$^1H\{^{31}P\}$ NMR [$(CD_3)_2CO$] δ δ 4.50 (s, 1H, C*H*$_{cage}$), 2.43 (s, 1H, C*H*$_{cage}$), 1.65 (s, 9H, C*H*$_3$).

$^1H\{^{11}B\}$ NMR ($CDCl_3$) δ includes -1.80 (br s, 1H, μ-H).

^{31}P NMR [$(CD_3)_2CO$] δ -6.9 (q, $^1J_{PB}$ = 151.2 Hz).

Mass Spectrometry (EI) Envelope centred on *m/z* 350.3 (M^+).
[MW = 350.7 g mol^{-1}].

***X*-Ray Diffraction** Solvent diffusion of 40-60 petroleum ether into a CH_2Cl_2 solution of purple product at 5 °C resulted in suitable quality colourless crystals for *X*-ray diffraction.

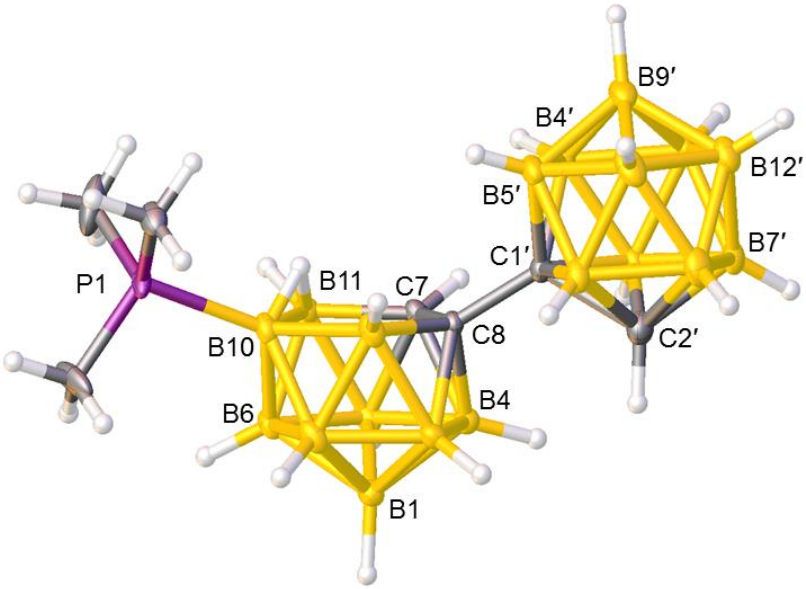

X85311

Compound 6:

[1-(1′-1′,2′-*closo*-$C_2B_{10}H_{11}$)-3-Cl-3-PMe_3-8-PMe_3-3,1,2-*closo*-$NiC_2B_9H_9$]

Elemental analysis (CHN) Required for $C_{10}H_{38}B_{19}ClNiP_2$: C 23.1, H 7.37%.
Found: No analysis due to trace amount.

$^{11}B\{^1H\}$ NMR ($CDCl_3$) δ -1.9 (1B), -3.3 (1B), -4.0 (1B), -5.3 (1B), -6.5 (1B), -8.1 to -15.2 multiple overlapping resonances with maxima at -9.6, -10.6, -12.6 (total integral of last three resonances 10B), -15.9 (1B), -17.7 (2B), -25.4 (1B).

^1H NMR ($CDCl_3$) δ 6.13 (s, 1H, C*H*$_{cage}$), 1.59 (s, 1H, C*H*$_{cage}$), 1.74 (d, $^2J_{PH}$ = 12.0 Hz, 9H, C*H*$_3$), 1.36 (d, $^2J_{PH}$ = 15.6 Hz, 9H, C*H*$_3$).

$^1H\{^{31}P\}$ NMR ($CDCl_3$) δ 6.13 (s, 1H, C*H*$_{cage}$), 1.59 (s, 1H, C*H*$_{cage}$), 1.74 (s, 9H, C*H*$_3$), 1.36 (s, 9H, C*H*$_3$).

^{31}P NMR ($CDCl_3$) δ -9.2 (q, $^1J_{PB}$ = 145.8 Hz, 1P), -20.7 (s, 1P)

Mass Spectrometry (EI) Envelope centred on *m/z* 519.9 (M^+).
[MW = 519.91 g mol^{-1}].

***X*-Ray Diffraction** Solvent diffusion of 40-60 petroleum ether into a $CDCl_3$ solution of purple product at 5 °C resulted in suitable quality purple crystals for *X*-ray diffraction.

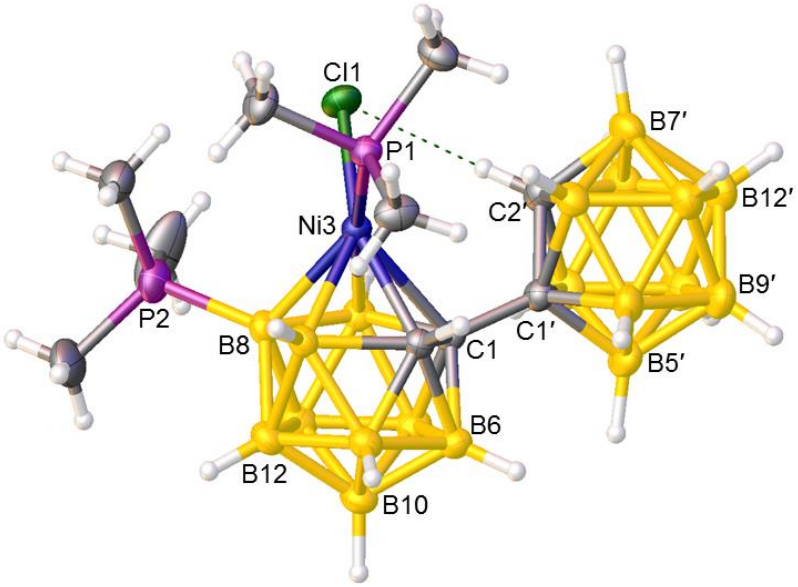

X85285

5.2.5 Synthesis of [1-(1′-1′,2′-*closo*-$C_2B_{10}H_{11}$)-3,3-$(PMe_2Ph)_2$-3,1,2-*closo*-$NiC_2B_9H_{10}$] (7) and [7-(1′-1′,2′-*closo*-$C_2B_{10}H_{11}$)-10-(PMe_2Ph)-7,8-*nido*-$C_2B_9H_{10}$] (8)

Salt $[HNMe_3]$**I** (0.20 g, 0.59 mmol) was treated with *n*-BuLi (0.51 mL of 2.5M solution in hexanes, 1.29 mmol) as described previously and then frozen at -196 °C. To this was added *cis*-$[NiCl_2(PMe_2Ph)_2]$ (0.25 g, 0.64 mmol) and the reaction mixture stirred overnight at room temperature. All volatiles were removed *in vacuo* and the crude mixture dissolved in DCM and filtered through Celite®. Preparative TLC using an eluent system of DCM and petrol in a ratio of 40:60 afforded a green band and a lavender purple band.

Crystallisation of lavender purple product results lavender purple and colourless solids, the latter in sufficient amount for it to be identified.

Green	R_f = 0.45	Yield = 93 mg, 25%	Compound **7**
Lavender purple	R_f = 0.50	Yield = trace amount	Compound **8** (colourless)

Compound 7:

[1-(1′-1′,2′-*closo*-$C_2B_{10}H_{11}$)-3,3-$(PMe_2Ph)_2$-3,1,2-*closo*-$NiC_2B_9H_{10}$]

Elemental analysis (CHN) Required for $C_{20}H_{43}B_{19}NiP_2$: C 24.7, H 8.10%.
Found for **7**: C 24.4, H 8.30%.

$^{11}B\{^1H\}$ NMR ($CDCl_3$) δ 1.6 (1B), -0.7 (1B), -2.4 (1B), -4.7 (1B), -8.7 to -16.2 multiple overlapping resonances with maxima at -8.7, -9.7, -12.1, -16.2 (total integral of last four resonances 14B), -21.6 (1B).

^1H NMR ($CDCl_3$) δ 7.83 (m, 2H, C_6H_5), 7.58-7.38 (m, 8H, C_6H_5), 4.00 (s, 1H, CH_{cage}), 1.74 (d, $^2J_{PH}$ = 10.0 Hz, 3H, CH_3), 1.54 (d, $^2J_{PH}$ = 10.0 Hz, 3H, CH_3), 1.37 (d, $^2J_{PH}$ = 8.0 Hz, 3H, CH_3), 1.18 (d, $^3J_{PH}$ = 14.0 Hz, 1H, CH_{cage}), 1.07 (d, $^2J_{PH}$ = 10.0 Hz, 3H, CH_3).

$^1H\{^{31}P\}$ NMR ($CDCl_3$) δ 7.84 (m, 2H, C_6H_5), 7.58-7.38 (m, 8H, C_6H_5), 4.00 (s, 1H, CH_{cage}), 1.75 (s, 3H, CH_3), 1.54 (s, 3H, CH_3), 1.38 (s, 3H, CH_3), 1.16 (s, 1H, CH_{cage}), 1.09 (s, 3H, CH_3).

^{31}P NMR ($CDCl_3$) δ -4.75 (d, $^2J_{PP}$ = 39.7 Hz, 1P), -14.9 (d, $^2J_{PP}$ = 39.7 Hz, 1P).

Mass Spectrometry (EI) Envelope centred on *m/z* 609.3 (M^+).
[MW = 609.61 g mol^{-1}].

***X*-Ray Diffraction** Solvent diffusion of 40-60 petroleum ether into a THF solution of **7** at 5 °C resulted in suitable quality crystals for *X*-ray diffraction.

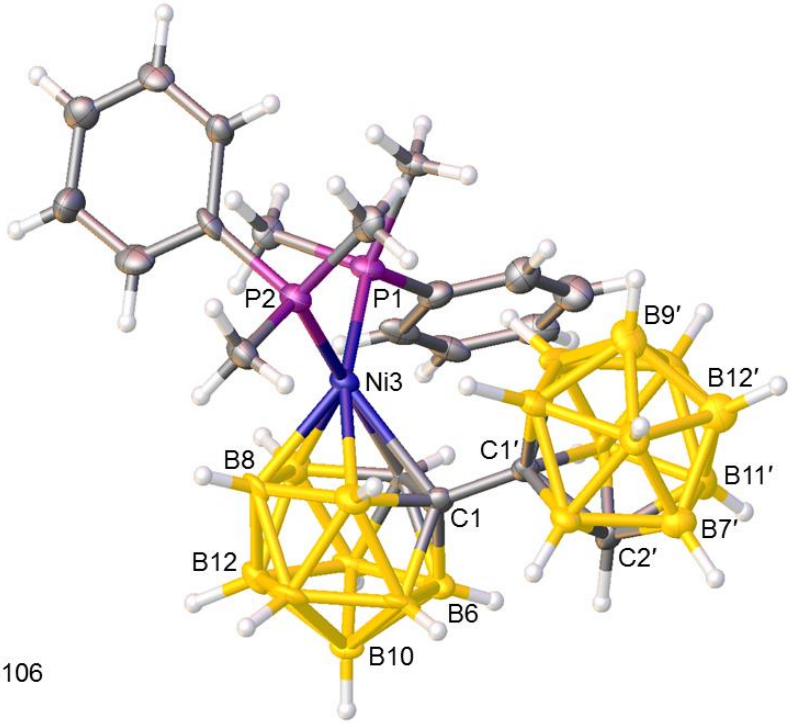

X85106

Compound 8:

[7-(1′-1′,2′-*closo*-$C_2B_{10}H_{11}$)-10-(PMe_2Ph)-7,8-*nido*-$C_2B_9H_{10}$]

Elemental analysis (CHN) Required for $C_{12}H_{32}B_{19}P$: C 34.9, H 7.81%.
Found for **8**: C 34.4, H 7.23%.

$^{11}B\{^1H\}$ NMR ($CDCl_3$) δ -2.7 (1B), -4.9 (1B), -8.5 to -18.4 multiple overlapping resonances with maxima at -8.5, -9.8, -10.7, -13.2, -15.0, -16.4, -17.5 (total integral of last seven resonances 15B), -33.4 (1B), -34.2 (1B).

^1H NMR ($CDCl_3$) δ 7.76-7.65 (m, 5H, C_6H_5), 3.66 (s, 1H, CH_{cage}), 2.49 (s, 1H, CH_{cage}), 1.79 (d, $^2J_{PH}$ = 10.8 Hz, 6H, CH_3).

$^1H\{^{31}P\}$ NMR ($CDCl_3$) δ 7.76-7.65 (m, 5H, C_6H_5), 3.66 (s, 1H, CH_{cage}), 2.49 (s, 1H, CH_{cage}), 1.79 (s, 6H, CH_3).

$^1H\{^{11}B\}$ NMR ($CDCl_3$) δ includes -1.93 (br s, 1H, μ-H).

^{31}P NMR ($CDCl_3$) δ -8.8 (q, $^1J_{PB}$ = 148.5 Hz).

Mass Spectrometry (EI) Envelope centred on *m/z* 412.7 (M^+).
[MW = 412.77 g mol^{-1}].

***X*-Ray Diffraction** Solvent diffusion of 40-60 petroleum ether into a $CDCl_3$ solution of purple product at 5 °C resulted in suitable quality colourless crystals for *X*-ray diffraction.

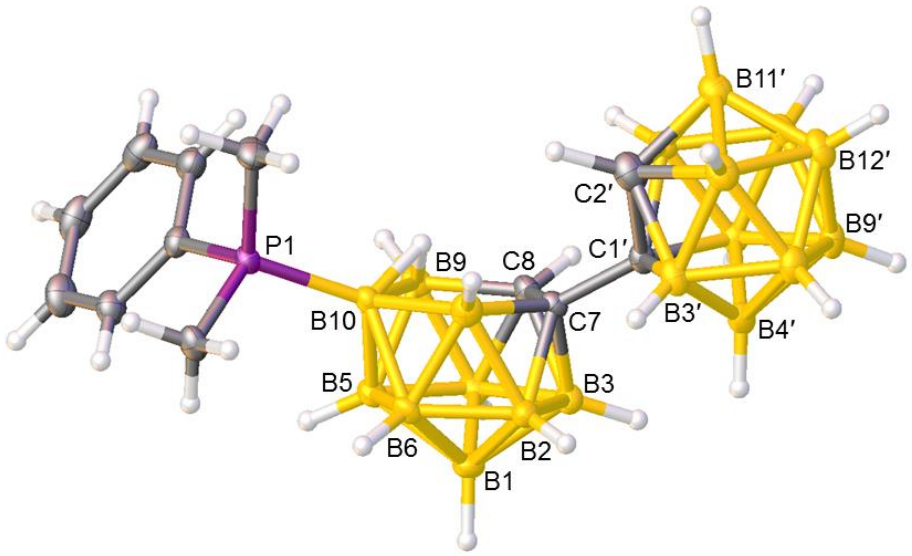

X85114

5.2.6 Synthesis of [2-(1′-1′,2′-*closo*-$C_2B_{10}H_{11}$)-4,4-$(PMePh_2)_2$-4,1,2-*closo*-$NiC_2B_9H_{10}$] (9)

Salt [$HNMe_3$]**I** (0.20 g, 0.59 mmol) was deprotonated with *n*-BuLi (0.51 mL of 2.5M solution in hexanes, 1.29 mmol) as above and frozen at -196 °C. *Cis*-[$NiCl_2(PMePh_2)_2$] (0.33 g, 0.64 mmol) added and the reaction mixture stirred overnight at room temperature. THF was removed *in vacuo* and the crude mixture dissolved in DCM and filtered through Celite®. Preparative TLC using an eluent system of DCM and petrol in a ratio of 40:60 afforded an olive-green band which was collected as solid.

Olive green $R_f = 0.48$ Yield = 90 mg, 20% Compound **9**

Compound 9:

[2-(1′-1′,2′-*closo*-$C_2B_{10}H_{11}$)-4,4-$(PMePh_2)_2$-4,1,2-*closo*-$NiC_2B_9H_{10}$]

Elemental analysis (CHN) Required for $C_{30}H_{47}B_{19}NiP_2$: C 49.1, H 6.46%.
Required for $C_{30}H_{45}B_{19}NiP_2 \cdot CH_2Cl_2$: C 45.5, H 5.92%.
Required for $C_{30}H_{45}B_{19}NiP_2 \cdot 0.5CH_2Cl_2$: C 47.2, H 6.23%.
Found for **9**: C 47.2, H 6.91%.

$^{11}B\{^1H\}$ NMR $[(CD_3)_2CO]$ δ 5.1 (1B), -1.6 to -17.3 multiple overlapping resonances with maxima at -1.6, -3.2, -6.9, -10.4, -13.1, -15.0, -17.3 (total integral of last seven resonances 18B).

^1H NMR $[(CD_3)_2CO]$ δ 5.33 (s, 1H, C*H*$_2$Cl$_2$), 7.73-7.67 (m, 4H, C$_6$*H*$_5$), 7.49-7.18 (m, 16H, C$_6$*H*$_5$), 4.13 (s, 1H, C*H*$_{cage}$), 2.82 (s, 1H, C*H*$_{cage}$), 1.89 [d + d (app. t), $^2J_{PH}$ = ca. 5 Hz, 5Hz, 6H, C*H*$_3$).[19]

$^1H\{^{31}P\}$ NMR $[(CD_3)_2CO]$ δ 7.72-7.23 (m, 20H, C$_6$*H*$_5$), 4.11 (s, 1H, C*H*$_{cage}$), 2.81 (s, 1H, C*H*$_{cage}$), 1.89 (s, 6H, C*H*$_3$).

^{31}P NMR $[(CD_3)_2CO]$ δ 13.9 (s).

Mass Spectrometry (EI) Envelope centred on *m/z* 733.4 (M^+).
[MW = 733.76 g mol^{-1}].

***X*-Ray Diffraction** Many attempts using several solvent systems failed to grow suitable quality crystals for *X*-ray diffraction.

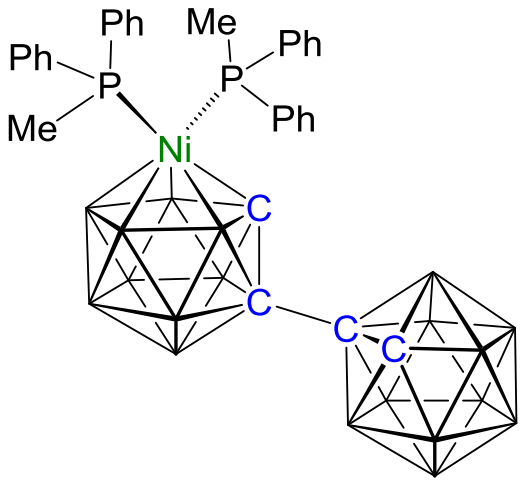
Ph
Me
Ph
Ph
P
P
Me
Ph
Ni
C
C
C
C

5.2.7 Synthesis of [1-(1′-1′,2′-*closo*-$C_2B_{10}H_{11}$)-3-Cl-3-PMe_3-8-PMe_3-3,1,2-*closo*-$PdC_2B_9H_9$] (10)

Salt [$HNMe_3$]**I** (0.10 g, 0.30 mmol) was deprotonated with *n*-BuLi (0.26 mL of 2.5M solution in hexanes, 0.66 mmol) as above and then frozen at -196 °C. *Cis*-[$PdCl_2(PMe_3)_2$] (0.97 g, 0.3 mmol) added and the reaction mixture stirred overnight at room temperature during which time the solution changed to brown. All volatiles were removed *in vacuo* and the crude mixture dissolved in DCM and filtered through Celite®. Following spot TLC (DCM:petrol, 70:30) purification by preparative TLC using the same eluent gave a single mobile band:

Greenish-yellow $R_f = 0.36$ Yield = 35 mg, 20.5% Compound **10**

Compound 10:

[1-(1′-1′,2′-*closo*-$C_2B_{10}H_{11}$)-3-Cl-3-PMe_3-8-PMe_3-3,1,2-*closo*-$PdC_2B_9H_9$]

Elemental analysis (CHN) Required for $C_{10}H_{38}B_{19}ClP_2Pd$: C 21.2, H 6.75%.
Found for **10**: C 21.1, H 6.33%.

$^{11}B\{^1H\}$ NMR ($CDCl_3$) δ 6.5 (d, $^2J_{PB}$ = 144.6 Hz, 1B), -2.5 to -18.0 multiple overlapping resonances with maxima at -2.5, -4.0, -8.6, -9.4, -10.4, -12.5, -15.7, -18.0 (total integral of last eight resonances 17B), -23.0 (1B).

^1H NMR ($CDCl_3$) δ 5.74 (s, 1H, C*H*$_{cage}$), 3.74 (s, 1H, C*H*$_{cage}$), 1.73 (d, $^2J_{PH}$ = 12.0 Hz, 9H, C*H*$_3$), 1.61 (d, $^2J_{PH}$ = 11.2 Hz, 9H, C*H*$_3$).

$^1H\{^{31}P\}$ NMR ($CDCl_3$) δ 5.74 (s, 1H, C*H*$_{cage}$), 3.74 (s, 1H, C*H*$_{cage}$), 1.73 (s, 9H, C*H*$_3$), 1.61 (d, 9H, C*H*$_3$)

^{31}P NMR (CD_2Cl_2) δ -11.3 (q, $^1J_{PB}$ = 144.6 Hz, 1P), -5.8 (s, 1P).

Mass Spectrometry (EI) *m/z* envelope centred on 567.2 (M^+).
[MW = 567.62 g mol^{-1}].

***X*-Ray Diffraction** Solvent evaporation of a $CDCl_3$ solution of **10** at room temperature (16 ^oC) resulted in suitable quality crystals for *X*-ray diffraction and unit cell determination reveals that this is isomorphous to compound **6**.

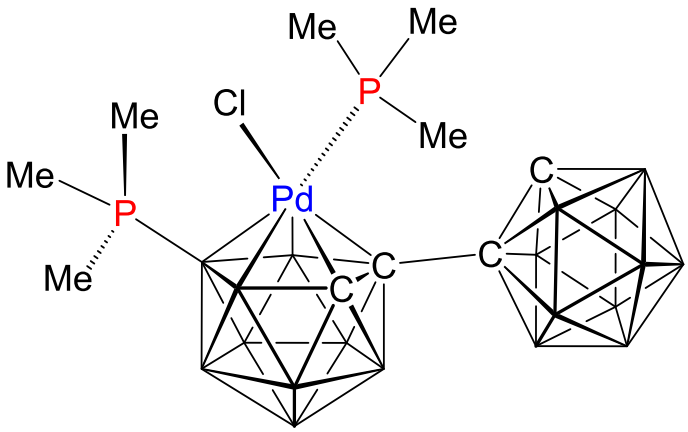
Me
Me
P
Me
Cl
Pd
Me
P
Me
C
C
C
C

5.2.8 Synthesis of [1-(1′-1′,2′-*closo*-$C_2B_{10}H_{11}$)-3-tmeda-3,1,2-*closo*-$PdC_2B_9H_{10}$] (11) and [8-(1′-1′,2′-*closo*-$C_2B_{10}H_{11}$)-2-tmeda-2,1,8-*closo*-$PdC_2B_9H_{10}$] (12)

Salt [$HNMe_3$]**I** (0.10 g, 0.30 mmol) was dissolved in dry THF (20 ml), *n*-BuLi (0.24 mL of 2.5M solution in hexanes, 0.59 mmol) was added dropwise at 0 °C and the solution was stirred at room temperature for 2 hrs. The pale yellow THF solution of Li_2[7-(1′-1′,2′-*closo*-$C_2B_{10}H_{11}$)-7,8-*nido*-$C_2B_9H_{10}$] was frozen at -196 °C, [$PdCl_2$(tmeda)] (0.34 g, 0.30 mmol) was added and the reaction mixture stirred overnight at room temperature, during which time the solution changed to brown. THF was removed *in vacuo* and the crude mixture dissolved in DCM and filtered through Celite®. Preparative TLC using an eluent system of DCM and petrol (50:50) afforded two mobile bands which were purified after several elutions in the same solvent system.

Orange-yellow	R_f = 0.33	Yield = 14 mg, 9.4%	Compound **11**
Orange yellow	R_f = 0.38	Yield = 13 mg, 9%	Compound **12**

Compound 11:

[1-(1′-1′,2′-*closo*-$C_2B_{10}H_{11}$)-3-tmeda-3,1,2-*closo*-$PdC_2B_9H_{10}$]

Elemental analysis (CHN) Required for $C_{10}H_{37}B_{19}N_2Pd$: C 24.2, H 7.50, N 5.63%. Found for **11**: C 24.0, H 7.45, N 5.45%.

$^{11}B\{^1H\}$ NMR ($CDCl_3$) δ -2.9 (1B), -5.5 to -17.0 multiple overlapping resonances with maxima at -5.5, -7.5, -10.0, -13.0, -17.0 (total integral of last five resonances 15B), -23.0 (1B), -25.4 (1B), -27.2 (1B).

^1H NMR ($CDCl_3$) δ 3.96 (s, 1H, CH_{cage}), 3.07 (s, 1H, CH_{cage}), 2.95-2.75 (m, 4H, N{CH_2}$_2$N), 2.83 (s, 3H, CH_3), 2.79 (s, 3H, CH_3), 2.72 (s, 3H, CH_3), 2.69 (s, 3H, CH_3).

Mass Spectrometry (EI) Envelope centred on *m/z* 497.3 (M^+).
[MW = 497.23 g mol^{-1}].

***X*-Ray Diffraction** Solvent diffusion of 40-60 petroleum ether into a $CDCl_3$ solution of **11** at 5 ^oC resulted in suitable quality crystals for *X*-ray diffraction.

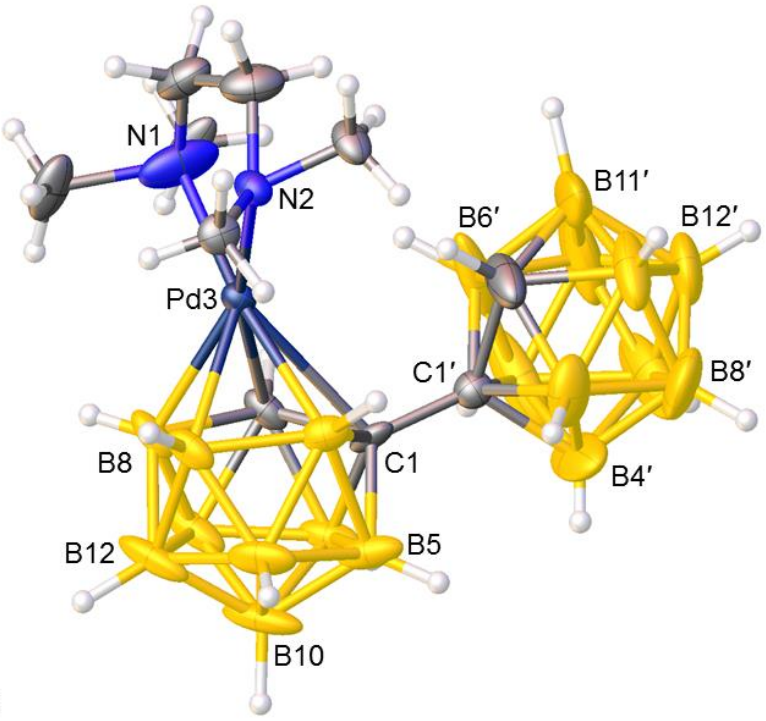

X85345

Compound 12:

[8-(1′-1′,2′-*closo*-$C_2B_{10}H_{11}$)-2-tmeda-2,1,8-*closo*-$PdC_2B_9H_{10}$]

Elemental analysis (CHN) Required for $C_{10}H_{37}B_{19}N_2Pd$: C 24.2, H 7.50, N 5.63%. Found for **12**: C 24.1, H 7.28, N 5.01%.

$^{11}B\{^1H\}$ NMR ($CDCl_3$) δ -3.1 to -22.4 multiple overlapping resonances with maxima at -3.1, -4.4, -6.1, -10.4, -13.6, -15.7, -19.6, -22.4 (total integral of last eight resonances 18B), -29.5 (1B).

^1H NMR ($CDCl_3$) δ 3.73 (s, 1H, C*H*$_{cage}$), 2.90-2.75 (m, 4H, N{C*H*$_2$}$_2$N), 2.80 (s, 3H, C*H*$_3$), 2.78 (s, 3H, C*H*$_3$), 2.65 (s, 3H, C*H*$_3$), 2.62 (s, 3H, C*H*$_3$), 2.52 (s, 1H, C*H*$_{cage}$).

Mass Spectrometry (EI) Envelope centred on *m/z* 497.3 (M^+).
[MW = 497.23 g mol^{-1}].

***X*-Ray Diffraction** Solvent diffusion of 40-60 petroleum ether into a $CDCl_3$ solution of **12** at 5 ^oC resulted in suitable quality crystals for *X*-ray diffraction.

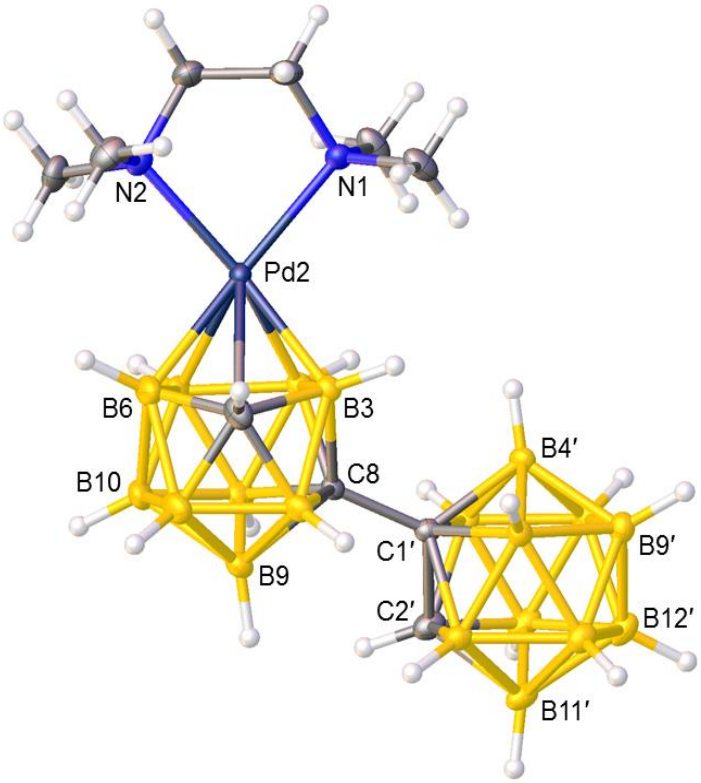

X85344

5.2.9 Synthesis of [1-(1′-1′,2′-*closo*-$C_2B_{10}H_{11}$)-3,3-{$P(OMe)_3$}$_2$-3,1,2-*closo*-$NiC_2B_9H_{10}$] (13) and [1-(1′-1′,2′-*closo*-$C_2B_{10}H_{11}$)-2,2-{$P(OMe)_3$}$_2$-2,1,8-*closo*-$NiC_2B_9H_{10}$] (14)

Salt [$HNMe_3$]**I** (0.15 g, 0.45 mmol) was lithiated with *n*-BuLi (0.36 mL of 2.5M solution in hexanes, 0.90 mmol) and frozen at -196 °C. [(Ni_3(tmeda)$_3Cl_5$)Cl] (0.11 g, 0.15 mmol) was added and the reaction mixture allowed to stir at room temperature to produce a greenish-blue solution. $P(OMe)_3$ (0.53 mL, 4.50 mmol) was added to the reaction solution in a dropwise fashion and the reaction mixture was stirred overnight at room temperature during which the solution turned brown. The THF was removed *in vacuo* and the crude mixture was dissolved in DCM and filtered through Celite®. Preparative TLC using an eluent system of DCM and petrol, 50:50, afforded a single mobile band.

Purple R_f = 0.38 Yield = 45 mg, 17% Compound **13**

Similarly, salt [$HNMe_3$]**I** (0.20 g, 0.59 mmol) was lithiated with *n*-BuLi (0.47 mL of 2.5M solution in hexanes, 1.18 mmol) and frozen at -196 °C. [Ni_3(tmeda)$_3Cl_5$]Cl (0.22 g, 0.30 mmol) was added and the reaction mixture allowed to stir for 2 h at room temperature to produce a greenish-blue solution. $P(OMe)_3$ (0.70 mL, 5.90 mmol) was added to the reaction solution in a dropwise fashion and the reaction mixture was stirred overnight at room temperature during which the solution turned brown. The THF was removed *in vacuo* and the crude mixture was dissolved in DCM and filtered through Celite®. Preparative TLC using an eluent system of DCM and petrol, 50:50, afforded two mobile bands which were collected as solids.

Purple R_f = 0.36 Yield = 10 mg, 3% Compound **13**
Yellow R_f = 0.46 Yield = 46 mg, 13% Compound **14**

Compound 13:

[1-(1′-1′,2′-*closo*-$C_2B_{10}H_{11}$)-3,3-{$P(OMe)_3$}$_2$-3,1,2-*closo*-$NiC_2B_9H_{10}$]

Elemental analysis (CHN) Required for $C_{10}H_{39}B_{19}NiO_6P_2$: C 20.7, H 6.76%.
Found for **13**: C 20.5, H 6.93%.

$^{11}B\{^1H\}$ NMR ($CDCl_3$) δ 1.3 (1B), -0.6 (1B), -2.2 (1B), -4.6 (1B), -6.3 (1B), -9.7 to -14.0 multiple overlapping resonances with maxima at -9.7, -10.2, -13.1, -14.0 (total integral of last four resonances 13B), -18.7 (1B).

^1H NMR ($CDCl_3$) δ 4.59 (s, 1H, C*H*$_{cage}$), 3.85 [d + d (app. t), $^3J_{PH}$ = *ca*. 11.0 Hz, 11.0 Hz, 18H, OC*H*$_3$], 2.52 (d, $^3J_{PH}$ = 10.0 Hz, 1H, C*H*$_{cage}$).

$^1H\{^{31}P\}$ NMR ($CDCl_3$) δ 4.58 (s, 1H, C*H*$_{cage}$), 3.87 (s, 9H, OC*H*$_3$), 3.84 (s, 9H, OC*H*$_3$), 2.52 (s, 1H, C*H*$_{cage}$).

$^{31}P\{^1H\}$ NMR ($CDCl_3$) δ 117.4 (d, $^2J_{PP}$ = 118.2 Hz, 1P), 113.1 (d, $^2J_{PP}$ = 118.2 Hz, 1P).

Mass Spectrometry (EI) Envelope centred on *m/z* 581.3 (M^+).
[MW = 581.47 g mol^{-1}]

***X*-Ray Diffraction** Solvent diffusion of 40-60 petroleum ether into a $CDCl_3$ solution of **13** at 5 °C resulted in suitable quality crystals for *X*-ray diffraction.

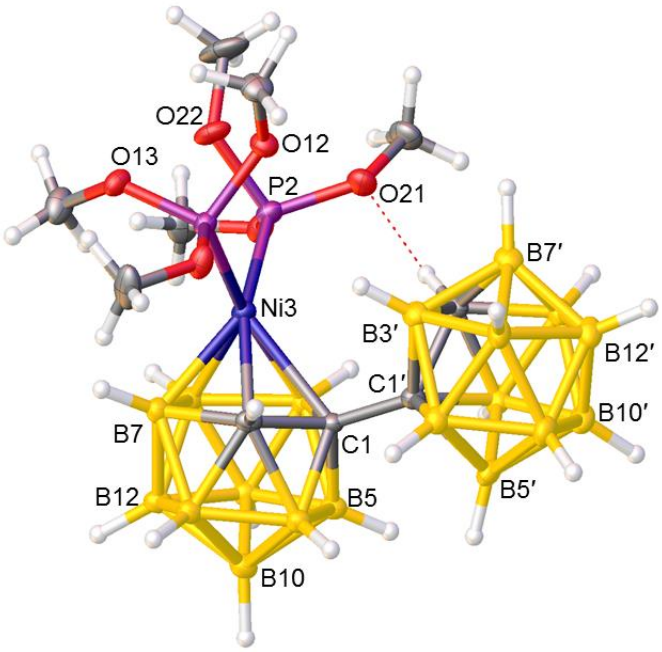

X85420

Compound 14

[1-(1′-1′,2′-*closo*-$C_2B_{10}H_{11}$)-2,2-{$P(OMe)_3$}$_2$-2,1,8-*closo*-$NiC_2B_9H_{10}$]

Elemental analysis (CHN) Required for $C_{10}H_{39}B_{19}NiO_6P_2$: C 20.7, H 6.76%.
Found for **14**: C 20.3, H 6.84%.

$^{11}B\{^1H\}$ NMR ($CDCl_3$) δ -2.5 (1B), -5.6 (2B), -8.2 to -9.8 multiple overlapping resonances with maxima at -8.2, -9.8 (total integral of last two resonances 8B), -13.2 (4), -17.6 (2B), -18.4 (2B).

^1H NMR ($CDCl_3$) δ 4.32 (s, 1H, C*H*$_{cage}$), 3.83 [d with additional structure, $^3J_{PH,}$ = *ca*. 10.4 Hz, 9H, OC*H*$_3$], 3.79 [d with additional structure, $^3J_{PH,}$ = *ca*. 10.4 Hz, 9H, OC*H*$_3$], 2.23 (s, 1H, C*H*$_{cage}$).

$^1H\{^{31}P\}$ NMR ($CDCl_3$) δ 4.31 (s, 1H, C*H*$_{cage}$), 3.83 (s, 9H, OC*H*$_3$), 3.79 (s, 9H, OC*H*$_3$), 2.22 (s, 1H, C*H*$_{cage}$).

$^{31}P\{^1H\}$ NMR ($CDCl_3$) δ 125.2-123.5 (m, overlapping of two doublets, 2P).

Mass Spectrometry (EI) Envelope centred on *m/z* 580.3 (M^+).
[MW = 581.47 g mol^{-1}]

***X*-Ray Diffraction** Solvent diffusion of 40-60 petroleum ether into a $CDCl_3$ solution of **14** at 5 ^oC resulted in suitable quality crystals for *X*-ray diffraction.

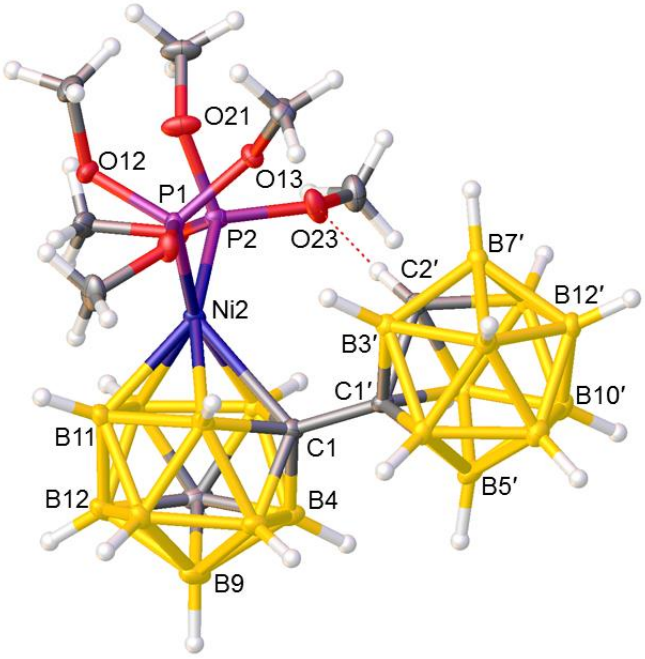

X85478

5.2.10 Synthesis of *cis*-[$NiBr_2${$P(OMe)_3$}$_2$] (15)

By following the literature method,[11] anhydrous $NiBr_2$ (0.50 g, 2.29 mmol) was taken in THF (20 ml) and stirred for 0.5 hr affording a brownish-orange solution. $P(OMe)_3$ (0.54 ml, 4.58 mmol) was added to the solution, which immediately changed to dark purple. The reaction mixture was stirred at room temperature for 2 hrs during which it remained as a dark purple solution. After removing THF, the remaining solid was dried under vacuum to afford a brown powder.

Yield = 0.76 g, 71% Compound **15**

Elemental analysis (CHN) Required for $C_6H_{18}Br_2NiO_6P_2$: C 15.4, H 3.89%.
Found for **15**: C 16.1, H 4.38%.

^{1}H NMR ($CDCl_3$) δ 3.87 (br s, OC*H*$_3$).

^{31}P{^{1}H} NMR ($CDCl_3$) δ 108.8 (br s).

5.2.11 Alternative synthesis of [1-(1′-1′,2′-*closo*-$C_2B_{10}H_{11}$)-3,3-{$P(OMe)_3$}$_2$-3,1,2-*closo*-$NiC_2B_9H_{10}$] (13)

Salt **I** (0.20 g, 0.59 mmol) was deprotonated with *n*-BuLi (0.51 mL of 2.5M solution in hexanes, 1.29 mmol) and then frozen at -196 °C. *Cis*-[$NiBr_2(P(OMe)_3)_2$] (0.28 g, 0.59 mmol) was added and the reaction mixture stirred overnight at room temperature during which time the initially brown solution turned to green. THF was removed *in vacuo* and the crude mixture dissolved in DCM, purified by preparative TLC using the eluent system DCM:petroleum ether, 60:40, to afford a single mobile band identified as compound **13** by ^{1}H, ^{31}P, $^{11}B\{^{1}H\}$, ^{11}B NMR spectroscopies.

Purple $R_f = 0.56$ Yield = 53 mg, 15% Compound **13**

5.2.12 Synthesis of [1-(1′-1′,2′-*closo*-$C_2B_{10}H_{11}$)-3,3-{$P(OEt)_3$}$_2$-3,1,2-*closo*-$NiC_2B_9H_{10}$] (16)

Salt **I** (0.20 g, 0.59 mmol) was lithiated with *n*-BuLi (0.51 mL of 2.5M solution in hexanes, 1.29 mmol) and then frozen at -196 °C. *Cis*-[$NiBr_2(P(OEt)_3)_2$] (0.33 g, 0.59 mmol) was added and the reaction mixture allowed to warm at room temperature. After overnight stirring the initially dark purple solution turned to brown. Solvents were removed under vacuum and the crude mixture dissolved in DCM. Preparative TLC using an eluent system of DCM and petrol (50:50) yielded a mobile band, collected as solid:

Purple $R_f = 0.52$ Yield = 68 mg, 17% Compound **16**

Compound 16:

[1-(1′-1′,2′-*closo*-$C_2B_{10}H_{11}$)-3,3-{$P(OEt)_3$}$_2$-3,1,2-*closo*-$NiC_2B_9H_{10}$]

Elemental analysis (CHN) Required for $C_{16}H_{51}B_{19}NiO_6P_2$: C 28.9, H 7.72%.
Found for **16**: C 28.5, H 7.93%.

$^{11}B\{^1H\}$ NMR ($CDCl_3$) δ 1.3 (1B), -0.4 (1B), -2.1 (1B), -4.6 (1B), -6.8 (1B), -9.7 to -16.1 multiple overlapping resonances with maxima at -9.7, -10.4, -14.3, -16.1 (total integral of last four resonances 13B), -18.9 (1B).

^1H NMR ($CDCl_3$) δ 5.01 (s, 1H, C*H*$_{cage}$), 4.30-4.05 (m, 12H, OC*H*$_2$), 2.44 (d, $^3J_{PH}$ = 13 Hz, 1H, C*H*$_{cage}$), 1.34 [td, $^3J_{HH}$ = 7.2 Hz, $^4J_{PH}$ = <1 Hz, 18H, C*H*$_3$]

$^1H\{^{31}P\}$ NMR ($CDCl_3$) δ 5.00 (s, 1H, C*H*$_{cage}$), 4.30-4.05 (m, 12H, OC*H*$_2$), 2.44 (s, 1H, C*H*$_{cage}$), 1.34 (t, $^3J_{HH}$ = 7.2 Hz, 18H, C*H*$_3$).

$^{31}P\{^1H\}$ NMR ($CDCl_3$) δ 109.9 (d, $^2J_{PP}$ = 116.1 Hz, 1P), 113.1 (d, $^2J_{PP}$ = 116.1 Hz, 1P).

Mass Spectrometry (EI) Envelope centred on *m/z* 665.6 (M^+).
[MW = 665.63 g mol^{-1}]

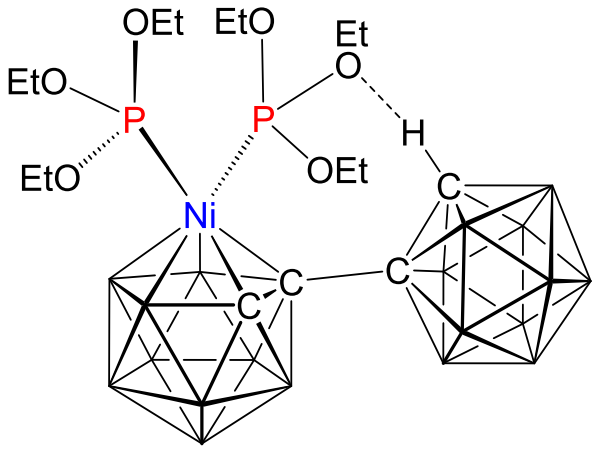

5.3.1 Synthesis of $[Tl]_2[1\text{-}(1'\text{-}3',1',2'\text{-}TlC_2B_9H_{10})\text{-}3,1,2\text{-}TlC_2B_9H_{10}]$ (17)

Potassium hydroxide (2.36 g, 42 mmol) was added to a solution of 1,1′-bis(*o*-carborane) (0.50 g, 1.75 mmol) in ethanol (30 mL) and the solution heated to reflux overnight. The solution was cooled to room temperature and the solvent removed *in vacuo*. The resultant white solid was then dissolved in deionised water (30 mL) and filtered before a solution of thallous acetate (1.94 g, 7.35 mmol) in deionised water (30 mL) was added to the filtrate. The yellow precipitate was collected and washed with ethanol (2 × 20 ml), followed by diethyl ether (2 × 20 ml). Drying *in vacuo* afforded a fine powder.

Yellow Yield = 89 mg, 23% Compound **17**

Elemental analysis (CHN) Required for $C_4H_{20}B_{18}Tl_4$: C 4.5, H 1.87%.
Found for **17**: C 4.4, H 1.78%.

5.3.2 Synthesis of *rac*-[1-(1′-3′-(dmpe)-3′,1′,2′-*closo*^{3}-$NiC_2B_9H_{10}$)-3-(dmpe)-3,1,2-*closo*^{3}-$NiC_2B_9H_{10}$] (18) and *meso*-[1-(1′-3′-(dmpe)-3′,1′,2′-*closo*^{3}-$NiC_2B_9H_{10}$)-3-(dmpe)-3,1,2-*closo*^{3}-$NiC_2B_9H_{10}$] (19)

Salt **17** (0.60 g, 0.56 mmol) was suspended in dry THF (15 ml) and the resulting yellow suspension degassed by freeze-pump-thaw (three cycles). Anhydrous [$NiCl_2$(dmpe)] (0.31 g, 1.1 mmol) was added at -196 °C. The reaction mixture was allowed to warm and stirred at room temperature overnight during which the colour of the reaction mixture changes to dark green. THF was removed *in vacuo* and the resultant dark green mixture filtered through silica with DCM to remove impurities. The solution was reduced in volume under low pressure and purified by preparative TLC using an eluent system of DCM and petrol (80:20) to afford two dark green bands which were collected as solids:

Dark-green	R_f = 0.84	Yield = 80 mg, 21%	Compound **18**
Dark-green	R_f = 0.63	Yield = 76 mg, 20%	Compound **19**

Compound 18:

rac-[1-(1′-3′-(dmpe)-3′,1′,2′-*closo*^{5}-$NiC_2B_9H_{10}$)-3-(dmpe)-3,1,2-*closo*^{5}-$NiC_2B_9H_{10}$]

Elemental analysis (CHN) Required for $C_{16}H_{52}B_{18}Ni_2P_4$: C 28.2, H 7.70%.
Required for $C_{16}H_{52}B_{18}Ni_2P_4 \cdot 0.5CH_2Cl_2$: C 27.4, H 7.39%.
Found for **18**$\cdot 0.5CH_2Cl_2$: C 27.4, H 7.57%.

$^{11}B\{^1H\}$ NMR (CD_2Cl_2) δ -2.7 (2B), -4.1 (2B), -7.3 (2B), -11.8 (2B), -13.6 (2B), -15.8 (4B), -21.1 (4B).

^1H NMR (CD_2Cl_2) δ 2.43 (d, $^3J_{PH}$ = 14.0 Hz, 2H, CH_{cage}), 2.14-1.90 (m, 8H, P{CH_2}$_2$P), 1.83 (d, $^2J_{PH}$ = 10.0 Hz, 6H, CH_3), 1.67 (d, $^2J_{PH}$ = 10.0 Hz, 6H, CH_3), 1.55 (d, $^2J_{PH}$ = 10.0 Hz, 12H, CH_3).

$^1H\{^{31}P\}$ NMR (CD_2Cl_2) δ 2.43 (s, 2H, CH_{cage}), 2.12-1.89 (m, 8H, P{CH_2}$_2$P), 1.83 (s, 6H, CH_3), 1.67 (s, 6H, CH_3), 1.56 (s, 12H, CH_3).

$^{31}P\{^1H\}$ NMR (CD_2Cl_2) δ 43.1 (d, $^2J_{PP}$ = 29.2 Hz, 2P), 33.0 (d, $^2J_{PP}$ = 29.2 Hz, 2P).

Mass Spectrometry (EI) Sharp peak at *m/z* 681.0 (M^+).
[MW = 680.47 g mol^{-1}].

***X*-Ray Diffraction** Solvent diffusion of 40-60 petroleum ether into a CH_2Cl_2 solution of **18** at 5 ^oC resulted in suitable quality crystals for *X*-ray diffraction.

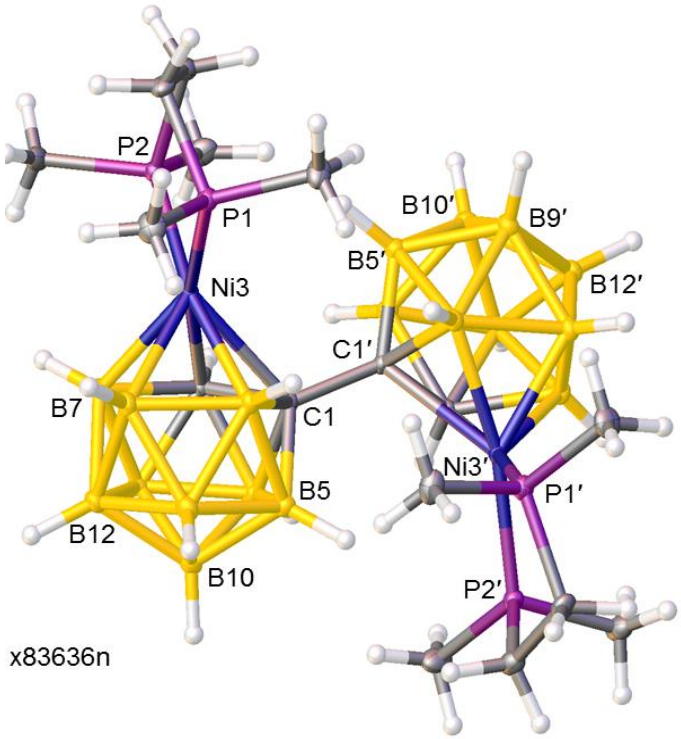
P2
P1
Ni3
B7
C1
B5
B12
B10
B10′
B9′
B5′
B12′
C1′
Ni3′
P1′
P2′
x83636n

Compound 19:

meso-[1-(1′-3′-(dmpe)-3′,1′,2′-*closo*^{5}-$NiC_2B_9H_{10}$)-3-(dmpe)-3,1,2-*closo*^{5}-$NiC_2B_9H_{10}$]

Elemental analysis (CHN) Required for $C_{16}H_{52}B_{18}Ni_2P_4$: C 28.2, H 7.70%.
Required for $C_{16}H_{52}B_{18}Ni_2P_4 \cdot CH_2Cl_2$: C 26.7, H 7.11%.
Required for $C_{16}H_{52}B_{18}Ni_2P_4 \cdot 3CH_2Cl_2$: C 24.4, H 6.25%.
Found for **19**$\cdot 3CH_2Cl_2$: C 24.6, H 7.41%.

$^{11}B\{^1H\}$ NMR (CD_2Cl_2) δ -1.5 (2B), -4.0 (2B), -10.4 (2B), -11.5 (2B), -14.5 (3B), -15.9 (5B), -20.4 (2B).

^1H NMR (CD_2Cl_2) δ 5.33 (s, 6H, C*H*$_2$Cl$_2$), 2.48 (d, $^3J_{PH}$ = 10.0 Hz, 2H, C*H*$_{cage}$), 2.16-1.79 (m, 8H, P{C*H*$_2$}$_2$P), 1.73 (d, $^2J_{PH}$ = 10.0 Hz, 6H, C*H*$_3$), 1.70 (d, $^2J_{PH}$ = 8.0 Hz, 6H, C*H*$_3$), 1.57 (d, $^2J_{PH}$ = 10.0 Hz, 6H, C*H*$_3$), 1.55 (d, $^2J_{PH}$ = 8.0 Hz, 6H, C*H*$_3$).

$^1H\{^{31}P\}$ NMR (CD_2Cl_2) δ 2.49 (s, 2H, C*H*$_{cage}$), 2.14-1.78 (m, 8H, P{C*H*$_2$}$_2$P), 1.74 (s, 6H, C*H*$_3$), 1.70 (s, 6H, C*H*$_3$), 1.57 (s, 6H, C*H*$_3$), 1.55 (s, 6H, C*H*$_3$).

$^{31}P\{^1H\}$ NMR (CD_2Cl_2) δ 43.7 (d, $^2J_{PP}$ = 28.4 Hz, 2P), 33.4 (d, $^2J_{PP}$ = 28.4 Hz, 2P).

Mass Spectrometry (EI) Sharp peak at *m/z* 679.6 (M^+).
[MW = 680.47 g mol^{-1}].

***X*-Ray Diffraction** Solvent diffusion of 40-60 petroleum ether into a CH_2Cl_2 solution of **19** at 5 ^oC resulted in suitable quality crystals for *X*-ray diffraction.

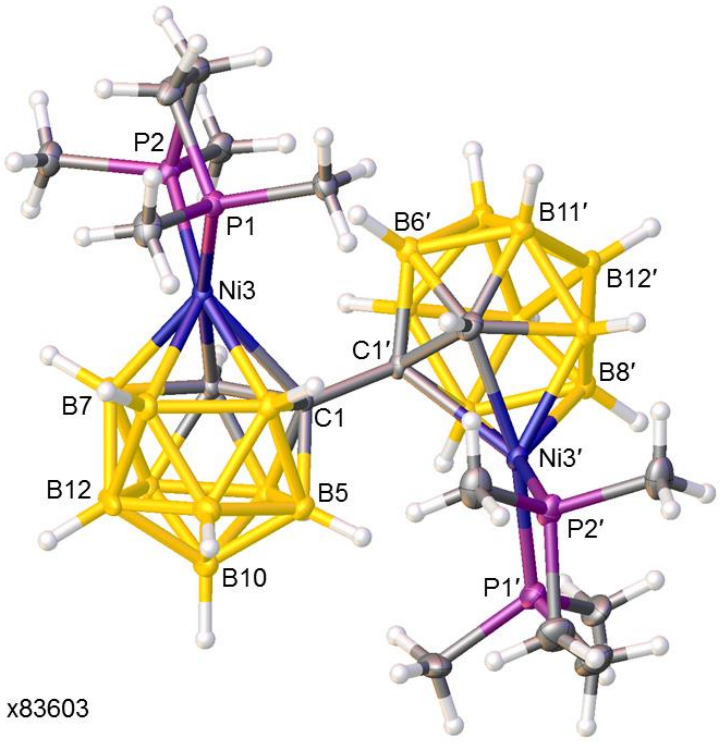
P2
P1
Ni3
B7
C1
B12
B5
B10
B6′
B11′
B12′
C1′
B8′
Ni3′
P2′
P1′
x83603

5.3.3 Thermal isomerisation of compound 18 to compounds 18 and 19

Compound **18** (0.040 g, 0.059 mmol) was dissolved in THF (10 mL) and the solution heated at reflux for 2.5 hr. After reflux the colour of the solution remained dark green. The solvent was removed *in vacuo* and the dark green residue purified by preparative TLC using an eluent system of DCM:petroleum ether (70:30) to afford two dark green bands which were identified by ^{1}H, $^{31}P\{^{1}H\}$ and $^{11}B\{^{1}H\}$ NMR spectroscopies.

Dark-green	$R_f = 0.64$	Yield = 18 mg, 45%	Compound **18**
Dark-green	$R_f = 0.60$	Yield = 17 mg, 43%	Compound **19**

5.3.4 Thermal isomerisation of compound 19 to compounds 18 and 19

Compound **19** (0.036 g, 0.053 mmol) was dissolved in THF (10 mL) and the solution heated at reflux for 2.5 hr. After reflux the colour of the solution remained dark green. The solvent was removed under vacuum and the product purified by preparative TLC using an eluent system of DCM:petroleum ether (70:30) to afford two dark green bands the identities of which were confirmed by NMR spectroscopies.

Dark-green	R_f = 0.64	Yield = 16 mg, 44%	Compound **18**
Dark-green	R_f = 0.60	Yield = 17 mg, 47%	Compound **19**

5.3.5 Thermal isomerisation of compounds 18 and 19 in toulene

Compound **18** (0.020 g, 0.029 mmol) was dissolved in toluene (10 mL) and the solution heated to reflux for 2.5 hr during which time the colour of the reaction mixture turned red-orange. The solvent was removed *in vacuo* and the solubility of the resultant material was checked in DCM, THF, acetone, acetonitrile and toluene and was found to be insoluble, therefore characterisation was not possible. Similarly, compound **19** (0.020 g, 0.029 mmol) was dissolved in toluene (10 ml) and the solution heated to reflux for 2.5 hr during which time the colour of the reaction mixture changes to red-orange. Due to limited solubility in DCM, THF, acetone, acetonitrile and toluene characterisation was not possible.

5.3.6 Synthesis of [7-(7′-7′,8′-*nido*-$C_2B_9H_{12}$)-7,8-*nido*-$C_2B_9H_{12}$] (20)

Salt **17** (0.50 g, 0.46 mmol) was suspended in dry petrol (15 ml) and the resulting yellow suspension was degassed by freeze-pump-thaw (three cycles). A solution of BI_3 (0.39 g, 1.02 mmol) in petrol was added in dropwise fashion *via* cannula at 0 °C. The reaction mixture was allowed to warm and stirred at room temperature 3 hrs affording a bright orange suspension. All volatiles were removed under low pressure. The residue was dissolved in DCM and filtered through silica. The colourless solution was evaporated to dryness to afford compound **20** as a white solid.

White Yield = 32 mg, 26% Compound **20**

Similarly treatment of salt **17** (0.50 g, 0.46 mmol) in dry petrol (15 ml) with BBr_3 (1.02 mL of 1M solution in hexanes, 1.02 mmol) as above and overnight stirring afforded a pale yellow suspension. Solvents were removed *in vacuo* and the crude reaction mixtures were passed through silica to remove impurities. The solution was evaporated under low pressure to yield compound **20**, identified by NMR spectroscopies.

White Yield = 27 mg, 22% Compound **20**

Compound 20:

[7-(7′-7′,8′-*nido*-$C_2B_9H_{12}$)-7,8-*nido*-$C_2B_9H_{12}$]

Elemental analysis (CHN) Required for $C_4H_{24}B_{18}$: C 18.0, H 9.07%.
Found for **20**: C 18.3, H 9.11%.

$^{11}B\{^1H\}$ NMR ($CDCl_3$) δ -7.0 (1B), 6.0 (1B), 2.9 (2B), -5.4 (4B), -12.4 (2B), -16.1 (2B), -24.7 (2B), -25.5 (2B), -26.6 (2B).

^1H NMR ($CDCl_3$) δ 3.73 (s, 2H, C*H*$_{cage}$).

Mass Spectrometry (EI) Envelope centred on *m/z* 262.3 (M^+-4H).
[MW = 266.83 g mol^{-1}].

***X*-Ray Diffraction** Solvent diffusion of 40-60 petroleum ether into a CH_2Cl_2 solution of **20** at 5 °C resulted in suitable quality colourless crystals for *X*-ray diffraction.

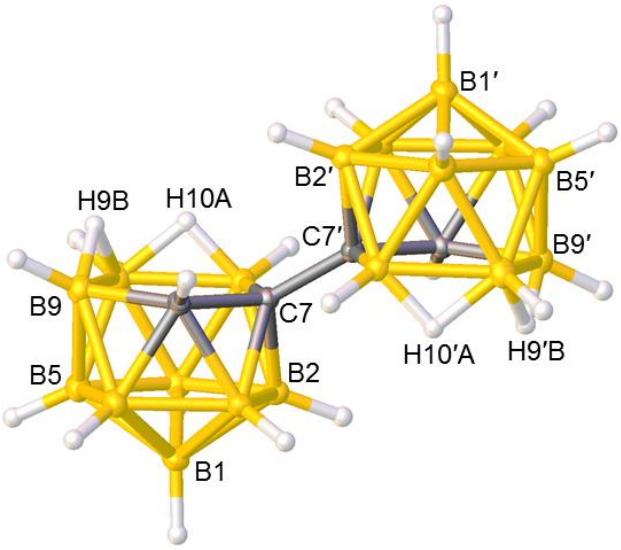

5.3.7 Synthesis of *rac*-[1-(1′-3′-Ph-1′,2′-*closo*$^{\circlearrowleft}$-$C_2B_{10}H_{10}$)-3-Ph-1,2-*closo*$^{\circlearrowleft}$-$C_2B_{10}H_{10}$] (21) and *meso*-[1-(1′-3′-Ph-1′,2′-*closo*$^{\circlearrowleft}$-$C_2B_{10}H_{10}$)-3-Ph-1,2-*closo*$^{\circlearrowleft}$-$C_2B_{10}H_{10}$] (22)

Salt $[HNMe_3]_2$**II** (0.12 g, 0.31 mmol) was suspended in dry ether (20 ml), *n*-BuLi (0.58 mL of 2.36M solution in hexanes, 1.37 mmol) was added dropwise at 0 °C and the cloudy solution was heated to reflux for 2 hrs. After cooling to room temperature, all volatiles (ether, amine) were removed *in vacuo* and the white residue was washed with dry petrol (15 ml) and dried. Filter degassed dry petrol (15 ml) was added affording a white suspension of Li_4[7-(7′-7′,8′-*nido*-$C_2B_9H_{10}$)-7,8-*nido*-$C_2B_9H_{10}$]. $PhBCl_2$ (0.10 mL, 0.68 mmol) was added in a dropwise fashion to a frozen suspension of Li_4[7-(7′-7′,8′-*nido*-$C_2B_9H_{10}$)-7,8-*nido*-$C_2B_9H_{10}$] in petrol at -196 °C. The reaction mixture was allowed to warm and stirred at room temperature for 18 hr during which time the reaction mixture turned light pink. All volatiles were removed under vacuum and the resultant product was filtered through silica with DCM. The solution was reduced in volume and preparative TLC using an eluent system of DCM and petrol (20:80) afforded two colourless but UV active bands collected as solids:

Colourless	R_f = 0.85	Yield = 30 mg, 22%	Compound **21**
Colourless	R_f = 0.75	Yield = 23 mg, 17%	Compound **22**

Compound 21:

rac-[1-(1′-3′-Ph-1′,2′-*closo*-$C_2B_{10}H_{10}$)-3-Ph-1,2-*closo*-$C_2B_{10}H_{10}$]

Elemental analysis (CHN) Required for $C_{16}H_{30}B_{20}$: C 43.8, H 6.89%.
Found for **21**: C 43.1, H 6.91%.

$^{11}B\{^1H\}$ NMR ($CDCl_3$) δ -0.8 (2B), -3.1 (2B), -8.2 to -11.0 multiple overlapping resonances with maxima at -8.2, -9.3 -11.0 (total integral of three resonances 14B), -13.9 (2B).

^1H NMR ($CDCl_3$) δ 7.61-7.47 (m, 10H, C_6H_5), 3.69 (s, 2H, CH_{cage}).

Mass Spectrometry (EI) Envelope centred on *m/z* 438.4 (M^+).
[MW = 438.64 g mol^{-1}].

***X*-Ray Diffraction** Solvent diffusion of 40-60 petroleum ether into a CH_2Cl_2 solution of **21** at room temperature resulted in suitable quality colourless crystals for *X*-ray diffraction.

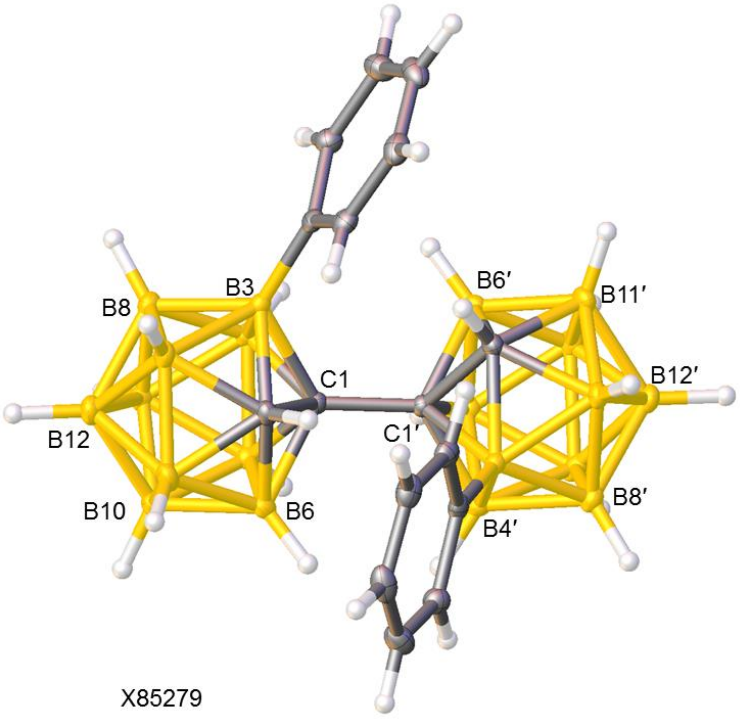

Compound 22:

meso-[1-(1′-3′-Ph-1′,2′-*closo*$^{\circlearrowleft}$-$C_2B_{10}H_{10}$)-3-Ph-1,2-*closo*$^{\circlearrowleft}$-$C_2B_{10}H_{10}$]

Elemental analysis (CHN) Required for $C_{16}H_{30}B_{20}$: C 43.8, H 6.89%.
Found for **22**: C 42.7, H 5.66%.

$^{11}B\{^1H\}$ NMR ($CDCl_3$) δ -0.5 (4B), -3.0 (2B), -7.1 (2B), -9.6 to -11.5 multiple overlapping resonances with maxima at -8.2, -10.6, -11.0 (total integral of three resonances 10B), -13.6 (2B).

^1H NMR ($CDCl_3$) δ 7.54-7.41 (m, 10H, C_6H_5), 4.19 (s, 2H, CH_{cage}).

Mass Spectrometry (EI) Envelope centred on *m/z* 438.4 (M^+).
[MW = 438.64 g mol^{-1}].

***X*-Ray Diffraction** Solvent diffusion of 40-60 petroleum ether into a CH_2Cl_2 solution of **22** at room temperature resulted in suitable quality colourless crystals for *X*-ray diffraction.

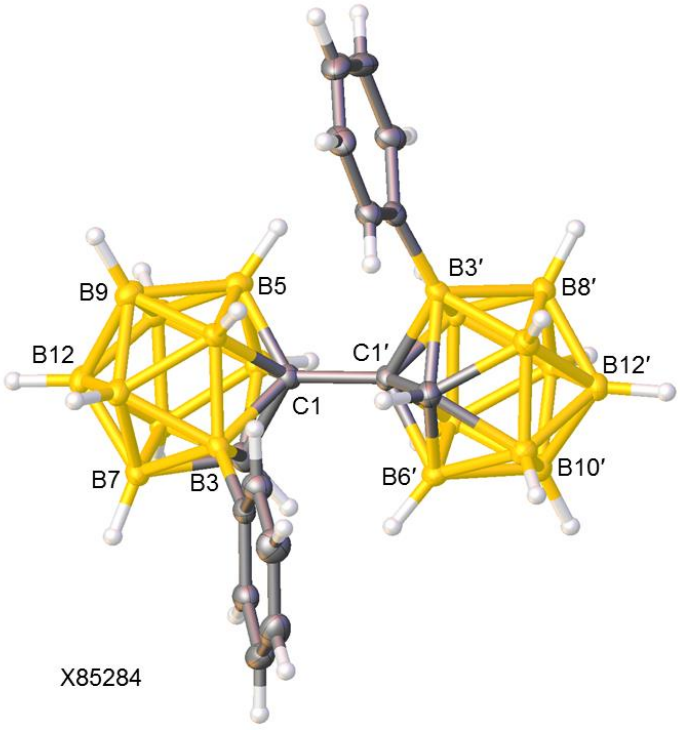

5.3.8 Synthesis of $[HNMe_3]_2[7\text{-}(7'\text{-}3'\text{-}Ph\text{-}7',8'\text{-}nido\text{-}C_2B_9H_{10})\text{-}3\text{-}Ph\text{-}7,8\text{-}nido\text{-}C_2B_9H_{10}]$ ($[HNMe_3]_2$[23]) as a *rac* and *meso* mixture and $[BTMA]_2[7\text{-}(7'\text{-}3'\text{-}Ph\text{-}7',8'\text{-}nido\text{-}C_2B_9H_{10})\text{-}3\text{-}Ph\text{-}7,8\text{-}nido\text{-}C_2B_9H_{10}]$ ($[BTMA]_2$[23]) as a *rac* and *meso* mixture

A *rac* (**21**) and *meso* (**22**) mixture of [1-(1′-3′-Ph-1′,2′-*closo*-$C_2B_{10}H_{10}$)-3-Ph-1,2-*closo*-$C_2B_{10}H_{10}$] (0.31 g, 0.71 mmol) and KOH (0.95 g, 17.0 mmol) were heated to reflux in EtOH (20 ml) for 18 hr. The solution was allowed to cool and excess KOH was removed by reaction with CO_2 (dry ice) and filtering off the K_2CO_3 formed. Then all volatiles were removed *in vacuo* and deionised water (10 ml) was added and the solution filtered. To the clear solution of K_2[7-(7′-3′-Ph-7′,8′-*nido*-$C_2B_9H_{10}$)-3-Ph-7,8-*nido*-$C_2B_9H_{10}$] was added an aqueous solution of [$HNMe_3$]Cl (0.15 g, 1.6 mmol) resulting in a white cloudy precipitate. This was extracted into DCM (3×15 ml) and dried over $MgSO_4$. A semi-solid white residue was recovered which, after applying high vacuum, gave a solid.

White Yield = 120 mg, 31% Compound ($[HNMe_3]_2$[**23**])

Similarly treatment of *rac* (**21**) and *meso* (**22**) mixture of [1-(1′-3′-Ph-1′,2′-*closo*-$C_2B_{10}H_{10}$)-3-Ph-1,2-*closo*-$C_2B_{10}H_{10}$] (0.09 g, 0.21 mmol) with KOH (0.28 g, 5.04 mmol) in EtOH (15 ml) followed by work up afforded K_2[7-(7′-3′-Ph-7′,8′-*nido*-$C_2B_9H_{10}$)-3-Ph-7,8-*nido*-$C_2B_9H_{10}$]. This was treated with an aqueous solution of [BTMA]Cl (0.09 g, 0.46 mmol) resulting in a white precipitate. Filtration followed by washing with deionised water (3×10 ml) and drying yielded a solid.

White Yield = 66 mg, 44% Compound ($[BTMA]_2$[**23**])

Compound ([HNMe$_3$]$_2$[23]):

[HNMe$_3$]$_2$[7-(7′-3′-Ph-7′,8′-*nido*-C$_2$B$_9$H$_{10}$)-3-Ph-7,8-*nido*-C$_2$B$_9$H$_{10}$] as a *rac* and *meso* mixture

Elemental analysis (CHN) Required for $C_{22}H_{50}B_{18}N_2$: C 49.2, H 9.38, N 5.21%.
Required for $C_{22}H_{50}B_{18}N_2 \cdot 0.5CH_2Cl_2$: C 46.6, H 8.87, N 4.83%.
Found for ([HNMe$_3$]$_2$[**23**])$\cdot 0.5CH_2Cl_2$: C 46.8, H 9.08, N 4.80%.

From the spectra ([HNMe$_3$]$_2$[**23**]) is a mixture of major and minor components arising from decapitation of the rac/meso precursor. Being unable to assign each component, the integral values are excluded for $^{11}B\{^1H\}$ and ^1H NMR spectra.

^{11}B{^{1}H} NMR [(CD$_3$)$_2$CO] δ -7.8, -9.5, -12.8, -13.6, -16.8 to -21.0 multiple overlapping resonances with maxima at -16.8, -18.9, -20.1, -21.0, -34.2, -35.0.

^{1}H NMR [(CD$_3$)$_2$CO] δ 7.74-6.99 (m, C$_6$*H*$_5$), 3.16 (s, N(C*H*$_3$)$_3$), 2.33 (s, C*H*$_{cage}$), 1.45 (s, C*H*$_{cage}$).

Compound ([BTMA]$_2$[23]):

[BTMA]$_2$[7-(7′-3′-Ph-7′,8′-*nido*-$C_2B_9H_{10}$)-3-Ph-7,8-*nido*-$C_2B_9H_{10}$] as a *rac* and *meso* mixture

Elemental analysis (CHN) Required for $C_{36}H_{62}B_{18}N_2$: C 60.3, H 8.71, N 3.90%.
Required for $C_{36}H_{62}B_{18}N_2 \cdot 0.5CH_2Cl_2$: C 57.7 H 8.36, N 3.69%.
Found for ([BTMA]$_2$[**23**])·$0.5CH_2Cl_2$: C 57.9, H 8.79, N 3.80%.

From the spectra ([BTMA]$_2$[**23**]) is a mixture of major and minor components arising from decapitation of the rac/meso precursor. Being unable to assign each component, the integral values are excluded for $^{11}B\{^1H\}$ and ^1H NMR spectra.

$^{11}B\{^1H\}$ NMR [$(CD_3)_2CO$] δ -7.8, -9.0, -12.7, -13.4, -16.9 to -21.0 multiple overlapping resonances with maxima at -16.8, -17.7, -18.6, -20.1, -21.0, -34.2, -35.0.

^1H NMR [$(CD_3)_2CO$] δ 7.75-6.97 (m, C_6H_5), 4.76 (s, CH_2), 3.33 (s, $N(CH_3)_3$), 2.35 (s, 1H, CH_{cage}), 1.46 (s, CH_{cage}).

***X*-Ray Diffraction** Solvent diffusion of 40-60 petroleum ether into a CH_2Cl_2 solution of ([BTMA]$_2$[**23**]) at 5 ºC resulted in suitable quality colourless crystals of the meso form of [BTMA]$_2$[7-(7′-3′-Ph-7′,8′-*nido*-$C_2B_9H_{10}$)-3-Ph-7,8-*nido*-$C_2B_9H_{10}$] for *X*-ray diffraction (at the overleaf structure counter cation, solvents are omitted for clarity).

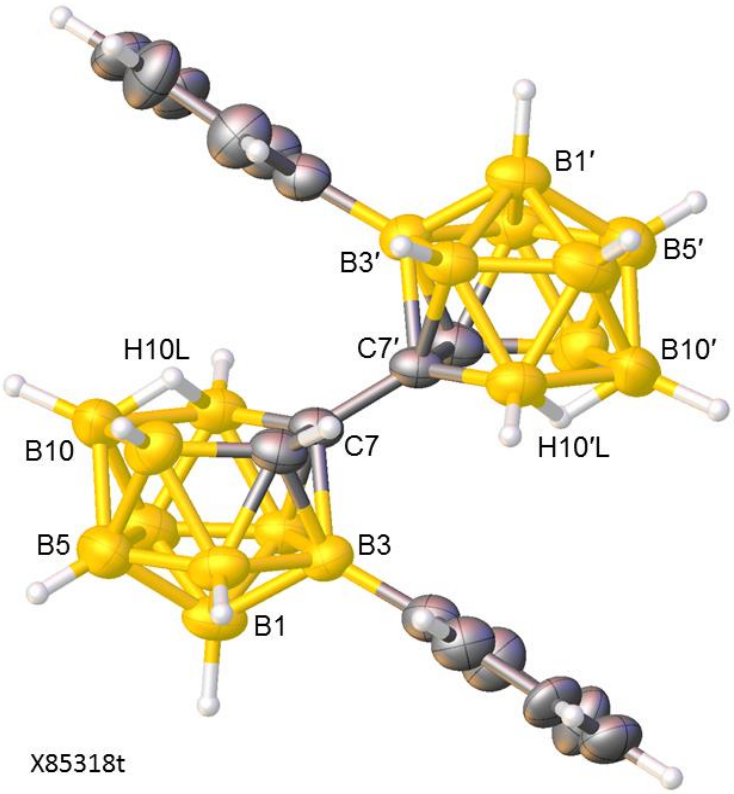
B1′
B3′
B5′
H10L
C7′
B10′
B10
C7
H10′L
B5
B3
B1
X85318t

5.3.9 Synthesis of *rac*-[1-(1′-3′-(dppe)-3′,1′,2′-*closo*^{5}-$NiC_2B_9H_{10}$)-3-(dppe)-3,1,2-*closo*^{5}-$NiC_2B_9H_{10}$] (24) and [1-(2′-4′-(dppe)-4′,1′,2′-*closo*^{5}-$NiC_2B_9H_{10}$)-3-(dppe)-3,1,2-*closo*^{5}-$NiC_2B_9H_{10}$] (25)

Salt **17** (0.60 g, 0.56 mmol) was suspended in dry THF (20 ml) and frozen at -196 °C. [$NiCl_2$(dppe)] (0.59 g, 1.1 mmol) added and the reaction mixture stirred overnight at room temperature affording a green suspension. THF was removed *in vacuo* and the resultant army green reaction mixture was filtered through silica with DCM. The solution was reduced in volume under low pressure and purified by preparative TLC with a mixed eluent of DCM and petrol (60:40). This yielded, along with a trace amount of purple band with R_f = 0.39, two major mobile components, collected as solids. Crystallisations of the lower band yielded compound **24** in pure form.

Army-green R_f = 0.28 Yield = 130 mg, 20% Compound **24**
Army-green R_f = 0.35 Yield = 122 mg, 19% Compound **25**

Compound 24:

rac-[1-(1′-3′-(dppe)-3′,1′,2′-*closo*$^{\upsilon}$-$NiC_2B_9H_{10}$)-3-(dppe)-3,1,2-*closo*$^{\upsilon}$-$NiC_2B_9H_{10}$]

Elemental analysis (CHN)	Required for $C_{56}H_{68}B_{18}Ni_2P_4$: C 57.2, H 5.82%. Found for **24**: C 56.1, H 6.26%.
$^{11}B\{^1H\}$ NMR (CD_2Cl_2)	δ 4.9 (2B), -2.5 (4B), -9.0 (2B), -14.7 (5B), -18.0 (5B).
^1H NMR (CD_2Cl_2)	δ 7.80-7.25 (m, 40H, C_6H_5), 3.29-1.96 (m, 8H, P{CH_2}$_2$P), 1.83 (d, $^3J_{PH}$ = 11.6 Hz, 2H, CH_{cage}).
$^1H\{^{31}P\}$ NMR (CD_2Cl_2)	δ 7.79-7.25 (m, 40H, C_6H_5), 3.29-1.97 (m, 8H, P{CH_2}$_2$P), 1.84 (s, 2H, CH_{cage}).
$^{31}P\{^1H\}$ NMR (CD_2Cl_2)	δ 51.6 (d, $^2J_{PP}$ = 19.9 Hz, 2P), 39.2 (d, $^2J_{PP}$ = 19.9 Hz, 2P).
Mass Spectrometry (EI)	Envelope centred on *m/z* 1176.6 (M^+). [MW = 1177.04 g mol^{-1}].
***X*-Ray Diffraction**	Solvent diffusion of 40-60 petroleum ether into a CH_2Cl_2 solution of **24** at 5 ^oC resulted in suitable quality crystals for *X*-ray diffraction.

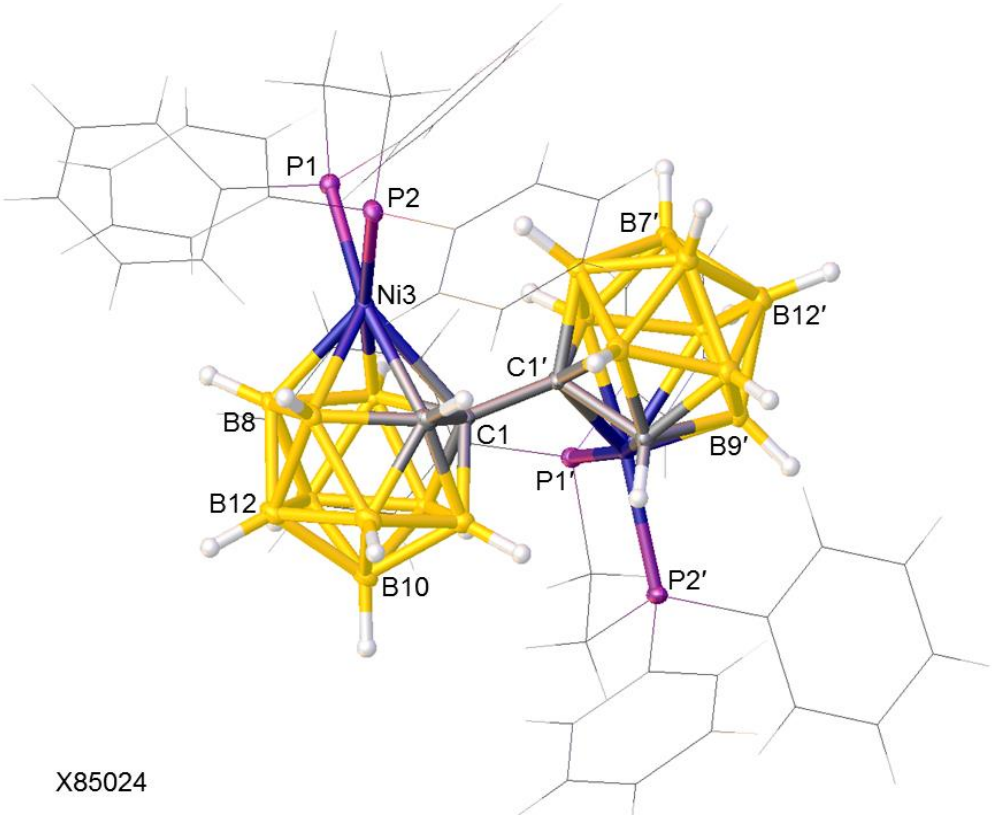

X85024

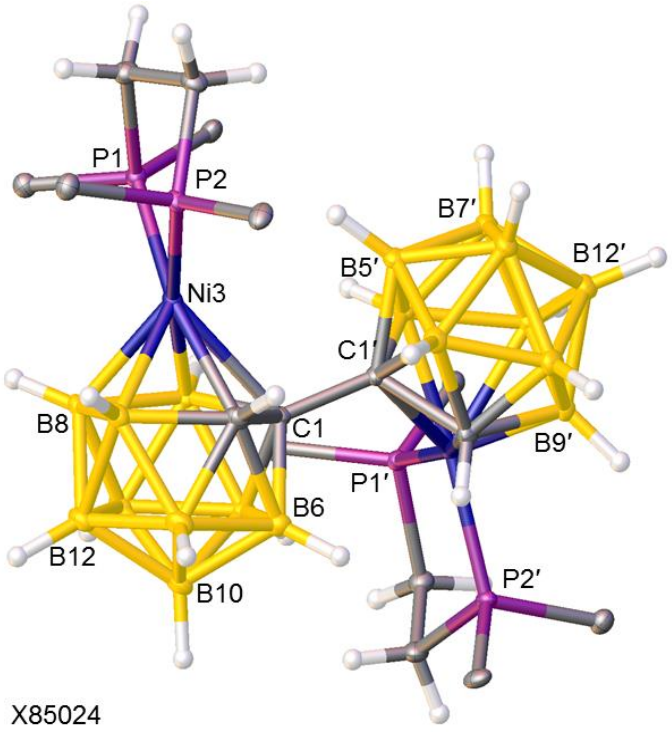

X85024

Compound 25:

[1-(2′-4′-(dppe)-4′,1′,2′-*closo*^{5}-$NiC_2B_9H_{10}$)-3-(dppe)-3,1,2-*closo*^{5}-$NiC_2B_9H_{10}$]

Elemental analysis (CHN) Required for $C_{56}H_{68}B_{18}Ni_2P_4$: C 57.2, H 5.82%.
Required for $C_{56}H_{68}B_{18}Ni_2P_4 \cdot CH_2Cl_2$: C 54.3, H 5.59%.
Found for **25**$\cdot CH_2Cl_2$: C 54.2, H 5.85%.

$^{11}B\{^1H\}$ NMR (CD_2Cl_2) δ 5.9 (1B), 1.7 (1B), -0.2 (1B), -4.6 (3B), -9.8 to -20.4 multiple overlapping resonances with maxima at -9.8, -13.5, -15.6, -16.8, -20.4 (total integral of last five resonances 12B).

^1H NMR (CD_2Cl_2) δ 8.01-7.02 (m, 40H, C_6H_5), 3.67-2.26 (m, 8H, P{CH_2}$_2$P), 1.94 (s, 1H, CH_{cage}), 1.66 (d, $^3J_{PH}$ = 11.2 Hz, 1H, CH_{cage}).

$^1H\{^{31}P\}$ NMR (CD_2Cl_2) δ 8.02-7.01 (m, 40H, C_6H_5), 3.68-2.25 (m, 8H, P{CH_2}$_2$P), 1.95 (s, 1H, CH_{cage}), 1.67 (s, 1H, CH_{cage}).

$^{31}P\{^1H\}$ NMR (CD_2Cl_2) δ 62.9 (s, 2P), 49.4 (d, $^2J_{PP}$ = 16.6 Hz, 1P), 47.5 (d, $^2J_{PP}$ = 16.6 Hz, 1P).

Mass Spectrometry (EI) Envelope centred on *m/z* 1176.6 (M^+).
[MW = 1177.04 g mol^{-1}].

***X*-Ray Diffraction** Solvent diffusion of 40-60 petroleum ether into a CH_2Cl_2 solution of **25** at 5 °C resulted in suitable quality crystals for *X*-ray diffraction.

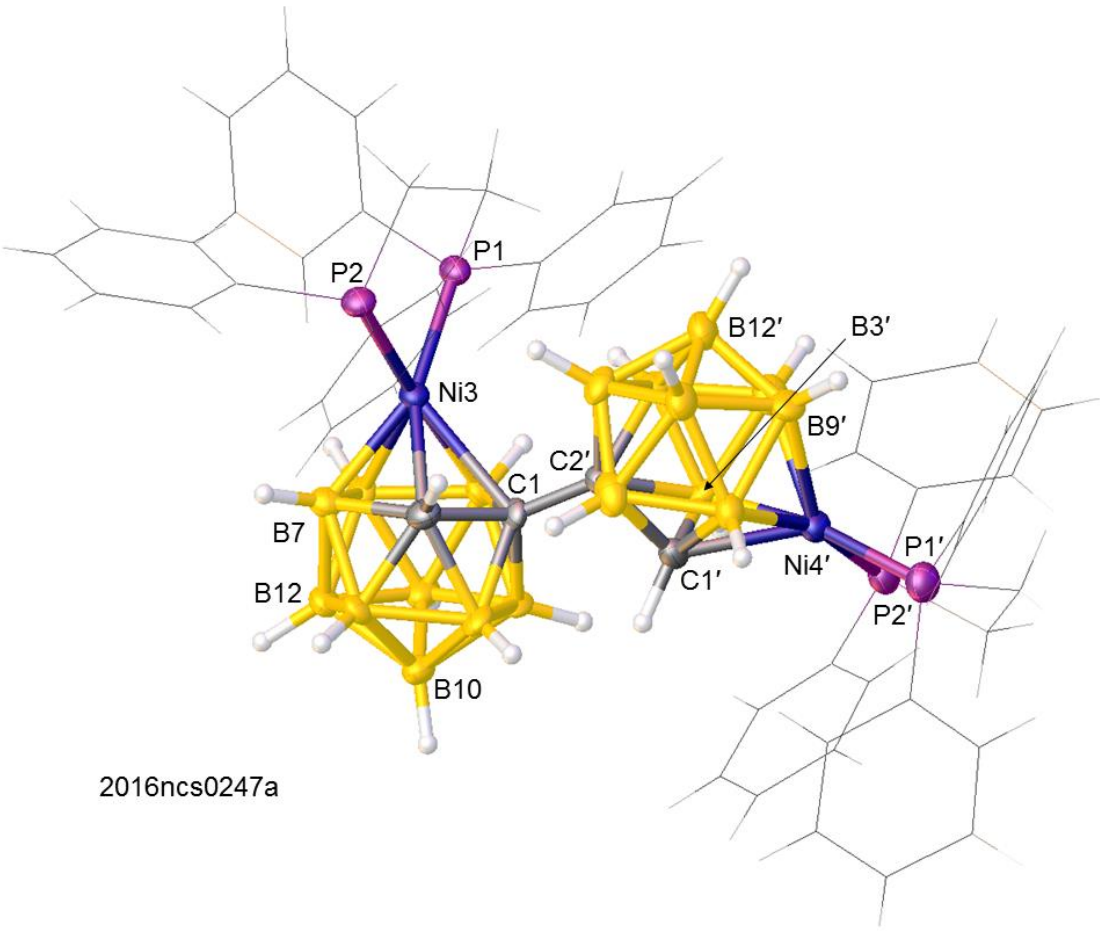

2016ncs0247a

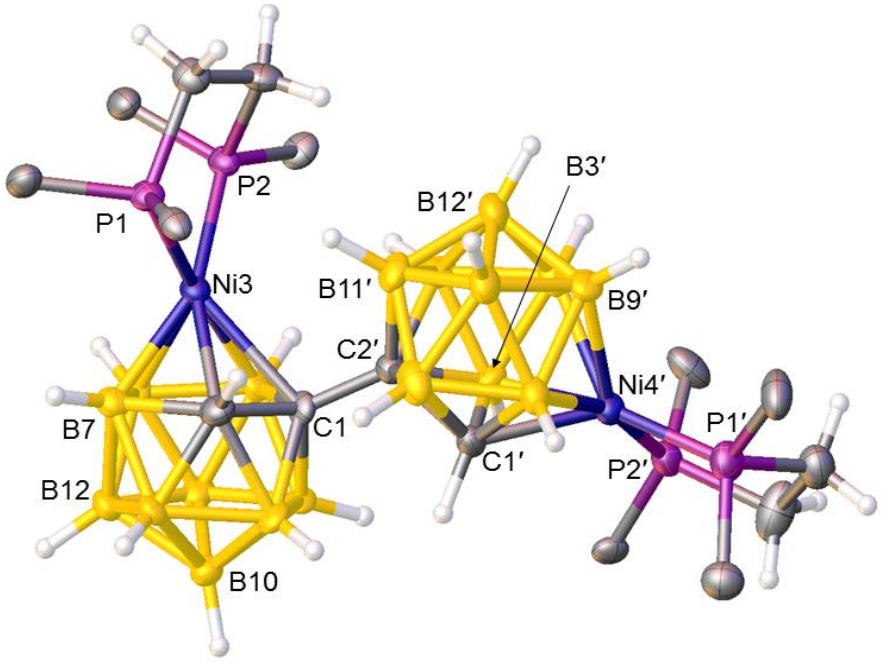

2016ncs0247a

5.3.10 Attempted thermal isomerisation of compound 24 in THF

Compound **24** (0.055 g, 0.047 mmol) was dissolved in THF (10 mL) and the solution heated at reflux for 2.5 hr during which time the colour of the solution remained green. The solvent was removed and purification by preparative TLC using an eluent system of DCM:petroleum ether (60:40) obtained only starting material compound **24**, confirmed by ^{1}H, ^{31}P and ^{11}B NMR spectroscopies.

5.2.11 Thermal isomerisation of compound 24 in toluene: synthesis of [2-(8′-2′-(dppe)-2′,1′,8′-*closo*$^{\circlearrowleft}$-$NiC_2B_9H_{10}$)-4-(dppe)-4,1,2-*closo*$^{\circlearrowleft}$-$NiC_2B_9H_{10}$] (26) and [2-(2′-4′-(dppe)-4′,1′,2′-*closo*$^{\circlearrowleft}$-$NiC_2B_9H_{10}$)-4-(dppe)-4,1,2-*closo*$^{\circlearrowleft}$-$NiC_2B_9H_{10}$] (27)

Compound **24** (0.048 g, 0.040 mmol) was dissolved in toluene (10 mL) and the solution heated at reflux for 2.5 hr, during which time the initially army green solution turned red purple. The solvent was removed under vacuum and the product purified by preparative TLC using an eluent system of DCM:petroleum ether (60:40) to afford, along with a trace yield of red purple band at $R_f = 0.68$, two red purple bands, collected as solids.

Red purple	$R_f = 0.27$	Yield = 15 mg, 31%	Compound **26**
Red purple	$R_f = 0.41$	Yield = 13 mg, 27%	Compound **27**

Compound 26:

[2-(8′-2′-(dppe)-2′,1′,8′-*closo*$^{\circlearrowleft}$-$NiC_2B_9H_{10}$)-4-(dppe)-4,1,2-*closo*$^{\circlearrowleft}$-$NiC_2B_9H_{10}$]

Elemental analysis (CHN) Required for $C_{56}H_{68}B_{18}Ni_2P_4$: C 57.2, H 5.82%.
Found for **26**: C 56.0, H 4.99%.

$^{11}B\{^1H\}$ NMR (CD_2Cl_2) δ 6.8 (2B), -0.2 to -20.5 multiple overlapping resonances with maxima at -0.2, -5.1, -6.7, -13.8, -16.5 -20.5 (total integral of last six resonances 16B).

^1H NMR (CD_2Cl_2) δ 7.78-7.35 (m, 40H, C_6H_5), 2.60-2.19 (m, 8H, $P\{CH_2\}_2P$), 1.98 (s, 1H, CH_{cage}), 1.81 (s, 1H, CH_{cage}).

$^{31}P\{^1H\}$ NMR (CD_2Cl_2) δ 62.7 (s, 2P), 61.5 (br s, very weak) at 298K.
δ 62.6 (s, 2P), 61.5 (br s) at 308K.
δ 68.7 (d, $^2J_{PP}$ = 36.0 Hz, 1P), 65.4 (br s, 1P), 62.2 (br s, 1P), 57.1 (d, $^2J_{PP}$ = 36.0 Hz, 1P) at 203 K.

$^{31}P\{^1H\}$ NMR ($CD_3C_6D_5$) δ 70.7 (s, 2P), 68.7 (br s, very weak) at 298 K.
δ 70.1 (s, 2P), 68.4 (s, 2P) at 343 K.
δ 74.5 (d, $^2J_{PP}$ = 31.6 Hz, 1P), 71.3 (s, 2P), 64.7 (d, $^2J_{PP}$ = 31.6 Hz, 1P) at 203 K.

Mass Spectrometry (EI) Envelope centred on *m/z* 1176.5 (M^+).
[MW = 1177.04 g mol^{-1}].

***X*-Ray Diffraction** Solvent diffusion of 40-60 petroleum ether into a THF solution of **26** at 5 °C resulted in suitable quality crystals for *X*-ray diffraction.

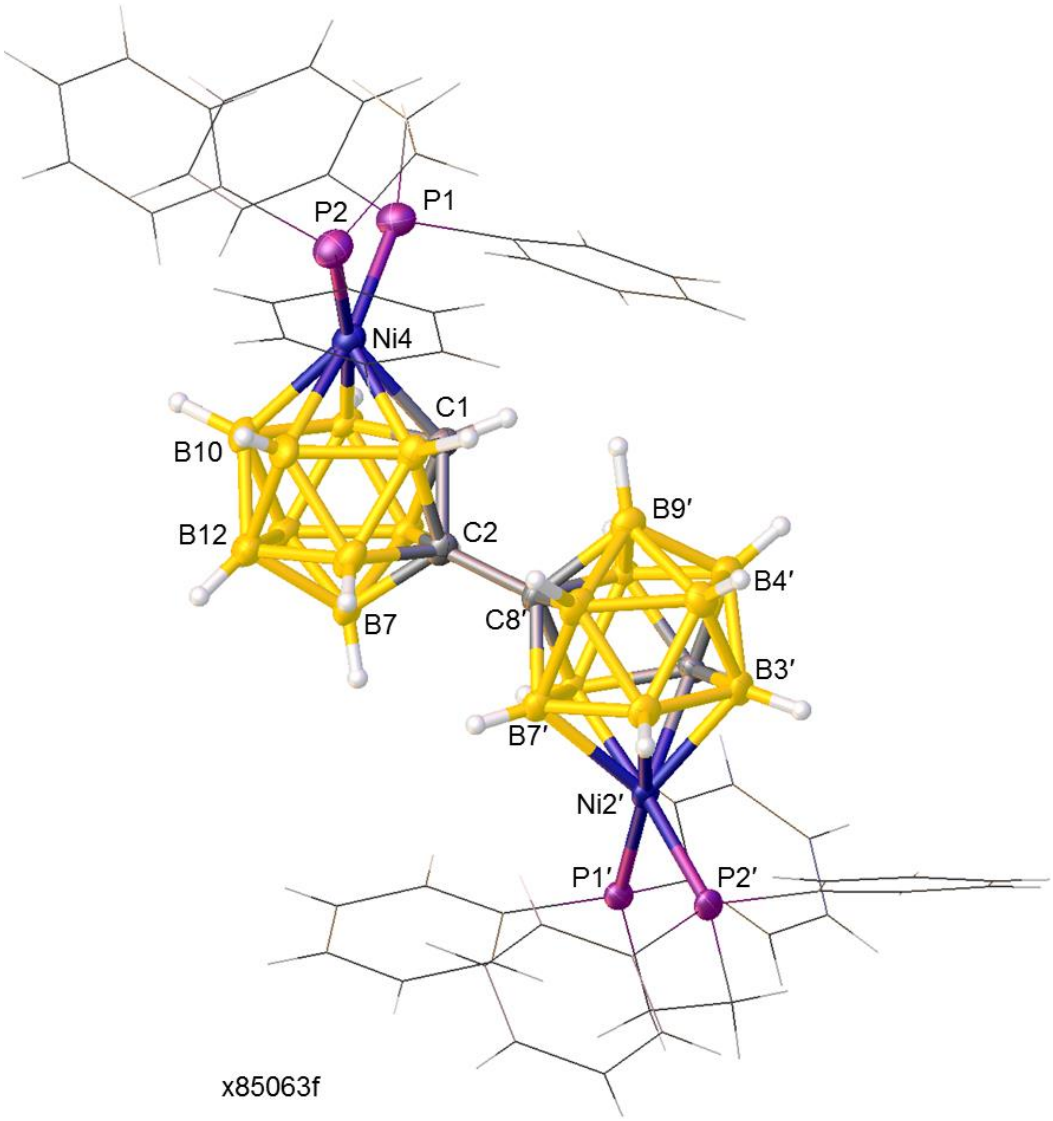
P2
P1
Ni4
C1
B10
B12
C2
B7
B9′
B4′
C8′
B3′
B7′
Ni2′
P1′
P2′
x85063f

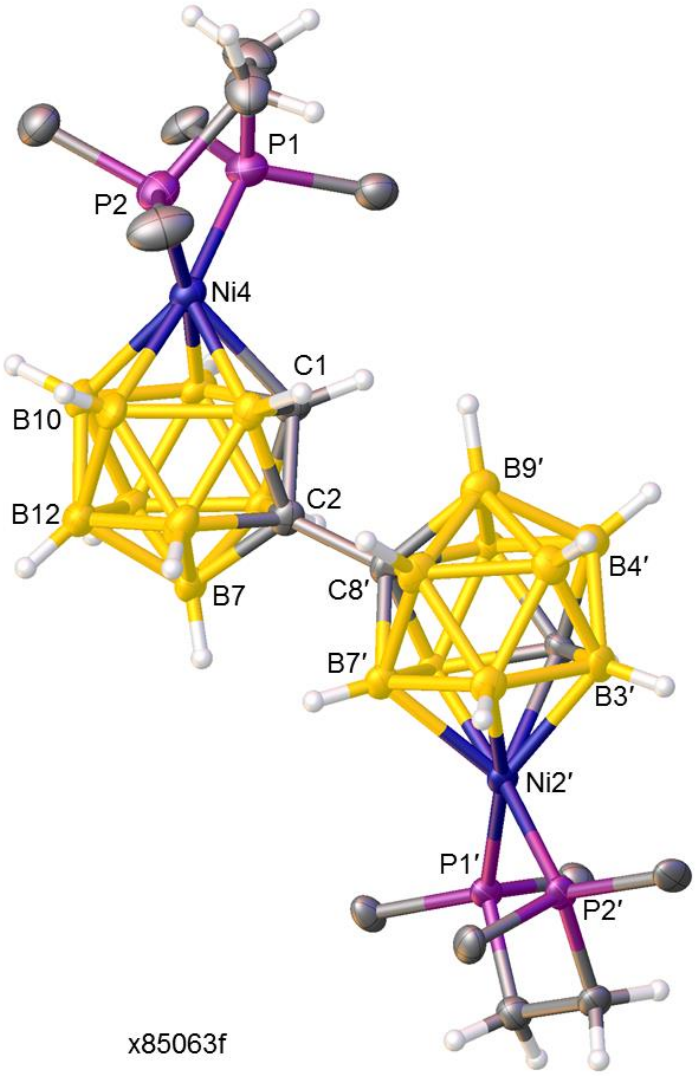
P1
P2
Ni4
C1
B10
B12
C2
B7
B9′
B4′
C8′
B7′
B3′
Ni2′
P1′
P2′
x85063f

Compound 27:

[2-(2′-4′-(dppe)-4′,1′,2′-*closo*^{5}-$NiC_2B_9H_{10}$)-4-(dppe)-4,1,2-*closo*^{5}-$NiC_2B_9H_{10}$]

Elemental analysis (CHN)	Required for $C_{56}H_{68}B_{18}Ni_2P_4$: C 57.2, H 5.82%. Found for **27**: C 56.1, H 5.52%.
$^{11}B\{^1H\}$ NMR (CD_2Cl_2)	δ 6.8 (2B), -5.2 (7B), -13.3 (4B), -16.6 (5B).
^1H NMR (CD_2Cl_2)	δ 7.73-7.35 (m, 40H, C_6H_5), 2.54-2.35 (m, 8H, $P\{CH_2\}_2P$), 2.03 (s, 2H, CH_{cage}).
$^{31}P\{^1H\}$ NMR (CD_2Cl_2)	δ 62.9 (s).
Mass Spectrometry (EI)	Envelope centred on *m/z* 1177.5 (M^+). [MW = 1177.04 g mol^{-1}].
***X*-Ray Diffraction**	Solvent diffusion of 40-60 petroleum ether into a DCM solution of **27** at 5 ^oC resulted in suitable quality crystals for *X*-ray diffraction.

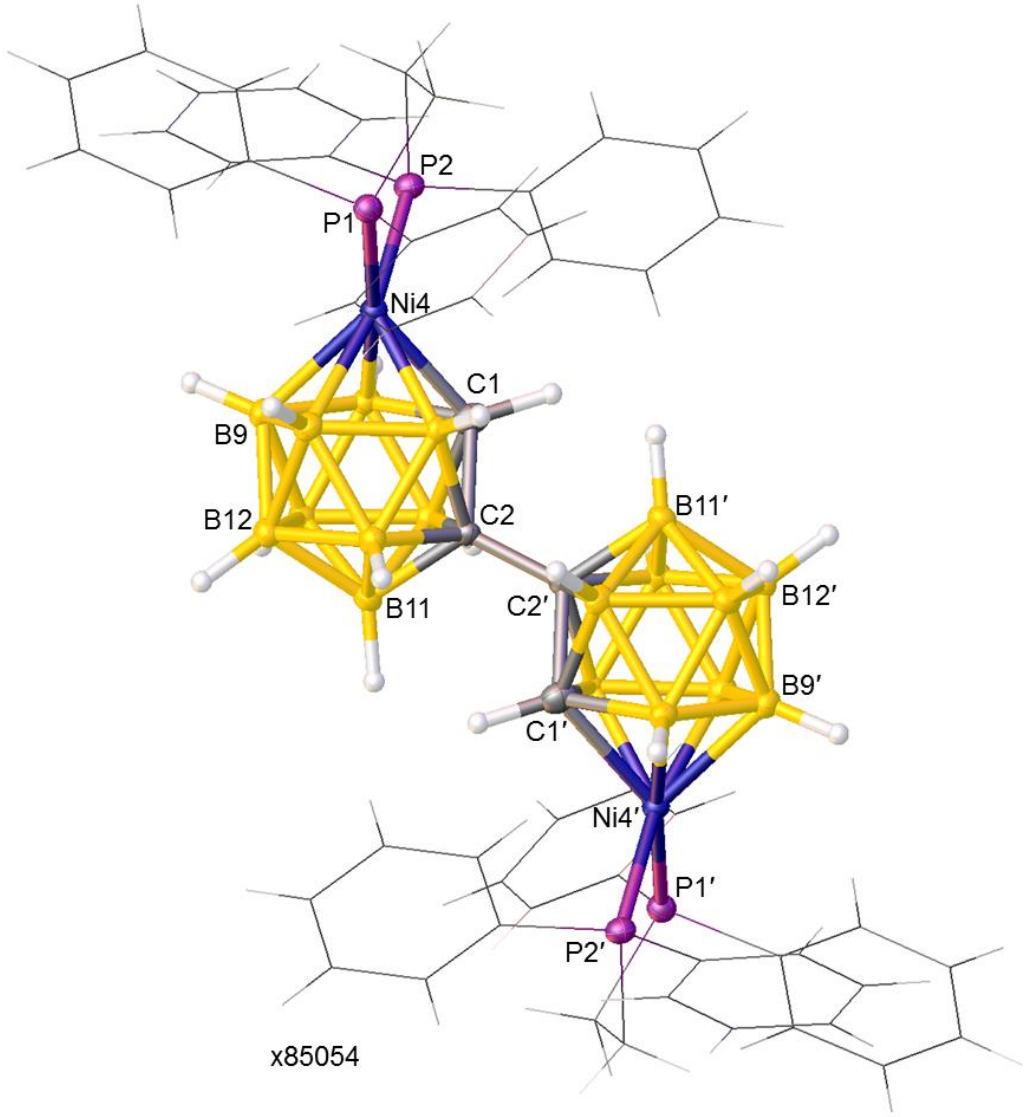
P2
P1
Ni4
C1
B9
B12
C2
B11
B11′
C2′
B12′
B9′
C1′
Ni4′
P1′
P2′
x85054

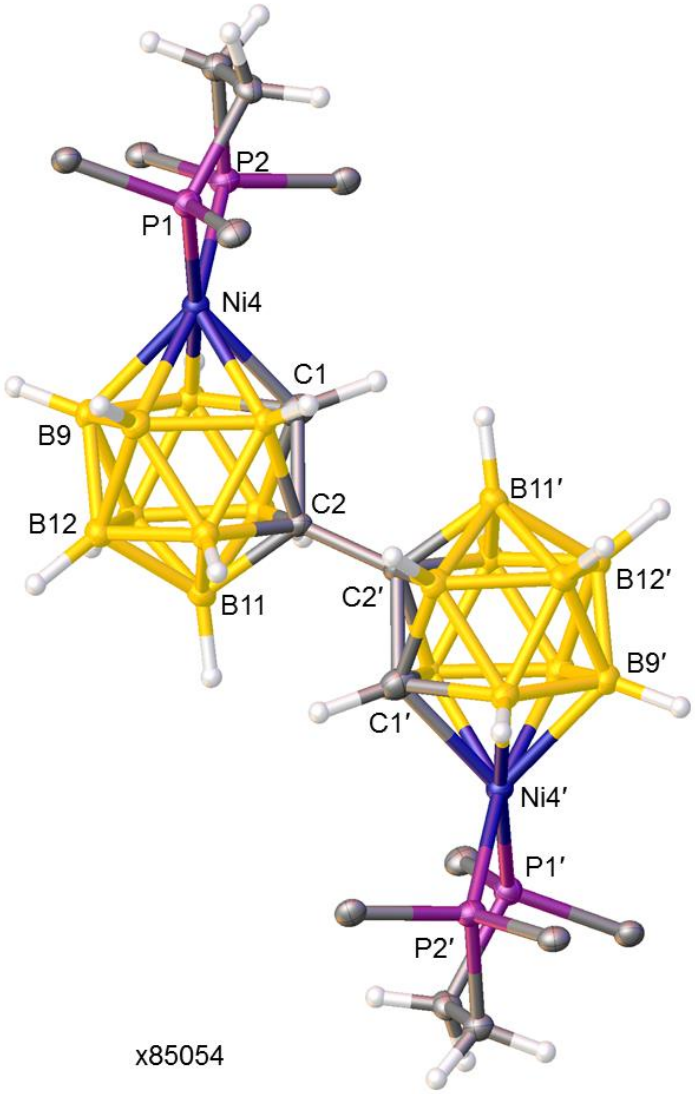
P2
P1
Ni4
C1
B9
B12
C2
B11
B11′
B12′
C2′
B9′
C1′
Ni4′
P1′
P2′
x85054

5.3.12 Attempted thermal isomerisation of compound 25 in THF

Compound **25** (0.045 g, 0.038 mmol) was dissolved in THF (10 mL) and the solution heated at reflux for 2.5 hr. The solution remained the same army green colour. All volatiles were removed under low pressure and purification by preparative TLC using an eluent system of DCM:petroleum ether (60:40) afforded only starting material, confirmed by ^{1}H, ^{31}P and ^{11}B NMR spectroscopies.

5.2.13 Thermal isomerisation of compound 25 in toluene: alternative synthesis of 26 and 27

Compound **25** (0.040 g, 0.033 mmol) was dissolved in toluene (10 mL) and the solution heated at reflux for 2.5 hr during which time the colour changed to red purple from army green. The solvent was removed under vacuum and the product purified by preparative TLC using an eluent system of DCM:petroleum ether (70:30) to afford two red purple bands, subsequently identified as compounds **26**, **27** by ^{1}H, ^{31}P and $^{11}B\{^{1}H\}$ NMR spectroscopies.

Red purple	$R_f = 0.36$	Yield = 16 mg, 40%	Compound **26**
Red purple	$R_f = 0.41$	Yield = 15 mg, 38%	Compound **27**

5.4.1 Thermal isomerisation of *rac* and *meso* isomers of [1-(1'-4'-Cp-4',1',6'-*closo*-$CoC_2B_{10}H_{11}$)-4-Cp-4,1,6-*closo*-$CoC_2B_{10}H_{11}$]: synthesis of *rac*-[1-(1'-4'-Cp-4',1',12'-*closo*-$CoC_2B_{10}H_{11}$)-4-Cp-4,1,12-*closo*-$CoC_2B_{10}H_{11}$] (28) and *meso*-[1-(1'-4'-Cp-4',1',12'-*closo*-$CoC_2B_{10}H_{11}$)-4-Cp-4,1,12-*closo*-$CoC_2B_{10}H_{11}$] (29)

0.20 g (0.37 mmol) of a *rac* and *meso* mixture of [1-(1'-4'-Cp-4',1',6'-*closo*-$CoC_2B_{10}H_{11}$)-4-Cp-4,1,6-*closo*-$CoC_2B_{10}H_{11}$] was dissolved in 15 ml xylenes and heated to reflux at 180 °C for 4 hrs. Following cooling and removal of solvent with a high vacuum pump, separation by preparative TLC* using an eluent system of DCM and petrol 40-60 in the ratio of 20:80 afforded several mobile bands. Two bands were collected as solids.

Orange	R_f = 0.62	Yield = 72 mg, 36%	Compound **28**
Orange	R_f = 0.53	Yield = 65 mg, 32%	Compound **29**

*Other possible isomers with lower R_f value have been observed.

Compound 28:

rac-[1-(1'-4'-Cp-4',1',12'-*closo*-$CoC_2B_{10}H_{11}$)-4-Cp-4,1,12-*closo*-$CoC_2B_{10}H_{11}$]

Elemental analysis (CHN) Required for $C_{14}H_{32}B_{20}Co_2$: C 31.4, H 6.03%.
Found for **28**: C 31.5, H 6.08%.

$^{11}B\{^1H\}$ NMR ($CDCl_3$) δ 8.07 (4B), 3.02 (4B), -3.82 (2B), -7.12 (2B), -8.33 (2B), -9.44 (2B), -15.22 (2B), -16.80 (2B).

^1H NMR ($CDCl_3$) δ 5.34 (s, 10H, C_5H_5), 3.37 (br s, 2H, $C_{cage}H$).

Mass Spectrometry (EI) Envelope centred on *m/z* 534.0 (M^+).
[MW = 534.5 g mol^{-1}].

***X*-Ray Diffraction** Vapour diffusion of petrol 40-60 into a THF solution of **28** at room temperature resulted in suitable quality crystals for *X*-ray diffraction.

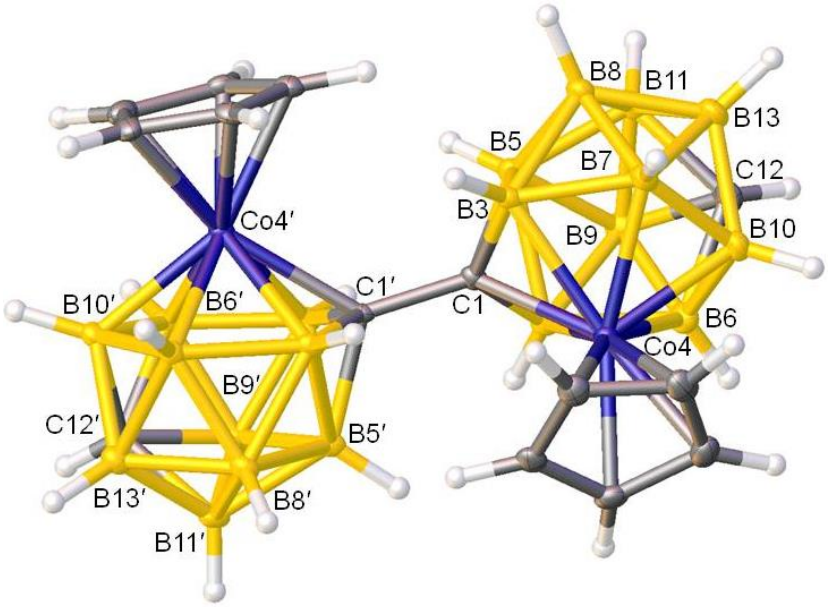

Compound 29:

meso-[1-(1'-4'-Cp-4',1',12'-*closo*-$CoC_2B_{10}H_{11}$)-4-Cp-4,1,12-*closo*-$CoC_2B_{10}H_{11}$]

Elemental analysis (CHN) Required for $C_{14}H_{32}B_{20}Co_2$: C 31.4, H 6.03%.
Found for **29**: C 30.6, H 6.15%.

$^{11}B\{^1H\}$ NMR ($CDCl_3$) δ 8.00 (5B), 3.15 (3B), -3.79 (2B), -7.03 (2B), -7.91 (2B), -9.37 (2B), -15.23 (2B), -16.58 (2B).

^1H NMR ($CDCl_3$) δ 5.41 (s, 5H, C_5H_5), 5.34 (s, 5H, C_5H_5), 3.35 (br s, 1H, $C_{cage}H$), 3.27 (br s, 1H, $C_{cage}H$).

Mass Spectrometry (EI) Envelope centred on *m/z* 534.0 (M^+).
[MW = 534.5 g mol^{-1}].

***X*-Ray Diffraction** Vapour diffusion of petrol 40-60 into a THF solution of **29** at room temperature resulted in suitable quality crystals for *X*-ray diffraction.

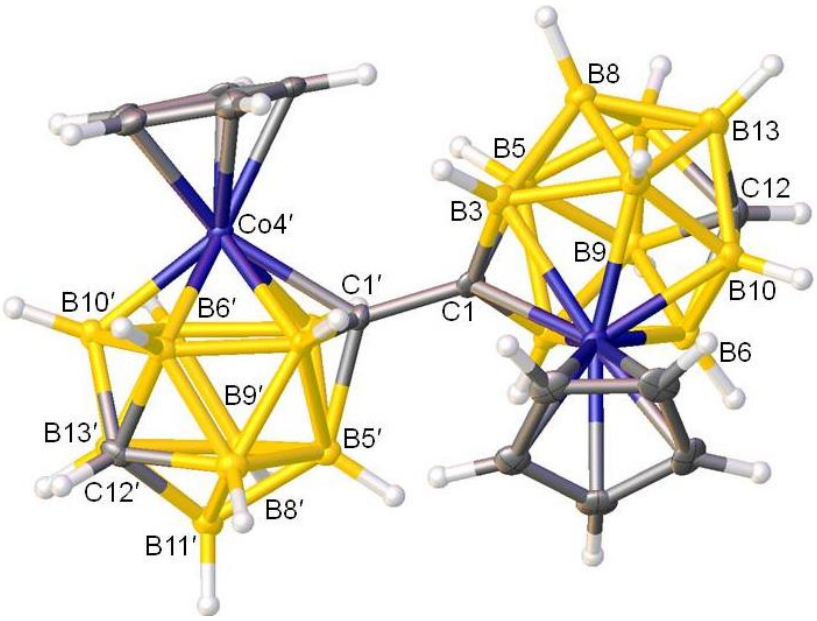

5.5 References

1 S. Ren and Z. Xie, *Organometallics*, 2008, **27**, 5167.

2 G. Thiripuranathar, W. Y. Man, C. Palmero, A. P. Y. Chan, B. T. Leube, D. Ellis, D. McKay, S. A. Macgregor, L. Jourdan, G. M. Rosair and A. J. Welch, *Dalton Trans*., 2015, **44**, 5628.

3 G. Thiripuranathar, *PhD thesis*, Heriot-Watt University, 2011.

4 G. Booth and J. Chatt, *J. Chem. Soc*., 1965, 3238.

5 (a) L. M. Venanzi, *J. Chem. Soc*., 1958, 719; (b) G. Booth and J. Chatt, *J. Chem. Soc*., 1960, 1718.

6 M. S. Kharasch, R. C. Seyler and F. R. Mayo, *J. Am. Chem. Soc*., 1938, **60**, 882.

7 G. Schultz, N. Yu. Subbotina, C. M. Jensen, J. A. Golen and I. Hargittai, *Inorg. Chim. Acta*, 1992, **191**, 85.

8 A. M. Z. Slawin, P. G. Waddell and J. D. Woollins, *Acta Cryst*., 2009, **E65**, m1391.

9 D. W. Meek, *Inorg. Chem*., 1965, **4**, 250.

10 D. A. Handly, P. B. Hitchcock and G. J. Leigh, *Inorg. Chim. Acta*, 2001, **314**, 1.

11 M. M. Lindner, U. Beckmann, W. Frank, and W. Kläui, *ISRN Inorg. Chem*. 2013, **2013**, 1.

12 Th. Renner, *Angew. Chem*., 1957, **69**, 478.

13 *Bruker AXS APEX2, version 2009-5*, Bruker AXS Inc., Madison, Wisconsin, USA, 2009.

14 O. V. Dolomanov, L. J. Bourhis, R. J. Gildea, J. A. K. Howard and H. Puschmann, *J. Appl. Cryst.*, 2009, **42**, 339.

15 L. J. Bourhis, O. V. Dolomanov, R. J. Gildea, J. A. K. Howard and H. Puschmann, *Acta Cryst*., 2015, A**71**, 59.

16 G. M. Sheldrick, *Acta Cryst.*, 2008, A**64**, 112.

17 A. McAnaw, G. Scott, L. Elrick, G. M. Rosair and A. J. Welch, *Dalton Trans*., 2013, **42**, 645.

18 A. McAnaw, M. E. Lopez, D. Ellis, G. M. Rosair and A. J. Welch, *Dalton Trans*., 2014, **43**, 5095.

19 See compound **4** in R. E. King, S. B. Miller, C. B. Knobler and M. F. Hawthorne, *Inorg. Chem*., 1983, **22**, 3548.

Appendix Crystal Data and Structure Refinements

Compound **1**
[1-(1′-1′,2′-*closo*-$C_2B_{10}H_{11}$)-3-dppe-3,1,2-*closo*-$NiC_2B_9H_{10}$]

Identification code	5038
Empirical formula	$C_{34.75}H_{54.75}B_{19}NiOP_2$
Formula weight	814.57
Temperature	100.0(2) K
Wavelength	λ = 0.71073 Å
Crystal system	Monoclinic
Space group	$P2_1/n$
Unit cell dimensions	a = 15.9009(8) Å α = 90°
	b = 15.8294(8) Å β = 109.606(2)°
	c = 18.1091(8) Å γ = 90°
Volume	4293.8(4) $Å^3$
Z	4
Density (calculated)	1.260 g/cm^3
Absorption coefficient	0.557 mm^{-1}
F(000)	1697.0
Crystal size	0.52 × 0.1 × 0.06 mm^3
Theta range for data collection	4.776 to 56.154°
Index ranges	$-20 \le h \le 17$, $-20 \le k \le 18$, $-23 \le l \le 23$
Reflections collected	71344
Independent reflections	10294 [R_{int} = 0.0994, R_{sigma} = 0.0743]
Completeness to theta = 28.08°	98.7%
Absorption correction	Multiscan
Max. and min. transmission	0.746 and 0.548
Refinement method	Full-matrix least-squares on F^2
Data / restraints / parameters	10294 / 0 / 532
Goodness-of-fit on F^2	0.969
Final R indices [I>=2sigma(I)]	R_1 = 0.0429, wR_2 = 0.0974
Final R indices (all data)	R_1 = 0.0731, wR_2 = 0.1055
Largest diff. peak and hole	0.37 and -0.71 e.$Å^{-3}$

Compound **2**
[2-(1′-1′,2′-*closo*-$C_2B_{10}H_{11}$)-4-dppe-4,1,2-*closo*-$NiC_2B_9H_{10}$]

Identification code	5029
Empirical formula	$C_{31}H_{47}B_{19}Cl_2NiP_2$
Formula weight	816.62
Temperature	100.0(2) K
Wavelength	λ = 0.71073 Å
Crystal system	Triclinic
Space group	P-1
Unit cell dimensions	a = 10.2951(8) Å α = 70.135(4)°
	b = 13.7359(10) Å β = 74.434(4)°
	c = 16.4159(13) Å γ = 74.312(4)°
Volume	2061.6(3) $Å^3$
Z	2
Density (calculated)	1.315 g/cm^3
Absorption coefficient	0.704 mm^{-1}
F(000)	840.0
Crystal size	0.44 × 0.24 × 0.08 mm^3
Theta range for data collection	5.402 to 67.978°
Index ranges	$-16 \le h \le 16$, $-20 \le k \le 21$, $-25 \le l \le 25$
Reflections collected	59426
Independent reflections	16558 [R_{int} = 0.0417, R_{sigma} = 0.0505]
Completeness to theta = 33.99°	98.4%
Absorption correction	Multiscan
Max. and min. transmission	0.747and 0.682
Refinement method	Full-matrix least-squares on F^2
Data / restraints / parameters	16558 / 0 / 572
Goodness-of-fit on F^2	1.030
Final R indices [I>=2sigma(I)]	R_1 = 0.0436, wR_2 = 0.0999
Final R indices (all data)	R_1 = 0.0624, wR_2 = 0.1089
Largest diff. peak and hole	1.23 and -0.89 e.$Å^{-3}$

Compound **3**
[8-(1′-1′,2′-*closo*-$C_2B_{10}H_{11}$)-2-dmpe-2,1,8-*closo*-$NiC_2B_9H_{10}$]

Identification code	X85030
Empirical formula	$C_{10}H_{37.05}B_{19}NiP_2$
Formula weight	483.49
Temperature	100.0(2) K
Wavelength	λ = 0.71073 Å
Crystal system	Triclinic
Space group	P-1
Unit cell dimensions	a = 9.0457(7) Å α = 112.101(4)°
	b = 12.1143(10) Å β = 97.903(4)°
	c = 13.0918(11) Å γ = 99.226(4)°
Volume	1280.96(18) $Å^3$
Z	2
Density (calculated)	1.254 g/cm^3
Absorption coefficient	0.883 mm^{-1}
F(000)	500.0
Crystal size	0.36 × 0.26 × 0.1 mm^3
Theta range for data collection	3.44 to 56.66°
Index ranges	$-11 \le h \le 11$, $-15 \le k \le 16$, $-17 \le l \le 16$
Reflections collected	21467
Independent reflections	6101 [R_{int} = 0.0328, R_{sigma} = 0.0380]
Completeness to theta = 28.33°	95.5%
Absorption correction	Multiscan
Max. and min. transmission	0.746 and 0.700
Refinement method	Full-matrix least-squares on F^2
Data / restraints / parameters	6101 / 12 / 384
Goodness-of-fit on F^2	0.980
Final R indices [I>=2sigma(I)]	R_1 = 0.0342, wR_2 = 0.0759
Final R indices (all data)	R_1 = 0.0429, wR_2 = 0.0811
Largest diff. peak and hole	0.76 and -0.62 e.$Å^{-3}$

Compound **4**
[1-(1′-1′,2′-*closo*-$C_2B_{10}H_{11}$)-3,3-$(PMe_3)_2$-3,1,2-*closo*-$NiC_2B_9H_{10}$]

Identification code	5112
Empirical formula	$C_{10}H_{39}B_{19}NiP_2$
Formula weight	485.45
Temperature	100.0(2) K
Wavelength	λ = 0.71073 Å
Crystal system	Monoclinic
Space group	$P2_1/n$
Unit cell dimensions	a = 10.3294(7) Å α = 90°
	b = 29.295(2) Å β = 116.545(3)°
	c = 10.5038(7) Å γ = 90°
Volume	2843.4(4) $Å^3$
Z	4
Density (calculated)	1.134 g/cm^3
Absorption coefficient	0.796 mm^{-1}
F(000)	1008.0
Crystal size	0.42 × 0.16 × 0.12 mm^3
Theta range for data collection	4.598 to 55.528°
Index ranges	$-13 \le h \le 13$, $-38 \le k \le 38$, $-13 \le l \le 13$
Reflections collected	48075
Independent reflections	6682 [R_{int} = 0.0575, R_{sigma} = 0.0427]
Completeness to theta = 27.76°	99.4%
Absorption correction	Multiscan
Max. and min. transmission	0.746 and 0.681
Refinement method	Full-matrix least-squares on F^2
Data / restraints / parameters	6682 / 0 / 359
Goodness-of-fit on F^2	1.072
Final R indices [I>=2sigma(I)]	R_1 = 0.0348, wR_2 = 0.0847
Final R indices (all data)	R_1 = 0.0475, wR_2 = 0.0894
Largest diff. peak and hole	0.35 and -0.30 e.$Å^{-3}$

Compound **5**
[7-(1′-1′,2′-*closo*-$C_2B_{10}H_{11}$)-10-(PMe_3)-7,8-*nido*-$C_2B_9H_{10}$]

Identification code	5311
Empirical formula	$C_7H_{30}B_{19}P$
Formula weight	350.67
Temperature	100.0(2) K
Wavelength	λ = 0.71073 Å
Crystal system	Monoclinic
Space group	$P2_1/n$
Unit cell dimensions	a = 6.6697(5) Å α = 90°
	b = 12.6409(8) Å β = 95.995(3)°
	c = 24.9422(17) Å γ = 90°
Volume	2091.4(3) $Å^3$
Z	4
Density (calculated)	1.114 g/cm^3
Absorption coefficient	0.121 mm^{-1}
F(000)	728.0
Crystal size	0.6 × 0.44 × 0.4 mm^3
Theta range for data collection	4.6 to 53.292°
Index ranges	$-8 \le h \le 8$, $-15 \le k \le 15$, $-31 \le l \le 31$
Reflections collected	29225
Independent reflections	4334 [R_{int} = 0.0409, R_{sigma} = 0.0289]
Completeness to theta = 26.65°	98.6%
Absorption correction	Multiscan
Max. and min. transmission	0.745 and 0.632
Refinement method	Full-matrix least-squares on F^2
Data / restraints / parameters	4334 / 0 / 321
Goodness-of-fit on F^2	1.188
Final R indices [I>=2sigma(I)]	R_1 = 0.0912, wR_2 = 0.2195
Final R indices (all data)	R_1 = 0.0972, wR_2 = 0.2219
Largest diff. peak and hole	0.40 and -0.50 e.$Å^{-3}$

Compound **6**
[1-(1′-1′,2′-*closo*-$C_2B_{10}H_{11}$)-3-Cl-3-PMe_3-8-PMe_3-3,1,2-*closo*-$NiC_2B_9H_9$]

Identification code	5285
Empirical formula	$C_{10}H_{38}B_{19}ClNiP_2$
Formula weight	519.89
Temperature	200 K
Wavelength	λ = 0.71073 Å
Crystal system	Monoclinic
Space group	$P2_1/n$
Unit cell dimensions	a = 11.2413(5) Å α = 90°
	b = 13.8817(6) Å β = 97.664(2)°
	c = 18.1169(7) Å γ = 90°
Volume	2801.9(2) $Å^3$
Z	4
Density (calculated)	1.232 g/cm^3
Absorption coefficient	0.904 mm^{-1}
F(000)	1072.0
Crystal size	0.4 × 0.24 × 0.2 mm^3
Theta range for data collection	3.708 to 57.096°
Index ranges	$-15 \le h \le 15$, $-18 \le k \le 15$, $-24 \le l \le 24$
Reflections collected	50624
Independent reflections	7045 [R_{int} = 0.0520, R_{sigma} = 0.0365]
Completeness to theta = 28.55°	98.7%
Absorption correction	Multiscan
Max. and min. transmission	0.746 and 0.634
Refinement method	Full-matrix least-squares on F^2
Data / restraints / parameters	7045 / 0 / 364
Goodness-of-fit on F^2	1.039
Final R indices [I>=2sigma(I)]	R_1 = 0.0331, wR_2 = 0.0862
Final R indices (all data)	R_1 = 0.0490, wR_2 = 0.0934
Largest diff. peak and hole	0.38 and -0.30 e.$Å^{-3}$

Compound **7**
[1-(1′-1′,2′-*closo*-$C_2B_{10}H_{11}$)-3,3-(PMe_2Ph)$_2$-3,1,2-*closo*-$NiC_2B_9H_{10}$]

Identification code	5106
Empirical formula	$C_{20}H_{43}B_{19}NiP_2$
Formula weight	609.58
Temperature	100.0(2) K
Wavelength	λ = 0.71073 Å
Crystal system	Monoclinic
Space group	$P2_1$
Unit cell dimensions	a = 9.8159(13) Å α = 90°
	b = 11.0792(15) Å β = 90.703(9)°
	c = 14.558(2) Å γ = 90°
Volume	1583.1(4) $Å^3$
Z	2
Density (calculated)	1.279 g/cm^3
Absorption coefficient	0.729 mm^{-1}
F(000)	632.0
Crystal size	0.22 × 0.2 × 0.03 mm^3
Theta range for data collection	4.62 to 49.65°
Index ranges	$-11 \le h \le 9$, $-13 \le k \le 10$, $-17 \le l \le 16$
Reflections collected	17876
Independent reflections	4833 [R_{int} = 0.1330, R_{sigma} = 0.1580]
Completeness to theta = 24.83°	88.0%
Absorption correction	Multiscan
Max. and min. transmission	0.745 and 0.490
Refinement method	Full-matrix least-squares on F^2
Data / restraints / parameters	4833 / 7 / 441
Goodness-of-fit on F^2	1.047
Final R indices [I>=2sigma(I)]	R_1 = 0.0699, wR_2 = 0.1353
Final R indices (all data)	R_1 = 0.1216, wR_2 = 0.1567
Largest diff. peak and hole	0.53 and -0.51 e.$Å^{-3}$
Flack parameter	0.44(4)

Compound **8**
[7-(1′-1′,2′-*closo*-$C_2B_{10}H_{11}$)-10-(PMe_2Ph)-7,8-*nido*-$C_2B_9H_{10}$]

Identification code	5114
Empirical formula	$C_{12}H_{32}B_{19}P$
Formula weight	412.73
Temperature	100.0(2) K
Wavelength	λ = 0.71073 Å
Crystal system	Monoclinic
Space group	$P2_1/n$
Unit cell dimensions	a = 7.0021(9) Å α = 90°
	b = 12.7125(16) Å β = 95.459(3)°
	c = 26.754(3) Å γ = 90°
Volume	2370.7(5) $Å^3$
Z	4
Density (calculated)	1.156 g/cm^3
Absorption coefficient	0.117 mm^{-1}
F(000)	856.0
Crystal size	0.32 × 0.25 × 0.12 mm^3
Theta range for data collection	5.596 to 56.556°
Index ranges	$-9 \le h \le 8$, $-16 \le k \le 16$, $-35 \le l \le 20$
Reflections collected	15432
Independent reflections	5764 [R_{int} = 0.0548, R_{sigma} = 0.0769]
Completeness to theta = 28.28°	97.9%
Absorption correction	Multiscan
Max. and min. transmission	0.746 and 0.699
Refinement method	Full-matrix least-squares on F^2
Data / restraints / parameters	5764 / 5 / 355
Goodness-of-fit on F^2	1.026
Final R indices [I>=2sigma(I)]	R_1 = 0.0587, wR_2 = 0.1334
Final R indices (all data)	R_1 = 0.0882, wR_2 = 0.1481
Largest diff. peak and hole	0.58 and -0.43 e.$Å^{-3}$

Compound **11**
1-(1′-1′,2′-*closo*-$C_2B_{10}H_{11}$)-3-tmeda-3,1,2-*closo*-$PdC_2B_9H_{10}$]

Identification code	5345x
Empirical formula	$C_{10}H_{37}B_{19}N_2Pd$
Formula weight	497.20
Temperature	100.0 K
Wavelength	λ = 0.71073 Å
Crystal system	Monoclinic
Space group	$P2_1/n$
Unit cell dimensions	a = 10.6803(8) Å α = 90°
	b = 14.3903(10) Å β = 90.885(4)°
	c = 16.2382(12) Å γ = 90°
Volume	2495.4(3) $Å^3$
Z	4
Density (calculated)	1.323 g/cm^3
Absorption coefficient	0.747 mm^{-1}
F(000)	1008.0
Crystal size	0.56 × 0.24 × 0.22 mm^3
Theta range for data collection	4.532 to 66.422°
Index ranges	$-16 \le h \le 15$, $-22 \le k \le 22$, $-24 \le l \le 23$
Reflections collected	67551
Independent reflections	9421 [R_{int} = 0.0359, R_{sigma} = 0.0234]
Completeness to theta = 33.21°	98.4%
Absorption correction	Multiscan
Max. and min. transmission	0.747 and 0.682
Refinement method	Full-matrix least-squares on F^2
Data / restraints / parameters	9421 / 0 / 416
Goodness-of-fit on F^2	1.177
Final R indices [I>=2sigma(I)]	R_1 = 0.0589, wR_2 = 0.1193
Final R indices (all data)	R_1 = 0.0678, wR_2 = 0.1232
Largest diff. peak and hole	1.80 and -1.74 e.$Å^{-3}$

Compound **12**
[8-(1′-1′,2′-*closo*-$C_2B_{10}H_{11}$)-2-tmeda-2,1,8-*closo*-$PdC_2B_9H_{10}$]

Identification code	5344
Empirical formula	$C_{10}H_{37}B_{19}N_2Pd$
Formula weight	497.21
Temperature	100.0 K
Wavelength	λ = 0.71073 Å
Crystal system	Triclinic
Space group	P-1
Unit cell dimensions	a = 9.2262(11) Å α = 113.603(6)°
	b = 11.8142(15) Å β = 99.756(6)°
	c = 13.2471(16) Å γ = 98.806(6)°
Volume	1264.4(3) $Å^3$
Z	2
Density (calculated)	1.306 g/cm^3
Absorption coefficient	0.738 mm^{-1}
F(000)	504.0
Crystal size	0.46 × 0.22 × 0.08 mm^3
Theta range for data collection	5.022 to 63.64°
Index ranges	$-13 \le h \le 12$, $-17 \le k \le 16$, $-19 \le l \le 19$
Reflections collected	31302
Independent reflections	8479 [R_{int} = 0.0408, R_{sigma} = 0.0455]
Completeness to theta = 31.82°	98.1%
Absorption correction	Multiscan
Max. and min. transmission	0.746 and 0.669
Refinement method	Full-matrix least-squares on F^2
Data / restraints / parameters	8479 / 0 / 398
Goodness-of-fit on F^2	1.053
Final R indices [I>=2sigma(I)]	R_1 = 0.0312, wR_2 = 0.0608
Final R indices (all data)	R_1 = 0.0381, wR_2 = 0.0632
Largest diff. peak and hole	1.02 and -1.08 e.$Å^{-3}$

Compound **13**
[1-(1′-1′,2′-*closo*-$C_2B_{10}H_{11}$)-3,3-{$P(OMe)_3$}$_2$-3,1,2-*closo*-$NiC_2B_9H_{10}$]

Identification code	5420
Empirical formula	$C_{10}H_{39}B_{19}O_6P_2Ni$
Formula weight	581.45
Temperature	100.0 K
Wavelength	λ = 0.71073 Å
Crystal system	Triclinic
Space group	P-1
Unit cell dimensions	a = 11.0321(11) Å α = 109.302(4)°
	b = 11.6703(12) Å β = 95.518(5)°
	c = 11.8503(11) Å γ = 93.573(6)°
Volume	1426.1(2) $Å^3$
Z	2
Density (calculated)	1.354 g/cm^3
Absorption coefficient	0.820 mm^{-1}
F(000)	600.0
Crystal size	0.36 × 0.16 × 0.08 mm^3
Theta range for data collection	5.522 to 52.09°
Index ranges	$-13 \le h \le 13$, $-14 \le k \le 13$, $0 \le l \le 14$
Reflections collected	28465
Independent reflections	5415 [R_{int} = 0.0850, R_{sigma} = 0.0666]
Completeness to theta = 26.05°	96.0%
Absorption correction	Multiscan
Max. and min. transmission	0.745 and 0.557
Refinement method	Full-matrix least-squares on F^2
Data / restraints / parameters	5415 / 0 / 413
Goodness-of-fit on F^2	1.020
Final R indices [I>=2sigma(I)]	R_1 = 0.0419, wR_2 = 0.0992
Final R indices (all data)	R_1 = 0.0655, wR_2 = 0.1106
Largest diff. peak and hole	0.45 and -0.51 e.$Å^{-3}$

Compound **14**
[1-(1′-1′,2′-*closo*-$C_2B_{10}H_{11}$)-2,2-{$P(OMe)_3$}$_2$-2,1,8-*closo*-$NiC_2B_9H_{10}$]

Identification code	5478
Empirical formula	$C_{10}H_{39}B_{19}O_6P_2Ni$
Formula weight	581.45
Temperature	100.0 K
Wavelength	λ = 0.71073 Å
Crystal system	Triclinic
Space group	P-1
Unit cell dimensions	a = 10.2399(12) Å α = 78.502(7)°
	b = 10.9998(13) Å β = 89.803(6)°
	c = 13.1020(15) Å γ = 78.700(6)°
Volume	1417.1(3) $Å^3$
Z	2
Density (calculated)	1.363 g/cm^3
Absorption coefficient	0.826 mm^{-1}
F(000)	600.0
Crystal size	0.38 × 0.32 × 0.08 mm^3
Theta range for data collection	5.012 to 62.176°
Index ranges	$-14 \le h \le 14$, $-15 \le k \le 12$, $-18 \le l \le 13$
Reflections collected	33480
Independent reflections	8810 [R_{int} = 0.0487, R_{sigma} = 0.0536]
Completeness to theta = 31.09°	96.9%
Absorption correction	Multiscan
Max. and min. transmission	0.746 and 0.689
Refinement method	Full-matrix least-squares on F^2
Data / restraints / parameters	8810 / 0 / 412
Goodness-of-fit on F^2	1.057
Final R indices [I>=2sigma(I)]	R_1 = 0.0376, wR_2 = 0.0809
Final R indices (all data)	R_1 = 0.0548, wR_2 = 0.0881
Largest diff. peak and hole	0.43 and -0.58 e.$Å^{-3}$

Compound **18**
rac-[1-(1′-3′-(dmpe)-3′,1′,2′-*closo*^{5}-$NiC_2B_9H_{10}$)-3-(dmpe)-3,1,2-*closo*^{5}-$NiC_2B_9H_{10}$]

Identification code	3636n
Empirical formula	$C_{16}H_{52}B_{18}P_4Ni_2$
Formula weight	680.45
Temperature	100.15 K
Wavelength	λ = 0.71073 Å
Crystal system	Monoclinic
Space group	P2/n
Unit cell dimensions	a = 13.6195(9) Å α = 90°
	b = 8.7239(5) Å β = 100.316(3)°
	c = 14.3241(9) Å γ = 90°
Volume	1674.41(18) Å^3
Z	2
Density (calculated)	1.350 g/cm^3
Absorption coefficient	1.328 mm^{-1}
F(000)	708.0
Crystal size	0.38 × 0.36 × 0.2 mm^3
Theta range for data collection	5.572 to 52.748°
Index ranges	-17 ≤ h ≤ 16, 0 ≤ k ≤ 10, 0 ≤ l ≤ 17
Reflections collected	46391
Independent reflections	3481 [R_{int} = 0.0436, R_{sigma} = 0.0270]
Completeness to theta = 26.37°	101.7%
Absorption correction	Multiscan
Max. and min. transmission	0.745 and 0.649
Refinement method	Full-matrix least-squares on F^2
Data / restraints / parameters	3481 / 0 / 216
Goodness-of-fit on F^2	1.056
Final R indices [I>=2sigma(I)]	R_1 = 0.0225, wR_2 = 0.0506
Final R indices (all data)	R_1 = 0.0260, wR_2 = 0.0519
Largest diff. peak and hole	0.30 and -0.27 e.Å^{-3}

Compound **19**
meso-[1-(1′-3′-(dmpe)-3′,1′,2′-*closo*^{5}-$NiC_2B_9H_{10}$)-3-(dmpe)-3,1,2-*closo*^{5}-$NiC_2B_9H_{10}$]

Identification code	X83603
Empirical formula	$C_{19}H_{58}B_{18}Cl_6Ni_2P_4$
Formula weight	935.24
Temperature	100(2) K
Wavelength	λ = 0.71073 Å
Crystal system	Triclinic
Space group	P-1
Unit cell dimensions	a = 11.4867(6) Å α = 96.986(3)°
	b = 12.5327(6) Å β = 90.037(3)°
	c = 15.0938(8) Å γ = 91.277(2)°
Volume	2156.21(19) Å^3
Z	2
Density (calculated)	1.440 g/cm^3
Absorption coefficient	1.412 mm^{-1}
F(000)	960.0
Crystal size	0.62 × 0.2 × 0.06 mm^3
Theta range for data collection	4.462 to 52.206°
Index ranges	-14 ≤ h ≤ 14, -15 ≤ k ≤ 15, -18 ≤ l ≤ 18
Reflections collected	29045
Independent reflections	8280 [R_{int} = 0.0517, R_{sigma} = 0.0657]
Completeness to theta = 26.1°	96.6%
Absorption correction	Multiscan
Max. and min. transmission	0.920 and 0.475
Refinement method	Full-matrix least-squares on F^2
Data / restraints / parameters	8280 / 6 / 520
Goodness-of-fit on F^2	1.030
Final R indices [I>=2sigma(I)]	R_1 = 0.0427, wR_2 = 0.0892
Final R indices (all data)	R_1 = 0.0752, wR_2 = 0.0996
Largest diff. peak and hole	0.87 and -0.79 e.Å^{-3}

Compound **20**
[7-(7′-7′,8′-*nido*-$C_2B_9H_{12}$)-7,8-*nido*-$C_2B_9H_{12}$]

Identification code	5153
Empirical formula	$C_4H_{24}B_{18}$
Formula weight	266.81
Temperature	100.0 K
Wavelength	λ = 0.71073 Å
Crystal system	Monoclinic
Space group	$P2_1/n$
Unit cell dimensions	a = 6.9679(14) Å α = 90°
	b = 9.5156(16) Å β = 90.414(11)°
	c = 12.319(2) Å γ = 90°
Volume	816.8(3) Å^3
Z	2
Density (calculated)	1.085 g/cm^3
Absorption coefficient	0.044 mm^{-1}
F(000)	276.0
Crystal size	0.38 × 0.18 × 0.1 mm^3
Theta range for data collection	5.41 to 61.552°
Index ranges	-9 ≤ h ≤ 9, -13 ≤ k ≤ 13, -17 ≤ l ≤ 17
Reflections collected	12027
Independent reflections	2531 [R_{int} = 0.0554, R_{sigma} = 0.0520]
Completeness to theta = 30.78°	99.6%
Absorption correction	Multiscan
Max. and min. transmission	0.746 and 0.679
Refinement method	Full-matrix least-squares on F^2
Data / restraints / parameters	2531 / 0 / 155
Goodness-of-fit on F^2	1.057
Final R indices [I>=2sigma(I)]	R_1 = 0.0485, wR_2 = 0.1251
Final R indices (all data)	R_1 = 0.0760, wR_2 = 0.1406
Largest diff. peak and hole	0.26 and -0.28 e.Å^{-3}

Compound **21**
rac-[1-(1′-3′-Ph-1′,2′-*closo*^{5}-$C_2B_{10}H_{10}$)-3-Ph-1,2-*closo*^{5}-$C_2B_{10}H_{10}$]

Identification code	5279
Empirical formula	$C_{16}H_{30}B_{20}$
Formula weight	438.60
Temperature	100.0 K
Wavelength	λ = 0.71073 Å
Crystal system	Monoclinic
Space group	C2/c
Unit cell dimensions	a = 12.9387(8) Å α = 90°
	b = 13.6960(10) Å β = 94.630(4)°
	c = 13.8958(8) Å γ = 90°
Volume	2454.4(3) Å^3
Z	4
Density (calculated)	1.187 g/cm^3
Absorption coefficient	0.055 mm^{-1}
F(000)	904.0
Crystal size	0.42 × 0.24 × 0.1 mm^3
Theta range for data collection	5.096 to 62.126°
Index ranges	-18 ≤ h ≤ 18, -19 ≤ k ≤ 19, -19 ≤ l ≤ 20
Reflections collected	25674
Independent reflections	3893 [R_{int} = 0.0564, R_{sigma} = 0.0394]
Completeness to theta = 31.06°	98.8%
Absorption correction	Multiscan
Max. and min. transmission	0.746 and 0.677
Refinement method	Full-matrix least-squares on F^2
Data / restraints / parameters	3893 / 0 / 193
Goodness-of-fit on F^2	1.041
Final R indices [I>=2sigma(I)]	R_1 = 0.0426, wR_2 = 0.1077
Final R indices (all data)	R_1 = 0.0643, wR_2 = 0.1201
Largest diff. peak and hole	0.36 and -0.24 e.Å^{-3}

Compound **22**
meso-[1-(1′-3′-Ph-1′,2′-*closo*$^{\cup}$-$C_2B_{10}H_{10}$)-3-Ph-1,2-*closo*$^{\cup}$-$C_2B_{10}H_{10}$]

Identification code	x85284
Empirical formula	$C_{16}H_{30}B_{20}$
Formula weight	438.60
Temperature	100.0(2) K
Wavelength	λ = 0.71073 Å
Crystal system	Monoclinic
Space group	$P2_1/n$
Unit cell dimensions	a = 15.1939(13) Å α = 90°
	b = 8.9446(7) Å β = 105.955(5)°
	c = 18.7010(14) Å γ = 90°
Volume	2443.6(3) Å^3
Z	4
Density (calculated)	1.192 g/cm^3
Absorption coefficient	0.055 mm^{-1}
F(000)	904.0
Crystal size	0.42 × 0.38 × 0.22 mm^3
Theta range for data collection	3.07 to 54.198°
Index ranges	-19 ≤ h ≤ 19, -11 ≤ k ≤ 11, -23 ≤ l ≤ 23
Reflections collected	42036
Independent reflections	5395 [R_{int} = 0.0641, R_{sigma} = 0.0446]
Completeness to theta = 27.10°	100%
Absorption correction	Multiscan
Max. and min. transmission	0.746 and 0.713
Refinement method	Full-matrix least-squares on F^2
Data / restraints / parameters	5395 / 0 / 385
Goodness-of-fit on F^2	1.030
Final R indices [I>=2sigma(I)]	R_1 = 0.0488, wR_2 = 0.1157
Final R indices (all data)	R_1 = 0.0725, wR_2 = 0.1281
Largest diff. peak and hole	0.24 and -0.27 e.Å^{-3}

Compound ([BTMA]$_2$[**23**])
[BTMA]$_2$[7-(7′-3′-Ph-7′,8′-*nido*-$C_2B_9H_{11}$)-3-Ph-7,8-*nido*-$C_2B_9H_{11}$]

Identification code	5318T
Empirical formula	$C_{36.85}H_{63.7}B_{18}Cl_{1.7}N_2$
Formula weight	789.64
Temperature	100.0 K
Wavelength	λ = 0.71073 Å
Crystal system	Monoclinic
Space group	C2/c
Unit cell dimensions	a = 31.758(7) Å α = 90°
	b = 10.095(2) Å β = 121.92(2)°
	c = 16.939(5) Å γ = 90°
Volume	4610(2) Å^3
Z	4
Density (calculated)	1.138 g/cm^3
Absorption coefficient	0.154 mm^{-1}
F(000)	1671.0
Crystal size	0.22 × 0.2 × 0.06 mm^3
Theta range for data collection	4.308 to 47.338°
Index ranges	-35 ≤ h ≤ 34, -10 ≤ k ≤ 11, -18 ≤ l ≤ 18
Reflections collected	19897
Independent reflections	3412 [R_{int} = 0.1633, R_{sigma} = 0.1695]
Completeness to theta = 23.67°	98.1%
Absorption correction	Multiscan
Max. and min. transmission	0.745 and 0.567
Refinement method	Full-matrix least-squares on F^2
Data / restraints / parameters	3412 / 2 / 349
Goodness-of-fit on F^2	1.001
Final R indices [I>=2sigma(I)]	R_1 = 0.0823, wR_2 = 0.1873
Final R indices (all data)	R_1 = 0.2114, wR_2 = 0.2465
Largest diff. peak and hole	0.35 and -0.20 e.Å^{-3}

Compound **24**
rac-[1-(1′-3′-(dppe)-3′,1′,2′-*closo*$^{\cup}$-$NiC_2B_9H_{10}$)-3-(dppe)-3,1,2-*closo*$^{\cup}$-$NiC_2B_9H_{10}$]

Identification code	5024
Empirical formula	$C_{59}H_{74}B_{18}Cl_6Ni_2P_4$
Formula weight	1431.76
Temperature	100.0 K
Wavelength	λ = 0.71073 Å
Crystal system	Monoclinic
Space group	C2/c
Unit cell dimensions	a = 25.0952(8) Å α = 90°
	b = 14.9165(5) Å β = 113.620(2)°
	c = 19.7053(6) Å γ = 90°
Volume	6758.4(4) Å^3
Z	4
Density (calculated)	1.407 g/cm^3
Absorption coefficient	0.929 mm^{-1}
F(000)	2944.0
Crystal size	0.32 × 0.2 × 0.16 mm^3
Theta range for data collection	5.584 to 58.27°
Index ranges	-34 ≤ h ≤ 34, -20 ≤ k ≤ 20, -26 ≤ l ≤ 26
Reflections collected	59135
Independent reflections	8989 [R_{int} = 0.0510, R_{sigma} = 0.0432]
Completeness to theta = 29.14°	98.8%
Absorption correction	Multiscan
Max. and min. transmission	0.746 and 0.689
Refinement method	Full-matrix least-squares on F^2
Data / restraints / parameters	8989 / 8 / 445
Goodness-of-fit on F^2	1.013
Final R indices [I>=2sigma(I)]	R_1 = 0.0391, wR_2 = 0.0883
Final R indices (all data)	R_1 = 0.0600, wR_2 = 0.0970
Largest diff. peak and hole	0.64 and -1.01 e.Å^{-3}

Compound **25**
[1-(2′-4′-(dppe)-4′,1′,2′-*closo*$^{\cup}$-$NiC_2B_9H_{10}$)-3-(dppe)-3,1,2-*closo*$^{\cup}$-$NiC_2B_9H_{10}$]

Identification code	2016ncs0247
Empirical formula	$C_{59}H_{74}B_{18}Ni_2P_4Cl_6$
Formula weight	1431.76
Temperature	100.0 K
Wavelength	λ = 0.71073 Å
Crystal system	Orthorhombic
Space group	$P2_12_12_1$
Unit cell dimensions	a = 10.2816(4) Å α = 90°
	b = 20.3356(9) Å β = 90°
	c = 32.3413(14) Å γ = 90°
Volume	6762.0(5) Å^3
Z	4
Density (calculated)	1.406 g/cm^3
Absorption coefficient	0.928 mm^{-1}
F(000)	2944.0
Crystal size	0.42 × 0.02 × 0.015 mm^3
Theta range for data collection	4.2 to 55.12°
Index ranges	-13 ≤ h ≤ 9, -26 ≤ k ≤ 26, -41 ≤ l ≤ 42
Reflections collected	45269
Independent reflections	15482 [R_{int} = 0.1066, R_{sigma} = 0.1363]
Completeness to theta = 27.56°	99.0%
Absorption correction	Multiscan
Max. and min. transmission	1.000 and 0.303
Refinement method	Full-matrix least-squares on F^2
Data / restraints / parameters	15482 / 33 / 792
Goodness-of-fit on F^2	0.953
Final R indices [I>=2sigma(I)]	R_1 = 0.0775, wR_2 = 0.1701
Final R indices (all data)	R_1 = 0.1200, wR_2 = 0.1879
Largest diff. peak and hole	0.52 and -0.72 e.Å^{-3}
Flack parameter	0.12(2)

Compound **26**
[2-(8′-2′-(dppe)-2′,1′,8′-*closo*$^{\circlearrowleft}$-$NiC_2B_9H_{10}$)-4-(dppe)-4,1,2-*closo*$^{\circlearrowleft}$-$NiC_2B_9H_{10}$]

Identification code	5063f
Empirical formula	$C_{76}H_{108}B_{18}P_4Ni_2O_5$
Formula weight	1537.50
Temperature	100.0 K
Wavelength	λ = 0.71073 Å
Crystal system	Monoclinic
Space group	C2/c
Unit cell dimensions	a = 30.740(5) Å α = 90°
	b = 13.951(2) Å β = 107.473(6)°
	c = 38.880(6) Å γ = 90°
Volume	15904(5) Å^3
Z	8
Density (calculated)	1.284 g/cm^3
Absorption coefficient	0.604 mm^{-1}
F(000)	6480.0
Crystal size	0.2 × 0.17 × 0.15 mm^3
Theta range for data collection	2.778 to 54.004°
Index ranges	-39 ≤ h ≤ 37, -17 ≤ k ≤ 13, -43 ≤ l ≤ 49
Reflections collected	116035
Independent reflections	17228 [R_{int} = 0.0653, R_{sigma} = 0.0597]
Completeness to theta = 27.00°	99.1%
Absorption correction	Multiscan
Max. and min. transmission	0.746 and 0.683
Refinement method	Full-matrix least-squares on F^2
Data / restraints / parameters	17228 / 0 / 781
Goodness-of-fit on F^2	1.111
Final R indices [I>=2sigma(I)]	R_1 = 0.0611, wR_2 = 0.1747
Final R indices (all data)	R_1 = 0.0898, wR_2 = 0.1843
Largest diff. peak and hole	0.60 and -0.54 e.Å^{-3}

Compound **27**
[2-(2′-4′-(dppe)-4′,1′,2′-*closo*$^{\circlearrowleft}$-$NiC_2B_9H_{10}$)-4-(dppe)-4,1,2-*closo*$^{\circlearrowleft}$-$NiC_2B_9H_{10}$]

Identification code	5054
Empirical formula	$C_{56}H_{68}B_{18}Ni_2P_4$
Formula weight	1176.98
Temperature	100.0 K
Wavelength	λ = 0.71073 Å
Crystal system	Monoclinic
Space group	$P2_1/n$
Unit cell dimensions	a = 11.3872(10) Å α = 90°
	b = 16.4978(14) Å β = 109.049(4)°
	c = 16.8857(15) Å γ = 90°
Volume	2998.5(5) Å^3
Z	2
Density (calculated)	1.304 g/cm^3
Absorption coefficient	0.773 mm^{-1}
F(000)	1220.0
Crystal size	0.18 × 0.16 × 0.12 mm^3
Theta range for data collection	4.542 to 52.368°
Index ranges	-13 ≤ h ≤ 14, -17 ≤ k ≤ 20, -17 ≤ l ≤ 20
Reflections collected	39285
Independent reflections	5931 [R_{int} = 0.1151, R_{sigma} = 0.1012]
Completeness to theta = 26.18°	98.7%
Absorption correction	Multiscan
Max. and min. transmission	0.745 and 0.684
Refinement method	Full-matrix least-squares on F^2
Data / restraints / parameters	5931 / 0 / 391
Goodness-of-fit on F^2	1.024
Final R indices [I>=2sigma(I)]	R_1 = 0.0494, wR_2 = 0.0934
Final R indices (all data)	R_1 = 0.1050, wR_2 = 0.1106
Largest diff. peak and hole	0.38 and -0.44 e.Å^{-3}

Compound **28**
rac-[1-(1′-4′-Cp-4′,1′,12′-*closo*-$CoC_2B_{10}H_{11}$)-4-Cp-4,1,12-*closo*-$CoC_2B_{10}H_{11}$)]

Identification code	4943
Empirical formula	$C_{22}H_{48}B_{20}Co_2O_2$
Formula weight	678.66
Temperature	100.0 K
Wavelength	λ = 0.71073 Å
Crystal system	Triclinic
Space group	P-1
Unit cell dimensions	a = 8.9219(5) Å α = 89.659(3)°
	b = 12.4145(7) Å β = 79.993(4)°
	c = 15.5650(9) Å γ = 76.920(3)°
Volume	1652.72(16) Å^3
Z	2
Density (calculated)	1.364 g/cm^3
Absorption coefficient	1.029 mm^{-1}
F(000)	700.0
Crystal size	0.4 × 0.16 × 0.06 mm^3
Theta range for data collection	4.22 to 63.906°
Index ranges	-13 ≤ h ≤ 13, -18 ≤ k ≤ 18, -22 ≤ l ≤ 23
Reflections collected	41114
Independent reflections	11163 [R_{int} = 0.0581, R_{sigma} = 0.0646]
Completeness to theta = 31.95°	97.6%
Absorption correction	Multiscan
Max. and min. transmission	0.746 and 0.669
Refinement method	Full-matrix least-squares on F^2
Data / restraints / parameters	11163 / 63 / 510
Goodness-of-fit on F^2	1.032
Final R indices [I>=2sigma(I)]	R_1 = 0.0440, wR_2 = 0.0991
Final R indices (all data)	R_1 = 0.0683, wR_2 = 0.1095
Largest diff. peak and hole	0.64 and -0.60 e.Å^{-3}

Compound **29**
meso-[1-(1′-4′-Cp-4′,1′,12′-*closo*-$CoC_2B_{10}H_{11}$)-4-Cp-4,1,12-*closo*-$CoC_2B_{10}H_{11}$)]

Identification code	5219
Empirical formula	$C_{14}H_{32}B_{20}Co_2$
Formula weight	534.46
Temperature	100.0(2) K
Wavelength	λ = 0.71073 Å
Crystal system	Monoclinic
Space group	C2/c
Unit cell dimensions	a = 43.247(5) Å α = 90°
	b = 8.8497(9) Å β = 90.104(6)°
	c = 13.4476(14) Å γ = 90°
Volume	5146.7(9) Å^3
Z	8
Density (calculated)	1.380 g/cm^3
Absorption coefficient	1.295 mm^{-1}
F(000)	2160.0
Crystal size	0.2 × 0.2 × 0.1 mm^3
Theta range for data collection	4.7 to 56.86°
Index ranges	-50 ≤ h ≤ 57, -11 ≤ k ≤ 11, -17 ≤ l ≤ 17
Reflections collected	39827
Independent reflections	6433 [R_{int} = 0.0735, R_{sigma} = 0.0574]
Completeness to theta = 28.43°	97.6%
Absorption correction	Multiscan
Max. and min. transmission	0.746 and 0.607
Refinement method	Full-matrix least-squares on F^2
Data / restraints / parameters	6433 / 0 / 392
Goodness-of-fit on F^2	1.253
Final R indices [I>=2sigma(I)]	R_1 = 0.0873, wR_2 = 0.1521
Final R indices (all data)	R_1 = 0.0987, wR_2 = 0.1565
Largest diff. peak and hole	0.56 and -1.57 e.Å^{-3}